

**Aus der Klinik für Plastische, Ästhetische und Handchirurgie
der Medizinischen Fakultät
der Otto-von-Guericke-Universität Magdeburg
Arbeitsgruppe Gravitationsbiologie und translationale regenerative Medizin**

Influence of Mechanical Stress on Biological Processes of Human Cells

Dissertation

zur Erlangung des Doktorgrades

Dr. rer. medic.

(doctor rerum medicarum)

an der Medizinischen Fakultät
der Otto-von-Guericke-Universität Magdeburg

vorgelegt von **M. Sc. Mohamed Zakaria Nassef**
aus **Kairo, Ägypten**
Magdeburg 2020

Angefertigt von **Juni 2017 bis April 2020** in der Klinik für Plastische, Ästhetische und Handchirurgie, Arbeitsgruppe Gravitationsbiologie und translationale regenerative Medizin von Frau Professor Daniela Grimm.

Klinikdirektor: **Herr Professor Dr. med. Manfred Infanger**

Betreuer: **Frau Professor Dr. med. Daniela Grimm**
 Herr Professor Dr. med. Manfred Infanger

Bibliographical Description:

Mohamed Zakaria Nassef:

Influence of Mechanical Stress on Biological Processes of Human Cells– 2020. – 150 Pg., 22 Fig., 4 Appx.

Abstract

With an increasing number of spaceflights, it is crucial that we understand the changes that occur to our cells in space. I was interested in testing the effects of real (r-) and simulated (s-) microgravity (μg) on human breast cancer cells with the objective of investigating cytoskeletal alterations, focal adhesion molecules, extracellular matrix proteins, inflammatory cytokines and the potential mechanism of spheroid formation during microgravity. Besides microgravity, astronauts are subjected to other factors during space travel, including vibration, hypergravity and cosmic radiation. Moreover, vibrations occur during parabolic flights. To evaluate whether vibration has any beneficial impact on chondrocytes, I examined the effect of low-frequency vibration on human chondrocytes. Microgravity is known to exert a negative impact on chondrocytes and vibration could be the countermeasure to prevent such a negative impact.

This thesis evaluated the impact of a 14-day-exposure of MCF-7 breast cancer cells to a random positioning machine (RPM). The cells exposed to the RPM divided into adherent and multicellular spheroids. A proteomics analysis examined the difference between adherent, spheroid and 1g control cells. The analysis revealed a reduction in E-cadherin in spheroids. This finding was confirmed by measuring the messenger RNA (mRNA) expression and protein content. There is a relation between E-cadherin regulation and spheroid formation.

Furthermore, I performed live-cell imaging of transfected MCF-7 cells with a spinning-disc fluorescence microscopy analysis system (FLUMIAS) microscope during a sounding rocket mission. The cells exhibited a rearrangement of F-actin and tubulin. Moreover, I detected filopodia- and lamellipodia-like structures in the F-actin cytoskeleton shortly after the beginning of the microgravity phase. I also investigated the effect of microgravity on MCF-7 cells during a parabolic flight campaign (PFC). The cells manifested elevated *KRT8*, *RDX*, *TIMP1* and *CXCL8* mRNA, while *VCL* was downregulated. Furthermore, E-cadherin protein was significantly downregulated. These changes indicate a transformation of the MCF-7 cells into a more invasive cell type.

In another study, I evaluated the effect of microgravity on the triple negative breast cancer cell line MDA-MB-231 during a PFC. The parabolic flight induced alterations in cell adhesion molecules, findings that are in agreement with previous data from other cell lines.

Finally, I evaluated the impact of low-frequency vibration on human chondrocytes. There were no morphological changes, cytoskeletal alterations or apoptotic cells. Moreover, there was an upregulation of *ANXA1*, *PXN* and *VCL* mRNA and downregulation of *ANXA2*. Thus, I concluded that there is a beneficial effect of low-frequency vibration on human chondrocytes.

Keywords:

Breast cancer; Sounding Rocket; Parabolic Flight; Real Microgravity; FLUMIAS Microscope; Live Cell Imaging; Simulated Microgravity; Random Positioning Machine; Cytoskeleton; Focal Adhesions; Extracellular Matrix; E-cadherin; Vibration; Cartilage; Chondrocytes.

Schlüsselwörter:

Mammakarzinom; Höhenforschungsrakete; Parabelflug; Reale Mikrogravitation; FLUMIAS Mikroskop; Live Cell Imaging; Simulierte Mikrogravitation; Random Positioning Machine; Zytoskelett; Fokale Adhäsionen; Extrazelluläre Matrix; E Cadherin; Vibration; Knorpel; Chondrozyten.

This thesis is based on the following publications:

1. Sahana J *, **Nassef MZ** *, Wehland M, Kopp S, Krüger M, Corydon TJ, Infanger M, Bauer J, Grimm D. Decreased E-Cadherin in MCF7 Human Breast Cancer Cells Forming Multicellular Spheroids Exposed to Simulated Microgravity. *Proteomics* 18: 1800015, 2018.

*both authors contributed equally to this work

2. **Nassef MZ**, Kopp S, Wehland M, Melnik D, Sahana J, Krüger M, Corydon TJ, Oltmann H, Schmitz B, Schütte A, Bauer TJ, Infanger M, Grimm D. Real Microgravity Influences the Cytoskeleton and Focal Adhesions in Human Breast Cancer Cells. *Int J Mol Sci* 20: 3156, 2019.
3. **Nassef MZ**, Kopp S, Melnik D, Corydon TJ, Sahana J, Krüger M, Wehland M, Bauer TJ, Liemersdorf C, Hemmersbach R, Infanger M, Grimm D. Short-Term Microgravity Influences Cell Adhesion in Human Breast Cancer Cells. *Int J Mol Sci* 20: 5730, 2019.
4. Lützenberg R, Wehland M, Solano K, **Nassef MZ**, Buken C, Melnik D, Bauer J, Kopp S, Krüger M, Riwaldt S, Hemmersbach R, Schulz H, Infanger M, Grimm D. Beneficial Effects of Low Frequency Vibration on Human Chondrocytes in Vitro. *Cell Physiol Biochem*. 2019;53:623–37.

The publication texts can be found in the appendix of this dissertation

Table of Contents

Abstract.....	I
Table of Contents	6
Abbreviations:.....	8
1. Preface	11
2. Aims.....	12
3. Hypothesis.....	12
4. Introduction.....	13
4.1. Health risks for humans in space	13
4.2. Microgravity research	14
4.2.1. Real microgravity.....	15
4.2.2. Simulated microgravity	16
4.3. Hypergravity and vibration.....	17
4.4. Cancer	18
4.4.1. Breast cancer.....	19
4.4.2. Breast cancer cell lines	20
4.5. Human chondrocytes.....	21
4.6. Perception of mechanical stimuli.....	22
4.7. Multicellular spheroids.....	22
5. Discussion of the publications.....	24
5.1. Decreased E-Cadherin in MCF7 Human Breast Cancer Cells Forming Multicellular Spheroids Exposed to Simulated Microgravity	24
5.2. Real Microgravity Influences the Cytoskeleton and Focal Adhesions in Human Breast Cancer Cells	28
5.3. Short-term Microgravity Influences Cell Adhesion in Human Breast Cancer Cells	34
5.4. Beneficial Effects of Low Frequency Vibration on Human Chondrocytes <i>in vitro</i>	42
5.5. Conclusions	43

5.6.	Summary	45
5.7.	Zusammenfassung.....	46
6.	References	48
7.	Figure Index	60
8.	Acknowledgement	63
9.	Statement.....	64
10.	Curriculum Vitae	65
11.	Appendix	70
11.1.	Publication #1	70
11.2.	Publication #2	81
11.3.	Publication #3	107
11.4.	Publication #4	135

Abbreviations:

2D	Two-dimensional
3D	Three-dimensional
<i>ACAN</i>	Aggrecan
<i>ACTB</i>	Actin beta
AD	Adherent
ADS	Airbus Defence and Space
<i>ANXA1</i>	Annexin A1
<i>ANXA2</i>	Annexin A2
<i>APC/C</i>	Anaphase-promoting complex
<i>ASAP1</i>	ArfGAP with SH3 domain, ankyrin repeat and PH domain 1
<i>ATM</i>	Ataxia telangiectasia mutated
<i>BAX</i>	BCL2 associated X
<i>BCAR1</i>	Breast cancer anti-estrogen resistance protein 1
<i>BCL2</i>	B-cell lymphoma 2
<i>BIRC2</i>	Baculoviral IAP repeat containing 2
<i>BIRC3</i>	Baculoviral IAP repeat containing 3
<i>BIRC5</i>	Baculoviral IAP repeat containing 5
<i>BRCA1</i>	Breast cancer 1
<i>BRCA2</i>	Breast cancer 2
BRIP1	BRCA1 interacting protein C-terminal helicase 1
<i>Casp3</i>	Caspase 3
<i>CD44</i>	Cell surface glycoprotein CD44
<i>CDC</i>	Cell division cycle
<i>CDH1</i>	E-Cadherin
<i>CHEK2</i>	Checkpoint kinase 2
<i>COL1A1</i>	Collagen type I alpha 1 chain
<i>COL2A1</i>	Collagen type II alpha 1 chain
<i>c-SRC</i>	proto-oncogene tyrosine-protein kinase c-Src
<i>CXCL8</i>	C-X-C motif chemokine ligand 8
<i>CYC</i>	Cytochrome C
DLR	Deutsches Zentrum für Luft- und Raumfahrt
ECM	Extracellular matrix
<i>ER</i>	Estrogen receptor
ERK	Extracellular signal-regulated kinase
<i>ERK1</i>	Extracellular signal-regulated kinase 1
<i>ERK2</i>	Extracellular signal regulated kinase 2
<i>EZR</i>	Ezrin
FA	Focal adhesion
<i>FADD</i>	Fas associated via death domain
<i>FAK1</i>	Focal adhesion kinase 1

<i>FAS</i>	Fas cell surface death receptor
FEI	Field Electron and Ion Company
FLUMIAS	spinning-disc Fluorescence Microscopy Analysis System
<i>FNI</i>	Fibronectin 1
FP	Filopodia
FTC-133	Human follicular thyroid carcinoma cell line
hAVICs	human aortic valve interstitial cells
<i>HER2</i>	Human epidermal growth factor receptor 2
Hyper-g	Hyper-gravity
<i>ICAM1</i>	Intercellular adhesion molecule 1
<i>IKBKγ</i>	Inhibitor NFKB kinase subunit gamma (NEMO)
<i>IL6</i>	Interleukin 6
<i>CXCL8</i>	Interleukin 8
<i>ISG15</i>	Interferon simulated gene 15
ISS	International space station
<i>ITGB1</i>	Integrin subunit beta 1
<i>IκB</i>	Inhibitor κ B
<i>JNK1</i>	mitogen-activated protein kinase 8 isoform JNK1 alpha1
<i>KRT8</i>	Keratin 8
<i>LAMA1</i>	Laminin subunit alpha 1
LFQ	Label-free quantification
LP	Lamellipodia
MAPK	Mitogen-activated protein kinase
<i>MAPK8</i>	Mitogen-Activated Protein Kinase 8
MCF-7	Michigan cancer foundation-7
MCS	Multicellular spheroids
MDA-MB-231	M.D. Anderson-metastasis breast cancer cell line-231
<i>MMP9</i>	Matrix metalloproteinase 9
mRNA	messenger RNA
<i>MSN</i>	Moesin
MuSIC	Multi sample incubator centrifuge
NASA	National Aeronautics and Space Administration
<i>NFKBIA</i>	NFKB inhibitor alpha
<i>NFKBIB</i>	NFKB inhibitor beta
<i>NFKBIE</i>	NFKB inhibitor epsilon
NF- κ B	Nuclear factor kappa
NF- κ B P50	Nuclear factor kappa-B P50 subunit
NF- κ B P52	Nuclear factor kappa-B P52 subunit
NF- κ B P65	Nuclear factor kappa-B P65 subunit
<i>NF-κB1</i>	Nuclear factor kappa B subunit 1
<i>NF-κB2</i>	Nuclear factor kappa B subunit 2
<i>NF-κB3</i>	Nuclear factor kappa B subunit 3
NGS	Next generation sequence

OHB	Otto Hydraulic Bremen
<i>PAIL/SERPINE1</i>	Serpin family E member 1
<i>PALB2</i>	Partner and localizer of BRCA2
<i>Paxillin-FAK</i>	Paxillin-focal adhesion kinase
PF	Parabolic flight
PFA	Paraformaldehyde
PFC	Parabolic flight campaign
<i>PR</i>	Progesterone receptor
<i>PRKCA</i>	Protein kinase C alpha
<i>PSMD4</i>	Proteasome 26S subunit non-ATPase 4
<i>PTEN</i>	Phosphatase and Tensin Homolog
PTH	Parathyroid hormone
<i>PTK2</i>	Protein tyrosine kinase 2
<i>PXN</i>	Paxillin
qPCR	quantitative polymerase chain reaction
r- μ g	Real microgravity
<i>Raf1</i>	Raf-1 Proto-Oncogene, Serine/Threonine Kinase
RCCS	Rotating cell culture system
<i>RDX</i>	Radixin
<i>RELA</i>	RELA proto-oncogene
RPM	Random positioning machine
RWV	Rotating wall vessel
s- μ g	Simulated microgravity
<i>SPP1</i>	Secreted phosphoprotein 1
<i>STK11</i>	Serine/threonine kinase 11
STRING	Search Tool for the Retrieval of Interacting Genes/Proteins
<i>TBX15</i>	T-Box Transcription Factor 15
TEXUS/TX	Technische Experimente unter Schwerelosigkeit
<i>TIMP1</i>	TIMP metalloproteinase inhibitor 1
<i>TLN1</i>	Talin 1
TNBC	Triple negative breast cancer
<i>TP53</i>	Tumor Protein P53
<i>TUBB</i>	Tubulin Beta
TUNEL	Terminal deoxynucleotidyl transferase dUTP nick end labeling
<i>UBE2C</i>	Ubiquitin conjugating enzyme E2 C
<i>VCAM1</i>	Vascular cell adhesion molecule 1
<i>VCL</i>	Vinculin
<i>VEGFA</i>	Vascular endothelial growth factor A

1. Preface

The work presented in this thesis was performed between June 2017 and April 2020 in the laboratories of Prof. Daniela Grimm in the Clinic for Plastic, Aesthetic and Hand Surgery, University Clinic, Otto-von-Guericke-University Magdeburg in Germany. Western blots experiments and some of the random positioning machine (RPM) simulation experiments were performed in the Department of Biomedicine, Pharmacology, Aarhus University. Mass spectrometry and pathway analysis were conducted in collaboration with the Max Planck Institute for Biochemistry in Martinsried, Germany.

Real microgravity ($r\text{-}\mu\text{g}$) experiments were performed during the Deutsches Zentrum für Luft- und Raumfahrt (DLR) parabolic flight campaigns 29 and 31 and the DLR Technische Experimente unter Schwerelosigkeit (TEXUS) sounding rocket mission 54. The parabolic flights were executed in the facility of the company Novespace, which is situated at the Bordeaux-Mérignac Airport in Bordeaux, France. The sounding rocket was launched from the SSC Esrange launch site, Kiruna, Sweden. The sounding rocket mission was supported by Airbus Defence and Space (ADS), the DLR, Otto Hydraulic Bremen (OHB)-system AG, Field Electron and Ion Company (FEI) Munich GmbH and the Esrange space station.

Supervisors:

Professor Daniela Grimm

Professor for Space Medicine and Pharmacology
Institute for Biomedicine, Pharmacology, Aarhus University,
Aarhus, Denmark
and

Guest Professor for Gravitational Biology and Translational Regenerative Medicine
Otto-von-Guericke-University, Magdeburg, Germany

Professor Manfred Infanger

Director of the Clinic for Plastic, Aesthetic and Hand Surgery
University Hospital, Otto-von-Guericke-University Magdeburg,
Magdeburg, Germany

Mentor:

Dr. Sascha Kopp

Gravitational Biology and Translational Regenerative Medicine group
Otto-von-Guericke-University, Magdeburg, Germany

2. Aims

When human breast cancer cells are exposed to conditions of simulated microgravity ($s\text{-}\mu g$) created by an RPM, they reveal a variety of changes in the cytoskeleton, the composition of the extracellular matrix (ECM) and they form three-dimensional (3D) aggregates during microgravity, among other changes. These 3D tissues are also called multicellular spheroids (MCS).

This thesis aimed to investigate the molecular and morphological alterations that occur in human breast cancer cells during r - and $s\text{-}\mu g$. Furthermore, I investigated the potential beneficial effect of vibration on human chondrocytes.

I studied samples of breast cancer cells and chondrocytes exposed to microgravity, hypergravity and vibration using microscopic techniques, quantitative real-time polymerase chain reaction (qPCR), Western blots, viability assays and pathway analyses. My principal aim was to detect and evaluate possible changes in breast cancer cells and chondrocytes induced by mechanical stress occurring during microgravity, hypergravity and vibration experiments.

3. Hypothesis

Human cells can sense microgravity and mechanical stressors through the cytoskeleton. The cytoskeleton plays an essential role in converting gravitational unloading (mechanical signal) into a chemical signal. Several cell lines have been tested in s - and $r\text{-}\mu g$ environments, and they have exhibited the conversion from 2D (two-dimensional) monolayers into 3D spheroids.

My hypotheses for this doctoral thesis were (1) the cytoskeletal alterations and mechanisms of spheroid formation in human breast cancer cells exposed to microgravity are similar to the alterations that occur in human follicular thyroid cancer cells; (2) E-cadherin and c-SRC (proto-oncogene tyrosine-protein kinase c-Src) are involved in MCS formation of breast cancer cells; and (3) intracellular adhesion molecule 1 (ICAM-1) and vascular cell adhesion molecule 1 (VCAM-1) and the rapid decrease in nuclear factor κB (NF- κB) subunit p-65 are fast-reacting, gravity-regulated and cell-protective mechanisms of triple-negative breast cancer (TNBC) cells exposed to altered gravity conditions.

Furthermore, vibration is known to be one of the stressors during a spaceflight and parabolic flights. It is important to study the impact of such stressors, especially with regard to future planned long-term spaceflights. A recent study hinted towards beneficial effects of vibration on human chondrocytes. Therefore, I tested the hypothesis that the impact of vibration on breast cancer cells and chondrocytes is moderate and of a cell-protective nature.

4. Introduction

Space-based research to investigate the alterations that occur in human cells exposed to microgravity is more necessary than ever. Astronauts spend longer times in space and mission durations are expected to increase with the commercialisation of space travels and the rising numbers of manned spaceflights as well as future plans to colonise the Moon and Mars (1).

4.1. Health risks for humans in space

Astronauts suffer from several health problems, especially when they spend longer periods of time in space. These medical health concerns include cardiovascular changes, reduction of bone density, risk of kidney stone formation, muscle atrophy and impaired immunity, among others (Fig. 1) (2–8).

Due to weightlessness in space, the human body is subjected to minimal gravitational force. Thus, the body adapts to weightlessness in space in different ways. Firstly, skeletal muscles lose some of their mass and strength. Furthermore, bone resorption increases, which leads to a decline in bone density and potential osteoporosis. As a secondary consequence of bone resorption, the parathyroid hormone (PTH) level decreases, which leads to a 50% increase in calcium excretion and a 50% reduction in calcium absorption (9). The increase in calcium excretion leads to a higher risk of renal stone formation.

Secondly, the immune system is negatively impacted by microgravity. Several infectious diseases, such as conjunctivitis, upper respiratory tract infections, pharyngitis, viral gastroenteritis and mild dermatologic problems, have been reported to occur during spaceflight missions (10, 11). Moreover, latent infectious diseases, including herpes simplex, are reportedly reactivated, possibly due to microgravity (12–14). While the immune system is hampered by microgravity, studies have also shown that some bacteria develop a higher pathogenicity and an altered response to antibiotics during spaceflights or s- μ g. For example *Salmonella typhimurium* exhibits increased resistance, survival and virulence in spaceflights (15, 16).

Thirdly, astronauts experience nausea and vomiting during spaceflights. However, such symptoms usually disappear after a few days (17–19). Moreover, there is a shift in the distribution of body of fluids due to lack of gravity. Body fluids such as blood and lymph are distributed towards the head, a phenomenon that results in puffy face and bird legs (20). Lastly, many astronauts suffer from orthostatic hypotension and a reduced exercise capacity post-flight (21). While many of these side effects might not represent a serious concern for short-term spaceflights, it is still crucial to understand how our cells behave in space to implement countermeasures for such complications, especially in regard to future long-term spaceflights (22, 23).

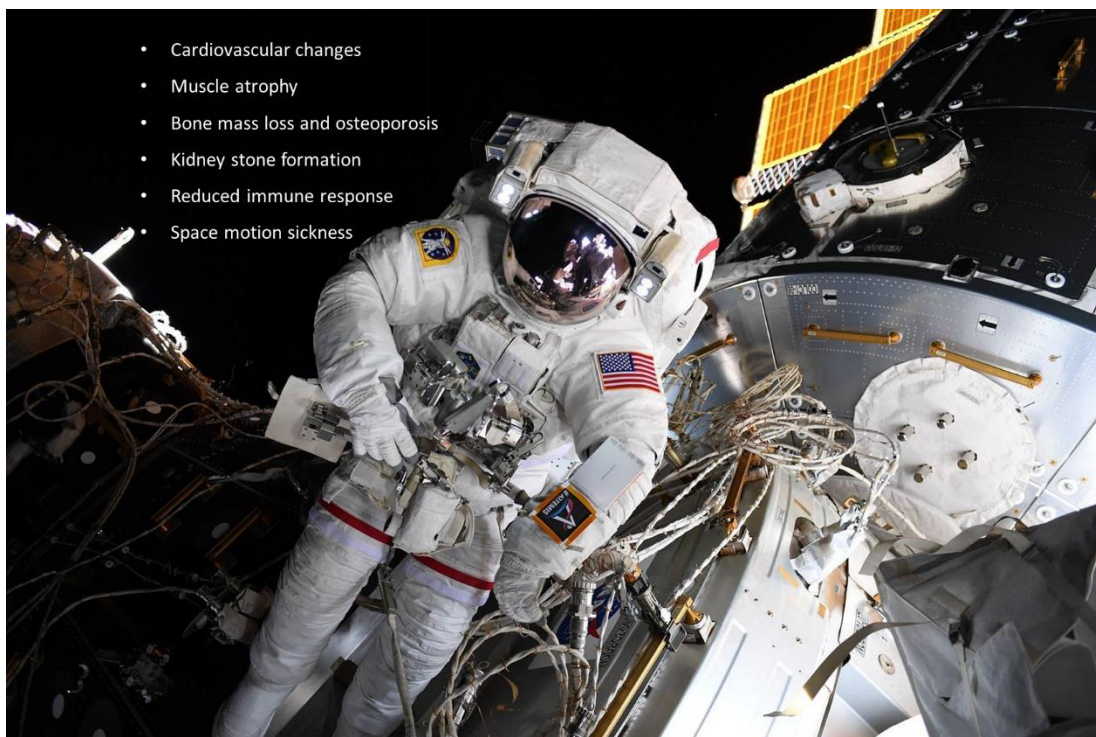


Fig. 1: A spaceflight can negatively affect the human body (modified from nasa.gov). A list of the most known health problems of humans in space is given.

4.2. Microgravity research

Prof. Grimm's group has prominent experience in performing flight missions and s- μ g experiments to investigate the impact of microgravity on cells. There are two main ways to investigate the effect of microgravity on cells: simulating devices (ground-based facility) or r- μ g flight missions.

4.2.1. Real microgravity

R- μ g represents conditions where the gravity force is diminished to almost zero. R- μ g is achievable through various platforms, such as unmanned BION or photon satellites, a spaceflight in orbit or to the International Space Station (ISS), parabolic flights and sounding rockets. Parabolic flights are very important for research in r- μ g, preparation of spaceflights and astronaut training. The German space agency Deutsches Zentrum für Luft- und Raumfahrt (DLR) organises parabolic flight campaigns on a regular basis to offer researchers the opportunity to perform experiments under r- μ g. Each flight comprises 31 consecutive parabolas. Each parabola contains two phases of 1.8g hyper-gravity (hyper-g) flanking one phase of μ g of up to 10^{-2} g quality. The first phase of a parabola begins with an ascent at 45 degrees for 22 s known as pull up, which is accompanied by a hyper-g of 1.8g, followed by decreasing thrust and following the ballistic trajectory of a parabola for 22 s in free fall (μ g phase). Finally, the pilot steers the aircraft back to fly horizontally. This last phase is known as pull out and lasts for 22 s with a hyper-g of 1.8g (Fig. 2A) (24, 25). The parabolic flight has the advantage of offering valuable r- μ g time, and it is the only platform that allows experiments that can be operated by the scientists themselves.

Another important platform to study cells in r- μ g are sounding rockets. The DLR offers opportunities for researchers to conduct their experiments on sounding rockets through the Technische Experimente unter Schwerelosigkeit (TEXUS) program (26–33). The TEXUS (TX) sounding rocket has the advantage of providing a relatively longer duration (6 min) of microgravity compared to parabolic flights. Besides, it has only one period of hyper-g and vibration at the beginning prior to the microgravity phase. The TX sounding rocket is composed of the payload and a two-stage solid propellant VSB 30 rocket. During its flight, the TX rocket usually reaches an apogee of ~250 km; it enters microgravity 75 s after launch. The microgravity phase of $< 10^{-4}$ g usually lasts for ~6 min. Following the microgravity phase, the rocket falls back to earth by a parachute-mediated deceleration (Fig. 2B). The payload is usually recovered on the same day.

Other platforms, such as unmanned BION or photon spaceflights, a spaceflight in orbit and ISS experiments, offer a longer non-interrupted r- μ g time. However, they are even more complicated to conduct and plan and are challenging both logistically and financially. Hence, s- μ g experiments are more economical and accessible for routine microgravity research (34).

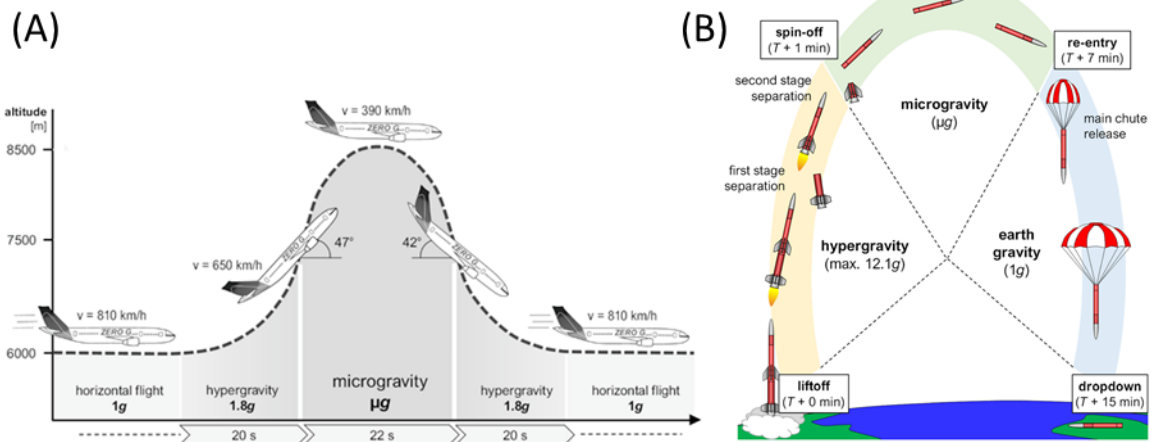


Fig. 2: Schematic sequences of parabolic and sounding rocket flights: (A) shows the altitude, speed and the three consecutive phases (hyper-g, microgravity and hyper-g) in each parabola during a parabolic flight, while (B) shows the launch and the re-entry of a sounding rocket (adapted from 35).

4.2.2. Simulated microgravity

Researchers might focus on s- μ g as a replacement for r- μ g missions in certain situations. S- μ g devices are a perfect platform to test new hypotheses or to confirm a finding. Moreover, they are always accessible, require little preparation time to conduct an experiment and offer the possibility of performing multi-time-point experiments. S- μ g experiments are performed in a ground-based facility with the help of microgravity simulation devices. It is possible to achieve s- μ g environment through 2D or 3D clinostats, RPM or rotating wall vessels (RWV). Such devices do not eliminate gravitational forces; instead, they work to achieve a microgravity perception on biological samples by randomising the direction of gravity over time (34) by rotating them around either one or all three axes in space.

A 2D clinostat is a microgravity-simulating device that rotates around one axis with a constant speed and direction. A clinostat nullifies the effect of gravity on biological samples by running in constant speed against the direction of the gravity vector. In contrast, 3D clinostats utilise two independent rotation axes with constant speed and direction. The 3D clinostats were first established in Japan and the Netherlands (36). Researchers have hypothesised that 3D clinostats provide a better a microgravity simulation by running two independent axes. Moreover, a 3D clinostat can serve as an RPM if the two axes run in randomised different speed and directions (34). In order to ensure correct execution of microgravity simulation experiments with an RPM and clinostat, cell culture flasks must be filled with medium that is

completely free from air bubbles in order to avoid any shear stress. They have to be kept near the centre of rotation to avoid any residual acceleration forces.

Another device that it is used in microgravity simulation is the RWV or rotating cell culture system (RCCS), which was first established by the US National Aeronautics and Space Administration (NASA) (37). The RWV is composed of a plexiglass cylinder with a wide central core mounted on a horizontal plane and a variable speed motor connected to the shaft (34). The RWV was designed to provide an s- μ g environment for cells and aquatic organisms (38). While s- μ g machines have contributed to a myriad of research, one must be careful about possible variability and differences between r- and s- μ g.

4.3. Hypergravity and vibration

It is important to investigate the impact of vibration and hyper-g on cells as these factors are involved in r- μ g experiments. Parabolic flight is an example of a platform that contains long phases of hyper-g and vibration. When it comes to spaceflights and long-term ISS missions, hyper-g is not a major factor to be considered. However, vibration can always be generated in space, either from the different machines that surround the astronauts or from the astronauts themselves during workouts (39).

As a consequence of having vibration and hyper-g as involving factors during r- μ g missions, there was a need for laboratory devices that can replicate the effect of vibration and hyper-g. As a vibration-simulating device, the Vibraplex was developed by the DLR to conduct vibration experiments on cells *in vitro* (Fig. 3C). The Vibraplex produces frequencies between 0.2 to 14 kHz. These frequencies are used to create vibrations that resemble a parabolic flight (40, 41). To investigate the impact of hyper-g on cells, the DLR developed a multi sample incubator centrifuge (MuSIC) (Fig. 3A, B). The MuSIC is capable of simulating the hyper-g phases that occur during a parabolic flight (39).

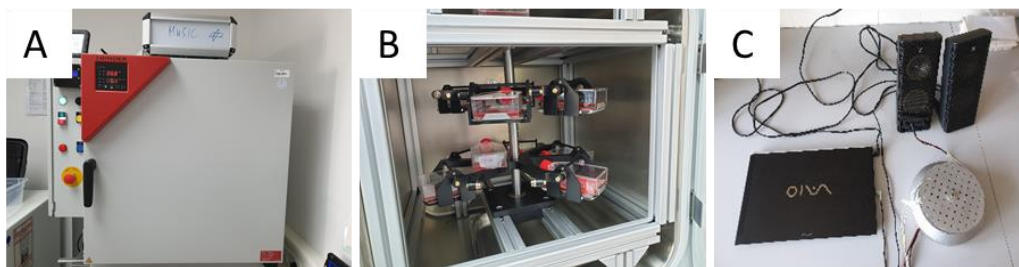


Fig. 3: (A) A view of the MuSIC from the outside; (B) cell culture flasks fixed to the MUSIC from the inside; (C) the Vibraplex connected to audio speakers to control the frequency produced by the device.

While hyper-*g* and vibration might induce genetic alterations in cells, μg has the strongest impact (39). More research must be conducted to reach a conclusive answer with regard to the impact of hyper-*g* and vibration on the human body.

4.4. Cancer

Cancer represents a huge health and economic burden on humankind. In 2018, cancer was responsible for 9.6 million deaths worldwide (42). The number of cancer patients is expected to rise every year. The most common cancer types in both sexes are lung cancer, breast cancer, prostate cancer and colorectal cancer (42). Environmental factors and inherited genetic factors are considered to be the main causes of cancer (43). Cancer is usually initiated by mutations in the DNA of oncogenes or tumour suppressor genes that lead to uncontrolled cell growth and malignant transformation (44). Cancer can be characterised by six general hallmarks: sustaining proliferative signals, evading growth suppressors, resisting programmed cell death (apoptosis), promoting blood vessel formation or angiogenesis, invasiveness or metastasis and unlimited number of cell division promoting immortality (45).

Furthermore, the immune system is thought to be involved in the process of cancer development, a phenomenon known as cancer immunoediting. The first phase of cancer immunoediting is elimination. In this phase, innate and adaptive immunity work together to eliminate any existing tumour. If the immune system is successful, the tumour will be fully eliminated. In other cases, the tumour will progress to the equilibrium phase. In this phase, adaptive immunity works to keep the tumour dormant. The equilibrium phase can last for years or even a lifetime in some subjects; hence, it is considered the longest phase of cancer immunoediting. Tumour cells express antigens that are recognised by adaptive immunity. Defects in antigen processing or presentation or antigen loss variants may lead to tumour cells that are unrecognisable to the immune system. This event leads to the last phase of cancer immunoediting: escape. The tumour cells enter a immunosuppressive state, which promotes cell growth and proliferation and clinical manifestation of the tumour (44). Evidently, more research needs to be performed to identify new targets and to develop new drugs against cancer. A previous study suggested that cancer cells may develop a less-aggressive phenotype when they grow in a microgravity environment (46). Studying the alterations that occur in cancer cells in microgravity could help us to identify potential targets to develop future treatments. One of my main focuses in this thesis is breast cancer.

4.4.1. Breast cancer

Breast cancer is the leading cause of cancer death in women worldwide, and there are increasing numbers of women diagnosed with it every year (47–49). Environmental and lifestyle factors are considered to be the main causes of breast cancer. Environmental risk factors include late maternal age for first pregnancy, early menarche, late-onset menopause and lack of breast-feeding. Early pregnancy and associated high levels of oestrogen during pregnancy have been linked to a lower risk of developing breast cancer (47, 50). A reduction in the progenitor or stem cell numbers and elimination of targets for malignant transformation during pregnancy might be the reason for lower risk of developing breast cancer (51). Genetic predisposition only accounts for 10% of breast cancer. For instance, mutations in high-penetrance genes, such as breast cancer 1 (*BRCA1*), breast cancer 2 (*BRCA2*), phosphatase and tensin homolog (*PTEN*), tumour protein P53 (*TP53*), E-cadherin (*CDH1*) and serine/threonine kinase 11 (*STK11*), have been associated with an up to an 80% lifetime risk of developing breast cancer (52). Other moderate-penetrance mutations in BRCA1 interacting protein C-terminal helicase 1 (*BRIP1*), ataxia telangiectasia mutated (*ATM*), partner and localiser of BRCA2 (*PALB2*) and checkpoint kinase 2 (*CHEK2*) genes have been linked with only a two-fold increased risk of breast cancer (52). Genetic evaluation for mutated genes is suggested on an individual basis, especially for women with a family history of breast cancer. Next generation sequencing (NGS) has become an essential tool to diagnose hereditary breast cancer. Moreover, it has provided clinicians with the ability to test for several mutations and disorders simultaneously. NGS is a comprehensive and indispensable tool in genetic disorder investigation in breast cancer (47, 52).

While it is not completely clear how breast cancer is initiated, it is possible to classify breast cancer into different subtypes depending on molecular characteristics (47). Breast cancer is divided into seven subtypes: luminal A, luminal B, basal like/triple-negative, human epidermal growth factor receptor (HER)-2 enriched, molecular apocrine, claudin-low and normal breast cancer-like (53–56). Utilising these biological classifications has improved therapy guidelines and helped to implement a new approach for each subtype. Moreover, the tumour is considered to be hormone-receptor-positive breast cancer if it possesses oestrogen receptor (ER) and/or progesterone receptor (PR). In contrast, it is considered TNBC if it does not possess ER, PR and HER-2. TNBC is associated with a poor prognosis because it does not respond to hormonal therapy (47). With improvements in health care and treatment guidelines, breast cancer has become curable in 70–80% of patients (47). However, it is still the cause of death for many women around the world. Research is the only way to overcome such socioeconomic burden by helping to identify new targets and to develop new drugs.

4.4.2. Breast cancer cell lines

Cell lines are excellent experimental models to study breast cancer and to investigate potential methods and drugs to decrease the disease progression. The Michigan Cancer Foundation (MCF)-7 cell line is one of the most widely used breast cancer cell lines; it has contributed to breast cancer research more than any other cell line (57). The MCF-7 cell line was established in 1973; it was derived from a breast cancer patient in the Michigan Cancer Foundation (Fig. 4A) (58). MCF-7 is a non-invasive and poorly aggressive cell line. It expresses the ER and PR, but is HER2 negative (59, 60). In the laboratory of Prof. Grimm, several s- μ g experiments—a sounding rocket experiment and parabolic flight experiments—have been performed with MCF-7 cells (61, 62). Furthermore, MCF-7 cells have been subjected to weightlessness in a photon capsule (63, 64). Overall, the cell line is robust and reliable for microgravity experiments in space and on Earth.

The second breast cancer cell line of interest to us is the M.D. Anderson-Metastasis Breast cancer (MDA-MB)-231 cell line. MDA-MB-231 cells are aggressive and invasive. The cell line was established in the 1970s (Fig. 4B) (65). Furthermore, MDA-MB-231 cells are triple negative because they do not express ER, PR and HER2 receptors (66, 67). The MDA-MB-231 cell line has been investigated in a s- μ g environment using an RPM (68). However, to my knowledge MDA-MB-231 cells have not yet been investigated under r- μ g conditions.

Both cell lines are representative for breast cancer and they have been used in many studies. Moreover, they respond to microgravity with alterations in the cytoskeleton and the formation of 3D aggregates, known as spheroids (62, 68). Thus, they are suitable candidates for r- and s- μ g experiments.

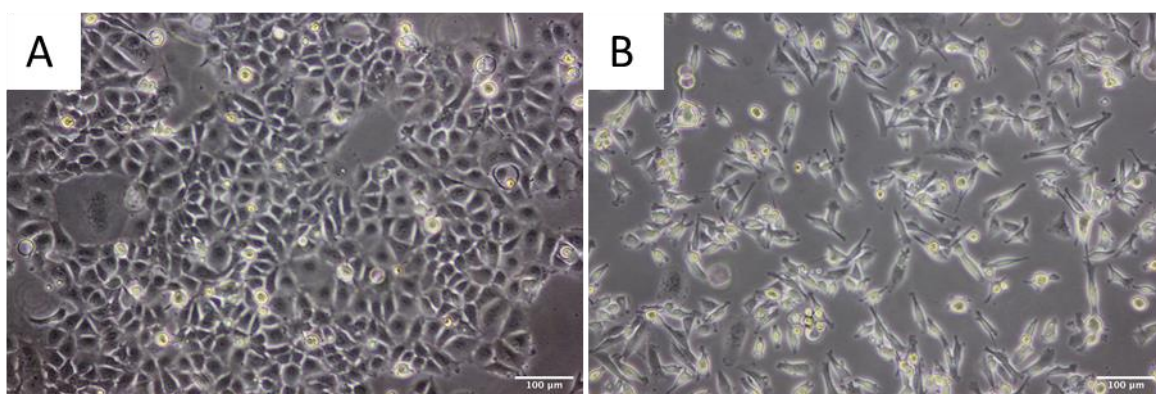


Fig. 4: Phase contrast images of MCF-7 (left) and MDA-MB-231 (right). The scale bar is equal to 100 μ m.

4.5. Human chondrocytes

Chondrocytes are the only cell type in cartilage tissue (Fig. 5). They synthesise ECM proteins such as fibronectin, proteoglycans and collagen type II. Besides these characteristics, they maintain the ECM homeostasis. To a certain extent, chondrocytes are metabolically inactive due to the absence of a vascular supply and innervation in the tissue (69). However, they can still sense mechanical stimuli, growth factors and cytokines. Several publications have highlighted the role of mechanical stress in modifying biological processes of chondrocytes, including proliferation, cell adhesion, differentiation and signal transduction (70, 71). Chondrocytes upregulate cytoskeletal genes upon exposure to $r\text{-}\mu\text{g}$ during a parabolic flight (41). Furthermore, they show a similar behaviour after culturing for 24 h in an RPM. Specifically, the chondrocytes exhibit alterations in the ECM during the reorganisation of the cytoskeleton before forming 3D aggregates (72, 73).

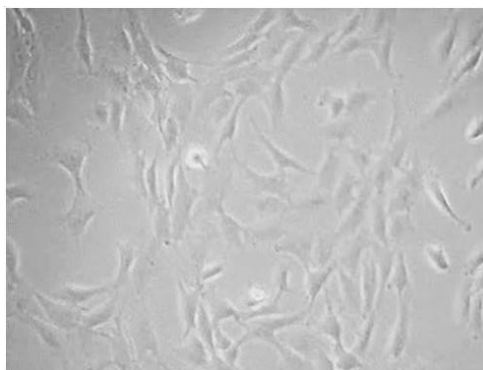


Fig. 5: Phase contrast image of chondrocytes

Recent studies have investigated the impact of 2- and 24-h vibration by the Vibraplex on human cartilage cells (40, 41). Short- and long-term vibration does not negatively influence the chondrocytes. Moreover, there is no apoptosis at either time point. However, long-term vibration reduces osteopontin protein and proteasome 26S subunit non-ATPase 4 (*PSMD4*) and T-Box transcription factor 15 (*TBX15*) gene expression. Osteopontin is elevated in osteoarthritis patients, indicating that this protein is linked to the progression of osteoarthritis (74). *PSMD4* is also involved in regulating the inflammatory response through activation of NF- κ B (75). *TBX15* is a possible calcification preventing factor in human aortic valve interstitial cells (hAVICs) (76). These modifications suggest a beneficial influence of long-term vibration on human chondrocytes (40). Further investigations on the effects of vibration on chondrocytes are needed, and I focused on these studies in my thesis.

4.6. Perception of mechanical stimuli

Some plant cells can sense gravity through special organelles called statoliths (77). In contrast, researchers have not yet identified specific gravity sensor in human cells. Nevertheless, the cytoskeleton is hypothesised to act as a gravity sensor for human cells. It is widely accepted that the cytoskeleton is the first structure that is altered by microgravity (78–80). The tensegrity model suggests that cells in all tissues may sense changes in gravity through disruption of the balance of forces between adhesion receptors and the cytoskeleton (81). The cytoskeleton comprises the actin network, the microtubule network and intermediate filaments (82). The role of the cytoskeleton in graviperception is central in converting mechanical signals into chemical signals. This conversion is achieved through mechanotransduction with the help of focal adhesion (FA) proteins and mechanosensitive ion channels. Mechanosensitive ion channels are transmembrane ion channels that can open or close due to changes in mechanical forces on the cell. FA proteins are a group of transmembrane complexes that connect the cytoskeleton to the ECM. FAs play an important role in environmental sensing and detecting the composition of ECM, actions that contribute to tumour cell resistance to chemotherapy and radiation (83–88). Moreover, research has suggested that FAs contribute to other cellular functions, such as migration (83). It is important to further study FAs due to their role in mechanotransduction and tumour cell resistance to therapy.

The cytoskeleton can sense the alterations in microgravity within seconds. However, the modification of the cytoskeleton is a dynamic process that can take days to be fully completed. This process can also be recovered after a certain amount of time (89). Therefore, it is important to test the impact of microgravity at several time points to understand the full picture. The cytoskeleton can sense microgravity and convert the mechanical signal into a chemical signal, but it also is able to sense shear stress or stiffness of the cellular substrate (90, 91).

4.7. Multicellular spheroids

In a 2D cell culture, the cells grow as a monolayer that is adherently attached to the plastic bottom of the cell culture flask. In this case, the cells interact with plastic more than with the ECM or other cells. In contrast to this growth behaviour, the majority of the cells in our body grow in a complex 3D structure. While the 2D cell culture technique has contributed to a lot of research around the world, it lacks the close resemblance to the growth of cells inside the real *in vivo* tissues. Therefore, there is a need for 3D cell culture systems that mimic the mechanical and biochemical environment *in vivo* (92).

In a scaffold-free environment in microgravity, many different types of cells tend to form 3D aggregates, which are called MCS (Fig. 6) (93). MCS usually have slightly different compositions depending on their size and the duration of exposure to microgravity (94). Spheroids larger than 500 μm usually take 3–5 days to develop, and they comprise an outer layer of proliferating cells that surrounds a viable quiescent layer of cells and a necrotic core (95–98). On the other hand, spheroids smaller than 200 μm take ~8 days to develop hypoxic core regions with necrotic areas (99, 100). MCS have an improved response to stimuli, migration, proliferation, morphology, angiogenesis stimulation, viability and differentiation (101). Spheroid formation can be induced by several methods, including via devices that simulate μg , long-term r- μg missions and Earth-based methods, e.g. liquid overlay, hanging drop and suspension cultures techniques, among others (94, 102, 103). Three-dimensional aggregates tend to resemble the tissue from which they are taken (62, 104). For instance, MCF-7 breast cancer cells exhibit duct-like spheroid formation after being cultured in an RPM for ≥ 5 days (68). Moreover, endothelial cells develop tube-like structures after 2 weeks of cell culture in an RPM (104). Using s- μg machines to form spheroids has proven to be advantageous in the field of tissue engineering because several cell types behave similar to a free-fall condition, promoting 3D self-assembly (105–107).

These 3D MCS are a valuable tool to study tumour proliferation, metastasis and drug delivery (102, 108, 109). For a drug to be delivered to a target cell, it must pass through several biological barriers, including other organs, ECM and intracellular compartments. Due to these barriers, the drug may be deactivated or trapped in other cells before it even reaches the target cells (109). Therefore, 2D monolayer cells do not offer the best model for a drug delivery system. In contrast, a 3D cell culture model like MCS offer a better environment to test the drug delivery *in vitro*. Spheroids can be specially suited for testing anti-cancer drugs because they possess necrotic core and hypoxic regions in the centre. This feature is thought to be one of the reasons of drug resistance in cancer therapy (109).

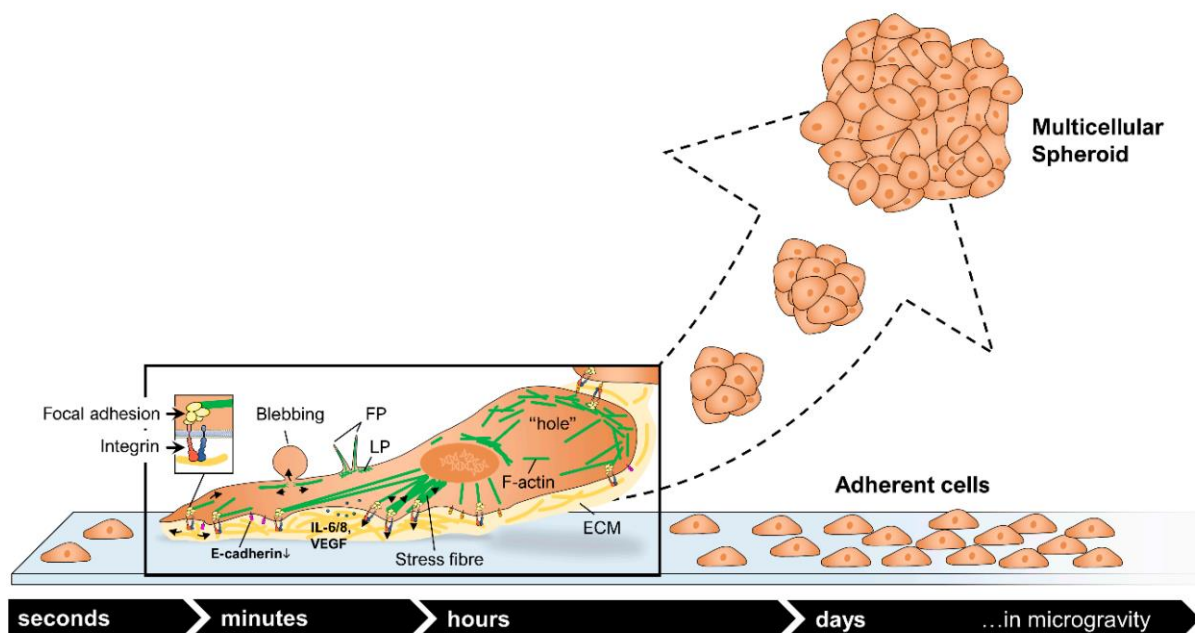


Fig. 6: The alterations of adherent cells and how they lead to the transformation into multicellular spheroids after exposure to microgravity. The figure in the box shows changes at the microscopic level. F-actin is displayed as green lines, while the ECM in yellow. Abbreviations: FP: filopodia, LP: lamellipodia (modified from 110).

5. Discussion of the publications

I will discuss and summarise four publications in this section.

5.1. Decreased E-Cadherin in MCF7 Human Breast Cancer Cells Forming Multicellular Spheroids Exposed to Simulated Microgravity

In this publication, I exposed human breast cancer cells MCF-7 to an RPM for 14 days. At the end of the 2-week RPM experiment, I harvested samples for mass spectrometry, Western blot analysis and messenger RNA (mRNA) expression analysis from adherent (AD) and 3D MCS cell cultures.

I analysed the protein samples of static 1g control cells, RPM-AD and RPM-MCS cells by mass spectrometry. I focused on proteins that form cell contacts with the cellular, non-cellular environment and on pathways regulating these processes. The proteome analysis revealed similar label-free quantification

(LFQ) scores for most of the proteins. Interestingly, other proteins in AD and MCS samples exhibited a two-fold deviation from 1g samples. There was an increase of ArfGAP with SH3 domain and ankyrin repeat and PH domain 1 (ASAP1), while breast cancer anti-oestrogen resistance protein 1 (BCAR1) and mitogen-activated protein kinase 8 (MAPK8) proteins were reduced in MCS cells. In earlier studies, there were similar alterations in FTC-133 thyroid cancer cells after 72-h culture in an RPM (111). To confirm these findings, I performed Western blot and qPCR. The protein and gene expression changes of *ASAP1*, *BCAR1* and *JNK/MAPK8* were consistent with the LFQ data. Therefore, I suggested that ASAP1 is involved in MCS formation in breast and thyroid cancer cells, while BCAR1 and MAPK8 are induced in adherent cells in both cell types when they remain in a monolayer on an RPM.

Moreover, the proteome analysis revealed an increase in the interferon simulated gene 15 (*ISG15*) (LFQ = 126.1×10^8) in MCS cells compared to AD (LFQ = 19.7×10^8) and 1g cells (LFQ = 62.4×10^8). Similar findings have been reported in FTC-133 follicular thyroid cancer cells when they were sent to space for more than 10 days (46). Most of the poorly differentiated follicular thyroid cancer cells transformed into MCS after 10 days in space. *ISG15* is reportedly the most upregulated of all genes investigated by microarray analysis (46, 112). ISG15 protein is induced by interferon and targets proteins associated with cell structure and motility according to a recent proteome study (113). The role of the ISG15 in spheroid formation is yet unknown. Nevertheless, the data suggested that ISG15 has an impact on stabilisation rather than on the formation of spheroids due to its time course of accumulation.

E-cadherin is another membrane protein that was affected by s- μ g. E-cadherin has an extracellular domain that is connected to another E-cadherin molecule of another cell. It also has an intracellular domain that is connected to the cytoskeleton. E-cadherin was diminished in the MCS samples in comparison to 1g and AD cells. E-cadherin of the MCS group had a LFQ score less than half of the score measured in 1g control samples. I verified this result by Western blot and qPCR analyses. The methods showed a significant reduction in the protein and mRNA levels, respectively.

Due to the reduction in E-cadherin in MCS cells, I concluded that proteins which downregulate E-cadherin are dominant. I investigated the (R-HAS-174084) pathway, which is known as 'Autodegradation of Cdh1 by Cdh1: APC/C', to gain insight on how proteins of this pathway could diminish E-cadherin (114). I used the Pathway Studio analysis program to investigate the interaction of the junction-related proteins detected with the E-cadherin-regulated proteins and with the R-HAS-174084 pathway proteins (Fig. 7).

blocker of E-cadherin regulator SRC on spheroid formation. I found that anti-E-cadherin promoted MCS formation (Fig. 8N), while PP2 prevented MCS formation (Fig.8J).

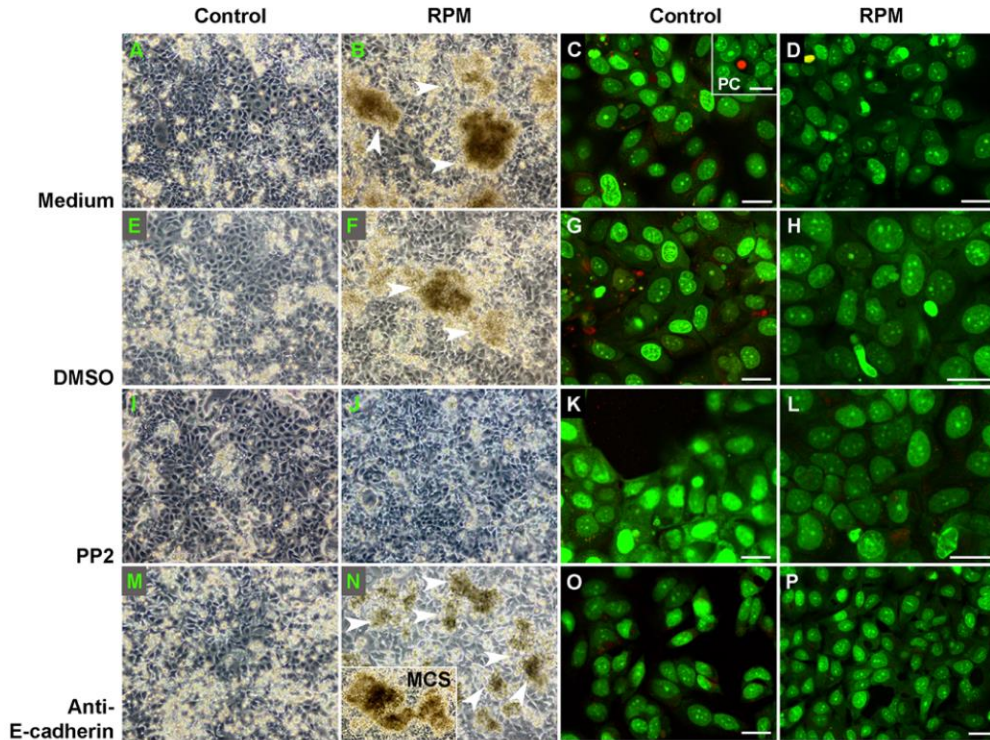


Fig. 8: Morphology and viability of MCF7 cells incubated at 1g (control) or on an RPM. Left side of the figure: phase contrast microscopy of MCF7 cells incubated at 1g (A, E, I, M) or on an RPM (B, F, J, N) for 14 days. Representative examples of spheroids formed on the RPM are marked by white arrowheads (B, F, N). J) Notably, no spheroids were formed on the RPM in the presence of the Src inhibitor PP2, N), whereas anti-E-cadherin (DECMA-1) stimulated the formation of spheroids. The inset in (N) shows an example of a large spheroid observed in the presence of anti-E-cadherin. Right side of figure: acridine orange/ethidium bromide staining revealed a green fluorescence in all cells of all groups (C, D, G, H, K, L, O, P), which indicates viability of MCF7 cells incubated on the RPM or at static 1g conditions. The inset in (C) represents positive control (PC) of the acridine orange/ethidium bromide assay after approximately 5 min incubation. The scale bars are 20 μ m.

In summary, E-cadherin plays an important role in spheroid formation, as shown by the proteome analysis and the blocking of spheroids formation by anti-E-cadherin antibodies. It is essential to investigate E-cadherin regulation in more detail in an animal xenograft model because a strong correlation between E-cadherin and the metastatic activity of cancer cells has been shown by several authors (119–121).

5.2. Real Microgravity Influences the Cytoskeleton and Focal Adhesions in Human Breast Cancer Cells

In this paper, I evaluated the effect of r- μ g on the cytoskeleton on human breast cancer cells during the TX54 sounding rocket mission. Initially, I transfected the MCF-7 cells with a LifeAct-eGFP-IRES-mCherry-Tubulin (LAGICT) expression cassette for the simultaneous visualisation of F-actin and α -tubulin through co-expression of Lifeact GFP and mCherry-tubulin fusion proteins, respectively.

I used the spinning-disc fluorescence microscopy analysis system (FLUMIAS) to perform live cell imaging of transfected MCF-7 cells in real time while they were cultured in microgravity. In May 2018, the TX54 sounding rocket was launched from the Esrange space station in Kiruna, Sweden (Fig. 9C). Shortly after the entry of the rocket into the microgravity phase, the first images were taken with the FLUMIAS microscope using the 488 nm and 568 nm diode lasers for visualisation of F-actin and α -tubulin. I compared all the images taken on board of the rocket to control images taken prior to launch. I examined the microscopic images to determine the effect of microgravity on the cytoskeleton. I observed disarrangement of F-actin bundles and the appearance of filopodia- and lamellipodia-like structures. Moreover, there were accumulations in the tubulin network and rearrangement in the F-actin and tubulin with holes (Fig. 10).

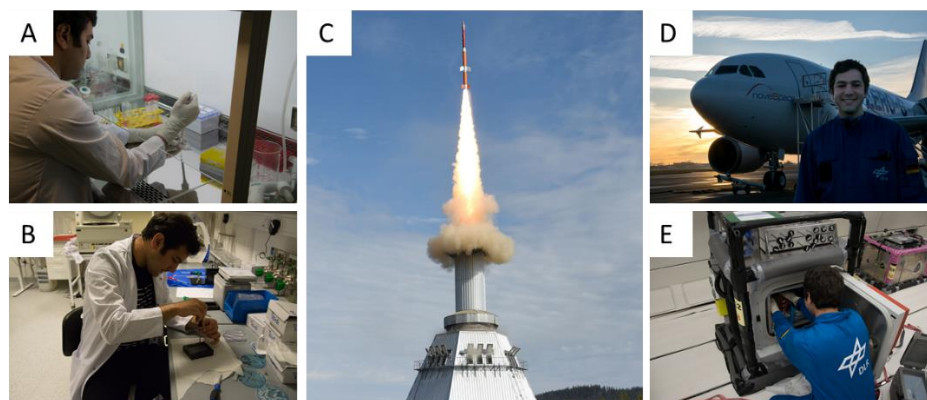


Fig. 9: (A) Cell culture and slide preparation for live microscopy. (B) Hardware preparation prior to the launch of the rocket. (C) Launch of the TX54 rocket (courtesy of Airbus Defence and Space). (D) Airbus 310 aircraft used for the parabolic flight. (E) Placing the cell culture flasks inside the incubator in the aircraft prior to take off.

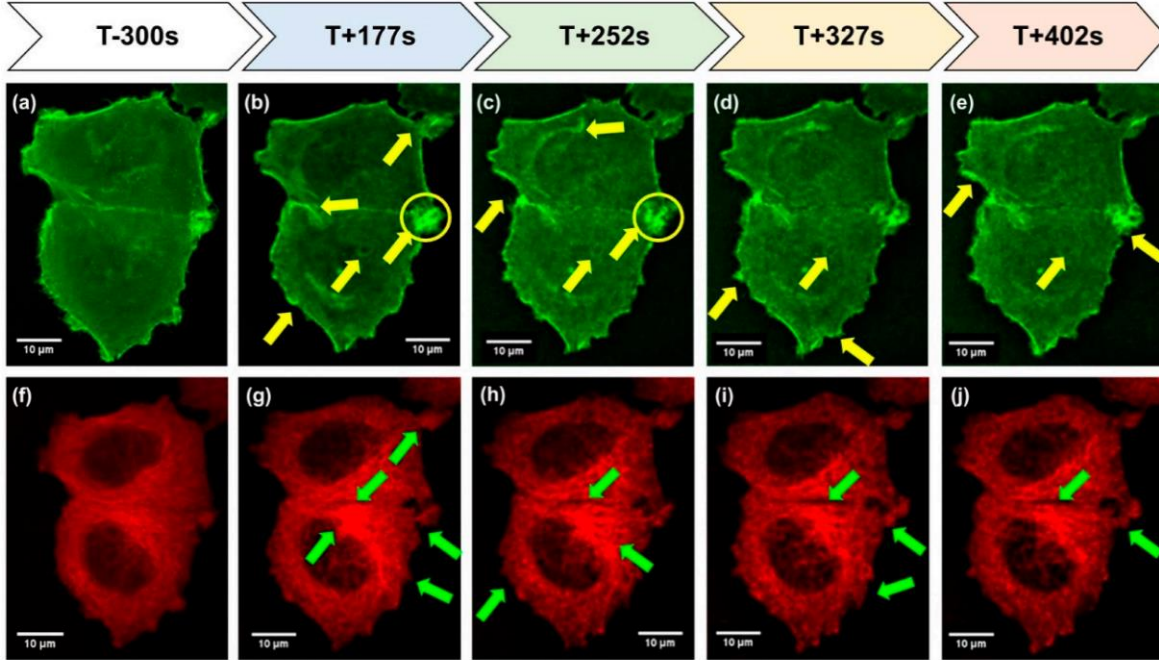


Fig. 10: Time course and images of FLUMIAS on TEXUS 54 (40×/1.2). The MCF-7 breast cancer cells 5 min before launch (T -300 s) of the rocket and during the r- μ g phase (T +177 s to T +402 s). The yellow arrows show the changes in F-actin (a–e; green fluorescence). The yellow circles include an area with F-actin accumulations. Filopodia and lamellipodia are found after 150 s and are more pronounced with time. The green arrows indicate changes in α -tubulin (f–j; red fluorescence). The tubulin network revealed holes after 150 s and a looser structure.

In addition to the live cell microscopy studies, I seeded regular MCF-7 cells into 18-well Ibidi slides. I fixed these slides with 4% paraformaldehyde (PFA) either at the end of the hyper-g phase or at the end of the microgravity phase and then compared them to 1g ground control slides fixed with 4% PFA. Later, I immunostained for matrix metalloproteinase (MMP)-9, vascular endothelial growth factor A (VEGFA), F-actin, interleukin 6 (IL-6) and interleukin 8 (CXCL8-8) proteins (Fig. 10a-l). Only F-actin and VEGFA exhibited a visible increase at the end of the microgravity phase in comparison to the control (Fig. 11d, e, n, o). However, F-actin was also upregulated after the end of the hyper-g phase (Fig. 11o). After the rocket launch, there is an initial phase of hyper-g that precedes the microgravity. Thus, the increase of F-actin protein in both hyper-g and microgravity phases indicates that the hyper-g phase is the main cause of upregulation because there was not enough time for F-actin to normalise at the end of the hyper-g phase. On the other hand, VEGFA exhibited a clear upregulation in the microgravity phase compared to the control (Fig. 11n). Similar findings of an upregulated *VEGFA* after parabola (P)1 and P31 in a parabolic flight (PF) mission have been reported earlier with follicular thyroid cancer cells (46).

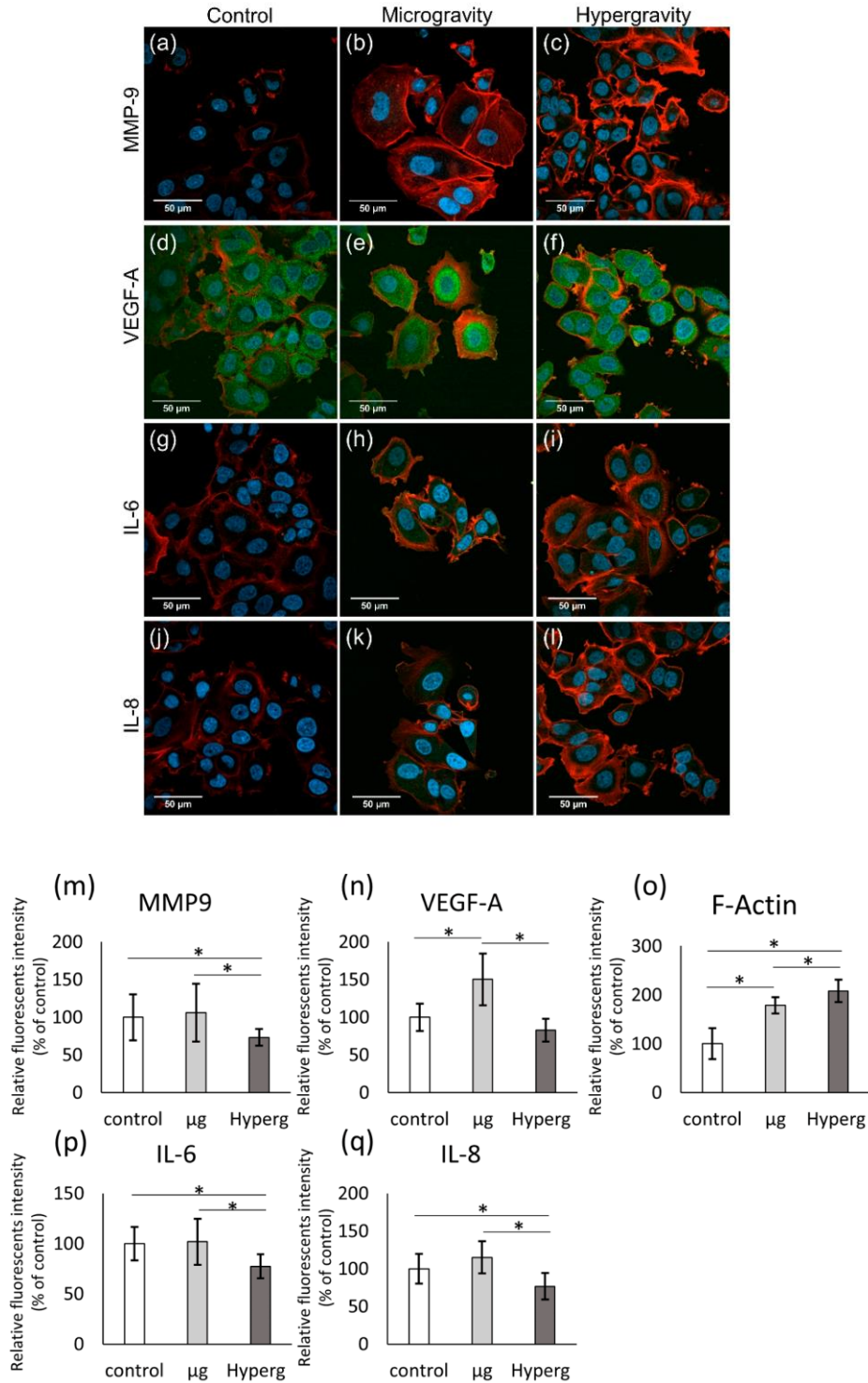


Fig. 11: Indirect immunofluorescence staining of PFA-fixed cells from the TEXUS 54 sounding rocket mission. I seeded 2500 MCF-7 cells into each well of the 18-well Ibidi slides. I fixed the cells either at the end of the hyper-g period or at the end of the microgravity period. I compared the two conditions to 1g ground control samples. The confocal laser scanning microscopy images (a-l) show either MMP9, VEGF-A, IL-6 or IL-8 in green, DAPI (in blue) and F-actin (in red). Scale bar is equal to 50 μm. I quantified the intensity of the staining by ImageJ (m-q). All data are shown as mean ± standard deviation; n = 10–14; * p < 0.05.

Moreover, I investigated the effect of r- μ g on breast cancer cells during the 31st DLR PFC (Fig. 9D). In this mission, I cultured MCF-7 cells in an incubator onboard of the PF (Fig. 9E). I fixed the cells with RNAlater either after the end of P1 or P31. I compared the PF samples to 1g control samples fixed with RNAlater on the ground in parallel to the flight. Subsequently, the samples were transported to the home laboratory for mRNA expression and protein content analysis. I investigated the effect of microgravity on early changes in the gene expression of cytoskeletal, FA, ECM and inflammatory cytokine genes.

To investigate alterations in the cytoskeleton, I evaluated the mRNA and protein expression of actin beta (*ACTB*), tubulin beta (*TUBB*), keratin 8 (*KRT8*), ezrin (*EZR*), radixin (*RDX*) and moesin (*MSN*) (Fig. 12a-f). Most of the cytoskeletal genes were not significantly altered. However, *KRT8* mRNA exhibited a significant upregulation after P1 and P31 (Fig. 12c). This finding fits with earlier results with thyroid cancer cells (122). In order to study adhesion molecules, I inspected the expression of several FA genes, such as *CDH1*, integrin subunit beta 1 (*ITGB1*) and vinculin (*VCL*; Fig. 13a-c). There was a significant downregulation of E-cadherin, β 1-integrin and vinculin protein expression (Fig. 13a-c). These findings are consistent with a recent publication where alterations in FA complexes were also found in melanoma cells in s- and r- μ g (123).

To study alterations of the ECM, I examined genes such as laminin subunit alpha 1 (*LAMA1*), laminin subunit alpha 3 (*LAMA3*), collagen type I alpha 1 chain (*COL1A1*), fibronectin 1 (*FNI*), TIMP metalloproteinase inhibitor 1 (*TIMP1*) and PAII/serpin family E member 1 (*SERPINE1*) (Fig. 14a-g). Most of the ECM genes exhibited no significant alterations during the PF. However, *TIMP1* showed a significant upregulation after P31 (Fig. 14e), while *SERPINE1* exhibited significant downregulation after P31 (Fig. 14g). Finally, I evaluated the expression of inflammatory cytokines *IL-6*, C-X-C motif chemokine ligand 8 (*CXCL8*) and growth factor *VEGFA* to investigate their involvement in the molecular process of microgravity sensation. *CXCL8* and *VEGFA* mRNA showed significant upregulation after P1 (Fig. 14i-j). Moreover, IL-8 protein showed significant upregulation after P1 and P31 (Fig. 15).

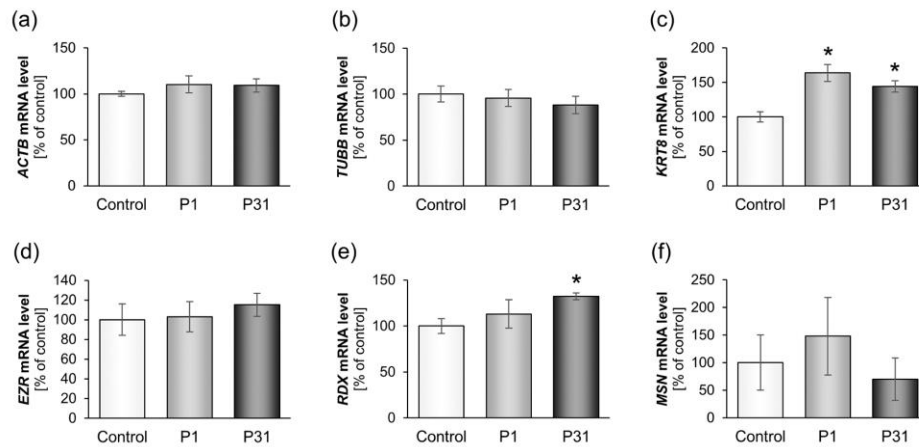


Fig. 12: Influence of short-term microgravity on the gene expression (mRNA) of cytoskeletal factors. The data are shown as mean \pm standard deviation; $n = 4$; * $p < 0.05$ vs. Control.

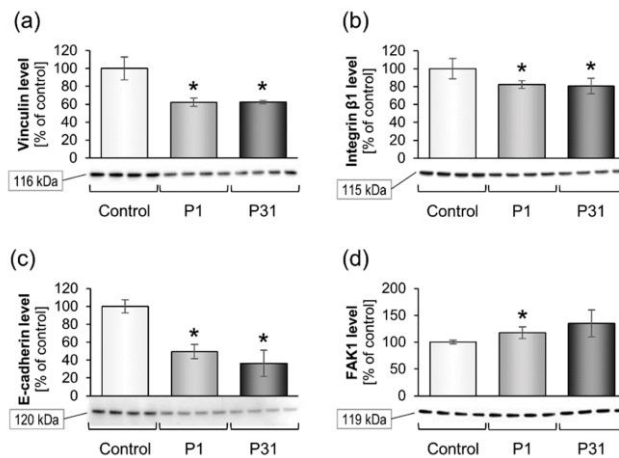


Fig. 13: Influence of short-term microgravity on the protein accumulation of focal adhesion complex components. The data is shown as mean \pm standard deviation; $n = 4$; * $p < 0.05$ vs. Control.

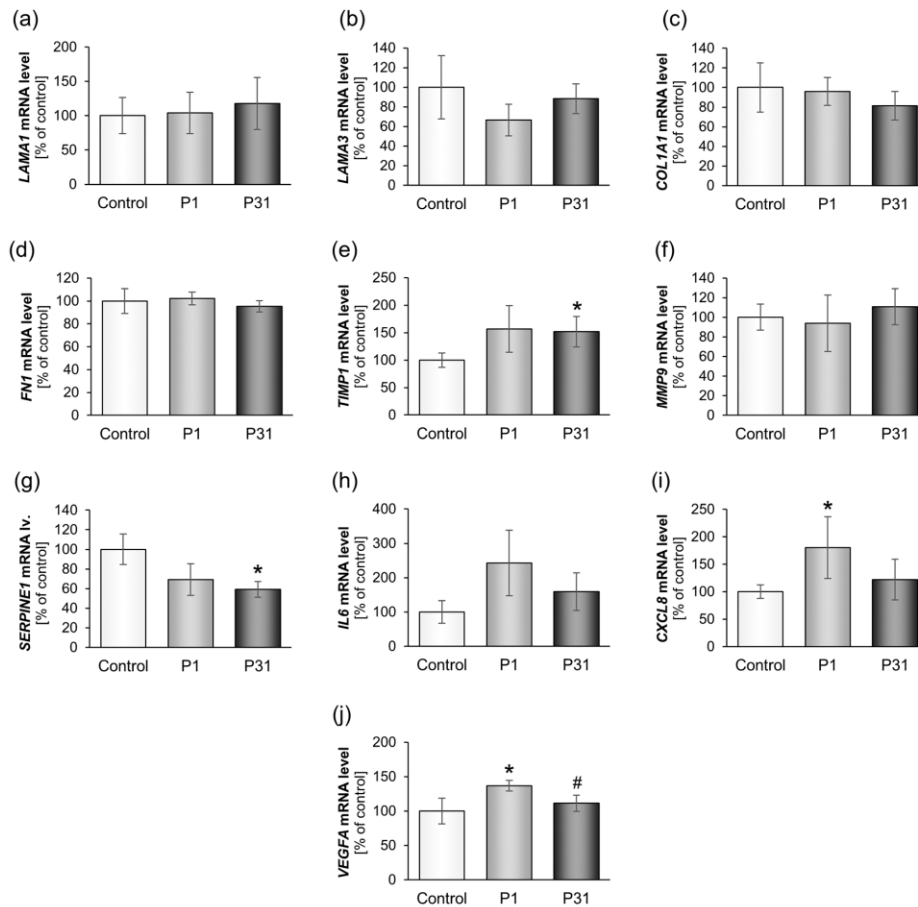


Fig. 14: Influence of short-term microgravity on expression of different ECM and cytokine genes. The data are shown as mean \pm standard deviation; n = 4; * p < 0.05 vs. Control; # p < 0.05 vs. P1.

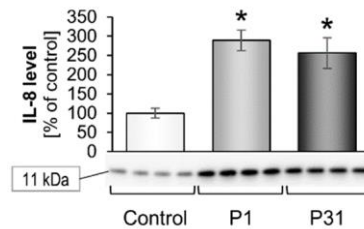


Fig. 15: Influence of short-term microgravity on the protein accumulation of IL-8. The data are shown as mean \pm standard deviation; n = 4; * p < 0.05 vs. Control.

To gain insight into the relationship between the genes investigated in this study, I performed a pathway analysis of all the investigated genes and proteins. *CDH1* and *VEGFA* play an important role in the network (Fig. 16). IL-6 and IL-8 control both genes by exerting an inhibitory effect on *CDH1* and a promoting effect on *VEGFA*. Exogenous IL-8 decreases the expression of E-cadherin mRNA in human gastric carcinoma cells (124). Furthermore, IL-6 downregulates E-cadherin in a dose-dependent manner (125). In contrast, IL-6 and IL-8 induce the expression of *VEGF* (126, 127).

The pathway analysis revealed many factors, other than IL-6 and IL-8, that are involved in regulating E-cadherin, including EZR, talin 1 (TLN1), protein tyrosine kinase 2 (PTK2), ITGB1 and MMP9 (Fig. 16). All of these proteins had an inhibitory effect on E-cadherin. Only vinculin exhibited a positive modulatory effect on E-cadherin. As it was demonstrated earlier, the E-cadherin downregulation promotes spheroid formation and metastasis. Furthermore, E-cadherin plays a central role in spheroids formation and it is strongly controlled by several proteins (as presented in Fig. 16).

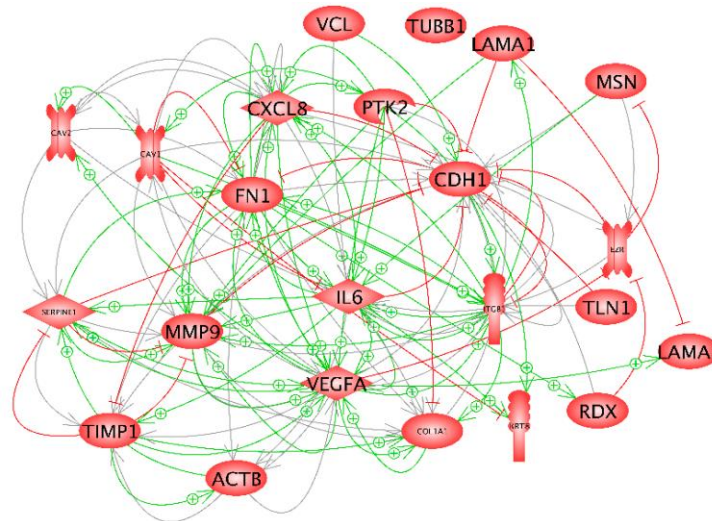


Fig. 16: Mutual interactions of the expression of the genes examined with qPCR. + Signs indicate an activity-enhancing effect and red lines indicate inhibition. The interaction networks were created using Elsevier Pathway Studio v11.

5.3. Short-term Microgravity Influences Cell Adhesion in Human Breast Cancer Cells

In this study, I investigated the effect of r- μ g on the TNBC MDA-MB-231 cell line. During PFC 29, I fixed the breast cancer cells with RNA*later* after P1 and P31. I focused on investigating cell adhesion, apoptosis, NF- κ B and MAPK signalling. Moreover, I evaluated the impact of vibration, RPM and hyper- g on these TNBC cells.

First, I investigated the rate of apoptosis of cells subjected to hyper- g , vibration and RPM by using the terminal deoxynucleotidyl transferase dUTP nick end labeling (TUNEL) assay. A previous study had revealed that some cancer cells become apoptotic after being subjected to microgravity and that apoptosis is involved in spheroids formation (105). However, our TUNEL assays revealed no apoptosis in breast cancer cells as a consequence of a 2-h exposure to vibration, hyper- g and RPM s- μ g experiments. To test the molecular effect of short-term microgravity on apoptosis in breast cancer cells, I assessed caspase-3

(*CASP3*), annexin A1 (*ANXA1*), annexin A2 (*ANXA2*), BCL2 associated X (*BAX*) and B cell lymphoma 2 (*BCL2*) mRNA expression (Fig. 17A, C, D, F, G). *Casp3* was upregulated after P1 and P31 (Fig. 17A); however, uncleaved caspase-3 was not detectable (Fig. 17B). Moreover, there were no changes in *CASP3* expression after the exposure of breast cancer cells to hyper-g, vibration and s- μ g (Fig. 18A, B). *ANXA1* and *ANXA2* were not regulated during parabolic flight (Fig. 17C, D), hyper-g or vibration (Fig. 18C, E). However, s- μ g resulted in significant downregulation of *ANXA2* (Fig. 18F). Additionally, *BCL2* mRNA was downregulated as a consequence of r- μ g after P1 and P31 (Fig. 17G), while vibration, s- μ g and hyper-g had no effect on *BCL2* mRNA (Fig. 18I, J). In contrast, *BAX* mRNA was not regulated by r- μ g (Fig. 17F), but it was downregulated by s- μ g (Fig. 18F). These findings show possible variation between the effect of r- and s- μ g on MDA-MB-231 cells.

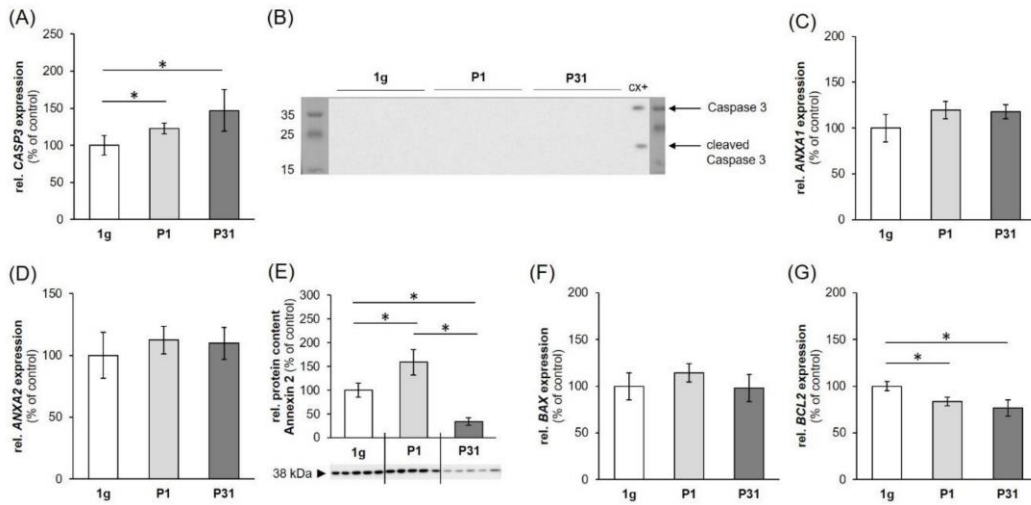


Fig. 17: The influence of short-term microgravity on the gene expression of (A) *CASP3*, (C) *ANXA1*, (D) *ANXA2*, (F) *BAX* and (G) *BCL2* and protein content of (B) caspase-3 and (E) annexin 2, all of which are regulators of apoptosis. The data are shown as mean \pm standard deviation; * $p < 0.05$ vs. 1g control. CX+ colon cancer cells served as the positive control for programmed cell death.

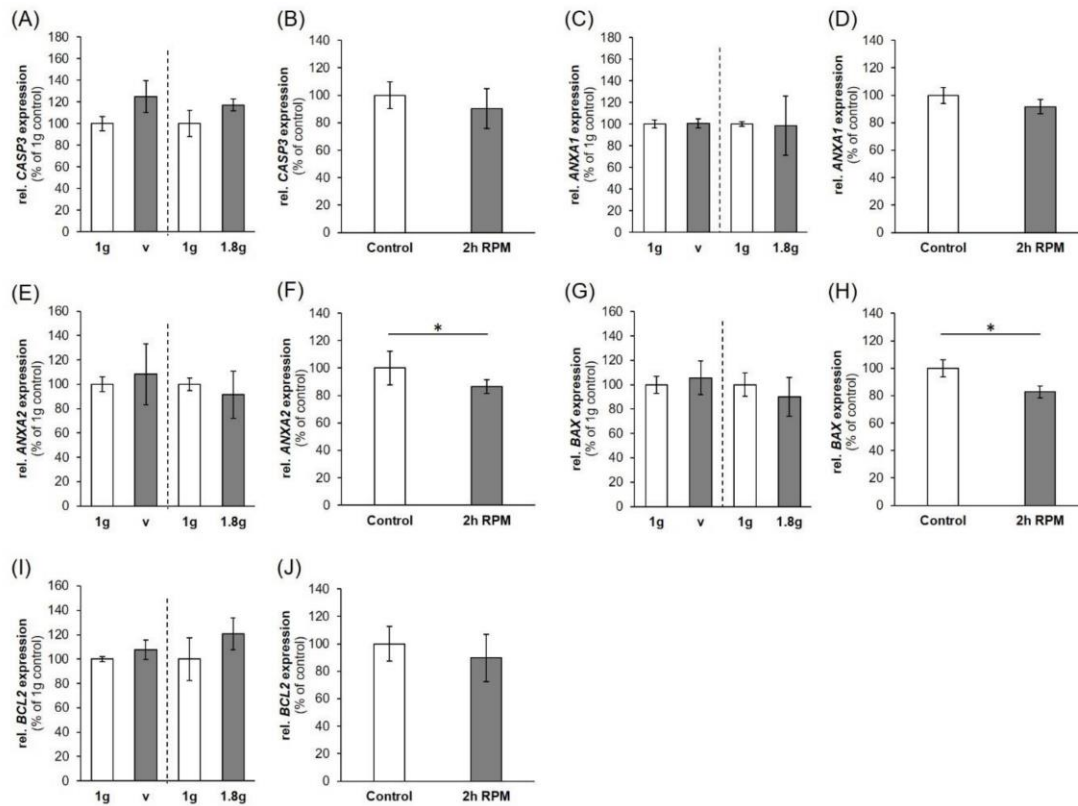


Fig. 18: The influence of a VIB (V), hyper-g and RPM-exposure on the gene expression of apoptosis signalling factors: (A,B) *CASP3*, (C,D) *ANXA1*, (E,F) *ANXA2*, (G,H) *BAX* and (I,J) *BCL2*. The data are shown as mean \pm standard deviation; n = 5; * p < 0.05 vs. 1g control. The dashed vertical line separates two independent experiments.

The NF- κ B pathway seems to be associated with spaceflight health problems (128). Moreover, the nuclear factor kappa-B P65 subunit (NF- κ B-P65) upregulation points to an increased aggressiveness of breast cancer cells and a poor prognosis (129). NF- κ B is generally associated with tumour promotion and negatively regulates apoptosis in tumour cells through several other genes. NF- κ B is also associated with endocrine therapy resistance (130). NF- κ B has three variant proteins: nuclear factor kappa-B P50 subunit (NF- κ B-P50), nuclear factor kappa-B P52 subunit (NF- κ B-p52) and NF- κ B-P65. These proteins are encoded by nuclear factor kappa B subunit 1 (*NFKB1*), nuclear factor kappa B subunit 2 (*NFKB2*) and nuclear factor kappa B subunit 3/RELA proto-oncogene (*NFKB3/RELA*) genes. Furthermore, the NF- κ B proteins are inhibited by inhibitor of κ B (*I κ B*) proteins (130). The NF- κ B P65 protein is upregulated with s- μ g on an RPM in FTC-133 follicular thyroid cancer cells and endothelial cells (105, 131).

Due to the importance of the NF- κ B pathway in microgravity and cancer cells, I evaluated the expression of *NFKB1*, *NFKB2* and *NFKB3*. *NFKB1* mRNA was upregulated after P31 (Fig. 19A), while *NFKB2*

showed no regulation (Fig. 19B). *NFKB3* revealed contradictory mRNA and protein data: the mRNA was upregulated after P1 (Fig.19C) and the protein content was downregulated after P1 and P31 (Fig. 19D). Downregulation of NF- κ B P65 protein after short-term microgravity is in concert with earlier microarray data from activated T cells cultured in space, where NF- κ B gene targets are suppressed after 1.5 h (132). Moreover, culturing T cells for 4 h on the RPM led to a similar result (133).

The I κ B proteins are the main regulators of NF- κ B through the canonical and non-canonical NF- κ B pathways (134). Therefore, I evaluated the expression of NF- κ B inhibitor alpha (*NFKBIA*), NF- κ B inhibitor beta (*NFKBIB*), NF- κ B inhibitor epsilon (*NFKBIE*) and inhibitor of NF- κ B kinase subunit gamma (*IKBKG*, *NEMO*) genes (Fig.19 E, G, H, I). *NFKBIA* and *NFKBIB* mRNA were elevated after the P31 (Fig. 19E, G), while *NFKBIE* and *IKBKG* mRNA expression and NEMO protein content were not regulated during the PF (Fig. 19H, I, J).

Vibration did not alter regulation of any of the inhibitory genes (Fig. 20), while hyper-g resulted in *NFKBIA* upregulation (Fig.20G). These data might indicate that hyper-g was the main cause of *NFKBIA* elevation especially given that RPM did not alter the mRNA expression of the gene.

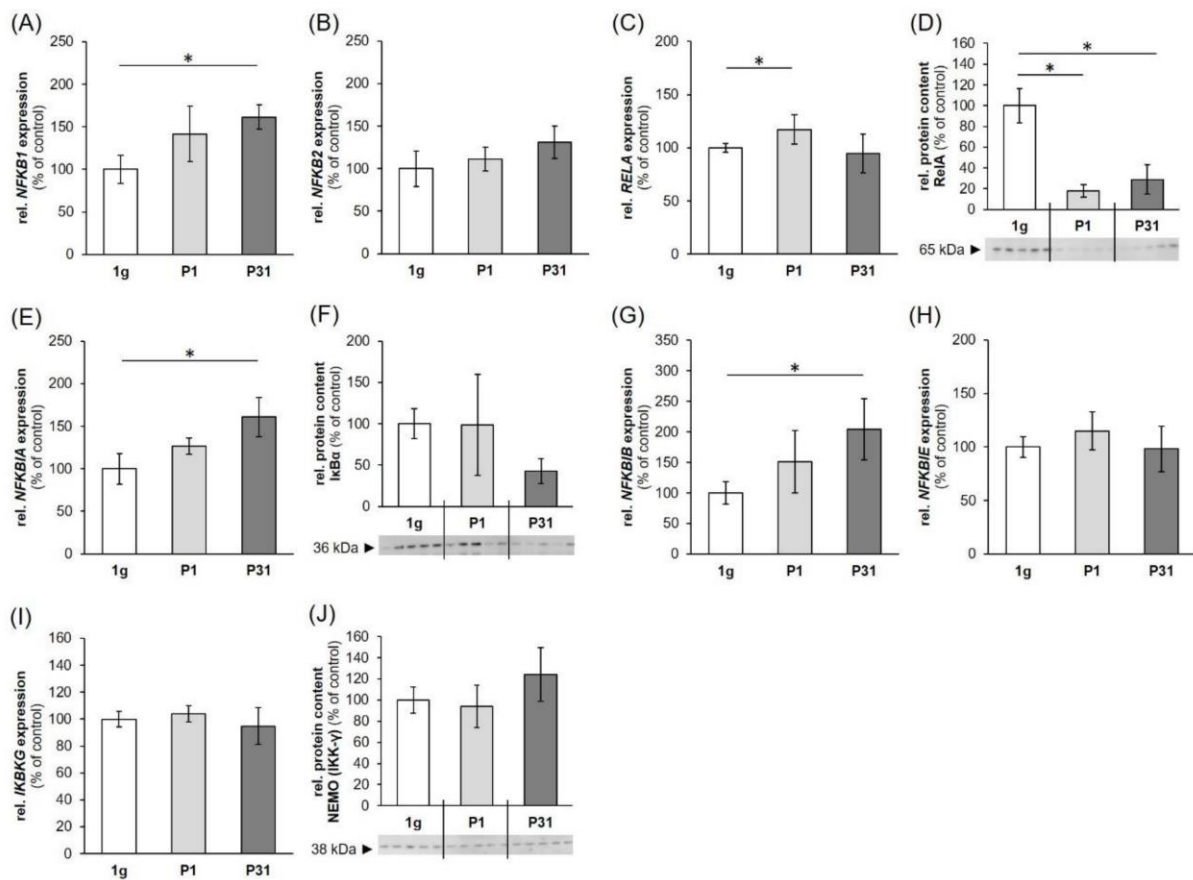


Fig. 19: The influence of short-term microgravity on the gene expression of (A) *NFKB1*, (B) *NFKB2*, (C) *RELA*, (E) *NFKBIA*, (G) *NFKBIB*, (H) *NFKBIE* and (I) *IKBKG* and the protein content of (D) RelA, (F) IκBα and (J) NEMO, all of which are NF-κB signalling factors. The data are shown as mean ± standard deviation; n = 5; * p < 0.05 vs.1g control.

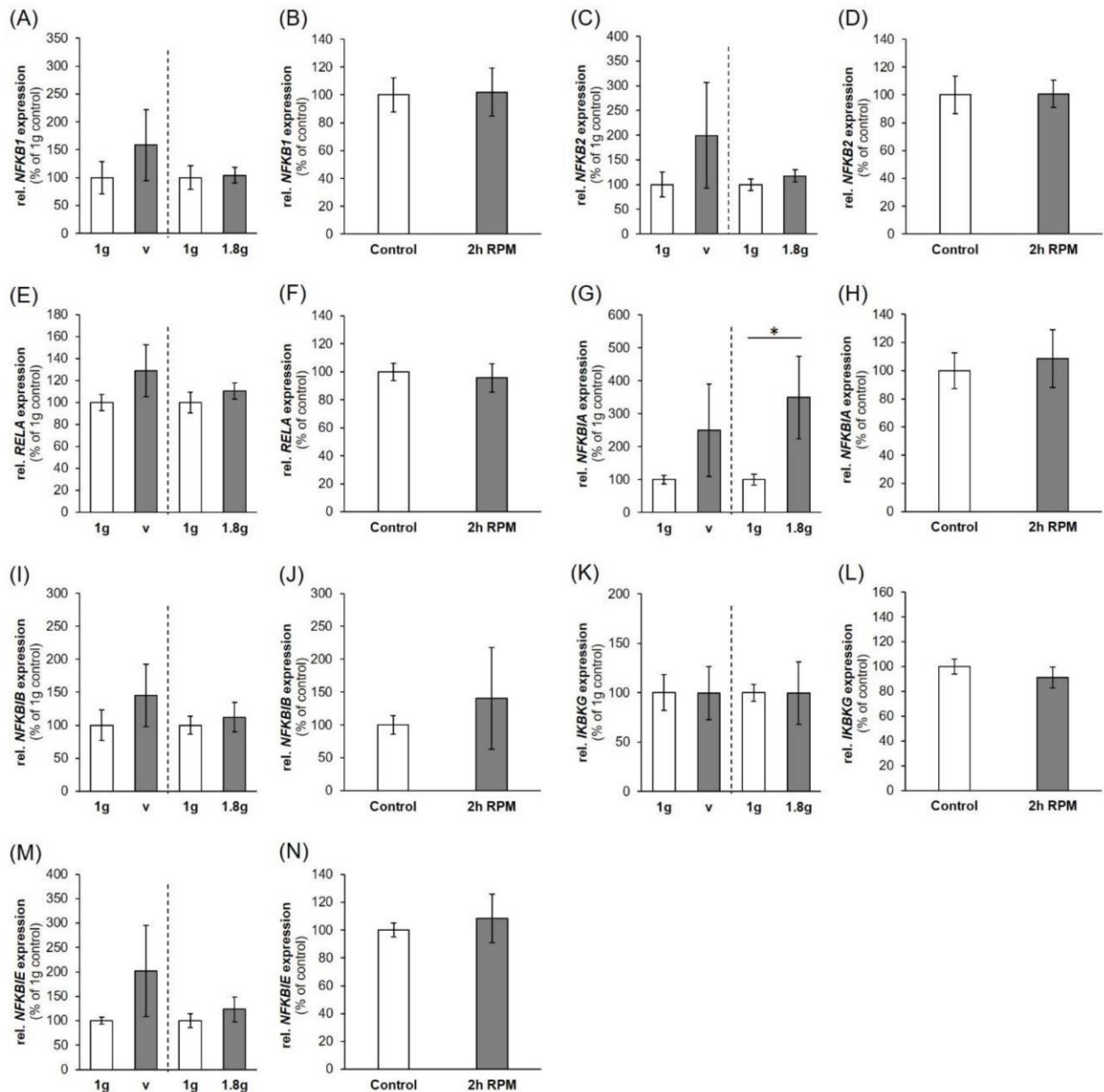


Fig. 20: The influence of VIB (V), hyper-g and iRPM-exposure on the gene expression of NF-κB signalling factors: (A,B) *NFKB1*, (C,D) *NFKB2*, (E,F) *RELA*, (G,H) *NFKBIA*, (I,J) *NFKBIB*, (K,L) *IKBKG* and (M,N) *NFKBIE*. The data are shown as mean ± standard deviation; n = 5; * p < 0.05 vs. corresponding 1g controls. The dashed vertical line separates two independent experiments.

FA molecules are influenced by microgravity and involved in the molecular transition from adherent cells to spheroids (77). Thus, I investigated the expression of *ICAM1*, *VCAM1*, cell surface glycoprotein CD44 (*CD44*) and secreted phosphoprotein 1 (*SPP1*) genes (Fig. 21A-H). *ICAM1* and *VCAM1* proteins were elevated after P31 (Fig. 21B, D), while hyper-g and vibration had no effect on the respective gene regulation (Fig. 22A, C). *ICAM1* and *VCAM1* are mediators of cell adhesion in cancer cells and lymphocytes to the

endothelium (135). ICAM1 was elevated in macrophage-like differentiated human U937 cells during the microgravity phase of PFs. Furthermore, CD44 mRNA and protein was elevated (Fig. 21G, H); however, hyper-g also elevated *CD44* mRNA (Fig. 22G). Therefore, I concluded that hyper-g might be the main reason for the elevated *CD44* mRNA expression and protein content. Additionally, *SPP1* mRNA was upregulated after P31 (Fig. 21E), whereas osteopontin protein exhibited a significant decrease after P1 and P31 (Fig. 21F). Hyper-g and vibration had no effect on *SPP1* (Fig. 22E). There is a reduction in osteopontin protein in FTC-133 thyroid cancer cells in adherent cells and MCS after a 24-hour RPM-exposure (105).

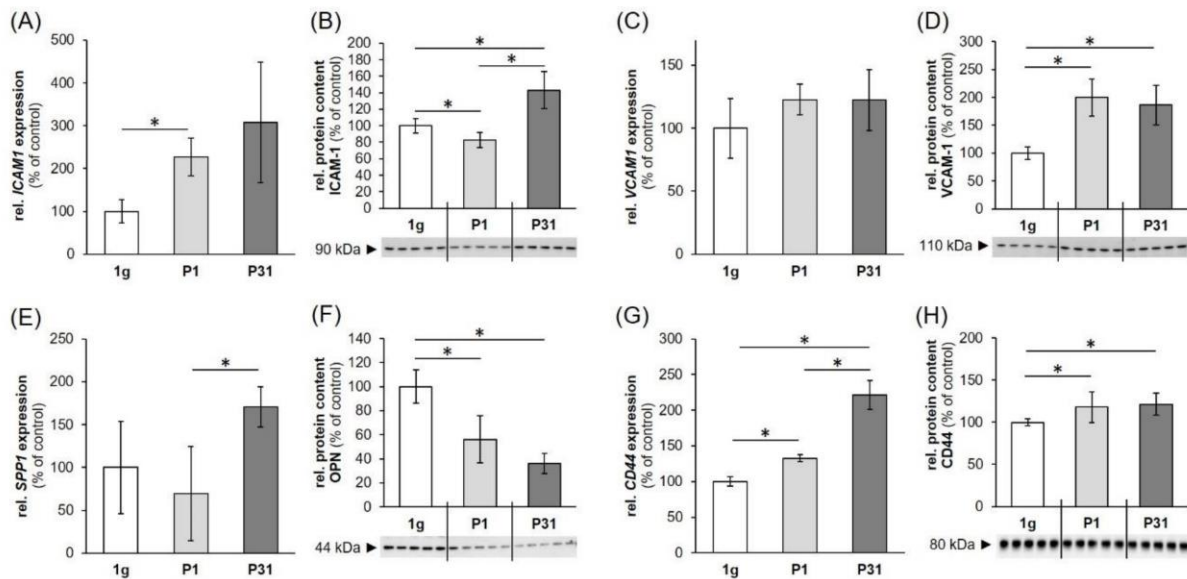


Fig. 21: Expression of the genes (A) *ICAM1*, (C) *VCAM1*, (E) *SPP1* and (G) *CD44* and proteins (B) ICAM-1, (D) VCAM-1, (F) OPN and (H) CD44, all of which are involved in cell adhesion. 1g: ground control; P1: parabola 1; P31: parabola 31. The data are shown as mean \pm standard deviation; * p < 0.05 vs. 1g control; ** p < 0.01 vs. 1g control.

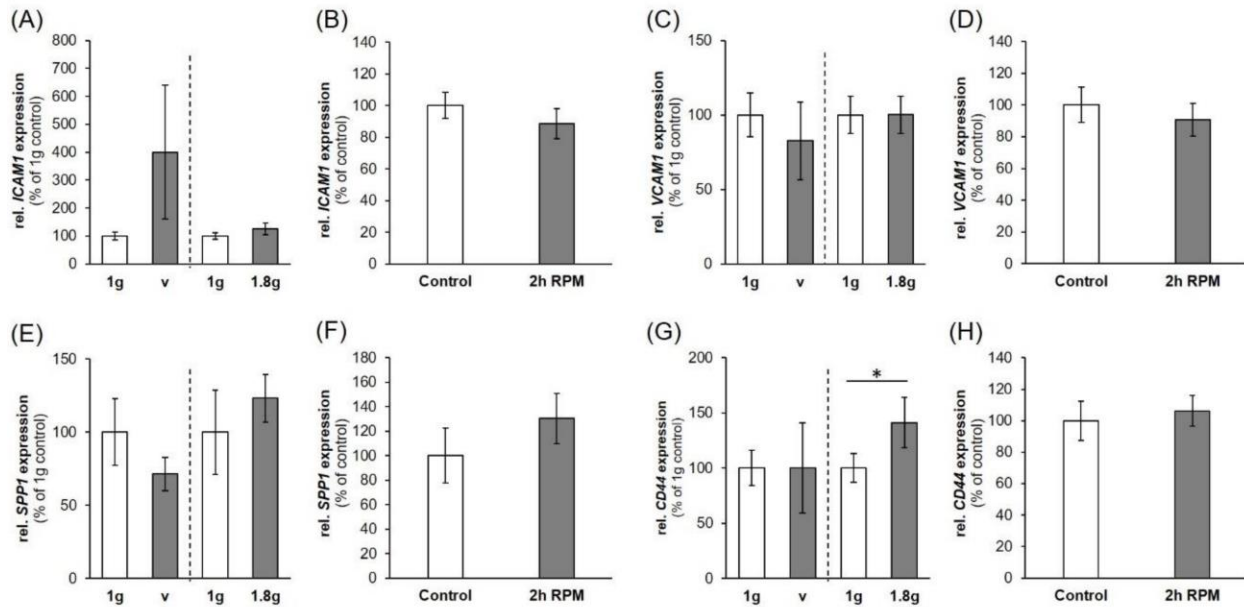


Fig. 22: The influence of VIB (V), hyper-g and iRPM-exposure on the gene expression of cell adhesion signalling factors: (A,B) *ICAM1*, (C,D) *VCAM1*, (E,F) *SPP1* and (G,H) *CD44*. 1g: ground control; V: 2 h of vibration; 1.8g: 2 h of hyper-g. The data are shown as mean \pm standard deviation. * $p < 0.05$ vs. 1g control. The dashed vertical line separates two independent experiments.

To investigate factors involved in enhancing cancer growth and spreading, I evaluated MAPK signalling factors, specifically protein kinase C alpha (*PRKCA*), Raf-1 proto-oncogene, serine/threonine kinase (*Raf1*), extracellular signal-regulated kinase 1 (*ERK1*), extracellular signal regulated kinase 2 (*ERK2*), focal adhesion kinase 1 (*FAK1*) and mitogen-activated protein kinase 8 isoform JNK1 alpha1 (*JNK1*) transcript levels. *PRKCA* and *Raf1* exhibited no significant alterations, while *ERK1* was elevated after P1. In addition, *ERK2* was only elevated after P31 in comparison to P1. The ERK subfamily is composed of atypical (ERK3/4/7/8) and typical (ERK1/2/5) members (136). The ERKs are known to be involved in regulating the epithelial-mesenchymal transition (EMT), which increases cancer migration and spread (136–138). *ERK1* upregulation after P1 might be the initial signal to start 3D aggregation in microgravity.

Additionally, *FAK1* mRNA was upregulated after P31 in comparison to the control. *FAK1* is translated into the PTK2 protein, which enhances cancer cell migration and metastatic dissemination to distant sites (139). Moreover, FAK depletion induces the formation of active invadopodia and impairs invasive cell migration (140). In contrast, *JNK1* mRNA was downregulated after P1 and readapted after P31. The JNK family of kinases is involved in the prevention of malignant transformation via the induction of apoptosis and in promoting cell survival in established tumours (141). Thus, a reduction in JNK might promote 3D formation of the TNBC cells in r- μ g conditions.

To gain insight into the relationship between the investigated genes and proteins, I performed an interaction analysis using the search tool for the retrieval of interacting genes/proteins (STRING) in the molecular action mode. The analysis revealed a strong regulation between the nuclear factors whose expression I analysed. In contrast, the remaining items formed a loose network. Moreover, NFKB1, NFKB2 and NFKB3 are strictly controlled at various levels (142). They are regulated by each other, with inhibitors such as NFKBIA, NFKBIB, NFKBIE and with kinases such as IKBKB.

This publication demonstrated alterations in cell adhesion in MDA-MB-231 breast cancer cells as a result of microgravity exposure. This finding further proves the importance of FA molecules in mechanotransduction. In addition, the early changes in ICAM-1 and VCAM-1, as well as the quick reduction of the NF- κ B subunit p-65, are involved in fast-reacting, gravity-regulated and cell-protective mechanisms of TNBC cells exposed to microgravity.

5.4. Beneficial Effects of Low Frequency Vibration on Human Chondrocytes *in vitro*

Humans experience vibration during space travel. Furthermore, vibration occurs during parabolic flights and normal passenger flights. In order to evaluate the effect of vibration on human chondrocytes, I subjected these cells to a 24-h low-frequency vibration experiment. I used chondrocytes from six different human donors for this study. I performed the vibration experiment *in vitro* using a Vibraplex device (Fig. 3C). There were no morphological alterations or cell death at the end of the 24-hour vibration experiment. This finding is consistent with previous data (40). Moreover, I investigated selected ECM, FA marker and intrinsic and extrinsic apoptosis factor genes. I tested the hypothesis that vibration has beneficial effects on human chondrocytes and eventually on cartilage.

To investigate ECM changes, I evaluated the gene expression pattern of *FNI*, aggrecan (*ACAN*), *COL1A1* and collagen type II alpha 1 chain (*COL2A1*). There were no significant mRNA changes after subjecting the cells to a 24-h vibration experiment.

This study also focused on the expression of *VCL*, *TLN1* and paxillin (*PXN*) to determine the effect of vibration on focal FA factors. *VCL* and *PXN* mRNA were upregulated at the end of the 24-h vibration experiment. Vinculin reportedly promotes the survival of mouse embryonal cancer cells through regulating paxillin-FAK (paxillin-focal adhesion kinase) interactions to alter extracellular signal-regulated kinase 1/2

(ERK1/2) activation (143). Moreover, paxillin induces anti-apoptotic and survival effects on mouse cells (144).

I examined the gene expression of *ANXA1*, *ANXA2*, *NFκB1*, *NFκB3/RELA*, baculoviral IAP repeat containing 2 (*BIRC2*), baculoviral IAP repeat containing 3 (*BIRC3*), baculoviral IAP repeat containing 5 (*BIRC5*), Fas associated via death domain (*FADD*), Fas cell surface death receptor (*FAS*), cytochrome C (*CYC*), *BAX* and *BCL2* to further investigate the biological process of apoptosis. *ANXA1*, *BAX* and *BCL2* were upregulated after 24-h vibration, while *ANXA2* was downregulated. The other genes did not exhibit any significant alterations. Additionally, RelA/NF-κB-P65 protein was downregulated as a consequence of vibration. *ANXA1* reportedly inhibits the NF-κB activation by binding to the P65 subunit (145). Moreover, *ANXA1* acts as anti-proliferative and anti-apoptotic substance and it is associated with survival in gastric cancer (146).

Finally, I performed a STRING analysis to assess the relationship between the investigated genes. These analyses hinted towards a beneficial effect of low-frequency vibration on human cartilage cells.

In summary, all these experiments indicated a beneficial influence of vibration on chondrocytes. In particular, upregulation of *VCL*, *PXN*, *ANXA1* and downregulation of *ANXA2* are involved in protecting chondrocytes and inhibiting differentiation.

5.5. Conclusions

In this thesis, I demonstrated the central role of E-cadherin in spheroid formation. E-cadherin is proposed to have a strong correlation with the metastatic activity of cancer cells (120). It is important to further study the mechanism of E-cadherin activity in microgravity to investigate whether spheroid formation depends on the level of E-cadherin expression or if post-translational modifications such as phosphorylation play an additive role. Once again, microgravity simulation experiments that utilised an RPM proved to be a suitable model to study cancer metastasis. Moreover, biological or chemical agents such as PP2 or anti-E-cadherin antibodies were helpful to study the mechanism of spheroid formation. Future knockin and knockout experiments to determine the importance of E-cadherin in detail are planned.

Additionally, I studied MCF-7 breast cancer cells with live-cell imaging in orbit during the TX54 mission. The FLUMIAS microscope was a reliable method for live-cell imaging on a sounding rocket. A modified version of the FLUMIAS microscope has also been used onboard the ISS (147). MCF-7 sensed

microgravity within minutes, denoted by alterations in the F-actin and microtubule cytoskeleton. Furthermore, I studied the MCF-7 cells during the PFC. MCF-7 exhibited an early upregulation in *CXCL8* and *VEGFA* mRNA as well as downregulations in *VCL* mRNA and E-cadherin protein. MCF-7 transformed into a more invasive cell line after the exposure of the cells to short-term $r\text{-}\mu\text{g}$. This finding is in agreement with earlier data with thyroid cancer cells exposed to microgravity during a parabolic flight (46). Further investigations of MCF-7 cancer cells are needed for longer times in space. A future plan to test MCF-7 on board of the ISS is in place. The test phase has already commenced.

I also studied the effect of short-term microgravity on MDA-MB-231 breast cancer cells during the 29th DLR PFC. MDA-MB-231 cells exhibited upregulated cell adhesion genes. This finding is consistent with earlier data from other cell types cultured in space or on the NASA-developed high-aspect ratio vessel (HARV) (148–150). Another interesting finding is the upregulation of *CD44* during microgravity and hyper-*g*, which may be explained as a compensative regulation to counteract apoptosis occurring in microgravity. Moreover, the regulation of cell adhesion molecules and MAPK pathway factors are thought to be involved in the adaptive response to perturbation of mechanical stress under $r\text{-}\mu\text{g}$. Finally, the thesis suggests that a fine balance between NF- κ B-p65 and osteopontin gene dosage is needed to regulate metastasis, survival and angiogenesis of MDA-MB-231 breast cancer cells. Long-term microgravity studies must be performed on MDA-MB-231 cells to gain insight into the prolonged alterations occurring to the cells in microgravity. Both MCF-7 and MDA-MB-231 cell lines have demonstrated that they respond to microgravity by alterations in FA. Thus, these data confirm the importance of focal adhesion factors in mechanotransduction.

Finally, I studied the effect of low-frequency vibration on human chondrocytes. Vibration induced alterations with focal adhesions, changes that hint about the beneficial effects of vibration on the chondrocytes. Microgravity is thought to have a negative impact on chondrocytes, and vibration might be of importance to counteract the effect of microgravity. Due to the increasing number of spaceflights and future space exploration missions, it is important to study all stressors involved in long-time space travel, including microgravity, vibration, hypergravity and cosmic radiation. Therefore, long-term vibration and microgravity studies on other cells lines, such as endothelial cells and lymphocytes, should be performed.

5.6. Summary

Space research has become a necessity with the expected rise in spaceflights in the near future. Microgravity-based research will improve our understanding about the alterations that occur in our cells and organs in space.

One aim of this thesis was to study the cytoskeletal alterations and possible mechanisms of spheroid formation in human breast cancer cells in microgravity. Therefore, I examined the effect of $s\text{-}\mu\text{g}$ on human breast cancer cells MCF-7 on an RPM for 14 days. After subjecting the cells to $s\text{-}\mu\text{g}$ for 2 weeks, there were AD and MCS cellular subpopulations. A proteome analysis investigated the difference in protein expression among AD, MCS and $1g$ control cells. E-cadherin protein was significantly reduced in MCS. A balance between the proteins which up- and downregulate E-cadherin was proposed to control the tendency of MCF-7 cells to form MCS during the RPM-exposure.

Furthermore, I investigated transfected MCF-7 cells with FLUMIAS live-cell imaging during the TX54 sounding rocket mission. The cells revealed alterations and rearrangements of the F-actin and tubulin cytoskeleton, with holes and accumulations in the tubulin network as well as the appearance of filopodia- and lamellipodia-like structures in the F-actin cytoskeleton. I also investigated the effect of $r\text{-}\mu\text{g}$ on MCF-7 cells during the 31st DLR PFC. The cells exhibited gene modifications, which indicate a transformation of MCF-7 cells into a more invasive cell line.

Additionally, I examined TNBC MDA-MB-231 cells in $r\text{-}\mu\text{g}$ during the 29th DLR PFC mission. PF manoeuvres induced gene alterations that point to changes in cell adhesion in response to short-term microgravity. Furthermore, I evaluated the effects of hyper- g and vibration on MDA-MB-231 cells. However, the cells exhibited only minor alterations. Both breast cancer cell lines—MCF-7 and MDA-MB-231 showed modified focal adhesions as a consequence to microgravity-exposure. These data further confirm the important role of focal adhesion molecules in mechanotransduction.

Finally, I examined the impact of low-frequency vibration on human chondrocytes. The aim was to further study the impact of vibration on chondrocytes and if it has an effect on apoptosis. I subjected the cells to a 24-h experiment via a Vibraplex. The vibration did not induce any changes in the morphology of the cells or the cytoskeleton and I did not detect any apoptotic cells. However, *VCL*, *PXN*, *ANXA1* and downregulation of *ANXA2* were upregulated. These alterations appear to protect human chondrocytes and inhibit differentiation. All the experiments seem to show a beneficial influence of vibration on human

chondrocytes. Vibration can be considered a potential countermeasure against the negative impact of microgravity on human chondrocytes.

5.7. Zusammenfassung

Durch den zu erwarteten Anstieg der Weltraumflüge in naher Zukunft gewinnt die Weltraumforschung an Bedeutsamkeit. Die Mikrogravitationsbasierende Forschung wird das Verständnis für Veränderungen, die in unseren Organen und Zellen im Weltraum auftreten, verbessern.

In dieser Doktorarbeit bestand ein Hauptziel darin, die Veränderungen des Zytoskeletts und mögliche Mechanismen der Sphäroidbildung in menschlichen Mammakarzinomzellen in der simulierten Schwerelosigkeit zu untersuchen. Daher wurde die Wirkung von $s\text{-}\mu\text{g}$ auf die menschlichen Brustkrebszellen MCF-7 untersucht. Diese wurden für 14 Tage auf der RPM kultiviert. Nach zwei Wochen Kultivierung in $s\text{-}\mu\text{g}$ wurden zwei verschiedene Subpopulationen von Zellen (AD und MCS) identifiziert, die auf der RPM in der Mikrogravitation wachsen. Um Unterschiede in der Proteinexpression zwischen AD, MCS und 1g Kontrollzellen zu finden, wurde eine Proteomanalyse durchgeführt. Diese zeigte eine signifikante Reduktion des Proteins E-Cadherin in MCS. Es wird vermutet, dass das Verhältnis der Proteine, die E-Cadherin hoch- und herunterregulieren, die Tendenz zur Bildung von MCS von MCF-7 Zellen während der RPM-Exposition kontrolliert.

Darüber hinaus wurden transfizierte MCF-7 Zellen mit dem FLUMIAS Live Cell Imaging Mikroskop während der Raketenmission TX54 untersucht. Die Zellen zeigten Veränderungen und Umlagerungen des F-Aktin und Tubulin Zytoskeletts während des Flugs. Es fanden sich Löcher und Ansammlungen im Tubulin Netzwerk, sowie das Auftreten von Filopodien- und Lamellipodien-ähnlichen Strukturen im F-Aktin Zytoskelett. Darüber hinaus wurde die Wirkung von $r\text{-}\mu\text{g}$ auf MCF-7 Zellen während der 31st DLR PFC untersucht. Die Zellen zeigten Genmodifikationen, die auf eine Transformation der MCF-7 Zellen in eine invasivere Zelllinie hinweisen.

Zusätzlich wurde eine weitere Mammakarzinomzelllinie (triple-negative MDA-MB-231 Zelllinie) in $r\text{-}\mu\text{g}$ während der 29th DLR PFC Mission untersucht. PF-Manöver induzierten Genveränderungen, die auf Veränderungen der Zelladhäsion als Reaktion auf die kurzzeitige Mikrogravitation hinweisen. Darüber hinaus wurden die Auswirkungen von Hyper-g und Vibration auf die MDA-MB-231 Zellen studiert. Die Zellen zeigten jedoch nur geringfügige Veränderungen. Beide Brustkrebszelllinien: MCF-7 und

MDA-MB-231 wiesen Veränderungen der fokalen Adhäsionen als Folge der Mikrogravitationsexposition auf. Diese Daten bestätigen die wichtige Rolle fokaler Adhäsionsmoleküle bei der Mechanotransduktion.

Abschließend wurde der Einfluss niederfrequenter Schwingungen auf menschliche Chondrozyten getestet. Ziel war es, den Einfluss von Vibrationen auf Chondrozyten und deren Auswirkungen auf die Apoptose weiter zu untersuchen. Hierzu wurden die Zellen für 24 Stunden auf der Vibraplex Maschine kultiviert. Die Vibrationen induzierten keine Veränderungen der Morphologie der Zellen oder des Zytoskeletts und es waren keine apoptotischen Zellen nachweisbar. Jedoch konnte eine Hochregulation der Genexpression von *VCL*, *PXN*, *ANXA1* und eine Herunterregulierung von *ANXA2* festgestellt werden. Diese Veränderungen scheinen menschliche Chondrozyten zu schützen und deren Differenzierung zu hemmen. Alle Experimente zeigen einen positiven Einfluss der Vibration auf menschliche Knorpelzellen. Vibration kann als mögliche Gegenmaßnahme gegen die negativen Auswirkungen der Mikrogravitation auf menschliche Chondrozyten angesehen werden.

6. References

1. Payne, M. W. C., Williams, D. R., and Trudel, G. (2007) Space flight rehabilitation. *Am. J. Phys. Med. Rehabil.* **86**, 583–591
2. Grimm, D., Grosse, J., Wehland, M., Mann, V., Reseland, J. E., Sundaresan, A., and Corydon, T. J. (2016) The impact of microgravity on bone in humans. *Bone* **87**, 44–56
3. White, R. J. and Averner, M. (2001) Humans in space. *Nature* **409**, 1115–1118
4. Vandenburg, H., Chromiak, J., Shansky, J., Del Totto, M., and Lemaire, J. (1999) Space travel directly induces skeletal muscle atrophy. *FASEB J.* **13**, 1031–1038
5. Smith, S. M., Zwart, S. R., Heer, M., Hudson, E. K., Shackelford, L., and Morgan, J. L. (2014) Men and Women in Space: Bone Loss and Kidney Stone Risk After Long-Duration Spaceflight. *J. Bone Miner. Res.* **29**, 1639–1645
6. Zayzafoon, M., Meyers, V. E., and McDonald, J. M. (2005) Microgravity: the immune response and bone. *Immunol. Rev.* **208**, 267–280
7. Pietsch, J., Bauer, J., Egli, M., Infanger, M., Wise, P., Ulbrich, C., and Grimm, D. (2011) The Effects of Weightlessness on the Human Organism and Mammalian Cells. *Curr. Mol. Med.* **11**, 350–364
8. Charles, J. B. and Lathers, C. M. (1991) Cardiovascular Adaptation to Spaceflight. *J. Clin. Pharmacol.* **31**, 1010–1023
9. Smith, S. M., Wastney, M. E., Morukov, B. V., Larina, I. M., Nyquist, L. E., Abrams, S. A., Taran, E. N., Shih, C. Y., Nillen, J. L., Davis-Street, J. E., Rice, B. L., and Lane, H. W. (1999) Calcium metabolism before, during, and after a 3-mo spaceflight: kinetic and biochemical changes. *Am. J. Physiol. Regul. Integr. Comp. Physiol.* **277**, 1–10
10. Taylor, P. W. and Sommer, A. P. (2005) Towards rational treatment of bacterial infections during extended space travel. *Int. J. Antimicrob. Agents* **26**, 183–187
11. Cervantes, J. L. and Hong, B. Y. (2016) Dysbiosis and Immune Dysregulation in Outer Space. *Int. Rev. Immunol.* **35**, 67–82
12. Cohrs, R. J., Mehta, S. K., Schmid, D. S., Gilden, D. H., and Pierson, D. L. (2008) Asymptomatic reactivation and shed of infectious varicella zoster virus in astronauts. *J. Med. Virol.* **80**, 1116–1122
13. Mehta, S. K., Laudenslager, M. L., Stowe, R. P., Crucian, B. E., Sams, C. F., and Pierson, D. L. (2014) Multiple latent viruses reactivate in astronauts during Space Shuttle missions. *Brain. Behav. Immun.* **41**, 210–217
14. Stowe, R. P., Sams, C. F., and Pierson, D. L. (2003) Effects of Mission Duration on Neuroimmune Responses in Astronauts. *Aviat. Sp. Environ. Med.* **74**, 1281–1284
15. Wilson, J. W., Ott, C. M., Quick, L., Davis, R., zu Bentrup, K. H., Crabbé, A., Richter, E., Sarker,

- S., Barrila, J., Porwollik, S., Cheng, P., McClelland, M., Tsaprailis, G., Radabaugh, T., Hunt, A., Shah, M., Nelman-Gonzalez, M., Hing, S., Parra, M., Dumars, P., Norwood, K., Bober, R., Devich, J., Ruggles, A., CdeBaca, A., Narayan, S., Benjamin, J., Goulart, C., Rupert, M., Catella, L., Schurr, M. J., Buchanan, K., Morici, L., McCracken, J., Porter, M. D., Pierson, D. L., Smith, S. M., Mergeay, M., Leys, N., Stefanyshyn-Piper, H. M., Gorie, D., and Nickerson, C. A. (2008) Media ion composition controls regulatory and virulence response of Salmonella in spaceflight. *PLoS One* **3**, e3923
16. Nickerson, C. A., Ott, C. M., Wilson, J. W., Ramamurthy, R., and Pierson, D. L. (2004) Microbial Responses to Microgravity and Other Low-Shear Environments. *Microbiol. Mol. Biol. Rev.* **68**, 345–361
 17. Hodkinson, P. D., Anderton, R. A., Posselt, B. N., and Fong, K. J. (2017) An overview of space medicine. *Br. J. Anaesth.* **119**, i143–i153
 18. Jennings, R. T. (1998) Managing space motion sickness. *J. Vestib. Res. Equilib. Orientat.* **8**, 67–70
 19. Heer, M. and Paloski, W. H. (2006) Space motion sickness: incidence, etiology, and countermeasures. *Auton. Neurosci. Basic Clin.* **129**, 77–79
 20. Williams, D., Kuipers, A., Mukai, C., and Thirsk, R. (2009) Acclimation during space flight: effects on human physiology. *CMAJ* **180**, 1317–1323
 21. Grenon, S. M., Saary, J., Gray, G., Vanderploeg, J. M., and Hughes-Fulford, M. (2012) Can I take a space flight? Considerations for doctors. *BMJ* **345**, e8124–e8124
 22. Demontis, G. C., Germani, M. M., Caiani, E. G., Barravecchia, I., Passino, C., and Angeloni, D. (2017) Human pathophysiological adaptations to the space environment. *Front. Physiol.* **8**, 547
 23. Ploutz-Snyder, L. (2016) Evaluating countermeasures in spaceflight analogs. *J. Appl. Physiol.* **120**, 915–921
 24. Corydon, T. J., Kopp, S., Wehland, M., Braun, M., Schütte, A., Mayer, T., Hülsing, T., Oltmann, H., Schmitz, B., Hemmersbach, R., and Grimm, D. (2016) Alterations of the cytoskeleton in human cells in space proved by life-cell imaging. *Sci. Rep.* **6**, 20043
 25. Shelhamer, M. (2016) Parabolic flight as a spaceflight analog. *J. Appl. Physiol.* **120**, 1442–1448
 26. Hemmersbach, R., Wilczek, M., Stieber, C., Braucker, R., and Ivanova, K. (2002) Variable acceleration influences cyclic AMP levels in Paramecium biaurelia. *J. Gravit. Physiol.* **9**, P267-8
 27. Hader, D. P., Vogel, K., and Schafer, J. (1990) Responses of the photosynthetic flagellate, *Euglena gracilis*, to microgravity. *Microgravity Sci. Technol.* **3**, 110–116
 28. Mehrle, W., Hampp, R., Naton, B., and Grothe, D. (1989) Effects of microgravitation on electrofusion of plant cell protoplasts. *Plant Physiol.* **89**, 1172–1177
 29. Hampp, R., Naton, B., Hoffmann, E., and Mehrle, W. (1990) Suspensions of plant cells in

- microgravity. *Microgravity Sci. Technol.* **3**, 168–172
30. Ubbels, G. A., Reijnen, M., Meijerink, J., and Narraway, J. (1994) *Xenopus laevis* embryos can establish their spatial bilateral symmetrical body pattern without gravity. *Adv. Space Res.* **14**, 257–269
 31. Ubbels, G. A., Berendsen, W., and Narraway, J. (1989) Fertilization of frog eggs on a Sounding Rocket in space. *Adv. Space Res.* **9**, 187–197
 32. Thiel, C. S., Tauber, S., Schütte, A., Schmitz, B., Nuesse, H., Moeller, R., and Ullrich, O. (2014) Functional Activity of Plasmid DNA after Entry into the Atmosphere of Earth Investigated by a New Biomarker Stability Assay for Ballistic Spaceflight Experiments. *PLoS One* **9**, e112979
 33. Albi, E., Ambesi-Impiombato, F. S., Peverini, M., Damaskopoulou, E., Fontanini, E., Lazzarini, R., Curcio, F., and Perrella, G. (2011) Thyrotropin Receptor and Membrane Interactions in FRTL-5 Thyroid Cell Strain in Microgravity. *Astrobiology* **11**, 57–64
 34. Herranz, R., Anken, R., Boonstra, J., Braun, M., Christianen, P. C. M., de Geest, M., Hauslage, J., Hilbig, R., Hill, R. J. A., Lebert, M., Medina, F. J., Vagt, N., Ullrich, O., van Loon, J. J. W. A., and Hemmersbach, R. (2013) Ground-based facilities for simulation of microgravity: organism-specific recommendations for their use, and recommended terminology. *Astrobiology* **13**, 1–17
 35. Kopp, S., Krüger, M., Feldmann, S., Oltmann, H., Schütte, A., Schmitz, B., Bauer, J., Schulz, H., Saar, K., Huebner, N., Wehland, M., Nassef, M. Z., Melnik, D., Meltendorf, S., Infanger, M., and Grimm, D. (2018) Thyroid cancer cells in space during the TEXUS-53 sounding rocket mission-The THYROID Project. *Sci. Rep.* **8**, 10355
 36. Van Loon, J. J. W. A. Some history and use of the random positioning machine, RPM, in gravity related research. *Adv. Space Res.* **39**, 1161–1165
 37. Schwarz, R. P., Goodwin, T. J., and Wolf, D. A. (1992) Cell culture for three-dimensional modeling in rotating-wall vessels: An application of simulated microgravity. *J. Tissue Cult. Methods* **14**, 51–57
 38. Moorman, S. J., Burrell, C., Cordova, R., and Slater, J. (1999) Stimulus dependence of the development of the zebrafish (*Danio rerio*) vestibular system. *J. Neurobiol.* **38**, 247–258
 39. Ma, X., Wehland, M., Aleshcheva, G., Hauslage, J., Waßer, K., Hemmersbach, R., Infanger, M., Bauer, J., and Grimm, D. (2013) Interleukin-6 Expression under Gravitational Stress Due to Vibration and Hypergravity in Follicular Thyroid Cancer Cells. *PLoS One* **8**, e68140
 40. Lützenberg, R., Solano, K., Buken, C., Sahana, J., Riwaldt, S., Kopp, S., Krüger, M., Schulz, H., Saar, K., Huebner, N., Hemmersbach, R., Bauer, J., Infanger, M., Grimm, D., and Wehland, M. (2018) Pathway Analysis Hints Towards Beneficial Effects of Long-Term Vibration on Human Chondrocytes. *Cell. Physiol. Biochem.* **47**, 1729–1741

41. Aleshcheva, G., Wehland, M., Sahana, J., Bauer, J., Corydon, T. J., Hemmersbach, R., Frett, T., Egli, M., Infanger, M., Grosse, J., and Grimm, D. (2015) Moderate alterations of the cytoskeleton in human chondrocytes after short-term microgravity produced by parabolic flight maneuvers could be prevented by up-regulation of BMP-2 and SOX-9. *FASEB J.* **29**, 2303–2314
42. Bray, F., Ferlay, J., Soerjomataram, I., Siegel, R. L., Torre, L. A., and Jemal, A. (2018) Global cancer statistics 2018: GLOBOCAN estimates of incidence and mortality worldwide for 36 cancers in 185 countries. *CA. Cancer J. Clin.* **68**, 394–424
43. Kolak, A., Kamińska, M., Sygit, K., Budny, A., Surdyka, D., Kukielka-Budny, B., and Burdan, F. (2017) Primary and secondary prevention of breast cancer. *Ann. Agric. Environ. Med.* **24**, 549–553
44. Schreiber, R. D., Old, L. J., and Smyth, M. J. (2011) Cancer immunoediting: integrating immunity's roles in cancer suppression and promotion. *Science* **331**, 1565–1570
45. Hanahan, D. and Weinberg, R. A. (2011) Hallmarks of cancer: the next generation. *Cell* **144**, 646–674
46. Ma, X., Pietsch, J., Wehland, M., Schulz, H., Saar, K., Hübner, N., Bauer, J., Braun, M., Schwarzwälder, A., Segerer, J., Birlem, M., Horn, A., Hemmersbach, R., Waßer, K., Grosse, J., Infanger, M., and Grimm, D. (2014) Differential gene expression profile and altered cytokine secretion of thyroid cancer cells in space. *FASEB J.* **28**, 813–835
47. Harbeck, N., Penault-Llorca, F., Cortes, J., Gnant, M., Houssami, N., Poortmans, P., Ruddy, K., Tsang, J., and Cardoso, F. (2019) Breast cancer. *Nat. Rev. Dis. Prim.* **5**, 66
48. Tao, Z., Shi, A., Lu, C., Song, T., Zhang, Z., and Zhao, J. (2015) Breast Cancer: Epidemiology and Etiology. *Cell Biochem. Biophys.* **72**, 333–338
49. Redig, A. J. and Mcallister, S. S. (2013) Breast cancer as a systemic disease: a view of metastasis. *J. Intern. Med.* **274**, 113–126
50. Britt, K., Ashworth, A., and Smalley, M. (2007) Pregnancy and the risk of breast cancer. *Endocr. Relat. Cancer* **14**, 907–933
51. Siwko, S. K., Dong, J., Lewis, M. T., Liu, H., Hilsenbeck, S. G., and Li, Y. (2008) Evidence that an early pregnancy causes a persistent decrease in the number of functional mammary epithelial stem cells--implications for pregnancy-induced protection against breast cancer. *Stem Cells* **26**, 3205–3209
52. Shiovitz, S. and Korde, L. A. (2015) Genetics of breast cancer: a topic in evolution. *Ann. Oncol.* **26**, 1291–1299
53. Prat, A., Parker, J. S., Karginova, O., Fan, C., Livasy, C., Herschkowitz, J. I., He, X., and Perou, C. M. (2010) Phenotypic and molecular characterization of the claudin-low intrinsic subtype of breast cancer. *Breast Cancer Res.* **12**, R68

54. Farmer, P., Bonnefoi, H., Becette, V., Tubiana-Hulin, M., Fumoleau, P., Larsimont, D., MacGrogan, G., Bergh, J., Cameron, D., Goldstein, D., Duss, S., Nicoulaz, A. L., Brisken, C., Fiche, M., Delorenzi, M., and Iggo, R. (2005) Identification of molecular apocrine breast tumours by microarray analysis. *Oncogene* **24**, 4660–4671
55. Dai, X., Li, T., Bai, Z., Yang, Y., Liu, X., Zhan, J., and Shi, B. (2015) Breast cancer intrinsic subtype classification, clinical use and future trends. *Am. J. Cancer Res.* **5**, 2929–2943
56. Soliman, N. A. and Yussif, S. M. (2016) Ki-67 as a prognostic marker according to breast cancer molecular subtype. *Cancer Biol. Med.* **13**, 496–504
57. Sweeney, E. E., McDaniel, R. E., Maximov, P. Y., Fan, P., and Craig Jordan, V. (2012) Models and mechanisms of acquired antihormone resistance in breast cancer: significant clinical progress despite limitations. *Horm. Mol. Biol. Clin. Investig.* **9**, 143–163
58. Soule, H. D., Vazquez, J., Long, A., Albert, S., and Brennan, M. (1973) A human cell line from a pleural effusion derived from a breast carcinoma. *J. Natl. Cancer Inst.* **51**, 1409–1416
59. Comşa, Ş., Cîmpean, A. M., and Raica, M. (2015) The story of MCF-7 breast cancer cell line: 40 years of experience in research. *Anticancer Res.* **35**, 3147–3154
60. Levenson, A. S. and Craig, V. (1997) MCF-7: The First Hormone-responsive Breast Cancer Cell Line. *Cancer Res.* **57**, 3071–3078
61. Kopp, S., Sahana, J., Islam, T., Graver Petersen, A., Bauer, J., Corydon, T. J., Schulz, H., Saar, K., Huebner, N., Slumstrup, L., Riwaldt, S., Wehland, M., Infanger, M., Luetzenberg, R., and Grimm, D. The role of NFκB in spheroid formation of human breast cancer cells cultured on the Random Positioning Machine. *Sci. Rep.* **8**, 921
62. Kopp, S., Slumstrup, L., Corydon, T. J., Sahana, J., Aleshcheva, G., Islam, T., Magnusson, N. E., Wehland, M., Bauer, J., Infanger, M., and Grimm, D. (2016) Identifications of novel mechanisms in breast cancer cells involving duct-like multicellular spheroid formation after exposure to the Random Positioning Machine. *Sci. Rep.* **6**, 26887
63. Vassy, J., Portet, S., Beil, M., Millot, G., Fauvel-Lafève, F., Karniguian, A., Gasset, G., Irinopoulou, T., Calvo, F., Rigaut, J. P., and Schoevaert, D. (2001) The effect of weightlessness on cytoskeleton architecture and proliferation of human breast cancer cell line MCF-7. *FASEB J.* **15**, 1104–1106
64. Vassy, J., Portet, S., Beil, M., Millot, G., Fauvel-Lafeve, F., Gasset, G., and Schoevaert, D. (2003) Weightlessness acts on human breast cancer cell line MCF-7. *Adv. Sp. Res.* **32**, 1595–1603
65. Cailleau, R., Young, R., Olivé, M., and Reeves, W. J. (1974) Breast Tumor Cell Lines From Pleural Effusions. *JNCI J. Natl. Cancer Inst.* **53**, 661–674
66. Chavez, K. J., Garimella, S. V., and Lipkowitz, S. (2010) Triple negative breast cancer cell lines: one tool in the search for better treatment of triple negative breast cancer. *Breast Dis.* **32**, 35–48

67. Cailleau, R., Olivé, M., and Cruciger, Q. V. J. (1978) Long-term human breast carcinoma cell lines of metastatic origin: Preliminary characterization. *In Vitro* **14**, 911–915
68. Grazia Masiello, M., Cucina, A., Proietti, S., Palombo, A., Coluccia, P., Dinicola, S., Pasqualato, A., Morini, V., and Bizzarri, M. (2014) Phenotypic Switch Induced by Simulated Microgravity on MDA-MB-231 Breast Cancer Cells. *Biomed. Res. Int.* **2014**, 652434
69. Goldring, M. B. (2006) Update on the biology of the chondrocyte and new approaches to treating cartilage diseases. *Best Pract. Res. Clin. Rheumatol.* **20**, 1003–1025
70. Davisson, T., Sah, R. L., and Ratcliffe, A. (2002) Perfusion increases cell content and matrix synthesis in chondrocyte three-dimensional cultures. *Tissue Eng.* **8**, 807–816
71. Chen, C. S. and Ingber, D. E. (1999) Tensegrity and mechanoregulation: From skeleton to cytoskeleton. *Osteoarthr. Cartil.* **7**, 81–94
72. Aleshcheva, G., Sahana, J., Ma, X., Hauslage, J., Hemmersbach, R., Egli, M., Infanger, M., Bauer, J., and Grimm, D. (2013) Changes in morphology, gene expression and protein content in chondrocytes cultured on a random positioning machine. *PLoS One* **8**, e79057
73. Aleshcheva, G., Bauer, J., Hemmersbach, R., Egli, M., Wehland, M., and Grimm, D. (2016) Tissue Engineering of Cartilage on Ground-Based Facilities. *Microgravity Sci. Technol.* **28**, 237–245
74. Pullig, O., Weseloh, G., Gauer, S., and Swoboda, B. (2000) Osteopontin is expressed by adult human osteoarthritic chondrocytes: protein and mRNA analysis of normal and osteoarthritic cartilage. *Matrix Biol.* **19**, 245–255
75. Karin, M. and Delhase, M. (2000) The I κ B kinase (IKK) and NF- κ B: key elements of proinflammatory signalling. *Semin. Immunol.* **12**, 85–98
76. Sun, W., Zhao, R., Yang, Y., Wang, H., Shao, Y., and Kong, X. (2013) Comparative study of human aortic and mitral valve interstitial cell gene expression and cellular function. *Genomics* **101**, 326–335
77. Vorselen, D., Roos, W. H., MacKintosh, F. C., Wuite, G. J. L., and Van Loon, J. J. W. A. (2014) The role of the cytoskeleton in sensing changes in gravity by nonspecialized cells. *FASEB J.* **28**, 536–547
78. Grenon, S. M., Jeanne, M., Aguado-Zuniga, J., Conte, M. S., and Hughes-Fulford, M. (2013) Effects of gravitational mechanical unloading in endothelial cells: association between caveolins, inflammation and adhesion molecules. *Sci. Rep.* **3**, 1494
79. Hughes-Fulford, M. (2003) Function of the cytoskeleton in gravisensing during spaceflight. *Adv. Space Res.* **32**, 1585–1593
80. Boonstra, J. (1999) Growth factor-induced signal transduction in adherent mammalian cells is sensitive to gravity. *FASEB J.* **13**

81. Najrana, T. and Sanchez-Esteban, J. (2016) Mechanotransduction as an adaptation to gravity. *Front. Pediatr.* **4**, 140
82. Pegoraro, A. F., Janmey, P., and Weitz, D. A. (2017) Mechanical Properties of the Cytoskeleton and Cells. *Cold Spring Harb. Perspect. Biol.* **9**, a022038
83. Maziveyi, M. and Alahari, S. K. (2017) Cell matrix adhesions in cancer: the proteins that form the glue. *Oncotarget* **8**, 48471–48487
84. Damiano, J. S., Hazlehurst, L. A., and Dalton, W. S. (2001) Cell adhesion-mediated drug resistance (CAM-DR) protects the K562 chronic myelogenous leukemia cell line from apoptosis induced by BCR/ABL inhibition, cytotoxic drugs, and γ -irradiation. *Leukemia* **15**, 1232–1239
85. Park, C. C., Zhang, H., Pallavicini, M., Gray, J. W., Baehner, F., Park, C. J., and Bissell, M. J. (2006) β 1 integrin inhibitory antibody induces apoptosis of breast cancer cells, inhibits growth, and distinguishes malignant from normal phenotype in three dimensional cultures and in vivo. *Cancer Res.* **66**, 1526–1535
86. Park, C. C., Zhang, H. J., Yao, E. S., Park, C. J., and Bissell, M. J. (2008) β 1 integrin inhibition dramatically enhances radiotherapy efficacy in human breast cancer xenografts. *Cancer Res.* **68**, 4398–4405
87. Eke, I., Deuse, Y., Hehlhans, S., Gurtner, K., Krause, M., Baumann, M., Shevchenko, A., Sandfort, V., and Cordes, N. (2012) β 1 Integrin/FAK/cortactin signaling is essential for human head and neck cancer resistance to radiotherapy. *J. Clin. Invest.* **122**, 1529–1540
88. Schiller, H. B., Hermann, M. R., Polleux, J., Vignaud, T., Zanivan, S., Friedel, C. C., Sun, Z., Raducanu, A., Gottschalk, K. E., Théry, M., Mann, M., and Fässler, R. (2013) β 1 - And α v -class integrins cooperate to regulate myosin II during rigidity sensing of fibronectin-based microenvironments. *Nat. Cell Biol.* **15**, 625–636
89. Lewis, M. L., Reynolds, J. L., Cubano, L. A., Hatton, J. P., Desales Lawless, B., and Piepmeier, E. H. (1998) Spaceflight alters microtubules and increases apoptosis in human lymphocytes (Jurkat). *FASEB J.* **12**, 1007–1018
90. Engler, A. J., Sen, S., Sweeney, H. L., and Discher, D. E. (2006) Matrix Elasticity Directs Stem Cell Lineage Specification. *Cell* **126**, 677–689
91. Ando, J. and Yamamoto, K. (2009) Vascular mechanobiology: endothelial cell responses to fluid shear stress. *Circ. J.* **73**, 1983–1992
92. Achilli, T.-M., Meyer, J., and Morgan, J. R. (2012) Advances in the formation, use and understanding of multi-cellular spheroids. *Expert Opin. Biol. Ther.* **12**, 1347–1360
93. Aleshcheva, G., Bauer, J., Hemmersbach, R., Slumstrup, L., Wehland, M., Infanger, M., and Grimm, D. (2016) Scaffold-free Tissue Formation Under Real and Simulated Microgravity Conditions.

94. Froehlich, K., Haeger, J. D., Heger, J., Pastuschek, J., Photini, S. M., Yan, Y., Lupp, A., Pfarrer, C., Mrowka, R., Schleußner, E., Markert, U. R., and Schmidt, A. (2016) Generation of Multicellular Breast Cancer Tumor Spheroids: Comparison of Different Protocols. *J. Mammary Gland Biol. Neoplasia* **21**, 89–98
95. Kunz-Schughart, L. A., Freyer, J. P., Hofstaedter, F., and Ebner, R. (2004) The use of 3-D cultures for high-throughput screening: The multicellular spheroid model. *J. Biomol. Screen.* **9**, 273–285
96. Timmins, N., Dietmair, S., and Nielsen, L. (2004) Hanging-drop multicellular spheroids as a model of tumour angiogenesis. *Angiogenesis* **7**, 97–103
97. Lin, R. Z. and Chang, H. Y. (2008) Recent advances in three-dimensional multicellular spheroid culture for biomedical research. *Biotechnol. J.* **3**, 1172–1184
98. Sutherland, R. M., Sordat, B., Bamat, J., Gabbert, H., Bourrat, B., and Mueller-Klieser, W. (1986) Oxygenation and Differentiation in Multicellular Spheroids of Human Colon Carcinoma. *Cancer Res.* **46**, 5320–5329
99. Grimes, D. R., Kelly, C., Bloch, K., and Partridge, M. (2014) A method for estimating the oxygen consumption rate in multicellular tumour spheroids. *J. R. Soc. Interface* **11**, 20131124
100. Kim, C. H., Jeon, H. M., Lee, S. Y., Ju, M. K., Moon, J. Y., Park, H. G., Yoo, M. A., Choi, B. T., Yook, J. I., Lim, S. C., Han, S. I., and Kang, H. S. (2011) Implication of Snail in metabolic stress-induced necrosis. *PLoS One* **6**, e18000
101. Antoni, D., Burckel, H., Josset, E., and Noel, G. (2015) Three-Dimensional Cell Culture: A Breakthrough in Vivo. *Int. J. Mol. Sci* **16**, 5517–5527
102. Svejgaard, B., Wehland, M., Ma, X., Kopp, S., Sahana, J., Warnke, E., Aleshcheva, G., Hemmersbach, R., Hauslage, J., Grosse, J., Bauer, J., Corydon, T. J., Islam, T., Infanger, M., and Grimm, D. (2015) Common Effects on Cancer Cells Exerted by a Random Positioning Machine and a 2D Clinostat. *PLoS One* **10**, 135157
103. Zhang, H., Cui, X., and Hartanto, Y. (2017) Advances in multicellular spheroids formation. *J. R. Soc. Interface* **14**, pii: 20160877
104. Grimm, D., Infanger, M., Westphal, K., Ulbrich, C., Pietsch, J., Kossmehl, P., Vadrucci, S., Baatout, S., Flick, B., Paul, M., and Bauer, J. (2009) A delayed type of three-dimensional growth of human endothelial cells under simulated weightlessness. *Tissue Eng. Part A* **15**, 2267–2275
105. Grosse, J., Wehland, M., Pietsch, J., Schulz, H., Saar, K., Hübner, N., Eilles, C., Bauer, J., Abou-El-Ardat, K., Baatout, S., Ma, X., Infanger, M., Hemmersbach, R., and Grimm, D. (2012) Gravity-sensitive signaling drives 3-dimensional formation of multicellular thyroid cancer spheroids. *FASEB J.* **26**, 5124–5140

106. Aleshcheva, G., Bauer, J., Hemmersbach, R., Slumstrup, L., Wehland, M., Infanger, M., and Grimm, D. (2016) Scaffold-free Tissue Formation Under Real and Simulated Microgravity Conditions. *Basic Clin. Pharmacol. Toxicol.* **119**, 26–33
107. Ulbrich, C., Westphal, K., Pietsch, J., Winkler, H. D. F., Leder, A., Bauer, J., Kossmehl, P., Grosse, J., Schoenberger, J., Infanger, M., Egli, M., and Grimm, D. (2010) Characterization of human chondrocytes exposed to simulated microgravity. *Cell. Physiol. Biochem.* **25**, 551–560
108. Huang, B.-W. and Gao, J.-Q. (2017) Application of 3D cultured multicellular spheroid tumor models in tumor- targeted drug delivery system research. *J. Control Release* **270**, 246–259
109. Mehta, G., Hsiao, A. Y., Ingram, M., Luker, G. D., and Takayama, S. (2012) Opportunities and challenges for use of tumor spheroids as models to test drug delivery and efficacy. *J. Control. Release* **164**, 192–204
110. Krüger, M., Melnik, D., Kopp, S., Buken, C., Sahana, J., Bauer, J., Wehland, M., Hemmersbach, R., Corydon, T. J., Infanger, M., and Grimm, D. (2019) Fighting thyroid cancer with microgravity research. *Int. J. Mol. Sci.* **20**, pii: E2553
111. Bauer, J., Kopp, S., Schlagberger, E. M., Grosse, J., Sahana, J., Riwaldt, S., Wehland, M., Luetzenberg, R., Infanger, M., and Grimm, D. (2017) Proteome analysis of human follicular thyroid cancer cells exposed to the random positioning machine. *Int. J. Mol. Sci.* **18**, pii: E546
112. Bauer, J., Wehland, M., Pietsch, J., Sickmann, A., Weber, G., and Grimm, D. (2016) Annotated Gene and Proteome Data Support Recognition of Interconnections Between the Results of Different Experiments in Space Research. *Microgravity Sci. Technol.* **28**, 357–365
113. Giannakopoulos, N. V., Luo, J. K., Papov, V., Zou, W., Lenschow, D. J., Jacobs, B. S., Borden, E. C., Li, J., Virgin, H. W., and Zhang, D. E. (2005) Proteomic identification of proteins conjugated to ISG15 in mouse and human cells. *Biochem. Biophys. Res. Commun.* **336**, 496–506
114. Reactome | Autodegradation of Cdh1 by Cdh1:APC/C [Internet]. [cited 2019 Dec 31]. Available from: <https://reactome.org/content/detail/R-HSA-174084>
115. Brockie, P. J., Maricq, A. V., WormBook, ed. The C. elegans Research Community 2006, WormBook, 1, 1, <https://doi.org/10.1895/wormbook.1.61.1>, <http://www.wormbook.org>
116. Schreiber, A., Stengel, F., Zhang, Z., Enchev, R. I., Kong, E. H., Morris, E. P., Robinson, C. V., Da Fonseca, P. C. A., and Barford, D. (2011) Structural basis for the subunit assembly of the anaphase-promoting complex. *Nature* **470**, 227–235
117. Nath, S., Banerjee, T., Sen, D., Das, T., and Roychoudhury, S. (2011) Spindle assembly checkpoint protein Cdc20 transcriptionally activates expression of ubiquitin carrier protein UbcH10. *J. Biol. Chem.* **286**, 15666–15677
118. Song, S., Cui, L., Jing, G., and Liu, C. (2013) Involvement of ubiquitin-conjugating enzyme E2C in

- proliferation and invasion of prostate carcinoma cells. *Oncol. Res.* **21**, 121–127
119. Peng, J., Qi, S., Wang, P., Li, W., Song, L., Liu, C., and Li, F. (2016) Meta-analysis of downregulated E-cadherin as a poor prognostic biomarker for cervical cancer. *Futur. Oncol.* **12**, 715–726
 120. Bremnes, R. M., Veve, R., Hirsch, F. R., and Franklin, W. A. (2002) The E-cadherin cell-cell adhesion complex and lung cancer invasion, metastasis, and prognosis. *Lung Cancer* **36**, 115–124
 121. Siitonen, S. M., Kononen, J. T., Helin, H. J., Rantala, I. S., Holli, K. A., and Isola, J. J. (1996) Reduced E-cadherin expression is associated with invasiveness and unfavorable prognosis in breast cancer. *Am. J. Clin. Pathol.* **105**, 394–402
 122. Ulbrich, C., Pietsch, J., Grosse, J., Wehland, M., Schulz, H., Saar, K., Hübner, N., Hauslage, J., Hemmersbach, R., Braun, M., Van Loon, J., Vagt, N., Egli, M., Richter, P., Einspanier, R., Sharbati, S., Baltz, T., Infanger, M., Ma, X., and Grimm, D. (2011) Differential gene regulation under altered gravity conditions in follicular thyroid cancer cells: relationship between the extracellular matrix and the cytoskeleton. *Cell. Physiol. Biochem.* **28**, 185–198
 123. Tan, X., Xu, A., Zhao, T., Zhao, Q., Zhang, J., Fan, C., Deng, Y., Freywald, A., Genth, H., and Xiang, J. (2018) Simulated microgravity inhibits cell focal adhesions leading to reduced melanoma cell proliferation and metastasis via FAK/RhoA-regulated mTORC1 and AMPK pathways. *Sci. Rep.* **8**, 3769
 124. Kitadai, Y., Haruma, K., Mukaida, N., Ohmoto, Y., Matsutani, N., Yasui, W., Yamamoto, S., Sumii, K., Kajiyama, G., Fidler, I. J., and Tahara, E. (2000) Regulation of disease-progression genes in human gastric carcinoma cells by interleukin 8. *Clin. Cancer Res.* **6**, 2735–2740
 125. Zhou, J., Zhang, C., Pan, J., Chen, L., and Qi, S. T. (2017) Interleukin-6 induces an epithelial-mesenchymal transition phenotype in human adamantinomatous craniopharyngioma cells and promotes tumor cell migration. *Mol. Med. Rep.* **15**, 4123–4131
 126. Martin, D., Galisteo, R., and Gutkind, J. S. (2008) CXCL8/IL8 stimulates VEGF expression and the autocrine activation of VEGFR2 in endothelial cells by activating NFkappa B through the CBM (Carma3/Bcl10/Mat1) complex. *J Biol Chem.* **284**, 6038–6042
 127. Cohen, T., Nahari, D., Cerem, L. W., Neufeld, G., and Levin, B. Z. (1996) Interleukin 6 induces the expression of vascular endothelial growth factor. *J. Biol. Chem.* **271**, 736–741
 128. Zhang, Y., Maria-Villanueva, M., Krieger, S., Ramesh, G. T., Neelam, S., and Wu, H. (2017) Transcriptomics, NF-KB pathway, and their potential spaceflight-related health consequences. *Int. J. Mol. Sci.* **18**, pii: E1166
 129. Sarkar, D. K., Jana, D., Patil, P. S., Chaudhari, K. S., Chattopadhyay, B. K., Chikkala, B. R., Mandal, S., and Chowdhary, P. (2013) Role of NF-κB as a Prognostic Marker in Breast Cancer: A Pilot Study

- in Indian Patients. *Indian J. Surg. Oncol.* **4**, 242–247
130. Khongthong, P., Roseweir, A. K., and Edwards, J. (2019) The NF- κ B pathway and endocrine therapy resistance in breast cancer. *Endocr. Relat. Cancer* **26**, R369–R380
 131. Ulbricht, C., Westphal, K., Baatout, S., Wehland, M., Bauer, J., Flick, B., Infanger, M., Kreutz, R., Vadrucci, S., Egli, M., Cogoli, A., Derradji, H., Pietsch, J., Paul, M., and Grimm, D. (2008) Effects of basic fibroblast growth factor on endothelial cells under conditions of simulated microgravity. *J. Cell. Biochem.* **104**, 1324–1341
 132. Chang, T. T., Walther, I., Li, C.-F., Boonyaratanakornkit, J., Galleri, G., Meloni, M. A., Pippia, P., Cogoli, A., and Hughes-Fulford, M. (2012) The Rel/NF- κ B pathway and transcription of immediate early genes in T cell activation are inhibited by microgravity. *J. Leukoc. Biol.* **92**, 1133–1145
 133. Boonyaratanakornkit, J. B., Cogoli, A., Li, C. F., Schopper, T., Pippia, P., Galleri, G., Meloni, M. A., and Hughes-Fulford, M. (2005) Key gravity-sensitive signaling pathways drive T cell activation. *FASEB J.* **19**, 2020–2022
 134. Gilmore, T. D. (2006) Introduction to NF- κ B: Players, pathways, perspectives. *Oncogene* **25**, 6680–6684
 135. Eibl, R. H. and Benoit, M. (2004) Molecular resolution of cell adhesion forces. *IEE Proc. Nanobiotechnol.* **151**, 128–132.
 136. Olea-Flores, M., Zuñiga-Eulogio, M. D., Mendoza-Catalán, M. A., Rodríguez-Ruiz, H. A., Castañeda-Saucedo, E., Ortuño-Pineda, C., Padilla-Benavides, T., and Navarro-Tito, N. (2019) Extracellular-Signal Regulated Kinase: A Central Molecule Driving Epithelial-Mesenchymal Transition in Cancer. *Int. J. Mol. Sci.* **20**, pii: E2885
 137. Kalluri, R. and Weinberg, R. A. (2009) The basics of epithelial-mesenchymal transition. *J. Clin. Invest.* **119**, 1420–1428
 138. Xie, L., Law, B. K., Chytil, A. M., Brown, K. A., Aakre, M. E., and Moses, H. L. (2004) Activation of the Erk pathway is required for TGF- β 1-induced EMT in vitro. *Neoplasia* **6**, 603–610
 139. Crapoulet, N., O'Brien, P., J. Ouellette, R., and A. Robichaud, G. (2012) Coordinated Expression of Pax-5 and FAK1 in Metastasis. *Anticancer Agents Med. Chem.* **11**, 643–649
 140. Chan, K. T., Cortesio, C. L., and Huttenlocher, A. (2009) Fak alters invadopodia and focal adhesion composition and dynamics to regulate breast cancer invasion. *J. Cell Biol.* **185**, 357–370
 141. Ashenden, M., Van Weverwijk, A., Murugaesu, N., Fearn, A., Campbell, J., Gao, Q., Iravani, M., and Isacke, C. M. (2017) An in vivo functional screen identifies JNK signaling as a modulator of chemotherapeutic response in breast cancer. *Mol. Cancer Ther.* **16**, 1967–1978
 142. Oeckinghaus, A., Hayden, M. S., and Ghosh, S. (2011) Crosstalk in NF- κ B signaling pathways. *Nat. Immunol.* **12**, 695–708

143. Subauste, M. C., Pertz, O., Adamson, E. D., Turner, C. E., Junger, S., and Hahn, K. M. (2004) Vinculin modulation of paxillin-FAK interactions regulates ERK to control survival and motility. *J. Cell Biol.* **165**, 371–381
144. Nah, A. S. and Chay, K. O. (2019) Roles of paxillin phosphorylation in IL-3 withdrawal-induced Ba/F3 cell apoptosis. *Genes Genomics* **41**, 241–248
145. Zhang, Z., Huang, L., Zhao, W., and Rigas, B. (2010) Annexin 1 induced by anti-inflammatory drugs binds to NF- κ B and inhibits its activation: anticancer effects in vitro and in vivo. *Cancer Res.* **70**, 2379–2388
146. Cheng, T. Y., Wu, M. S., Lin, J. T., Lin, M. T., Shun, C. T., Huang, H. Y., Hua, K. T., and Kuo, M. L. (2012) Annexin A1 is associated with gastric cancer survival and promotes gastric cancer cell invasiveness through the formyl peptide receptor/extracellular signal-regulated kinase/integrin beta-1-binding protein 1 pathway. *Cancer* **118**, 5757–5767
147. Thiel, C. S., Tauber, S., Seebacher, C., Schropp, M., Uhl, R., Lauber, B., Polzer, J., Neelam, S., Zhang, Y., and Ullrich, O. (2019) Real-time 3D high-resolution microscopy of human cells on the international space station. *Int. J. Mol. Sci.* **20**
148. Li, N., Wang, C., Sun, S., Zhang, C., Lü, D., Chen, Q., and Long, M. (2018) Microgravity-Induced Alterations of Inflammation-Related Mechanotransduction in Endothelial Cells on Board SJ-10 Satellite. *Front. Physiol.* **9**, 1025
149. Kumei, Y., Morita, S., Katano, H., Akiyama, H., Hirano, M., Oyha, K., and Shimokawa, H. (2006) Microgravity signal ensnarls cell adhesion, cytoskeleton, and matrix proteins of rat osteoblasts: Osteopontin, CD44, osteonectin, and α -tubulin. *Ann. N. Y. Acad. Sci.* **1090**, 311–317
150. Ingram, M., Techy, G. B., Saroufeem, R., Yazan, O., Narayan, K. S., Goodwin, T. J., and Spaulding, G. F. (1997) Three-dimensional growth patterns of various human tumor cell lines in simulated microgravity of a nasa bioreactor. *Vitr. Cell. Dev. Biol. Anim.* **33**, 459–466

7. Figure Index

Fig. 1: A spaceflight can negatively affect the human body (modified from nasa.gov). A list of the most known health problems of humans in space is given.	14
Fig. 2: Schematic sequences of parabolic and sounding rocket flights: (A) shows the altitude, speed and the three consecutive phases (hyper-g, microgravity and hyper-g) in each parabola during a parabolic flight, while (B) shows the launch and the re-entry of a sounding rocket (adapted from 35).....	16
Fig. 3: (A) A view of the MuSIC from the outside; (B) cell culture flasks fixed to the MUSIC from the inside; (C) the Vibraplex connected to audio speakers to control the frequency produced by the device..	17
Fig. 4: Phase contrast images of MCF-7 (left) and MDA-MB-231 (right). The scale bar is equal to 100 μ m.	20
Fig. 5: Phase contrast image of chondrocytes.....	21
Fig. 6: The alterations of adherent cells and how they lead to the transformation into multicellular spheroids after exposure to microgravity. The figure in the box shows changes at the microscopic level. F-actin is displayed as green lines, while the ECM in yellow. Abbreviations: FP: filopodia, LP: lamellipodia (modified from 110).	24
Fig. 7: Pathway Studio analysis of detected proteins involved in the formation and regulation of junctions as well as in CDH1 autodegradation. The proteins that belong to the group involved in the formation and regulation of junctions are indicated by a yellow coloured lower half-rim around the protein symbols, while the proteins that belong to the CDH1 autodegradation pathway are indicated by a red coloured lower half-rim around the protein symbols. Blue upper half-rims indicate upregulation, green upper half-rims indicate downregulation and violet upper half-rims show unregulated proteins. Regulation means that the LFQ of a protein in MCS is at least twofold enhanced or diminished as compared to controls. Grey, green and red lines or arrows show the type of interaction. Green lines or arrows indicate a supportive and red ones indicate an inhibitory type of interaction. Grey lines and arrows show that an interaction is described but not yet clearly defined. The interactions are shown on the gene and gene product levels.....	26
Fig. 8: Morphology and viability of MCF7 cells incubated at 1g (control) or on an RPM. Left side of the figure: phase contrast microscopy of MCF7 cells incubated at 1g (A, E, I, M) or on an RPM (B, F, J, N) for 14 days. Representative examples of spheroids formed on the RPM are marked by white arrowheads (B, F, N). J) Notably, no spheroids were formed on the RPM in the presence of the Src inhibitor PP2, N), whereas anti-E-cadherin (DECMA-1) stimulated the formation of spheroids. The inset in (N) shows an example of a large spheroid observed in the presence of anti-E-cadherin. Right side of figure: acridine orange/ethidium bromide staining revealed a green fluorescence in all cells of all groups (C, D, G, H, K, L, O, P), which indicates viability of MCF7 cells incubated on the RPM or at static 1g conditions. The inset in (C) represents	

positive control (PC) of the acridine orange/ethidium bromide assay after approximately 5 min incubation. The scale bars are 20 μm 27

Fig. 9: (A) Cell culture and slide preparation for live microscopy. (B) Hardware preparation prior to the launch of the rocket. (C) Launch of the TX54 rocket (courtesy of Airbus Defence and Space). (D) Airbus 310 aircraft used for the parabolic flight. (E) Placing the cell culture flasks inside the incubator in the aircraft prior to take off..... 28

Fig. 10: Time course and images of FLUMIAS on TEXUS 54 (40 \times /1.2). The MCF-7 breast cancer cells 5 min before launch (T -300 s) of the rocket and during the r- μg phase (T +177 s to T +402 s). The yellow arrows show the changes in F-actin (a–e; green fluorescence). The yellow circles include an area with F-actin accumulations. Filopodia and lamellipodia are found after 150 s and are more pronounced with time. The green arrows indicate changes in α -tubulin (f–j; red fluorescence). The tubulin network revealed holes after 150 s and a looser structure..... 29

Fig. 11: Indirect immunofluorescence staining of PFA-fixed cells from the TEXUS 54 sounding rocket mission. I seeded 2500 MCF-7 cells into each well of the 18-well Ibidi slides. I fixed the cells either at the end of the hyper-g period or at the end of the microgravity period. I compared the two conditions to 1g ground control samples. The confocal laser scanning microscopy images (a–l) show either MMP9, VEGF-A, IL-6 or IL-8 in green, DAPI (in blue) and F-actin (in red). Scale bar is equal to 50 μm . I quantified the intensity of the staining by ImageJ (m–q). All data are shown as mean \pm standard deviation; n = 10–14; * p < 0.05..... 30

Fig. 12: Influence of short-term microgravity on the gene expression (mRNA) of cytoskeletal factors. The data are shown as mean \pm standard deviation; n = 4; * p < 0.05 vs. Control..... 32

Fig. 13: Influence of short-term microgravity on the protein accumulation of focal adhesion complex components. The data is shown as mean \pm standard deviation; n = 4; * p < 0.05 vs. Control..... 32

Fig. 14: Influence of short-term microgravity on expression of different ECM and cytokine genes. The data are shown as mean \pm standard deviation; n = 4; * p < 0.05 vs. Control; # p < 0.05 vs. P1. 33

Fig. 15: Influence of short-term microgravity on the protein accumulation of IL-8. The data are shown as mean \pm standard deviation; n = 4; * p < 0.05 vs. Control..... 33

Fig. 16: Mutual interactions of the expression of the genes examined with qPCR. + Signs indicate an activity-enhancing effect and red lines indicate inhibition. The interaction networks were created using Elsevier Pathway Studio v11. 34

Fig. 17: The influence of short-term microgravity on the gene expression of (A) CASP3, (C) ANXA1, (D) ANXA2, (F) BAX and (G) BCL2 and protein content of (B) caspase-3 and (E) annexin 2, all of which are regulators of apoptosis. The data are shown as mean \pm standard deviation; * p < 0.05 vs. 1g control. CX+ colon cancer cells served as the positive control for programmed cell death. 35

Fig. 18: The influence of a VIB (V), hyper-g and RPM-exposure on the gene expression of apoptosis signalling factors: (A,B) CASP3, (C,D) ANXA1, (E,F) ANXA2, (G,H) BAX and (I,J) BCL2. The data are shown as mean \pm standard deviation; n = 5; * p < 0.05 vs. 1g control. The dashed vertical line separates two independent experiments..... 36

Fig. 19: The influence of short-term microgravity on the gene expression of (A) NFKB1, (B) NFKB2, (C) RELA, (E) NFKBIA, (G) NFKBIB, (H) NFKBIE and (I) IKBKG and the protein content of (D) RelA, (F) I κ B α and (J) NEMO, all of which are NF- κ B signalling factors. The data are shown as mean \pm standard deviation; n = 5; * p < 0.05 vs.1g control. 38

Fig. 20: The influence of VIB (V), hyper-g and iRPM-exposure on the gene expression of NF- κ B signalling factors: (A,B) NFKB1, (C,D) NFKB2, (E,F) RELA, (G,H) NFKBIA, (I,J) NFKBIB, (K,L) IKBKG and (M,N) NFKBIE. The data are shown as mean \pm standard deviation; n = 5; * p < 0.05 vs. corresponding 1g controls. The dashed vertical line separates two independent experiments..... 39

Fig. 21: Expression of the genes (A) ICAM1, (C) VCAM1, (E) SPP1 and (G) CD44 and proteins (B) ICAM-1, (D) VCAM-1, (F) OPN and (H) CD44, all of which are involved in cell adhesion. 1g: ground control; P1: parabola 1; P31: parabola 31. The data are shown as mean \pm standard deviation; * p < 0.05 vs. 1g control; ** p < 0.01 vs. 1g control..... 40

Fig. 22: The influence of VIB (V), hyper-g and iRPM-exposure on the gene expression of cell adhesion signalling factors: (A,B) ICAM1, (C,D) VCAM1, (E,F) SPP1 and (G,H) CD44. 1g: ground control; V: 2 h of vibration; 1.8g: 2 h of hyper-g. The data are shown as mean \pm standard deviation. * p < 0.05 vs. 1g control. The dashed vertical line separates two independent experiments. 41

8. Acknowledgement

I would like to thank Prof. Daniela Grimm for giving me the opportunity to do my doctoral thesis in her laboratory at the OVGU Magdeburg. During my doctoral thesis, I could participate in DLR parabolic flight and TEXUS sounding rocket missions. And I am grateful to be a part of such missions.

Special thanks to Dr. Sascha Kopp. He offered me help and guidance whenever I had a problem with my project. I express my gratitude to my fellow laboratory mates for helping me with my project and for all the fun, we had together.

Many thanks to my family who supported me through the time of my PhD study. I am happy for having them in my life.

9. Statement

Ich erkläre, dass ich die an der Medizinischen Fakultät der Otto-von-Guericke-Universität zur Promotion eingereichte Dissertation mit dem Titel:

“Influence of Mechanical Stress on Biological Processes of Human Cells”

in der Klinik für Plastische, Ästhetische und Handchirurgie ohne Hilfe durchgeführt und bei der Abfassung der Dissertation außer den genannten Hilfsmitteln keine weiteren benutzt habe.

Bei der Abfassung der Dissertation sind Rechte Dritter nicht verletzt worden.

Ich habe diese Dissertation bisher an keiner in- oder ausländischen Hochschule zur Promotion eingereicht. Ich übertrage der Medizinischen Fakultät das Recht, weitere Kopien meiner Dissertation herzustellen und zu vertreiben.

Magdeburg, den

Mohamed Zakaria Nassef

10. Curriculum Vitae

Personal information

- Address: Raiffeisenstraße 24, 39112 Magdeburg
- Phone Number: 0176 7567 7993
- Email Address: mohamed.nassef@med.ovgu.de
- Birth Date: 30th September 1989
- Nationality: Egyptian

Education

- **Education to Dr. rer. medic. in Gravitational biology and Translational Regenerative Medicine, Otto-von- Guericke-University Magdeburg**
2017 – Present, Magdeburg, Germany
- **MSc in Neurosciences, University of Bonn**
2014 – 2016, Bonn, Germany
GPA: 1.8/1.0 (very good)
- **Bachelor of Pharmaceutical Sciences, Faculty of Pharmacy, Cairo University**
2006 – 2011, Cairo, Egypt
GPA: 3.74/4.0 (Excellent) Distinction with honor

Work Experience

- **PhD candidate** / Prof. Daniela Grimm's group at the Gravitational Biology and Translational Regenerative Medicine department, Otto-von-Guericke-University Magdeburg
Jun 2017 – Present, Magdeburg, Germany
- **Thesis:** Influence of Mechanical Stress on Biological Processes of Human Cells
- **Skills:** cell culture and general handling of MCF-7, transfected MCF-7, other cell lines: MDA-MB-231, FTC-133, ML-1, RO82-W-1 and EA.hy926. RNA isolation, qPCR, protein isolation, western blot, immunocytochemistry, confocal microscopy, live-cell imaging with the FLUMIAS microscope, random positioning machine, clinostat, hypergravity experiments, Vibraplex device.

- **Conferences:** ISSR&D 2018, ISGP & ESA Life Sciences Meeting 2018, IAC 2018.
- **Achievements:** Team member of the NASA-ESA SPHEROIDS project, 29th and 31st DLR Parabolic flight campaign and the TEXUS 53 & 54 sounding rocket missions. Travel grant recipient from OVGU Magdeburg.

- **Student assistant (MSc) - Research assistant** / Prof. Neumann's group at the Institute of Reconstructive Neurobiology, Life & Brain, University of Bonn
 Jan 2016 - Sep 2016, Bonn, Germany
 Apr 2017 - Jun 2017, Bonn, Germany
- **Master's thesis:** Anti-inflammatory effect of milk oligosaccharides on mouse microglia.
- **Skills:** cell culture and general handling of ESdM cell line, RNA isolation, qPCR, flow cytometry, MTT viability assay, HPLC, ion exchange chromatography, cryostat sectioning, immunohistochemistry, confocal microscopy
- **Conferences:** Bonn Brain Meeting 2016, 2017

- **Teaching assistant** / Department of Pharmacology & Therapeutics, October 6 University
 Sep 2012 - Jul 2014, Cairo, Egypt

- **Pharmacist** / Retail Pharmacy
 Sep 2011 - Sep 2012, Cairo, Egypt

Internships

- Lab rotation, Institute of Neuropathology - supervisor Prof. Dr. Susanne Schoch, University of Bonn. **(Oct - Dec 2015, Bonn, Germany)**
Skills: molecular cloning, bacterial transformation, DNA preparation, general animal handling, mouse perfusion, vibratome brain sectioning, immunohistochemistry, fluorescent microscopy
- Lab rotation, Institute of Reconstructive Neurobiology - supervisor Prof. Dr. Harald Neumann, University of Bonn. **(Aug - Oct 2015, Bonn, Germany)**
Skills: cell culture and general handling of Hepa-1c1c7 cell line, flow cytometry
- Training in retail pharmacy. **(Jul – Sep 2010, Cairo, Egypt)**
- Clinical pharmacist, Children's Cancer Hospital (57357). **(Jul – Aug 2009, Cairo, Egypt)**

- Clinical Pharmacist, National Cancer Institute (NCI). **(Jul – Aug 2008, Cairo, Egypt)**
- Industrial pharmacist, Amoun Pharmaceutical Company. **(Jul 2007, Cairo, Egypt)**

Languages

- Arabic: Native
- English: Excellent (TOEFL C1)
- German: very good (DAF B2 certificate from OVGU Magdeburg)

Computer Skills

MS Office, ImageJ, Flowjo, IBM SPSS, Graphpad Prism

Publications

1. Sorensen, L. M.; Grimm, D.; Simonsen, U.; Kruger, M.; Nassef, M. Z.; Wehland, M.; Infanger, M. A Special Focus on Selexipag - Treatment of Pulmonary Arterial Hypertension. *Curr. Pharm. Des.* **2017**, *23* (34), 1–9. <https://doi.org/10.2174/1381612823666170908114227>.
 2. Sahana, J.*; Nassef, M. Z.*; Wehland, M.; Kopp, S.; Krüger, M.; Corydon, T. J.; Infanger, M.; Bauer, J.; Grimm, D. Decreased E-Cadherin in MCF7 Human Breast Cancer Cells Forming Multicellular Spheroids Exposed to Simulated Microgravity. *Proteomics* **2018**, *18* (13), 1800015. <https://doi.org/10.1002/pmic.201800015>.
- *both authors contributed equally to this work
3. Kopp, S.; Krüger, M.; Feldmann, S.; Oltmann, H.; Schütte, A.; Schmitz, B.; Bauer, J.; Schulz, H.; Saar, K.; Huebner, N.; Wehland, M.; **Nassef, M. Z.**; Melnik, D.; Meltendorf, S.; Infanger, M.; Grimm, D. Thyroid Cancer Cells in Space during the TEXUS-53 Sounding Rocket Mission-The THYROID Project. *Sci. Rep.* **2018**, *8* (1), 10355. <https://doi.org/10.1038/s41598-018-28695-1>.
 4. Kopp, S.; Krüger, M.; Bauer, J.; Wehland, M.; Corydon, T.; Sahana, J.; **Nassef, M.**; Melnik, D.; Bauer, T.; Schulz, H.; et al. Microgravity Affects Thyroid Cancer Cells during the TEXUS-53 Mission Stronger than Hypergravity. *Int. J. Mol. Sci.* **2018**, *19* (12), 4001. <https://doi.org/10.3390/ijms19124001>.
 5. **Nassef, M.**; Kopp, S.; Melnik, D.; Krüger, M.; Wehland, M.; Corydon, T.; Bauer, J.; Infanger, M.; Grimm, D. Alterations of the Cytoskeleton in Breast Cancer Cells during Microgravity Visualised by FLUMIAS Live-Cell Imaging. *Front. Physiol.* **2018**, *9*. <https://doi.org/10.3389/conf.fphys.2018.26.00008>.
 6. **Nassef, M. Z.**; Kopp, S.; Wehland, M.; Melnik, D.; Sahana, J.; Krüger, M.; Corydon, T. J.; Oltmann, H.; Schmitz, B.; Schütte, A.; et al. Real Microgravity Influences the Cytoskeleton and Focal Adhesions in Human Breast Cancer Cells. *Int. J. Mol. Sci.* **2019**, *20* (13), 3156. <https://doi.org/10.3390/ijms20133156>.

7. Lützenberg, R.; Wehland, M.; Solano, K.; **Nassef, M. Z.**; Bukena, C.; Melnik, D.; Kopp, S.; Bauer, J.; Krüger, M.; Riwaldt, S.; et al. Beneficial Effects of Low Frequency Vibration on Human Chondrocytes in Vitro. *Cell Physiol Biochem* **2019**, *53* (4), 623–637. <https://doi.org/10.33594/000000161>.
8. **Nassef, M. Z.**; Kopp, S.; Melnik, D.; Corydon, T. J.; Sahana, J.; Krüger, M.; Wehland, M.; Bauer, T. J.; Liemersdorf, C.; Hemmersbach, R.; et al. Short-Term Microgravity Influences Cell Adhesion in Human Breast Cancer Cells. *Int. J. Mol. Sci.* **2019**, *20* (22). <https://doi.org/10.3390/ijms20225730>.
9. Melnik, D.; Sahana, J.; Corydon, T.J.; Kopp, S.; **Nassef, M.Z.**; Wehland, M.; Infanger, M.; Grimm, D.; Krüger, M. Dexamethasone Inhibits Spheroid Formation of Thyroid Cancer Cells Exposed to Simulated Microgravity. *Cells* **2020**, *9* (2), 367. <https://doi.org/10.3390/cells9020367>.
10. Hybel, T. E.; Dietrichs, D.; Sahana, J.; Corydon, T. J.; **Nassef, M. Z.**; Wehland, M.; Krüger, M.; Magnusson, N. E.; Bauer, J.; Utpatel, K.; et al. Simulated Microgravity Influences VEGF, MAPK, and PAM Signaling in Prostate Cancer Cells. *Int. J. Mol. Sci.* **2020**, *Vol. 21, Page 1263* **2020**, *21* (4), 1263. <https://doi.org/10.3390/IJMS21041263>.

Magdeburg, den

Mohamed Zakaria Nassef

11. Appendix

11.1. Publication #1

Sahana J *, **Nassef MZ** *, Wehland M, Kopp S, Krüger M, Corydon TJ, Infanger M, Bauer J, Grimm D. Decreased E-Cadherin in MCF7 Human Breast Cancer Cells Forming Multicellular Spheroids Exposed to Simulated Microgravity. *Proteomics* 18: 1800015, 2018.

*both authors contributed equally to this work

Decreased E-Cadherin in MCF7 Human Breast Cancer Cells Forming Multicellular Spheroids Exposed to Simulated Microgravity

Jayashree Sahana, Mohamed Zakaria Nassef, Markus Wehland, Sascha Kopp, Marcus Krüger, Thomas J. Corydon, Manfred Infanger, Johann Bauer, and Daniela Grimm*

MCF7 human breast cancer cells were cultured under normal gravity (1 g) and on a random positioning machine (RPM) preventing sedimentation. After 2 weeks, adherent 1 g-control and adherent RPM cells (AD) as well as multicellular spheroids (MCS) were harvested. AD and MCS had been exposed to the RPM in the same culture flask. In a subsequent proteome analysis, the majority of the proteins detected showed similar label-free quantification (LFQ) scores in each of the respective subpopulations, but in both AD or MCS cultures, proteins were also found whose LFQs deviated at least twofold from their counterparts in the 1 g-control cells. They included the cell junction protein E-cadherin, which was diminished in MCS cells, where proteins of the E-cadherin autodegradation pathway were enhanced and c-Src (proto-oncogene tyrosine-protein kinase c-Src) was detected. Spheroid formation was prevented by inhibition of c-Src but promoted by antibodies blocking E-cadherin activity. An interaction analysis of the detected proteins that are involved in forming and regulating junctions or adhesion complexes and in E-cadherin autodegradation indicated connections between the two protein groups. This suggests that the balance of proteins that up- or downregulate E-cadherin mediates the tendency of MCF7 cells to form MCS during RPM exposure.

monolayers are exposed to conditions similar to weightlessness that prevent their sedimentation, their growth behavior is altered. While some cells remain within the monolayer, many cells detach from the bottom of a culture flask and assemble to form 3D aggregates called spheroids.^[1,2] This transition from 2D to 3D growth is accompanied by changes in a number of molecular and cellular characteristics, which may occur at the gene as well as at the gene product level. After 4 h of annulled gravity, cells begin to leave the monolayer.^[3] After 24 h, a considerable number of 3D aggregates are observed. After 7 days of RPM exposure, cells adhering to the bottom of the culture flasks can still be observed as well as floating cell aggregates, which are rounded or show cellular structures resembling the organ from which the cells are derived.^[4-7]

Cell sedimentation can be prevented by sending cells into space or by mounting culture flasks on a random positioning machine (RPM). Studying cells

in vitro under these conditions may help to advance tissue engineering techniques,^[2] to enhance learning about diseases that may affect astronauts or space tourists,^[8] or allow investigation of mechanisms of metastasis of malignant cells.^[9] Metastasis and spheroid formation under microgravity resemble each other, as

1. Introduction

Cell populations derived from human tissues such as the thyroid, the liver, the kidneys, the mammary gland, the cartilage, or the veins usually form monolayers when cultured in vitro under normal gravity conditions (1 g). If such

J. Sahana, Prof. T. J. Corydon, Prof. D. Grimm
Department of Biomedicine
Aarhus University
8000 Aarhus C, Denmark
E-mail: dgg@biomed.au.dk

M. Z. Nassef, Dr. M. Wehland, S. Kopp, Dr. M. Krüger, Prof. M. Infanger,
Prof. D. Grimm
Clinic for Plastic, Aesthetic and Hand Surgery
Otto-von-Guericke-University Magdeburg
39120 Magdeburg, Germany

Prof. T. J. Corydon,
Department of Ophthalmology
Aarhus University Hospital
8000 Aarhus C, Denmark

Dr. J. Bauer
Max-Planck Institute of Biochemistry
82152 Martinsried, Germany

Prof. D. Grimm
Gravitational Biology and Translational Regenerative Medicine, Faculty of
Medicine and Mechanical Engineering
Otto-von-Guericke-University Magdeburg
39120 Magdeburg, Germany

DOI: 10.1002/pmic.201800015

Significance Statement

Cell exposure to a random positioning machine (RPM) mimics culturing cells in Space, where human tissue cancer cells split in a population, which continues to grow as a monolayer and another one forming multicellular spheroids (MCS). Investigating the proteome of MCF7 human breast cancer cells (BCC), in this study we expand the knowledge of proteins involved in triggering cells to leave the monolayer and grow within MCS subsequently. While ISG15 appears to play a role in the stabilization of MCS of BCC, like it was suggested earlier for thyroid cancer cells, ASAP1 is associated with the formation of MCS and BCAR1 and MAPK8 are enhanced in both types of cells, when they remain in a monolayer cultured on an RPM. In addition, SRC was detected in MCS but not in AD cells, while E-cadherin content was lower in MCS than in AD cells. Anti-E-cadherin antibodies reducing E-cadherin activity favor MCS formation, and PP2, blocking the E-cadherin regulator SRC, prevents MCS formation. As several authors have found a strict correlation between E-cadherin expression and metastatic activity of cancer cells in patients, studies on tumor cells exposed to an RPM can be considered to be a suitable model for studying metastatic mechanisms *in vitro*.

in both processes, a part of an existing cell population leaves its primary site of growth and moves to another one, where it joins or builds new 3D aggregates.^[4,6] Spheroid formation has already been investigated in various types of cancer cells.^[5] Microscopic observations clearly indicate a change of intercellular contacts, as spheroid cells are in contact with other cells that surround them in a 3D structure, while the adherent monolayer cells contact neighboring cells in one plane and the bottom of the culture flask, perpendicularly. Proteome analyses indicate a number of proteins that are differentially regulated during the change of these cell–cell contacts.^[7,10–13] Regulated proteins include compounds of the extracellular matrix (ECM), of cell–cell adhesion complexes, and of apoptosis. But the exact mechanism of the transition from a 2D to a 3D kind of growth is not known yet. At the moment, it is thought that cells polarize before they leave a monolayer, but it is not sure, whether they subsequently pass through a period of lack of anchorage resembling the situation in a suspension culture.^[6]

In recent studies, we have investigated the behavior of RPM-exposed breast cancer cells. Malignant breast cancer is still widespread with 1.7 million cases in 2012 with a high death rate, and urgently needs further research studies in this field.^[6,14] Breast cancer is currently treated with several approved drugs, such as the tyrosine kinase inhibitor sorafenib, or with approved therapeutic antibodies such as bevacizumab, ramucirumab, or trastuzumab.^[15,16] However, with the current state of technology, it is difficult to eliminate all of the cancer cells in any given patient in order to achieve healing. One solution could be to learn more about the proteins involved when cancer cells leave their primary site of growth and form new cell structures at another site.^[5]

In this study, we identified proteins present in MCF7 breast cancer cells cultured under normal laboratory conditions or

exposed to an RPM.^[6] For this purpose, we applied a highly developed technique to determine a large number of cellular proteins.^[17] In 2006, early approaches to identify the proteins in breast cancer cells were undertaken.^[18,19] Later, the cellular proteins of breast cancer cells were determined focusing on special aspects, such as the differences between various breast cancer cell lines or cell clones^[20,21] or on different types of proteins such as membrane proteins, mitochondrial proteins, glycolytic enzymes, or cell cycle promoting proteins.^[22–25] In recent years, clear differences have been detected in the proteins of different breast cancer cell lines with different degrees of malignancy, and between proteins of cells derived from tumors from patients suffering from different grades of breast cancer.^[26,27] In addition, protein differences were observed in cells treated with metformin, a drug that reduces blood glucose levels and is associated with a lower incidence of cancer.^[28] In this study, we analyzed the proteins of the breast cancer cell line MCF7 and focused on quantitative differences in proteins detected in the cells of three MCF7 subpopulations, respectively. The subpopulations comprised adherent monolayer cells cultured under normal gravity (1 g-controls), as well as adherent monolayer cells (AD) and spheroid forming (multicellular spheroids [MCS]) cells, which were cultured on a RPM in the same culture flask. Evaluating these protein data, we focused on proteins involved in forming cell contacts with the cellular or noncellular environment, and on the pathways regulating these processes. We also tested the involved proteins' cell line specificity in comparison with previously investigated FTC-133 thyroid cancer cells^[13,29,30] and found two agents influencing their behavior.

2. Experimental Section

2.1. Cell Culture and Harvest

MCF7 human breast adenocarcinoma cells were purchased from Sigma-Aldrich (order no. 86012803). Cells were cultivated in RPMI 1640 medium (Life Technologies) supplemented with 10% fetal calf serum (FCS; Biochrom, S0115) and 1% penicillin/streptomycin (Biochrom, A2213) at 37 °C and 5% CO₂. One day prior to the experimental run on the RPM, cells were seeded in T25 vented cell culture flasks (Sarstedt, Numbrecht, Germany). For microscopic investigations a second experiment was performed using slide flasks (Nunc™ Lab-Tek™ Flask on Slide; Thermo Fisher Scientific). When indicated, rat monoclonal antibodies against the ectodomain of E-cadherin (5 μl mL⁻¹, DECMA-1, U3254, Sigma-Aldrich)^[31] or 5 × 10⁶ mol L⁻¹ PP2 (c-Src inhibitor, Calbiochem, San Diego, CA, USA) dissolved in DMSO were added.^[32] Before starting the run, flasks were completely filled up with medium, ensuring that no air bubbles remained, as described by Kopp, et al.^[6] After 2 weeks of culturing, the cells were harvested according to the protocol described by Bauer, et al.^[13] First, the supernatant of each T25 culture flask from the RPM cultures was collected and centrifuged at 4 °C for MCS collection. After centrifugation, the supernatant was carefully aspirated, and the MCS were collected, washed in phosphate buffered saline (PBS, Life Technologies), and either stored in liquid nitrogen or prepared for microscopy. To harvest the adherent cells from the RPM AD and 1 g cultures, the supernatant was

removed and 5 mL of ice-cold PBS was carefully added to each T25 flask after removal of the supernatant. The PBS was then aspirated and the cells were detached with a scraper. The cell suspension was collected and centrifuged at 4 °C. The PBS was discarded and the dry pellet was washed with PBS and either stored in liquid nitrogen or prepared for microscopy.

2.2. Acridine Orange/Ethidium Bromide Staining

MCF7 cells of all groups were stained with acridine orange/ethidium bromide (Molecular Probes, Darmstadt, Germany) after exposure to the RPM and their controls, respectively, as performed in previous studies.^[33] The stained MCF7 cells were immediately investigated by using a Zeiss LSM 710 confocal laser scanning microscope (Zeiss, Jena, Germany). To check for cell death, the slides were left for drying and images were taken after 5 min.

2.3. Microscopy

The cells were observed and photographed using an Axiovert 25 Microscope (Carl Zeiss Microscopy, LLC, USA) and a Canon EOS 550D camera (Canon GmbH, Krefeld, Germany).

2.4. Random Positioning Machine

A desktop RPM (Airbus Defense and Space, former Dutch Space, Leiden, The Netherlands) was located in a standard incubator at 37 °C and 5% CO₂. The RPM was operated in real random mode with random directions and intervals and a maximum speed of 12.5 revolutions per minute. Sample flasks to be tested were placed onto the middle frame with a maximal distance of 7 cm from the center of rotation allowing a theoretical μ g quality of between 10⁻⁴ and 10⁻² g. The method has been extensively studied and described in other publications.^[34,35] Static controls were placed beside the RPM in the same incubator.

2.5. RNA and Protein Isolation and Quantitative Real-Time PCR

RNA and protein isolation were performed according to routine protocols^[4,36] using the AllPrep RNA/Protein Kit (Qiagen GmbH, Hilden, Germany) following the manufacturer's instructions. Biomolecule concentration determination was performed spectrophotometrically using an Ultrospec 2100 pro (Amersham Biosciences, Amersham, Great Britain). Complementary DNA was produced using the First Strand cDNA Synthesis Kit (Thermo Scientific, Waltham, Massachusetts, USA) following the manufacturer's instructions. Quantitative real-time PCR (qPCR) was performed using the SYBR Select Master Mix (Applied Biosystems, Darmstadt, Germany) and the 7500 Real-Time PCR System (Applied Biosystems) to determine the expression levels of *BCAR1*, *MAPK8* (*JNK1*), and *CDH1* (*E-cadherin*) genes. Specific primers were designed to span exon–exon boundaries and to have a T_m of 60 °C using Primer Express software (Applied Biosystems), and were synthesized by TIB Molbiol (Berlin,

Germany). Samples were measured in triplicate and were normalized to the housekeeper 18S rRNA.

The sequences of the primers used for qPCR were

BCAR1-F: CCAAGATGTCCGTGCCTATGAA; BCAR1-R: TG-GCAGGCATGTTCTGTCTT; CDH1-F: GCTGGACCGAGAGA-GTTTCC; CDH1-R: CAGCTGTTGCTGTTGTGCTT; MAPK8-F: TCTCCTTAGGTGCAGCAGTG; MAPK8-R: CAGAGGCAAAGTCGGATCT; as well as

18S-rRNA-F: GGAGCCTGCGGCTTAATTT; 18S-rRNA-R: CA-ACTAAGAACGGCCATGCA for the housekeeper gene. All sequences are given in the 5'-3' direction.

The comparative threshold cycle ($\Delta\Delta$ CT) method was used for relative quantification of transcription levels, with 1 g set as 100%.

2.6. Mass Spectrometry

Cells were lysed in a buffer containing 6 M guanidinium hydrochloride, 20 mM TCEP (tris(2-carboxyethyl)phosphine), and 40 mM chloroacetamide in 25 mM Tris pH 8.0. Lysis buffer pre-heated to 95 °C was added to the cells and the mixture was sonicated using a Bioruptor plus water bath sonicator (Diagnode, Seraing, Belgium). The lysates were again heated to 95 °C for 2 min followed by one more sonication at the maximum power setting for ten cycles. Following complete lysis, the sample was diluted tenfold with 25 mM Tris pH 8.0 and digested overnight at 37 °C with endoproteinase lysC (Wako Chemicals GmbH, Neuss, Germany) and mass spectrometry grade trypsin (V511, Promega) at a 1:50 enzyme:protein ratio. The digested peptides were then purified and concentrated on three plugged SDB-XC StageTips.^[37]

For the liquid chromatography, mass spectrometry analysis of about 2 μ g of peptides were loaded onto a 50 cm, 75 μ m I.D. column packed with 1.9 μ m C18 beads (Dr Maisch GmbH, Ammerbuch, Germany) using a Thermo EASY-nLC 1200 system (Thermo Scientific, Waltham, USA). The peptides were separated over a 215 min gradient with buffer A (0.1% formic acid) and buffer B (0.1% formic acid and 80% acetonitrile). The LC column was maintained at a constant temperature of 60 °C using a column oven (Sonation, Biberach, Germany). The peptides eluting from the column were directly sprayed into a Q Exactive HF mass spectrometer (Thermo Scientific) via a nano-electrospray ionization source (Thermo Scientific).^[38]

The mass spectrometer was operated in a data-dependent top 15 mode. Survey scans and fragmentation scans were acquired at resolution of 60 000 and 15 000, respectively ($m/z = 200$). Fragmentation was performed on precursors isolated within a window of 1.4 m/z with a normalized collision energy setting of 27.

Raw data from the mass spectrometer were processed using the MaxQuant computational proteomics platform version 1.5.7.9^[39] using the standard parameters. Relative protein quantification analysis was performed using the label-free quantification (LFQ) algorithm as described elsewhere.^[40]

2.7. Western Blot Analysis

Western blot analysis, gel electrophoresis, trans-blotting, and densitometry were carried out following routine protocols as

described previously.^[12] Twenty microliters of lysate per sample containing $2 \mu\text{g } \mu\text{L}^{-1}$ protein were loaded onto SDS-Polyacrylamide gels. A total number of six samples per cell population plus one positive control CX+ were analyzed after 14 days of culturing. Primary antibodies were applied against BCAR1 (Abcam, dilution 1:1000), MAPK8 (Cell Signaling, dilution 1:1000), and E-cadherin (Abcam, dilution 1:1000). HRP-linked secondary antibody was used at a dilution of 1:2000 (Dako Denmark A/S). A final analysis was performed in a Clarity Western ECL Substrate (Bio Rad, Hercules, CA, USA). Ponceau S red staining was used as an alternative to housekeeping genes as loading controls. The membranes were analyzed using ImageJ software (U.S. National Institutes of Health, Bethesda, MD, USA; <http://rsb.info.nih.gov/ij/>), for densitometric quantification of the bands. Ponceau S was evaluated according to Bauer et al.^[13]

2.8. Pathway Analysis

To investigate and visualize localizations and interactions of proteins, we entered relevant UniProtKB entry numbers into the Pathway Studio v.11 software (Elsevier Research Solutions, Amsterdam, The Netherlands).^[13,30] To estimate the belonging of the detected proteins to known pathways, the Reactome pathway

database was searched, also entering relevant UniProtKB entry numbers.^[41]

2.9. Statistical Evaluation

Statistical evaluation was performed using SPSS 15.0 (SPSS, Inc., Chicago, IL, USA). The Mann–Whitney *U* test was used to compare the 1 *g* and RPM conditions, as well as AD cells and MCS cells. All data are presented as means \pm standard deviation (SD) with a significance level of $p < 0.05$.

3. Results and Discussion

3.1. Harvest of Three Different MCF7 Subpopulations

After 2 weeks of incubation, three types of cells from the MCF7 cell line were harvested (Figure 1A,B). 1 *g*-control cells were grown under normal gravity and remained adherent until the day of harvest (Figure 1A). These cells were passaged once on the seventh day after a 1 to 5 dilution. Adherent cells and cells growing in MCS had been incubated on an RPM in the same culture flasks without any passaging (Figure 1B). Under the same culture conditions, the uniform MCF7 cell population had split in two different types of cells, which we call subpopulations in this

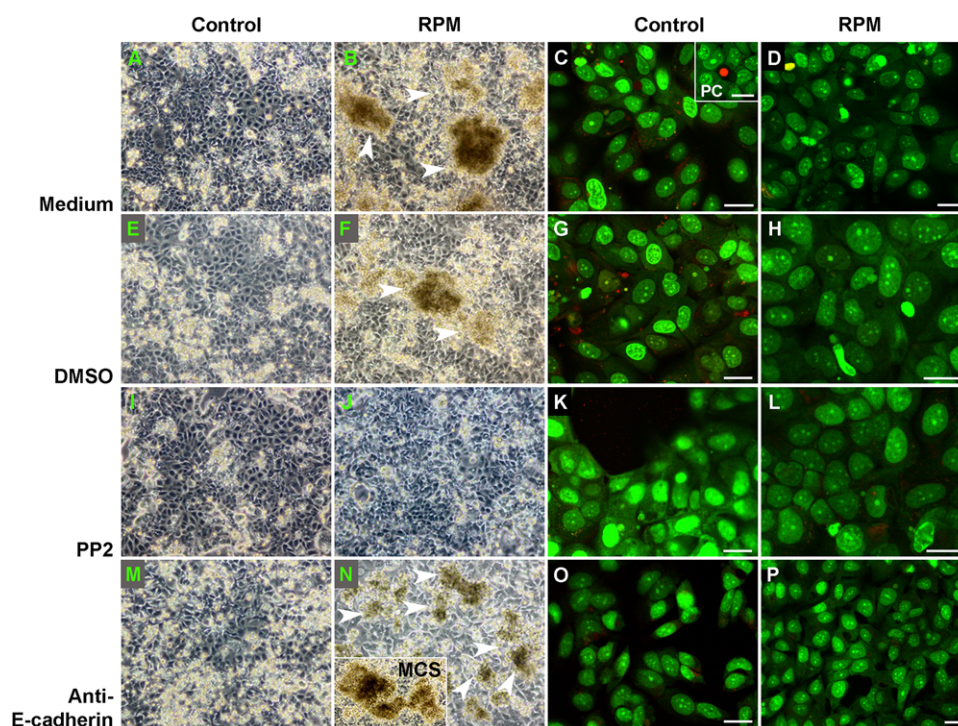


Figure 1. Morphology and viability of MCF7 cells incubated at 1 *g* (control) or on the RPM. Left side of the figure: phase contrast microscopy of MCF7 cells incubated at 1 *g* (A, E, I, M) or on the RPM (B, F, J, N) for 14 days. Representative examples of spheroids formed on the RPM are marked by white arrowheads (B, F, N). J) Notably, no spheroids were formed on the RPM in the presence of the Src inhibitor PP2, N) whereas anti-E-cadherin (DECMA-1) stimulated the formation of spheroids. Insert in (N) shows an example of a large spheroid observed in the presence of anti-E-cadherin. Right side of figure: acridine orange/ethidium bromide staining revealed a green fluorescence in all cells of all groups (C, D, G, H, K, L, O, P) which indicates viability of MCF7 cells incubated on the RPM or at static 1 *g*-conditions. Insert in (C) represents positive control (PC) of the acridine orange/ethidium bromide assay after approximately 5 min incubation. Scale bars 20 μm .

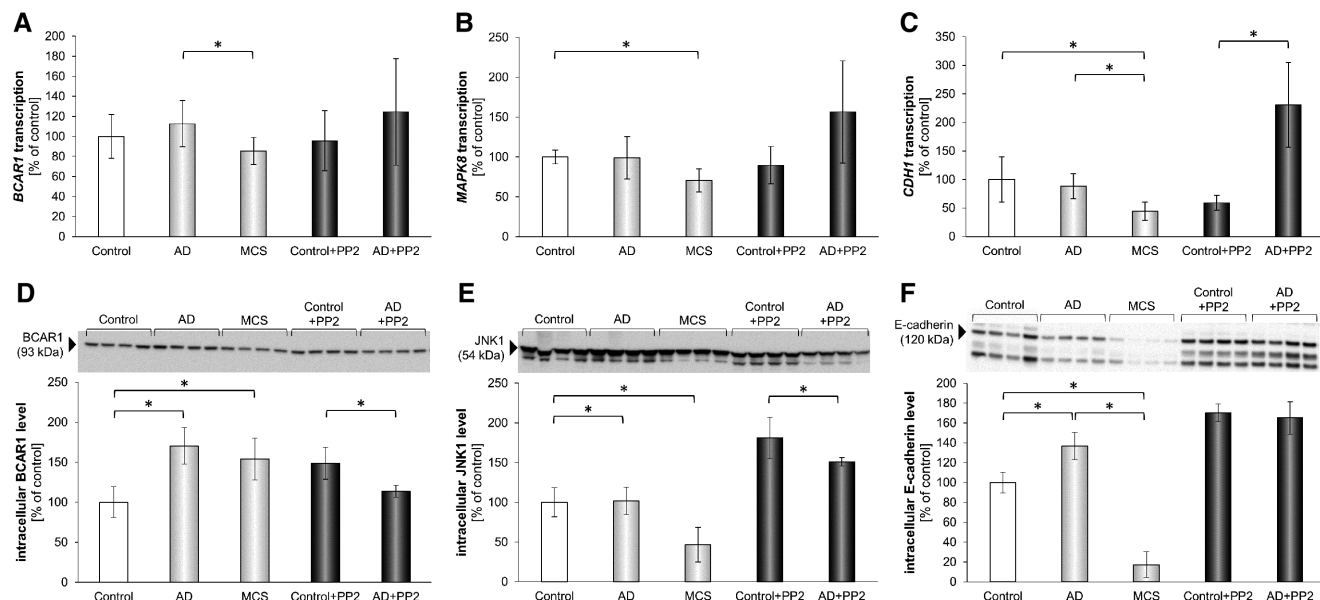


Figure 2. Relative expression of (A) *BCAR1*, (B) *MAPK8*, and (C) *CDH1*. Transcription was analyzed after 2 weeks at 1 g conditions or on the RPM in absence and presence of PP2. All values are given as mean \pm standard deviation. Western blot analysis of (D) *BCAR1*, (E) *JNK1*, and (F) *E-cadherin* proteins. Intracellular levels were determined after 2 weeks of RPM exposure in the absence and presence of PP2. * $p < 0.05$. AD, adherent cells; MCS, multicellular spheroids, after RPM-exposure.

manuscript. The MCS comprised cells that had detached from the bottom of the culture flask and formed 3D aggregates, while the AD cells had remained adherent until harvest.

3.2. Proteome Analysis

After harvest, proteins present in the various subpopulations of MCF7 cells were identified by mass spectrometry. The analysis revealed 6580 different proteins in 1 g-control cells, 6464 proteins in AD cells, and 6261 in MCS cells. These proteins, which together represented 6968 unique human proteins, could be identified with LFQ scores above 10^7 .^[40] They were evaluated with regard to their LFQ values detectable in the different subpopulations of MCF7 cells, respectively. In a first approach, we focused on proteins involved in the cell contacts with their environment, that is, with neighboring cells or with the bottom of the culture flasks and compared the current results with recent observations made on thyroid cancer cells cultivated for 3 days according to an equal protocol.^[13,42–44]

Arf-GAP with SH3 domain, ANK repeat, and PH domain-containing protein 1 (ASAP1), which had been found in thyroid MCS and control cells, but not in thyroid AD cells,^[13] was detected in MCF7 control cells with an LFQ value of 14.68×10^8 , in AD cells with a score of 19×10^8 , and in MCS cells with a 22.5×10^8 LFQ score. Breast cancer anti-estrogen resistance protein 1 (BCAR1) and mitogen activated protein kinase 8 (MAPK8), which were absent in thyroid MCS cells and present in thyroid AD and control cells,^[13] were detected with LFQ values for BCAR1 of 10.01×10^8 (1 g), 9.3×10^8 (AD), and 7.71×10^8 (MCS) and with LFQ scores for MAPK8 of 2.1×10^8 (1 g), 2.1×10^8 (AD), and 1.75×10^8 (MCS). Increased ASAP1 and simultaneously reduced BCAR1 and MAPK8 in MCS suggested that these proteins

were changed in MCF7 cells after 2 weeks in a similar manner to the same proteins in thyroid cells switching from a 2D to a 3D growth during the first 72 h of culturing on the RPM.^[13] This finding suggests that ASAP1 is associated with the formation of 3D aggregates of thyroid and breast cancer cells, while BCAR1 and MAPK8 are enhanced in both types of cells when their cells remain in a monolayer on a RPM. In order to verify the LFQ values, we performed western blot (WB) analyses. **Figure 2D,E** indicates a higher concentration of BCAR1 and MAPK8 (JNK1) in AD than in MCS cells. The protein changes correspond rather well to the LFQ values as well as to the corresponding mRNA expression in MCS cells (Figure 2A,B).

Comparing these 2 week long experiments with the recent study on 3 day old spheroids,^[13] it has to be considered that spheroid formation progresses in a time-dependent manner.^[3,45] Therefore, the current results were also compared with those obtained when FTC-133 thyroid cells were sent into space and incubated for more than 10 days, during which most of the cells formed spheroids.^[46,47] At that time, we found that the interferon stimulated gene 15 (*ISG15*) was the highest upregulated of all genes investigated with the microarray technology,^[29,46] while in the analysis of 3 day old FTC-133 spheroids, the *ISG15* protein was found to be reduced in MCS.^[13] In the current experiment on MCF7 cells, we again detected *ISG15* protein. It was enhanced in MCS cells with an LFQ value of 126.1×10^8 , when compared with AD (LFQ = 19.7×10^8) and 1 g cells (LFQ = 62.4×10^8). The role of *ISG15* protein in spheroid formation is as yet unknown. The protein is normally induced by interferon and modifies a number of cellular proteins co-translationally by ISGylation. A proteome analysis has revealed *ISG15* target proteins, including proteins involved in cell structure and motility.^[48] The time course of its accumulation suggests a role of *ISG15* in the stabilization rather than in the formation of the spheroids.^[13,29,46]

Table 1. Number of proteins detected in AD and MCS cells with quantitative changes more than twofold compared with the corresponding proteins in 1 g-control cells. The number of proteins indicated in the right column was used for searching pathways in the Reactome database.

Proteins detected in A	Proteins of A compared with equal proteins in B	Twofold enhanced A versus B	Detected in A, not detected in B	Used for searching Reactome database
AD cells (group 1)	1 g cells	359	97	456
1 g cells (group 2)	AD cells	446	213	659
MCS cells (group 3)	1 g cells	458	109	567
1 g cells (group 4)	MCS cells	664	427	1091

In order to focus on additional proteins that could have an influence on the behavior of MCF7 cells exposed to the RPM, we compared the quantities of the various proteins found in each subpopulation. The majority of the human proteins detected in AD and MCS cells indicated LFQ values that were changed less than twofold in either direction compared with the corresponding proteins in 1 g-control cells. Only LFQ values for 359 proteins were found at levels twofold higher in AD cells than in 1 g cells, while 446 proteins were found to be twofold higher in 1 g cells than in AD cells. Ninety-seven of the AD cell proteins were not detected in 1 g cells, but 213 of the 1 g cell proteins were not detected in AD cells. Furthermore, LFQ values for 458 proteins were detected being twofold higher in MCS cells than in 1 g cells and 664 proteins were found to be twofold higher in 1 g cells than in MCS cells. One hundred and nine of the MCS cell proteins were not detected in 1 g cells, while 427 proteins of the 1 g cells were not seen in MCS cells (Table 1).

3.3. Pathway Identification

As shown in Figure 1, the way that cells contact their neighbors or the bottom of the culture flask is different in MCS and AD cells, although the gravitational forces acting on the cells are similar. Attachment of cells to their solid environment is either mediated by ECM proteins or occurs by direct cell–cell interaction via various types of so-called junctions.^[49] Only three of the more than 300 ECM proteins were detected in MCS formed on the RPM with at least twofold enhanced LFQ values (Table 2). Therefore, we evaluated the junction proteins in more detail. Each of these junctions is linked to a set of proteins forming signaling pathways, which may be retrieved from the Reactome database.^[41] Therefore, we searched the Reactome database using either all of the 6968 different proteins identified in this analysis or, for comparison, proteins of each of the four groups indicated in Table 1, right hand column individually. Subsequently, we depicted those proteins in our analysis, that were included at least once in the pathways R-HSA-196025, R-HSA-191650, R-HSA-191647, R-HSA-157858, R-HSA-190828, R-HSA-190861, R-HSA-420029, R-HSA-418990, R-HSA-421270, R-HSA-446728, and/or R-HSA-190873, because the proteins comprising these pathways are involved in the formation, regulation, or maintenance of junctions.^[41]

When the whole set of detected proteins was matched against the Reactome database, 60 relevant proteins were found. Nineteen of these proteins were also recognized, when the four groups of proteins strongly affected by RPM exposure (Table 1) were matched individually. Fourteen were found to belong to

junction-related pathways (Table 2), when the proteins of group 4 indicated in Table 1 were matched against Reactome. The LFQs of these proteins were at least halved in MCS cells compared with the 1 g-controls. Another five proteins were identified when the proteins of group 2 (Table 1) were used to search the Reactome database (Table 2). Three of them were present in MCS and control cells at similar concentrations but were not detectable in AD cells. Only the focal adhesion protein beta-parvin (PARVB), which was not detectable in AD cells, was more than doubled in MCS cells compared with 1 g-control cells.^[50] Taken together, MCS cells appear to contain smaller amounts of distinct proteins that form and regulate junctions than control cells (Table 2).

E-cadherin is the most abundant of the 14 proteins detected in MCS cells with LFQ scores less than half of those in 1 g-controls (Table 2). Its decrease in MCS was also shown by WB analysis (Figure 2F) and corresponds with a slight reduction of mRNA expression (Figure 2C). E-cadherin is a multi-domain membrane protein. Its extracellular domain interacts with the same domain of another E-cadherin molecule belonging to another cell in a calcium-dependent manner establishing connections between neighboring cells.^[51] Its intracellular domains are connected to the cytoskeleton and its stability is regulated by catenin D1.^[52] Associating with the juxtamembrane domain of E-cadherin, catenin D1 affects cell–cell adhesion.^[53] Catenin D1 was also detected in our preceding study on thyroid cancer cells. At that time, the catenin D1 content in MCS cells was reduced by 30% compared with 1 g-control cells. E-cadherin had not been detected in one of our preceding proteome analyses performed on thyroid cancer cells and endothelial cells.^[7,12,13] According to the literature, E-cadherin is under the direct influence of proteins, which we earlier proposed to be involved in the regulation of MCS formation.^[13] According to the literature, E-cadherin is upregulated by ISG15 as well as by CLDN3 and FERMT2 shown in Table 2,^[54–56] which were all detected in MCS cells with higher LFQs than in controls. In addition, E-cadherin is downregulated by MAPK8 and BCAR1, which are accumulated to a higher level in AD than in MCS cells, as well as by PSMD10 and SRC, which are absent in AD but present in MCS cells (Table 2).^[57–60] As our measurements clearly indicated a reduction of E-cadherin in MCS cells, it may be concluded that the proteins effecting lower amounts of E-cadherin are dominant.

The downregulation of E-cadherin could also be supported by members of the so-called “Autodegradation of Cdh1 by Cdh1:APC/C” (R-HSA-174084) pathway. They were identified when the Reactome database was searched using the proteins of group 3 (doubled in the MCS cells compared with the 1 g-controls) indicated in Table 1. The R-HSA-174084 pathway includes 63 proteins, of which 54 were found in the present

Table 2. Accumulated ECM proteins and proteins belonging either to junction-related pathways (upper part) or to the CDH1 autodegradation pathway (lower part).

Protein ID	Protein name	Σ LFQ ($\cdot 10^8$) of four independent experiments		
		1 g-control	AD	MCS
P02751	Fibronectin	5.8	0.6	196
P23142	Fibulin-1	0.62	0.19	13.9
P39060	Collagen alpha-1(XVIII) chain	13.8	22	32.8
P12830	Cadherin-1 (E-cadherin)	163	134	76
O60716	Catenin delta-1	158	158	77
P09497	Clathrin light chain B	79.7	60.9	28
P16144	Integrin beta 4	29.5	24.6	12.5
O15551	Claudin-3	12.6	3.15	1.8
Q96AC1	Fermitin family homolog 2	8.43	5.79	3.52
P15151	Poliovirus receptor	6.42	8.98	1.16
Q03001	Dystonin	5.35	4.97	1.42
Q96NY8	Nectin-4	5.06	7.87	2.04
P53675	Clathrin heavy chain 2	4.42	1.1	1.38
P22223	Cadherin-3	1.08	1.56	0.16
P56749	Claudin-12	0.71	0.79	0.18
Q9BY67	Cell adhesion molecule 1	3.4	2.04	n.d.
E9PEQ4	Dynammin-2	1.05	1.54	n.d.
Q7Z5N4	Protein sidekick-1	2.05	0.57	1.6
P12931	Proto-oncogene tyrosine-protein kinase Src	1.45	n.d.	1.49
Q3ZCM7	Tubulin beta-8 chain	1.74	n.d.	1.87
P48509	CD151 antigen; tetraspanin	0.98	n.d.	0.99
Q9HBI1	Beta-parvin	0.07	n.d.	1.48
P25788	Proteasome subunit alpha type-3	17.5	20.7	35.4
P60900	Proteasome subunit alpha type-6	10.1	7.88	34.6
O75832	26S proteasome non-ATPase regulatory subunit 10	5.7	4.02	13.5
P49720	Proteasome subunit beta type-3	4.2	2.48	10
Q9UJX3	Anaphase-promoting complex subunit 7	3.2	1.44	8.1
P51668	Ubiquitin-conjugating enzyme E2 D1	n.d.	n.d.	4.68
P40306	Proteasome subunit beta type-10	0.26	n.d.	2.43
Q13042	Cell division cycle protein 16 homolog	0.53	1.61	2.42
Q9UM13	Anaphase-promoting complex subunit 10	0.34	n.d.	1.73
Q9UJX2	Cell division cycle protein 23 homolog	4.56	1.92	6.03
P28070	Proteasome subunit beta type-4	3.49	7.45	6.16

analysis. Nine of the 54 proteins belonging to the pathway were twofold higher in MCS cells compared with 1 g cells (Table 2, lower part). Another two proteins (Q9UJX2, P28070) belonging to the E-cadherin autodegradation pathway were detected when proteins of group 1 and group 2 (Table 1) were used to search for pathways. These proteins were enhanced by 50% in MCS cells compared with 1 g-controls (Table 2). The R-HSA-174084 pathway comprises mainly proteasomes, ubiquitin, and cell cycle proteins including CDC23, CDC16, AnaPC10, and AnaPC7 (Table 2). In order to elucidate how the proteins of this pathway could diminish cellular E-cadherin, we made a closer examination of the interaction of the 60 junction-related proteins detected with the E-cadherin regulator proteins described above and with the R-HSA-174084

pathway proteins applying Pathway Studio.^[30] A direct link between the CDC23/CDC16/Anapc7 and E-cadherin has been described for *Caenorhabditis elegans*.^[61] However, the influence of the mentioned proteins appears to be mediated via the additional proteins CDC27, AnaPC2, and UBE2C, which were detected in this analysis with very similar LFQ values in all three MCF7 subpopulations (**Figure 3**). The CDC16 and CDC23 peptides assemble with CDC27^[62] forming a sub-complex, which represents about 50% of the molecular mass of the whole APC-complex and bears a great a number of phosphorylation sites.^[63] The pattern of phosphorylation of these sites has an influence on the activity of the complex.^[64] CDC27 is required for UBE2C promoter activity^[65] and UBE2C can suppress the expression of E-cadherin.^[66] Since E-cadherin was diminished in MCS, we

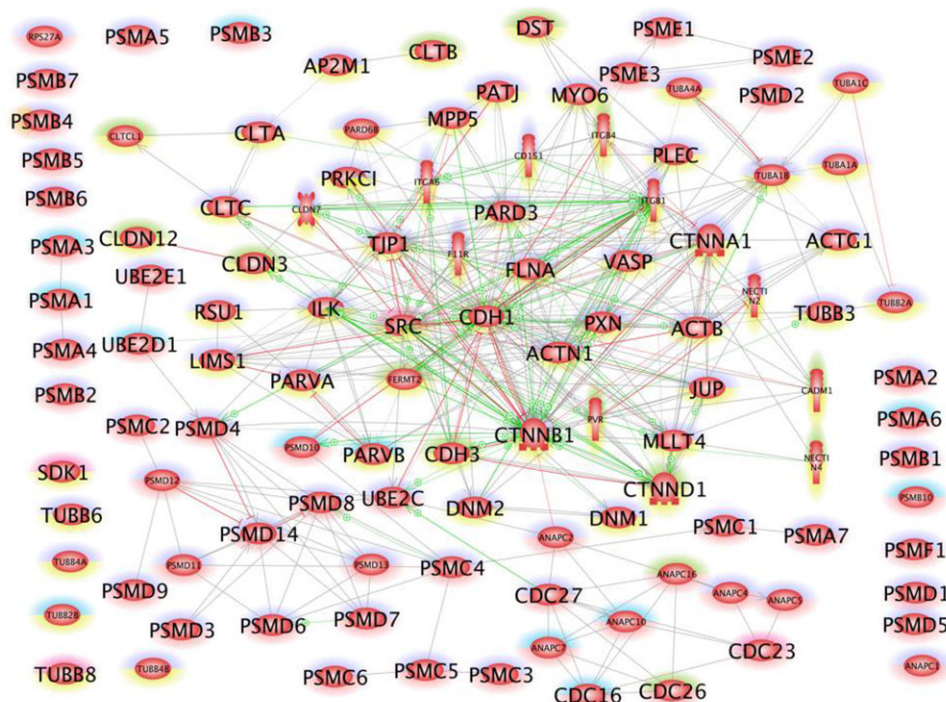


Figure 3. Pathway studio analysis of detected proteins involved in the formation and regulation of junctions and in CDH1 autodegradation. The belonging to the group of proteins involved in the formation and regulation of junctions is indicated by a yellow colored lower half-rim around the protein symbols, while the belonging to the group of proteins of the CDH1 autodegradation pathway is indicated by a red colored lower half-rim around the protein symbols. Blue upper half-rims indicate upregulation, green upper half-rims indicate downregulation, and violet upper half-rims show unregulated proteins. Regulation means that the LFQ of a protein in MCS is at least twofold enhanced or diminished as compared to controls. Grey, green, and red lines or arrows show the type of interaction. Green lines or arrows indicate supporting and red ones indicate inhibiting type of interaction. Grey lines and arrows show that an interaction is described but not yet clearly defined. The interactions are shown on the gene and gene product levels.

concluded that E-cadherin activity could counteract MCS formation. In order to prove this hypothesis, we performed cultivation experiments according to the same protocol as described for the proteome analysis but added anti-E-cadherin function-blocking antibodies or PP2, which blocks c-Src, a non-receptor tyrosine kinase that has been reported to inhibit the surface expression and function of E-cadherin^[32] (Figure 1), to the culture medium. Microscopic analyses of the cultured cells show that the anti-E-cadherin antibodies promoted MCS formation (Figure 1M,N), while PP2 inhibited this process (Figure 1I,J). Simultaneously, PP2 enhanced MAPK8 and E-cadherin slightly in 1 g-controls and AD cells (Figure 2E,F). A significant upregulation was found for the *CDH1* gene of AD (Figure 2C). Addition of DMSO, the solvent of PP2, had no effect (Figure 1E,F). In all flasks, the cells remained viable, as demonstrated by acridine orange/ethidium bromide staining and shown by the green fluorescence in Figure 1C, D,G,H,K,L,O,P.

4. Concluding Remarks

Biological experiments supported the central role of E-cadherin in spheroid formation as it was concluded from the proteome analysis. A further study of E-cadherin regulation is important

because several authors have found a strict correlation between E-cadherin expression and metastatic activity of cancer cells.^[67–69] It is of interest to investigate the mechanism of E-cadherin activity in cells exposed to the microgravity in order to see if it depends on the level of E-cadherin expression^[70] or if post-translational modifications such as phosphorylation play an additive role. Studies of cells changing their growth behavior under RPM exposure, revealed again to be a very suitable model to promote research on the metastatic activity of cancer cells in Earth-bound patients. It allows to combine biological and biochemical experiments to address questions on the mechanisms that enable the cells to leave a monolayer and to survive a possible anchorage free period.^[71–75] As demonstrated in this study, the application of immunological or chemical agents will be of great help for future investigations on these questions.

Acknowledgements

J.S. and M.Z.N. contributed equally to this work. This study was supported by the German Space Agency DLR (D.G.) (BMW grant 50WB1524), and Aarhus University, Denmark (D.G.). We thank Dr. Nagarjuna Nagaraj and the members of the biochemistry core facility at the Max-Planck Institute of Biochemistry for performing proteomic sample preparation and measurements. D.G. and J.B. designed the experiment. J.S. and M.Z.N. executed the RPM experiments, collected the material, and performed the western

blot analyses. S.K., M.Z.N., and M.K. performed qrtPCR analyses. T.J.C. performed the viability tests. J.B. performed the pathway analyses. J.B., J.S., M.W., and D.G. wrote the manuscript. M.I. and D.G. contributed reagents, materials, and analysis tools. All authors reviewed the manuscript.

Conflict of Interest

The authors declare no conflict of interest.

Keywords

cell interaction, ISG15, proteome data, Reactome, signaling pathways, simulated microgravity

Received: January 12, 2018
Revised: April 27, 2018
Published online: May 21, 2018

- [1] J. Pietsch, J. Bauer, M. Egli, M. Infanger, P. Wise, C. Ulbrich, D. Grimm, *Curr. Mol. Med.* **2011**, *11*, 350.
- [2] D. Grimm, M. Wehland, J. Pietsch, G. Aleshcheva, P. Wise, J. van Loon, C. Ulbrich, N. E. Magnusson, M. Infanger, J. Bauer, *Tissue Eng. Part B Rev.* **2014**, *20*, 555.
- [3] E. Warnke, J. Pietsch, M. Wehland, J. Bauer, M. Infanger, M. Gorog, R. Hemmersbach, M. Braun, X. Ma, J. Sahana, D. Grimm, *Cell Commun. Signal.* **2014**, *12*, 32.
- [4] S. Kopp, E. Warnke, M. Wehland, G. Aleshcheva, N. E. Magnusson, R. Hemmersbach, T. J. Corydon, J. Bauer, M. Infanger, D. Grimm, *Sci. Rep.* **2015**, *5*, 16691.
- [5] D. Grimm, J. Pietsch, M. Wehland, P. Richter, S. M. Strauch, M. Lebert, N. E. Magnusson, P. Wise, J. Bauer, *Expert Rev. Proteomics* **2014**, *11*, 465.
- [6] S. Kopp, L. Slumstrup, T. J. Corydon, J. Sahana, G. Aleshcheva, T. Islam, N. E. Magnusson, M. Wehland, J. Bauer, M. Infanger, D. Grimm, *Sci. Rep.* **2016**, *6*, 26887.
- [7] X. Ma, A. Sickmann, J. Pietsch, R. Wildgruber, G. Weber, M. Infanger, J. Bauer, D. Grimm, *Proteomics* **2014**, *14*, 689.
- [8] R. J. White, M. Averner, *Nature* **2001**, *409*, 1115.
- [9] J. L. Becker, G. R. Souza, *Nat. Rev. Cancer* **2013**, *13*, 315.
- [10] D. Grimm, J. Bauer, P. Kossmehl, M. Shakibaei, J. Schoberger, H. Pickenhahn, G. Schulze-Tanzil, R. Vetter, C. Eilles, M. Paul, A. Cogoli, *FASEB J.* **2002**, *16*, 604.
- [11] J. Pietsch, R. Kussian, A. Sickmann, J. Bauer, G. Weber, M. Nissum, K. Westphal, M. Egli, J. Grosse, J. Schonberger, R. Wildgruber, M. Infanger, D. Grimm, *Proteomics* **2010**, *10*, 904.
- [12] J. Pietsch, J. Bauer, G. Weber, M. Nissum, K. Westphal, M. Egli, J. Grosse, J. Schönberger, C. Eilles, M. Infanger, D. Grimm, *Microgravity Sci. Technol.* **2011**, *23*, 381.
- [13] J. Bauer, S. Kopp, E. M. Schlagberger, J. Grosse, J. Sahana, S. Riwaldt, M. Wehland, R. Luetzenberg, M. Infanger, D. Grimm, *Int. J. Mol. Sci.* **2017**, *18*, 546.
- [14] J. Ferlay, I. Soerjomataram, R. Dikshit, S. Eser, C. Mathers, M. Rebelo, D. M. Parkin, D. Forman, F. Bray, *Int. J. Cancer* **2015**, *136*, E359.
- [15] D. Grimm, M. Wehland, J. Pietsch, M. Infanger, J. Bauer, *Curr. Pharm. Des.* **2011**, *17*, 272.
- [16] M. Wehland, J. Bauer, M. Infanger, D. Grimm, *Curr. Pharm. Des.* **2012**, *18*, 4244.
- [17] R. Aebersold, M. Mann, *Nature* **2016**, *537*, 347.
- [18] H. A. Sarvaiya, J. H. Yoon, I. M. Lazar, *Rapid Commun. Mass Spectrom.* **2006**, *20*, 3039.
- [19] J. Hardouin, L. Canelle, C. Vlieghe, J.-P. Lasserre, M. Caron, R. Joubert-Caron, *Cancer Genomics Proteomics* **2006**, *3*, 355.
- [20] S. Nie, S. P. McDermott, Y. Deol, Z. Tan, M. S. Wicha, D. M. Lubman, *Proteomics* **2015**, *15*, 3772.
- [21] A. Aka, S. X. Lin, *PLoS One* **2012**, *7*, e31532.
- [22] C. Pionneau, L. Canelle, J. Bousquet, J. Hardouin, J. Bigeard, M. Caron, R. Joubert-Caron, *Cancer Genomics Proteomics* **2005**, *2*, 199.
- [23] R. Lamb, H. Harrison, J. Hulit, D. L. Smith, M. P. Lisanti, F. Sotgia, *Oncotarget* **2014**, *5*, 11029.
- [24] J. P. Murphy, D. M. Pinto, *J. Proteome. Res.* **2011**, *10*, 604.
- [25] M. J. Tenga, I. M. Lazar, *Proteomics* **2013**, *13*, 48.
- [26] T. Geiger, S. F. Madden, W. M. Gallagher, J. Cox, M. Mann, *Cancer Res.* **2012**, *72*, 2428.
- [27] S. Tyanova, R. Albrechtsen, P. Kronqvist, J. Cox, M. Mann, T. Geiger, *Nat. Commun.* **2016**, *7*, 10259.
- [28] F. Sacco, A. Silvestri, D. Posca, S. Pirro, P. F. Gherardini, L. Castagnoli, M. Mann, G. Cesareni, *Cell Syst.* **2016**, *2*, 159.
- [29] J. Bauer, M. Wehland, J. Pietsch, A. Sickmann, G. Weber, D. Grimm, *Microgravity Sci. Technol.* **2016**, *28*, 357.
- [30] J. Bauer, M. Bussen, P. Wise, M. Wehland, S. Schneider, D. Grimm, *Expert Rev. Proteomics* **2016**, *13*, 697.
- [31] X. Qian, T. Karpova, A. M. Sheppard, J. McNally, D. R. Lowy, *EMBO J.* **2004**, *23*, 1739.
- [32] P. Fan, F. A. Agboke, R. E. McDaniel, E. E. Sweeney, X. Zou, K. Creswell, V. C. Jordan, *Eur. J. Cancer* **2014**, *50*, 457.
- [33] S. Kopp, J. Sahana, T. Islam, A. G. Petersen, J. Bauer, T. J. Corydon, H. Schulz, K. Saar, N. Huebner, L. Slumstrup, S. Riwaldt, M. Wehland, M. Infanger, R. Luetzenberg, D. Grimm, *Sci. Rep.* **2018**, *8*, 921.
- [34] A. G. Borst, J. J. W. A. van Loon, *Microgravity Sci. Technol.* **2008**, *21*, 287.
- [35] E. Warnke, S. Kopp, M. Wehland, R. Hemmersbach, J. Bauer, J. Pietsch, M. Infanger, D. Grimm, *Microgravity Sci. Technol.* **2016**, *28*, 247.
- [36] E. Caló, V. V. Khutoryanskiy, *Eur. Polym. J.* **2015**, *65*, 252.
- [37] J. Rappsilber, M. Mann, Y. Ishihama, *Nat. Protoc.* **2007**, *2*, 1896.
- [38] N. Nagaraj, N. A. Kulak, J. Cox, N. Neuhauser, K. Mayr, O. Hoerning, O. Vorm, M. Mann, *Mol. Cell. Proteomics* **2012**, *11*, M111.013722.
- [39] J. Cox, M. Mann, *Nat. Biotechnol.* **2008**, *26*, 1367.
- [40] J. Cox, M. Y. Hein, C. A. Luber, I. Paron, N. Nagaraj, M. Mann, *Mol. Cell. Proteomics* **2014**, *13*, 2513.
- [41] M. Milacic, R. Haw, K. Rothfels, G. Wu, D. Croft, H. Hermjakob, P. D'Eustachio, L. Stein, *Cancers* **2012**, *4*, 1180.
- [42] J. Pietsch, A. Sickmann, G. Weber, J. Bauer, M. Egli, R. Wildgruber, M. Infanger, D. Grimm, *Proteomics* **2011**, *11*, 2095.
- [43] S. Riwaldt, J. Pietsch, A. Sickmann, J. Bauer, M. Braun, J. Segerer, A. Schwarzwald, G. Aleshcheva, T. J. Corydon, M. Infanger, D. Grimm, *Proteomics* **2015**, *15*, 2945.
- [44] S. Riwaldt, J. Bauer, J. Pietsch, M. Braun, J. Segerer, A. Schwarzwald, T. J. Corydon, M. Infanger, D. Grimm, *Int. J. Mol. Sci.* **2015**, *16*, 28296.
- [45] M. Infanger, C. Ulbrich, S. Baatout, M. Wehland, R. Kreutz, J. Bauer, J. Grosse, S. Vadrucci, A. Cogoli, H. Derradji, M. Neefts, S. Kusters, M. Spain, M. Paul, D. Grimm, *J. Cell Biochem.* **2007**, *101*, 1439.
- [46] X. Ma, J. Pietsch, M. Wehland, H. Schulz, K. Saar, N. Hubner, J. Bauer, M. Braun, A. Schwarzwald, J. Segerer, M. Birlem, A. Horn, R. Hemmersbach, K. Wasser, J. Grosse, M. Infanger, D. Grimm, *FASEB J.* **2014**, *28*, 813.
- [47] J. Pietsch, X. Ma, M. Wehland, G. Aleshcheva, A. Schwarzwald, J. Segerer, M. Birlem, A. Horn, J. Bauer, M. Infanger, D. Grimm, *Bio-materials* **2013**, *34*, 7694.
- [48] N. V. Giannakopoulos, J. K. Luo, V. Papov, W. Zou, D. J. Lenschow, B. S. Jacobs, E. C. Borden, J. Li, H. W. Virgin, D. E. Zhang, *Biochem. Biophys. Res. Commun.* **2005**, *336*, 496.
- [49] S. Sluysmans, E. Vasileva, D. Spadaro, J. Shah, F. Rouaud, S. Citi, *Biol. Cell* **2017**, *109*, 139.
- [50] G. Rosenberger, I. Jantke, A. Gal, K. Kutsche, *Hum. Mol. Genet.* **2003**, *12*, 155.
- [51] F. van Roy, G. Berx, *Cell Mol. Life Sci.* **2008**, *65*, 3756.

- [52] A. B. Reynolds, *Biochim. Biophys. Acta* **2007**, 1773, 2.
- [53] N. Ishiyama, M. Ikura, *Subcell Biochem.* **2012**, 60, 39.
- [54] Y. C. Tsai, S. Pestka, L. H. Wang, L. W. Runnels, S. Wan, Y. L. Lyu, L. F. Liu, *PLoS One* **2011**, 6, e24291.
- [55] X. Shang, X. Lin, E. Alvarez, G. Manorek, S. B. Howell, *Neoplasia* **2012**, 14, 974.
- [56] C. Ren, J. Du, C. Xi, Y. Yu, A. Hu, J. Zhan, H. Guo, W. Fang, C. Liu, H. Zhang, *Biochem. Biophys. Res. Commun.* **2014**, 446, 187.
- [57] C. Cellurale, G. Sabio, N. J. Kennedy, M. Das, M. Barlow, P. Sandy, T. Jacks, R. J. Davis, *Mol. Cell. Biol.* **2011**, 31, 1565.
- [58] N. Tikhmyanova, E. A. Golemis, *PLoS One* **2011**, 6, e22102.
- [59] L. Gao, H. Xie, L. Dong, J. Zou, J. Fu, X. Gao, L. Ou, S. Xiang, H. Song, *Mol. Med. Rep.* **2014**, 9, 1032.
- [60] F. Palacios, J. S. Tushir, Y. Fujita, C. D'Souza-Schorey, *Mol. Cell. Biol.* **2005**, 25, 389.
- [61] P. J. Brockie, A. V. Maricq, WormBook, ed. The *C. elegans* Research Community **2006**, WormBook, 1, 1, <https://doi.org/10.1895/wormbook.1.61.1>, <http://www.wormbook.org>.
- [62] A. Schreiber, F. Stengel, Z. Zhang, R. I. Enchev, E. H. Kong, E. P. Morris, C. V. Robinson, P. C. da Fonseca, D. Barford, *Nature* **2011**, 470, 227.
- [63] C. Kraft, F. Herzog, C. Gieffers, K. Mechtler, A. Hagting, J. Pines, J. M. Peters, *EMBO J.* **2003**, 22, 6598.
- [64] J. A. Steen, H. Steen, A. Georgi, K. Parker, M. Springer, M. Kirchner, F. Hamprecht, M. W. Kirschner, *Proc. Natl. Acad. Sci. U.S.A.* **2008**, 105, 6069.
- [65] S. Nath, T. Banerjee, D. Sen, T. Das, S. Roychoudhury, *J. Biol. Chem.* **2011**, 286, 15666.
- [66] S. Shuliang, C. Lei, J. Guangwu, L. Changjie, *Oncol. Res.* **2013**, 21, 121.
- [67] S. M. Siitonen, J. T. Kononen, H. J. Helin, I. S. Rantala, K. A. Holli, J. J. Isola, *Am. J. Clin. Pathol.* **1996**, 105, 394.
- [68] R. M. Bremnes, R. Veve, F. R. Hirsch, W. A. Franklin, *Lung Cancer* **2002**, 36, 115.
- [69] J. Peng, S. Qi, P. Wang, W. Li, L. Song, C. Liu, F. Li, *Future Oncol.* **2016**, 12, 715.
- [70] B. Angres, A. Barth, W. J. Nelson, *J. Cell Biol.* **1996**, 134, 549.
- [71] S. K. Wu, A. K. Lagendijk, B. M. Hogan, G. A. Gomez, A. S. Yap, *Cell Cycle* **2015**, 14, 315.
- [72] A. G. Grieve, C. Rabouille, *J. Cell Sci.* **2014**, 127, 3331.
- [73] P. Paoli, E. Giannoni, P. Chiarugi, *Biochim. Biophys. Acta* **2013**, 1833, 3481.
- [74] D. Grimm, M. Infanger, K. Westphal, C. Ulbrich, J. Pietsch, P. Kossmehl, S. Vadrucchi, S. Baatout, B. Flick, M. Paul, J. Bauer, *Tissue Eng. Part A* **2009**, 15, 2267.
- [75] M. G. Masiello, A. Cucina, S. Proietti, A. Palombo, P. Coluccia, F. D'Anselmi, S. Dinicola, A. Pasqualato, V. Morini, M. Bizzarri, *Biomed. Res. Int.* **2014**, 2014, 652434.

11.2. Publication #2

Nassef MZ, Kopp S, Wehland M, Melnik D, Sahana J, Krüger M, Corydon TJ, Oltmann H, Schmitz B, Schütte A, Bauer TJ, Infanger M, Grimm D. Real Microgravity Influences the Cytoskeleton and Focal Adhesions in Human Breast Cancer Cells. *Int J Mol Sci* 20: 3156, 2019.



Article

Real Microgravity Influences the Cytoskeleton and Focal Adhesions in Human Breast Cancer Cells

Mohamed Zakaria Nassef ¹, Sascha Kopp ¹, Markus Wehland ¹, Daniela Melnik ¹, Jayashree Sahana ², Marcus Krüger ¹ , Thomas J. Corydon ^{2,3}, Hergen Oltmann ⁴, Burkhard Schmitz ⁴, Andreas Schütte ⁴, Thomas J. Bauer ¹, Manfred Infanger ¹ and Daniela Grimm ^{1,2,5,*}

¹ Clinic for Plastic, Aesthetic and Hand Surgery, Otto von Guericke University Magdeburg, D-39120 Magdeburg, Germany

² Department of Biomedicine, Aarhus University, DK-8000 Aarhus C, Denmark

³ Department of Ophthalmology, Aarhus University Hospital, DK-8000 Aarhus C, Denmark

⁴ Airbus Defence and Space GmbH, Airbus-Allee 1, D-28199 Bremen, Germany

⁵ Gravitational Biology and Translational Regenerative Medicine, Faculty of Medicine and Mechanical Engineering, Otto von Guericke University Magdeburg, D-39120 Magdeburg, Germany

* Correspondence: dgg@biomed.au.dk; Tel.: +45-871-69693

Received: 23 May 2019; Accepted: 26 June 2019; Published: 28 June 2019



Abstract: With the increasing number of spaceflights, it is crucial to understand the changes occurring in human cells exposed to real microgravity ($r\text{-}\mu\text{g}$) conditions. We tested the effect of $r\text{-}\mu\text{g}$ on MCF-7 breast cancer cells with the objective to investigate cytoskeletal alterations and early changes in the gene expression of factors belonging to the cytoskeleton, extracellular matrix, focal adhesion, and cytokines. In the Technische Experimente unter Schwerelosigkeit (TEXUS) 54 rocket mission, we had the opportunity to conduct our experiment during 6 min of $r\text{-}\mu\text{g}$ and focused on cytoskeletal alterations of MCF-7 breast cancer cells expressing the Lifeact-GFP marker protein for the visualization of F-actin as well as the mCherry-tubulin fusion protein using the Fluorescence Microscopy Analysis System (FLUMIAS) for fast live-cell imaging under $r\text{-}\mu\text{g}$. Moreover, in a second mission we investigated changes in RNA transcription and morphology in breast cancer cells exposed to parabolic flight (PF) maneuvers (31st Deutsches Zentrum für Luft- und Raumfahrt (DLR) PF campaign). The MCF-7 cells showed a rearrangement of the F-actin and tubulin with holes, accumulations in the tubulin network, and the appearance of filopodia- and lamellipodia-like structures in the F-actin cytoskeleton shortly after the beginning of the $r\text{-}\mu\text{g}$ period. PF maneuvers induced an early up-regulation of *KRT8*, *RDX*, *TIMP1*, *CXCL8* mRNAs, and a down-regulation of *VCL* after the first parabola. E-cadherin protein was significantly reduced and is involved in cell adhesion processes, and plays a significant role in tumorigenesis. Changes in the E-cadherin protein synthesis can lead to tumor progression. Pathway analyses indicate that *VCL* protein has an activating effect on *CDH1*. In conclusion, live-cell imaging visualized similar changes as those occurring in thyroid cancer cells in $r\text{-}\mu\text{g}$. This result indicates the presence of a common mechanism of gravity perception and sensation.

Keywords: microgravity; breast cancer cells; cytoskeleton; tubulin; F-actin; focal adhesion; E-cadherin; vinculin; live-cell imaging

1. Introduction

Cancer is a burden of mankind with a high morbidity and mortality and is responsible for an estimated 9.6 million deaths, according to the World Health Organization (WHO) Global Cancer Observatory (GLOBOCAN) data indicated in 2018 [1]. The GLOBOCAN statistics from 2018 published

that breast cancer is the most common cancer in women and the second leading cause of cancer deaths worldwide [1]. More women are diagnosed with breast cancer in 2019 than with any other cancer, besides skin cancer. In 2019, an estimated 268,600 women in the United States will be diagnosed with invasive breast cancer, and 62,930 women with in situ breast cancer [2]. In addition, an estimated 2670 men in the United States will be diagnosed with breast cancer.

Due to the high mortality, new ways must be taken to find new approaches and therapeutic strategies in cancer research. Experiments performed in the space environment are not typically the main topic of cancer researchers [3]. However, a stay in orbit on the International Space Station (ISS) provides physical conditions that are not achievable on Earth. Studying the mechanisms of microgravity-dependent cellular and molecular changes is necessary to improve space medicine and to develop new treatment strategies for cancer patients [4].

Gravity is the most familiar force in human life [5]. In space, the gravity force is lowered, resulting in microgravity (μg). Although human cells do not have a gravity sensor, they can still sense μg through the cytoskeleton [6]. The response of cells to early μg , together with changes in actin and microtubules, has been reported for different kinds of cells [7–10]. Moreover, human thyroid cancer cells have demonstrated a response to early μg by alterations in the cytoskeleton such as disturbance of F-Actin bundles, formation of lamellipodia- and filopodia-like structures and cellular detachment [11]. When cells are subjected to μg for a longer duration, they tend to form three-dimensional (3D) aggregates, so-called multicellular spheroids (MCS) [12].

There are several options to study cells real microgravity ($r\text{-}\mu g$), such as parabolic flights, sounding rockets missions, unmanned BION and photon spaceflights or a spaceflight in orbit or to the ISS with a commercial carrier. The Technische Experimente unter Schwerelosigkeit (TEXUS, TX) sounding rocket program, offered by the Deutsches Zentrum für Luft- und Raumfahrt (DLR, German Aerospace Center), offers researchers six minutes of μg to conduct their experiments [11,13,14]. We participated in the TX54 mission with the main objective of study cytoskeletal alterations of breast cancer cells in $r\text{-}\mu g$. Moreover, we attended the 31st DLR parabolic flight campaign (PFC) and investigated morphological changes and focused on the gene expression of selected genes of interest. The Michigan cancer foundation (MCF)-7 cell line was chosen as a suitable candidate for both the TX 54 mission and the PFC. As an alternative to conducting experiment in $r\text{-}\mu g$, which often is very expensive and time consuming, researchers may choose to investigate biological processes in simulated μg . The simulation of μg is achievable by using the rotating wall vessel (RWV), the random positioning machine (RPM), a 2D or 3D clinostat, and magnetic levitation [15]. These special conditions had been applied to study changes in cell growth and the function of different benign cell types and cancer cells, and may to some extent resemble the findings provided by $r\text{-}\mu g$ [16].

The MCF-7 cell line had been investigated for several times under altered μg conditions in space and on Earth. The MCF-7 cell line showed a robust behavior in μg , and MCF-7 cells had been tested in space in a Photon capsule [17]. The MCF-7 cells reacted by exhibiting alterations in microtubules [17]. In addition, the MCF-7 cells exerted a loosening of the perinuclear cytokeratin network [18]. RPM-exposure experiments of the MCF-7 cells revealed changes in their growth behavior.

In this paper, we report for the first-time live-cell imaging of breast cancer cells on board a sounding rocket (TX 54). Live-cell imaging was performed with a spinning-disc Fluorescence Microscopy Analysis System (FLUMIAS) [11]. The objective of this study was first to focus on changes in the microtubule and F-actin cytoskeleton. Second, we investigated the changes in expression, distribution and localization of selected proteins by indirect immunofluorescence of fixed cells during μg . Third, we examined MCF-7 cells exposed to PF maneuvers and addressed changes in the gene expression patterns of genes encoding for components of the cytoskeleton, the extracellular matrix (ECM), focal adhesion molecules and cytokines.

2. Results

The TEXUS program is an established DLR-sponsored sounding rocket program which offers researchers precious μg time to test their hypotheses [19]. The sounding rocket has the advantage of providing a relatively longer time (6 min) period of r- μg compared to the parabolic flights. Moreover, it has only one period of hypergravity (hyper-g) and vibration at the beginning prior to the r- μg phase.

2.1. TEXUS 54 Sounding Rocket Mission: “Live-Cell Imaging of Human Breast Cancer Cells in Short-Term Weightlessness”

The cytoskeleton is a highly dynamic structure playing a crucial role in adaptation and cell signaling processes in μg . We first examined human MCF-7 breast cancer cells on a sounding rocket and studied the early cytoskeletal alterations (F-actin, α -tubulin).

MCF-7 cells exhibited three forms of growth when cultured for 24 days and five days under s- μg conditions. One part grew adherently on the cell culture flask bottom, a second group formed duct-like multicellular spheroids and a third group revealed compact spheroids on the RPM after a five-day exposure, whereas after 24h only adherent cells and compact MCS were visible [20,21]. The MCF-7 cells were transfected with a Sleeping Beauty transposon-based (pSB-LAGICT) expression construct to visualize F-actin and α -tubulin. The LAGICT (LifeAct-eGFP-IRES-mCherry-Tubulin) expression cassette enables simultaneous examination of F-actin and α -tubulin, through co-expression of Lifeact GFP and mCherry-tubulin fusion proteins, respectively. Transfected MCF-7 cells were examined with the FLUMIAS microscope with 488 nm and 568 nm diode lasers prior to launch and during r- μg . All the images taken at r- μg were compared to control images (Figure 1) which were taken before launch. We showed that MCF-7 cells respond to r- μg within four minutes and demonstrate similar changes as the FTC-133 thyroid cancer cells studied in previous campaigns [11]. This indicates a general gravitational mechanism in human cancer cells. During the r- μg phase of the TEXUS flight, various changes in the cytoskeleton were seen, including a clear influence on the F-actin bundles and the appearance of filopodia/lamellipodia-like structures (Figure 1).

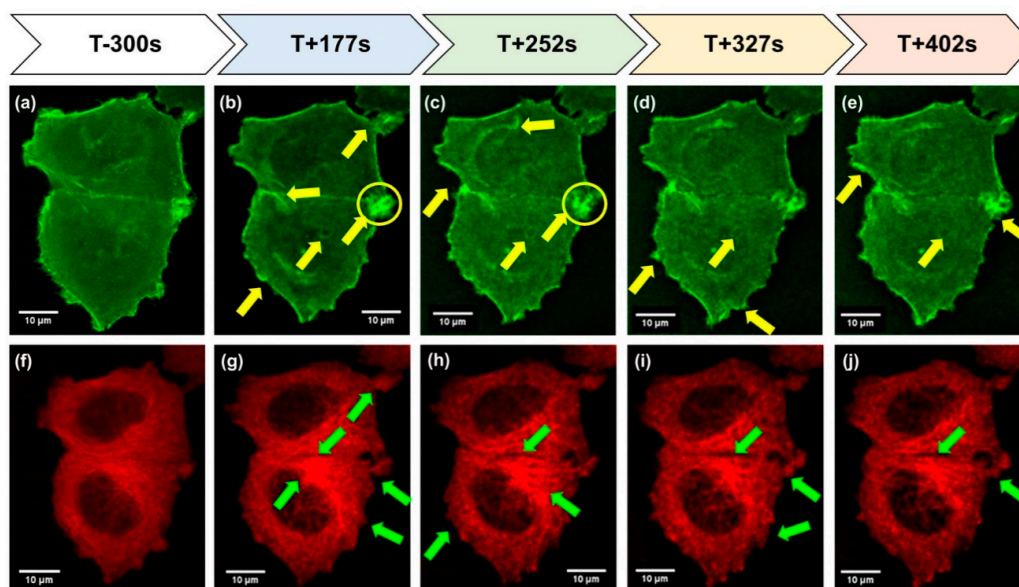


Figure 1. Time course and images of FLUMIAS on TEXUS 54 (40 \times /1.2). The MCF-7 breast cancer cells 5 min before launch (T-300 s) of the rocket and during the r- μg phase (T + 177s–T + 402s). The yellow arrows show the changes in F-actin (a–e; green fluorescence). The yellow circles include an area with F-actin accumulations. Filopodia and lamellipodia are found after 150s, which are more pronounced with time. The green arrows indicate changes in α -tubulin (f–j; red fluorescence). The tubulin network reveals holes after 150s and a looser structure.

2.2. Immunostaining of MCF 7 Cells Exposed to $r\text{-}\mu\text{g}$ during the TEXUS 54 Sounding Rocket Mission and Fixed in Orbit

In addition to the live-cell imaging studies of the transfected MCF-7 cells, regular MCF-7 cells were seeded into 18-well Ibidi slides which were fixed with 4% PFA at the end of the μg period and the hyper-g period. These slides were compared to a control slide fixed with 4% PFA on ground. Thus, we had the opportunity to investigate the changes in expression and distribution of the designated proteins. We tested the antibodies MMP9, VEGFA (c-term), IL-6 and IL-8. Phalloidin rhodamine and DAPI stains were used additionally for all the slides from the TX 54 mission.

Upon visual inspection of the microscopic images, there was no apparent difference in the protein distribution between the different conditions for all the tested antibodies (Figure 2a–l). In order to provide an indication on whether the level of the visualized proteins may have changed, the microscopic images were analyzed at the end of the hyper-g and μg phases in comparison to the controls by using the ImageJ program. At the end of the hyper-g phase, the analysis indicated that the level of F-actin was increased (Figure 2c,f,i,l,o) compared to the controls (Figure 2a,d,g,j), while the level of MMP9 (Figure 2a,c), IL-6 (Figure 2g,i) and IL-8 (Figure 2j,l) apparently was reduced (Figure 2m,p,q). VEGF exhibited no changes at the end of hyper-g phase (Figure 2d,f,n). Furthermore, the microscopic images at the end of the $r\text{-}\mu\text{g}$ phase were also investigated in comparison to the controls. The levels of VEGF and F-actin appeared to be increased (Figure 2n,o), while the levels of MMP9, IL-6 and IL-8 apparently were unchanged (Figure 2m,p,q).

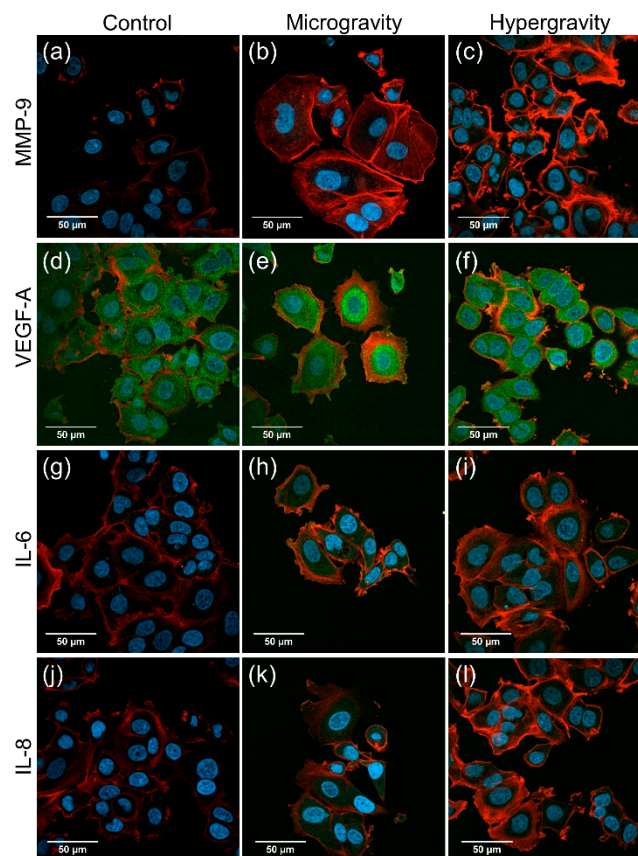


Figure 2. Cont.

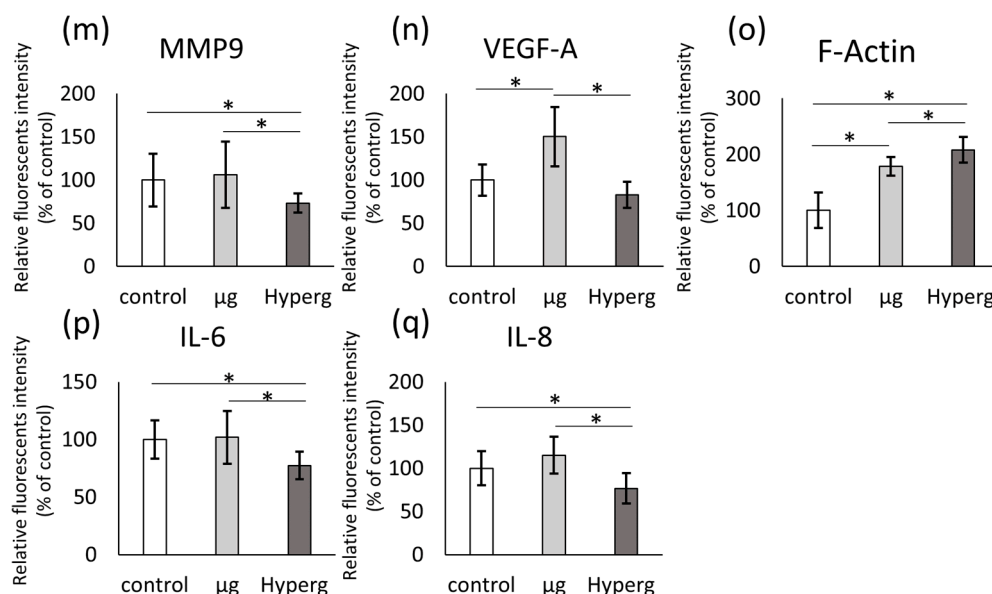


Figure 2. Indirect immunofluorescence staining of PFA-fixed cells from the TEXUS 54 sounding rocket mission. 2500 MCF-7 cells were seeded into each well of the 18 well Ibidi slides. The cells were fixed either at the end of the hyper-g period or at the end of the μg period. The two conditions were compared to 1g-ground control samples. The confocal laser scanning microscopy images (a–l) show either MMP9, VEGF-A, IL-6 or IL-8 in green, DAPI (in blue) and F-Actin (in red). Scale bar is equal to 50 μm . The intensity of the staining was quantified by ImageJ (m–q). All data are shown as mean \pm SD, $n = 10$ –14, with significance indicated by * $p < 0.05$.

2.3. Results of the 31st DLR Parabolic Flight Campaign: “Effects Of Short-Term Microgravity on Human Breast Cancer Cells”

The PFCs were organized by the DLR in close collaboration with the company Novespace, Bordeaux-Mérignac, France. A parabolic flight consisted of 31 consecutive parabolas. Each parabola contains two phases of 1.8 g hyper-g spanning one phase of 10^{-2} g r- μg . The first phase of a parabola begins with flying at 45 degrees for 22 s known as pull-up, followed by decreasing thrust and following the trajectory of a parabola for 22 s of free-fall. Thus, the r- μg phase lasts for the 22 s of the free-fall. The last phase is known as pull-out which begins pulling out the plane to fly back on a horizontal line trajectory. The pull-up phase lasts for 22 s with hyper-g of 1.8 g [16,22,23]. Not only does the parabolic flight have the advantage of offering valuable r- μg time to researchers, but also it gives the scientists access to their experiment on board of the flight.

The 31st DLR PFC took place in March 2018 at the company Novespace at the Bordeaux-Mérignac airport in France. The breast cancer cells (MCF-7 cell line) were examined after parabola 1 (P1) and after 31 parabolas (P31). At the same time, the ground control experimentation took place in the laboratories of Novespace. Subsequently, the fixed cells were transported to the Otto von Guericke University Magdeburg, Germany, where they were examined by molecular biology. We performed qPCR, Western blot and pathway analyses. The results are shown in the following Figures 3–10. Figures 3–8 each show the following groups: static ground controls (1g), P1 and P31.

2.3.1. Studies on Cytoskeletal Genes

Figure 3 gives the expression of the cytoskeletal genes and Figure 4 shows the levels of the corresponding proteins. There were no changes after P1 for the *ACTB*, *TUBB*, *EZR*, *RDX* and *MSN* mRNAs. However, there was a significant up-regulation of *KRT8* after P1 and P31 compared to 1g (Figure 3c) and of *RDX* after P31 (Figure 3e). The cytokeratin protein synthesis was also significantly increased after the first parabola but returned to control levels after 31 parabolas (Figure 4c).

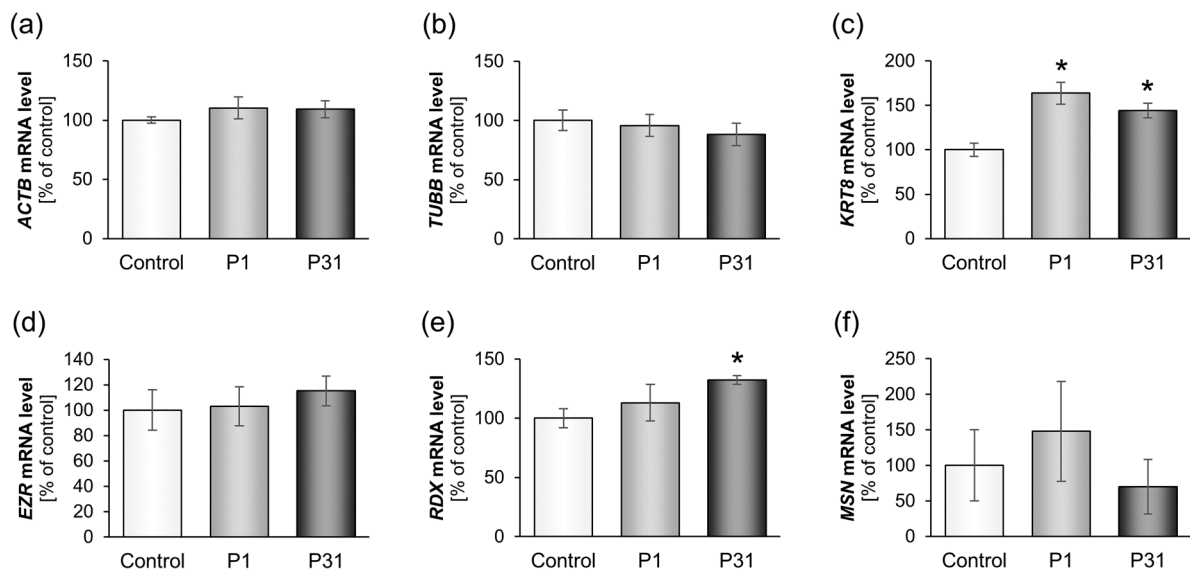


Figure 3. Influence of short-term microgravity on the gene expression (mRNA) of cytoskeletal factors. The data are given as mean \pm standard deviation. * $p < 0.05$ vs. Control.

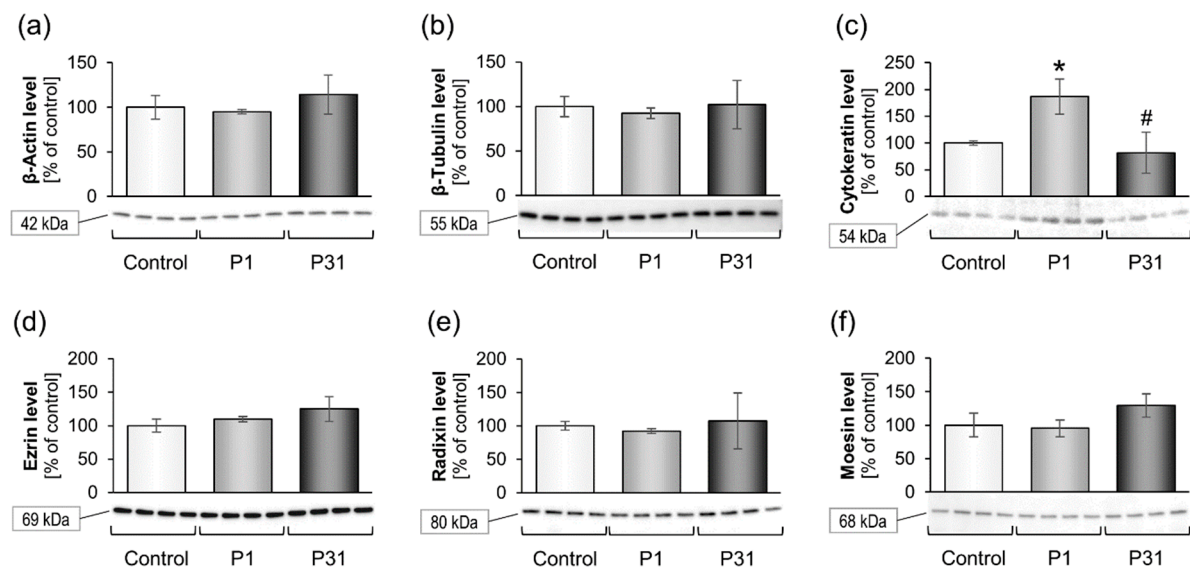


Figure 4. Influence of short-term microgravity on the protein accumulation of cytoskeletal factors. The data are given as mean \pm standard deviation. * $p < 0.05$ vs. Control; # $p < 0.05$ vs. P1.

2.3.2. Altered Expression of Genes of the Focal Adhesion Complex

Furthermore, we examined the mRNA expression and protein content of focal adhesion molecules (Figures 5 and 6). The *VCL* gene and corresponding vinculin protein were significantly reduced under $r\text{-}\mu\text{g}$ (Figures 5a and 6a). *TLN1*, *ITGB1*, *CDH1*, *PTK2*, *CAV1* and *CAV2* remained unchanged under $r\text{-}\mu\text{g}$, while the E-cadherin protein (Figure 6c) as well as β_1 -integrin protein (Figure 6b) were significantly reduced. FAK1 protein was elevated after P1 (Figure 6d).

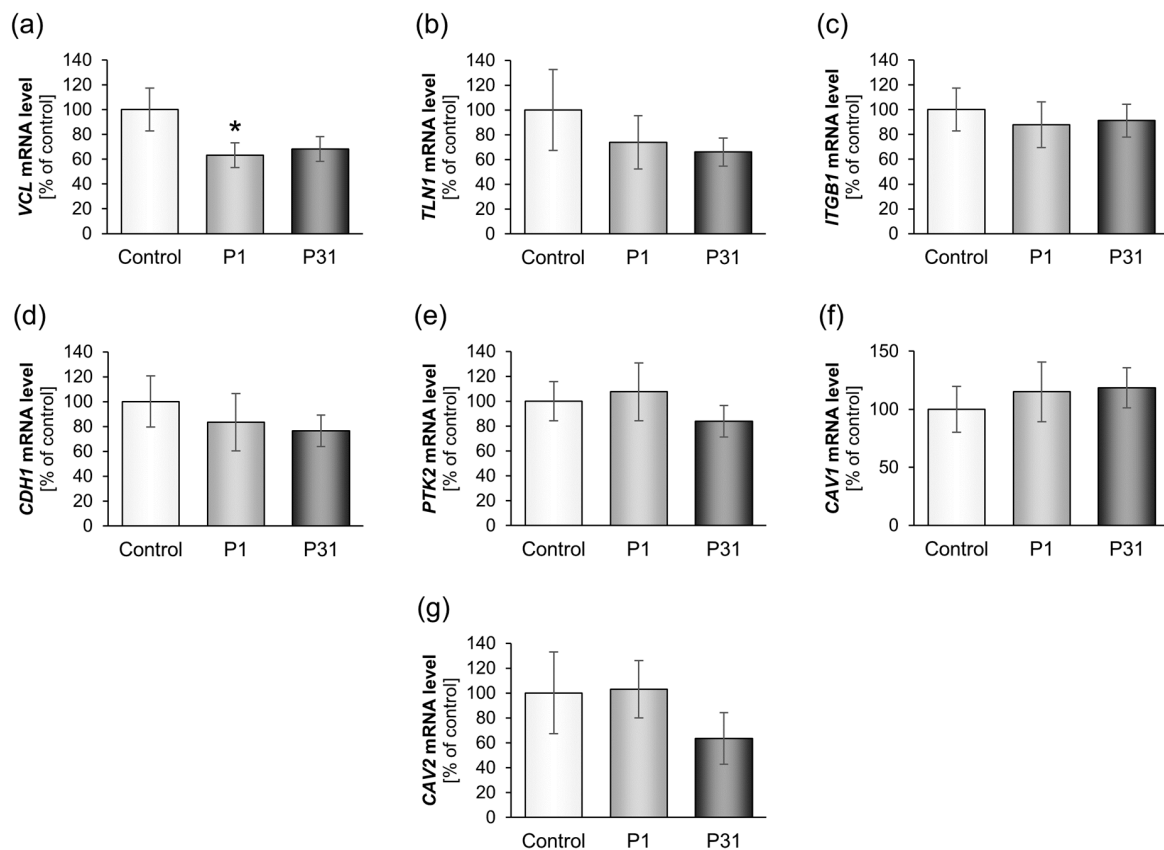


Figure 5. Influence of short-term microgravity on the expression (mRNA) of focal adhesion complex components. The data is given as mean \pm standard deviation. * $p < 0.05$ vs. Control.

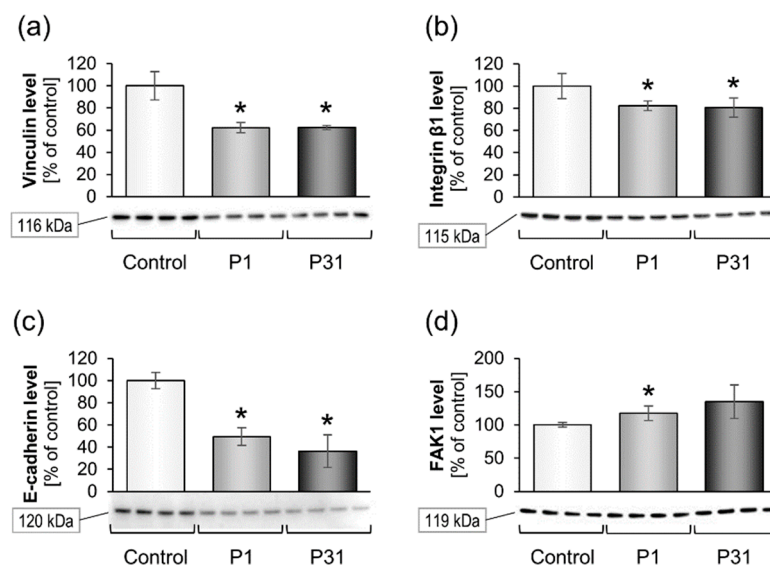


Figure 6. Influence of short-term microgravity on the protein accumulation of focal adhesion complex components. The data is given as mean \pm standard deviation. * $p < 0.05$ vs. Control.

2.3.3. Changes of Extracellular Matrix and Cytokine Gene Expression

The results on the extracellular matrix proteins are shown in Figures 7 and 8. There were no changes in the gene expression for *LAMA1*, *LAMA3*, *COL1A1*, *FN1*, *MMP9* and *PAI1* (*SERPINE1*). The *TIMP1* mRNA was significantly elevated after P31 compared with ground control samples (Figure 7e). In addition, we investigated the expression of the cytokines IL-6 and IL-8, which play

a major role in spheroid formation. The *IL6* mRNA was not significantly changed, but there was a tendency of an up-regulation after P1 and P31 (Figure 7h). In contrast, *CXCL8* was significantly up-regulated after P1, and slightly elevated after P31 (Figure 7i). A similar behavior showed the corresponding IL-8 protein synthesis, which was significantly increased after P1 and P31 (Figure 8). Moreover, a significant elevation of the *VEGFA* mRNA was detectable (Figure 7j).

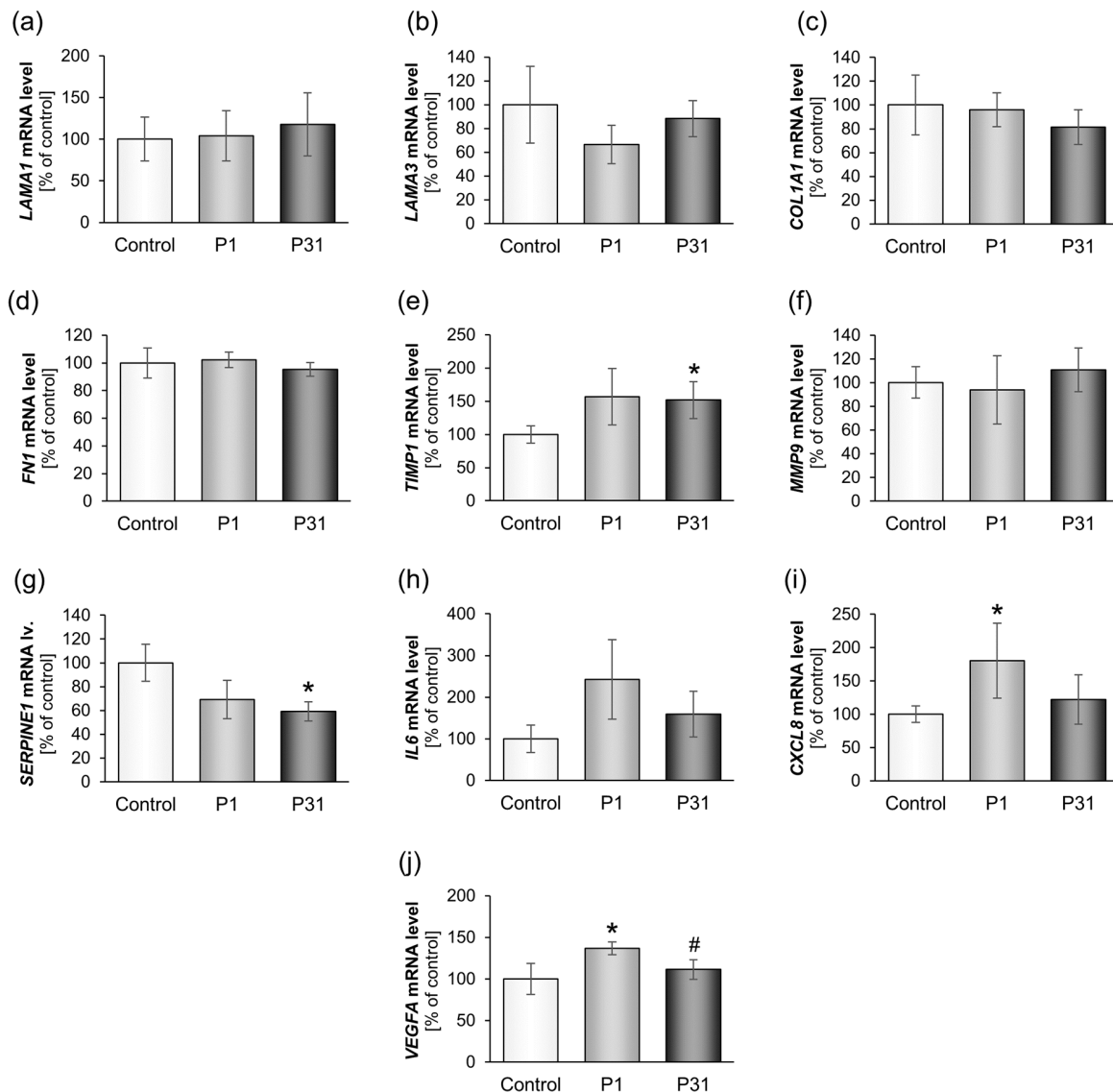


Figure 7. Influence of short-term microgravity on expression of different ECM and cytokine genes.

* $p < 0.05$ vs. Control; # $p < 0.05$ vs. P1.

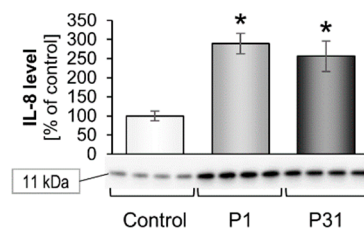


Figure 8. Influence of short-term microgravity on the protein accumulation of IL-8. The data is given as mean \pm standard deviation. * $p < 0.05$ vs. Control.

2.3.4. Pathway Analyses

The results of the pathway analysis given in Figure 9 indicate a clear role for *ITGB1*, *FN1*, *TLN1*, *CDH1*, *PTK2* and *VCL* in gravity sensing of MCF-7 breast cancer cells exposed to short-term r- μ g.

FN1, *VEGFA*, *TLN1* and *TIMP1* proteins are positively influencing β_1 -integrin which is inducing *PTK2* and fibronectin. *TLN1* is interacting with *PTK2* and *FN1*. Vinculin is activating E-cadherin, whereas ezrin has a negative influence on *CDH1*. Moreover, *TIMP1* is inhibiting *MMP9*.

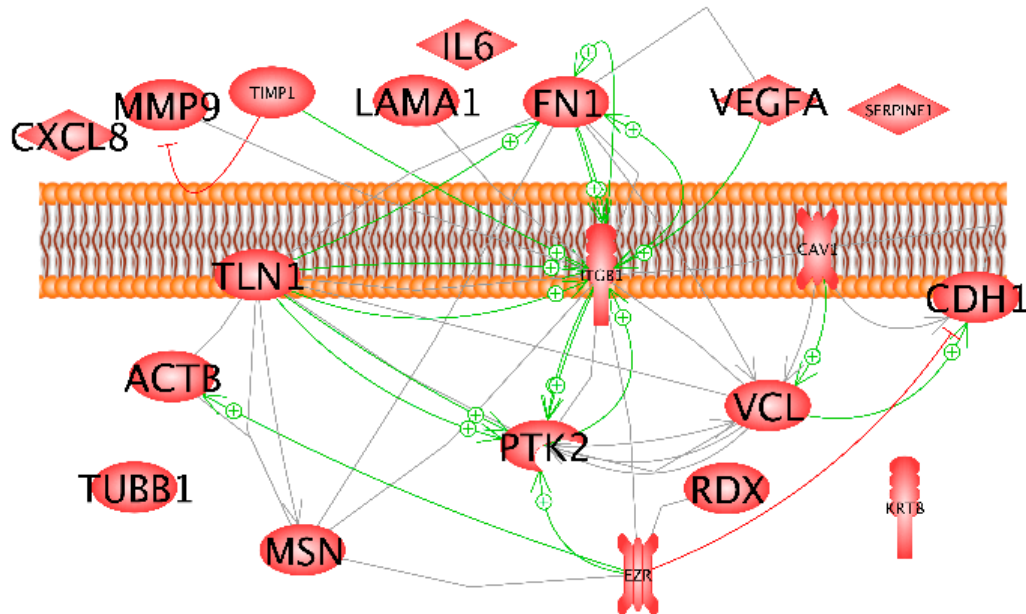


Figure 9. Interaction and localization of proteins detected in the cells by Western blot (red margins). Solid lines indicate the bond. Filled arrows show the directional interaction and dashed arrows show the influence. + Signs indicate activity – inducing effect and red lines indicate inhibition.

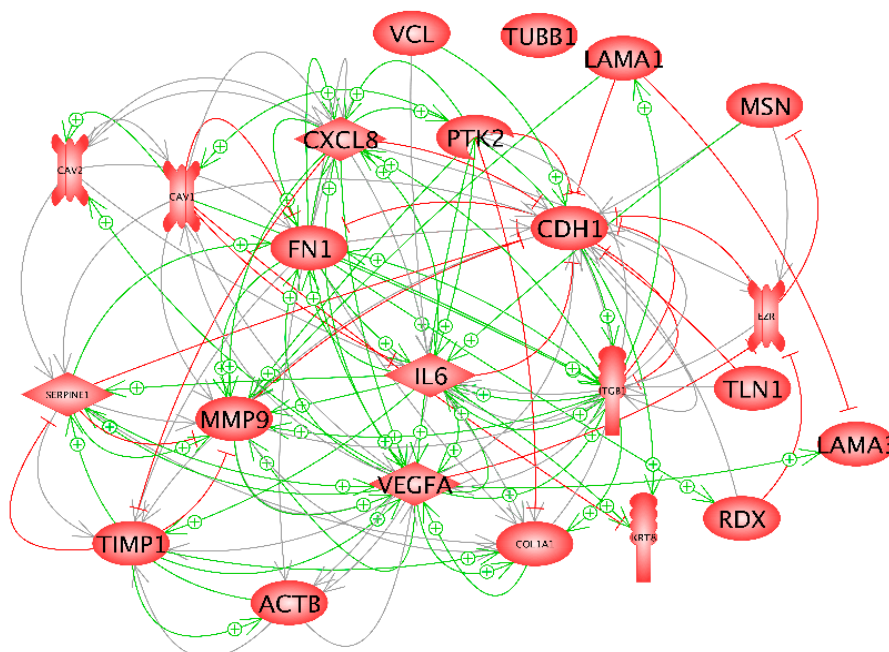


Figure 10. Mutual interactions of expression of the genes examined with qPCR and shown in Figures 2–4. + Signs indicate an activity-enhancing effect and red lines indicate inhibition. The interaction networks were created using Elsevier Pathway Studio v11.

The interaction network shown in Figure 10 indicates a fast significant up-regulation of *KRT8*, *RDX*, *TIMP1* and *CXCL8*, while *VCL* is down-regulated. Simultaneously, *TLN1* and *CDH1* indicate a slight but non-significant reduction of gene expression. Considering the red lines together with the qPCR results cell adhesion via *CDH1* seems to be attenuated. Various genes demonstrate an inhibitory effect on *CDH1* (Figure 9).

3. Discussion

In this study we investigated MCF-7 breast cancer cells in real microgravity using two experimental platforms offered by a sounding rocket mission and a parabolic flight. Live-cell imaging visualized similar changes as those occurring in thyroid cancer cells, when they were exposed to r- μ g. Our results now indicate the presence of a common cellular mechanism for sensing gravity. After entering microgravity, the MCF-7 cells showed a rearrangement of F-actin and tubulin comprising holes, accumulations in the tubulin network, and the appearance of filopodia- and lamellipodia-like structures. Up-regulation of *VEGF* and down-regulation of E-cadherin during parabolic flight maneuvers indicated a temporary change to a more invasive phenotype of MCF-7 cells. This finding also supports earlier data gained from thyroid cancer cells and may hint at a general cellular answer of cancer cells to short-term microgravity.

There is evidence that in vitro cell cultures respond to altered gravity conditions. Studies suggest that this response might be involved in the physiological changes and fundamental health problems of humans during spaceflight [24]. Microgravity alters adhesion, migration, proliferation, differentiation, growth, signaling and gene expression [25]. The cytoskeleton is discussed as the initial gravity sensor [26]. For example, bone cells exposed to r- and s- μ g show changes in their cytoskeleton and focal adhesions, two major mechanosensitive structures [27,28]. Similar results were obtained when investigating thyroid cancer and melanoma cells cultured under μ g-conditions [14,29].

Live-cell imaging of benign and tumor cells is possible using the FLUMIAS microscope which was flown on parabolic flight missions, sounding rocket missions and a more advanced version to the ISS [11,30].

3.1. Cytoskeletal Alterations Visualized during the TEXUS 54 Mission

The principal aim of our experiment onboard the TX 54 sounding rocket was to investigate the effect of r- μ g on the cytoskeleton of human breast cancer cells.

During the flight, MCF-7 cells exhibited alterations in the F-actin and microtubule cytoskeleton. The appearance of filopodia- and lamellipodia-like structures shortly after the beginning of the r- μ g period is comparable to the results which we have obtained with FTC-133 thyroid cancer cells during the TX 52 mission [11]. This data indicates that the gravi-sensing is similar in both cancer types. We could visualize impressing changes of alpha-tubulin during the r- μ g phase. This supports earlier results [20]. Investigating suspensions of purified tubulin, Moos et al. [31] found a significant difference between microtubules assembled in the 30 s μ g phase and the 2g hyper-g phase of a PF. These data reveal that microtubule polymerization is altered by altered gravity. These results were substantiated by sounding rocket [32] and shuttle flight [33] experiments.

In addition, an immunofluorescence staining on MCF-7 cells was performed. The cell fixation was done automatically during the r- μ g phase of the TX 54 mission. The quantitative analysis of VEGF exhibited an up-regulation of the protein in the r- μ g condition compared to the controls. We also measured an accumulation of F-actin. While VEGFA was up-regulated only in the r- μ g condition, F-actin was increased in both the hyper-g and r- μ g conditions. The significant up-regulation of a protein in both μ g and hyper-g conditions indicates that hyper-g was the main inducer for the up-regulation, because the hyper-g period precedes the μ g period. The F-actin content was elevated in A431 epidermoid carcinoma cells after a 7-min μ g-exposure during a sounding rocket flight [34]. Boonstra concluded that the actin microfilament system is sensitive to altered gravity conditions

and that its remodeling may affect signal transduction [34]. Reflecting our results, we can support this hypothesis.

Therefore, we can conclude that only VEGF showed a clear up-regulation in r- μ g compared to the control. This data fits to earlier results obtained during a PF mission, where VEGF was significantly up-regulated after P1 and P31 [16]. VEGF is a key inducer of angiogenesis and enhances spreading and metastasis [35,36]. Serum VEGF was significantly elevated in patients with metastatic differentiated thyroid cancer but not in those with poorly differentiated thyroid cancer metastases [37]. The release of VEGF by FTC-133 exposed to space conditions during the Shenzhou-8 spaceflight was high but not significantly different in 1g samples and r- μ g samples, but the gene expression of VEGFA was down-regulated after a 10-day mission [16].

3.2. MCF-7 Breast Cancer Cells Exposed to PF Maneuvers during the 31st DLR PFC

Earlier experiments investigating chondrocytes, endothelial cells, and thyroid cancer cells revealed that a short-term r- μ g-exposure (22 s) during PF maneuvers induced early cytoskeletal changes and an altered gene expression pattern in these different cell types [22,38,39]. These studies showed that the gravi-response of cancer and benign cells occurred very early, within the first few seconds [22,38,39]. Several gravi-sensitive signaling elements, such as AMP-activated protein kinase alpha 1 and integrins are involved in the reaction of endothelial cells to altered gravity conditions [38]. Down-regulated *MTSS1* and up-regulated *LIMA1* were key factors stabilizing the cytoskeleton of tumor cells under μ g conditions [39].

ECM proteins, focal adhesion and cytoskeletal components form a dynamic network interacting with signaling molecules as an adaptive response to altered gravity. These focal adhesions are integrin-containing structures that form mechanical links between intracellular actin bundles and the extracellular space of a cell. Focal adhesions are dynamic protein complexes through which the cytoskeleton of a cell connects to the ECM. The adhesion dynamics play a central role in cellular migration. Focal complexes are formed at the leading edge of the cell in lamellipodia.

We had first investigated the gene expression of cytoskeletal factors. Most cytoskeletal genes were not significantly altered but there was a significant up-regulation of the *KRT8* mRNA after P1 and P31. This finding is similar to earlier results with thyroid cancer cells [39].

Studying the genes of the focal adhesion complex we found a decrease in E-cadherin protein as well as β_1 -integrin protein. Changes in the focal adhesion complex were also found in cells exposed to s- μ g and r- μ g. Tan et al. [29] reported about a reduction in focal adhesions in melanoma cells exposed to s- μ g. In space on board the SJ-10 satellite, the mechanosensitive molecules β_1 -integrin, β -actin, α -tubulin, and others were elevated, whereas among others vinculin was down-regulated in bone marrow-derived mesenchymal stem cells [40]. In addition, the authors observed an accumulation of microtubules and vimentin through the altered expression and location of focal adhesion complexes [40].

Several ECM genes such as *FN1* were not altered during short-term μ g in MCF-7 breast cancer cells. This is different to the results which we obtained from low-differentiated ML-1 thyroid cancer cells [39]. During this PFC we detected an up-regulation of the *FN1* mRNA, which indicates a cancer type-specific reaction to μ g.

β_1 -integrin, fibronectin, and PTK2 play essential roles, when cells bind to the extracellular matrix. β_1 -integrin is involved in the proliferation and differentiation as well as in the development of epithelial tissues [41]. It is important for adhesion dynamics and essential for the control of cell migration and, therefore, is a marker for a poor prognosis in breast cancer [41]. β_1 -integrin forms heterodimers with various α -types integrins. Some of these dimers are able to bind to fibronectin. After binding, signals are forwarded to FAK1 (Focal adhesion kinase 1 coded by *PTK2*) and talin (*TLN1*) [42].

Binding of β_1 -integrin to fibrillar fibronectin promotes the phosphorylation of STAT3, which is known to participate in the induction of the epithelial mesenchymal transition [43]. In addition, β_1 -integrin facilitates the secretion of fibronectin in a way which is poorly understood. Fibronectin remaining intracellular is directly interacting with the actin cytoskeleton [43], which is changed when the

cells are exposed to microgravity [20]. Moreover, β_1 -integrin controls the VE-cadherin localization and blood vessel stability in the mouse retina [44]. VEGF can promote angiogenesis through up-regulation and/or activation of integrins [45]. The VEGF activity is dependent on β_1 -integrin function.

FAK1 and talin are members of the focal adhesion complexes. Talin mediates cell-cell adhesion linking the integrins to the actin cytoskeleton and in the activation of integrins [46]. Talin was differentially regulated in AD and MCS of thyroid cancer cells exposed to simulated microgravity [47]. FAK1 is a cytoplasmic protein tyrosine kinase which is found to be concentrated in the focal adhesions. It promotes the organization of the fibronectin matrix and fibrillar adhesions [48]. In addition, FAK1 triggers the recruitment of talin to nascent adhesions independently of integrin. It plays a key role in the migration process and FAK1 inhibition decreases mobility and metastasis. The β_1 -Integrin-FAK pathway is involved in cell survival and on the role of FAK in breast cancer development and progression [49]. In this study, the *PTK2* mRNA was stable in the breast cancer cells, but the corresponding protein showed an elevation after P1 (Figure 6d). This is different to the data obtained with thyroid cancer cells, where the *PTK2* mRNA in FTC-133 thyroid cancer cells was differentially expressed in the TEXUS samples, but the FAK1 protein content was significantly reduced in RPM samples [14].

The pathway analysis of the investigated genes revealed important roles of *CDH1* and *VEGFA* in the network. These genes are under the influence of IL-6 and IL-8, which both exert inhibitory effects on CDH1 and promoting effects on VEGFA. IL-6 promotes e-cadherin repression [50] and treating human gastric carcinoma cells with exogenous IL-8 decreased expression of E-cadherin mRNA [51]. IL-6 and IL-8 induce the expression of VEGF [52,53]. The *CDH1* gene encodes e-cadherin, which establishes cell-cell junctions [54]. After a 2-week RPM-exposure, E-cadherin, was diminished in MCF-7 MCS cells, where proteins of the E-cadherin autodegradation pathway were enhanced as well as c-Src (proto-oncogene tyrosine-protein kinase c-Src) [55]. Blocking the E-cadherin activity by specific antibodies promoted spheroid formation. As indicated by the high number of red lines shown in Figure 10, *CDH1* gene expression is strongly controlled by a number of proteins. Of the investigated components, only vinculin has a positive modulatory influence (green arrow) [56].

But, in addition to IL-6 and IL-8, EZR, talin, PTK2, ITGB1 and MMP9 were already found to have inhibitory effects. E-cadherin and EZR are involved in tumor growth. In a patient study, the ezrin expression was upregulated, while that of E-cadherin was decreased in breast cancer as compared to the control specimen. Ezrin expression was negatively correlated to the E-cadherin expression in a subpopulation of breast cancer patients with a high expression of ezrin [ezrin(high)] and a low expression of E-cadherin [E-cad(low)] [57]. Talin regulates the stability of E-cadherin transcriptional repressors [58]. An increased expression of E-cadherin was observed after reducing the level of β_1 -integrin in B16-F10 melanoma cells [59]. Treatment with recombinant MMP-9 or transient expression of MMP-9 is sufficient to reduce E-cadherin levels in differentiated ovarian tumor cells [60].

VEGFA encodes the vascular endothelial growth factor, which supports (neo)-vascularization of healthy and malignant tissues [61]. As mentioned above, IL-6 and IL-8 favor its expression. In addition, human astrocytoma cells expressed increased levels of fibronectin and VEGF upon transformation with a versican G3 construct [62] and VEGF expression was positively linked to MMP-9 levels in gastric carcinoma [63]. Overexpression of TIMP1 and PAI-1 in endothelial cells blocks vascular tube regression [64].

3.3. Microgravity-Induced Cytoskeleton Changes and Potent Physiological Responses

The cytoskeleton directs a number of essential cell functions, such as maintenance of cell shape, support of vacuole formation or fixation of organelles. The cytoskeleton is dynamic and not static, and it can disassemble and reassemble to contribute to cell mobility (Figure 11). It is involved in migration which is necessary for tissue repair and tumor spreading, progression and metastasis [65]. It is important for cellular signaling.

In this study, we demonstrate for the first time using live-cell imaging in real μg that MCF-7 cells reveal a rearrangement of the F-actin and microtubule cytoskeleton with holes, accumulations in the tubulin network, and the appearance of filopodia- and lamellipodia-like structures in the F-actin cytoskeleton (Figure 1). In lamellipodia are ribs of actin called microspikes spreading beyond the lamellipodium frontier are then called filopodia, which are involved in cell adhesion and migration, healing processes and others. The initiation and elongation of filopodia is depending on polymerization, convergence and crosslinking of actin filaments [66]. Filopodia and filopodia-like structures are involved in 3D cell migration and thus in tumor dissemination, growth and metastasis [67]. Filopodia are normally situated at the front of invading cancer cells [68,69] and filopodia-like structures promote cancer cell survival at metastatic sites [70,71]. In Figure 11 the possible mechanism is demonstrated how these μg -induced alterations of the cytoskeleton are involved in 3D growth and in the formation of multicellular spheroids, which resemble in vivo microtumors and metastases [65].

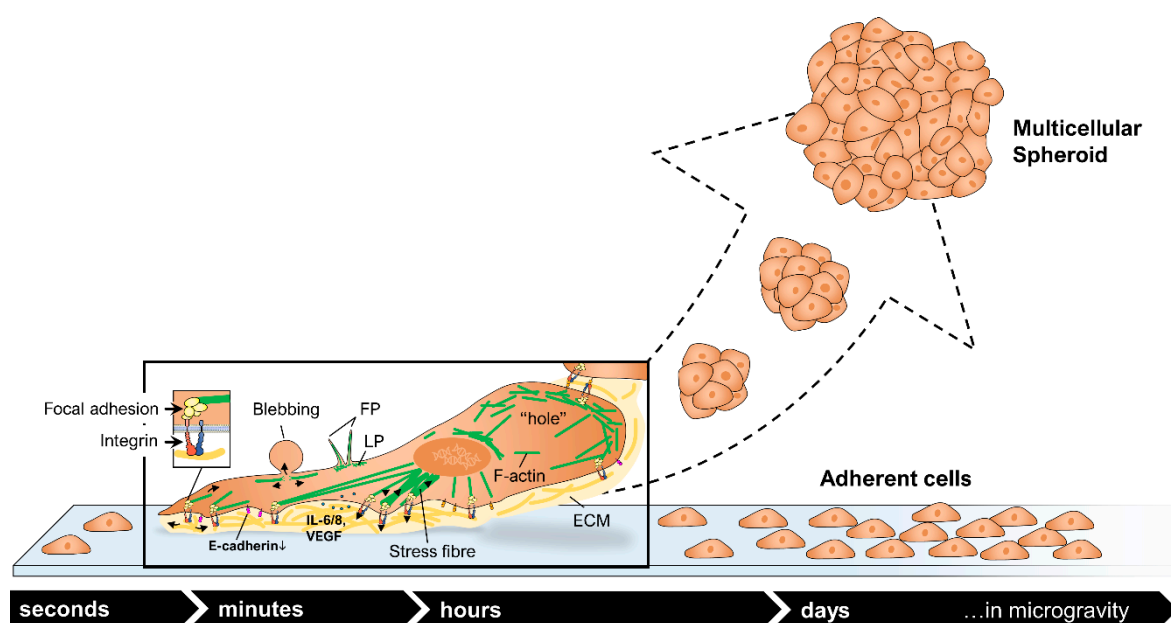


Figure 11. Alterations of adherently growing cancer cells after exposure to microgravity (modified from [65]). The figure in the box shows changes at the microscopic level. F-actin is displayed as green lines, the ECM in yellow. FP: filopodia, LP: lamellipodia.

In this study PF maneuvers induced a downregulation of *VCL* mRNA and the corresponding protein in MCF-7 breast cancer cells. Pathway analyses indicated that *VCL* protein has an activating effect on *CDH1*. E-cadherin is involved in cell adhesion and in tumorigenesis. Changes in the E-cadherin protein synthesis can lead to tumor progression. In addition, blockage of E-cadherin and a down-regulation of *CDH1* leads to enhanced spheroid formation of MCF-7 breast cancer cells [55,65].

$r\text{-}\mu\text{g}$ -induced changes in the cytoskeleton and/or in focal adhesion components of human cells as for example cancer cells and normal cells like osteoblasts, chondrocytes and cancer cells are the two major mechanosensitive responses [8,14,28]. The cytoskeleton responds to changes in the mechanical environment because of its connection to the ECM through focal adhesions. Exposure of human cells to μg impaired their cytoskeleton stability and reduced cellular tension, as well as focal adhesion formation and stability [8].

The ECM-membrane receptors-cytoskeleton system is known to be involved in cancer and metastasis [72]. Growth factor receptors, adhesion proteins and ion channels in association with the sub-membranous system of the actin cytoskeleton control the actin microfilament's force generating capacity. Perturbations of the actin microfilament system in cell motility and migration and their role in cancer pathophysiology are currently a hot topic [72].

The exact mechanisms how the cells transform the mechanical signal (microgravity) into a biochemical signal is still not known. The widely acknowledged tensegrity model hypothesis proposed by Ingber [73] explains that the cells are hardwired by the cytoskeleton components. The cells are spanned open and are under continuous tension [26,73]. An imbalance between adhesion and the cytoskeleton network might induce a cell shape change and has a direct impact on cell signaling [26,73]. This theory is supported by data of cytoskeletal changes in various benign and malignant cell types after short-term exposure to microgravity [11,16,21,22,38,74].

When microgravity conditions influence human adherent MCF-7 breast cancer cells, the microtubules (tubulin) rapidly reorient themselves and actin stress fibers increase in density in order to reinforce their mechanical strength. These changes in the F-actin and in microtubule network are followed by changes in adhesion, shedding of membrane receptors, cell detachment, migration, growth behavior, differentiation, and apoptosis [12,20,38,75]. These physiological changes have been detected in real microgravity and on Earth using various μ g-simulation devices [15].

In summary, an early up-regulation of *KRT8*, *RDX*, *TIMP1*, *CXCL8*, and down-regulation of *VCL* were found after the PF maneuvers. E-cadherin protein was reduced after the PF maneuvers. This result is very important because E-cadherin is not only involved in the cell adhesion process but plays a significant role in tumorigenesis. Changes in the E-cadherin protein can lead to tumor progression. VCL protein has an activating effect on *CDH1* (Figure 9). However, many of the genes investigated lead to an inhibition of *CDH1* (Figure 10). *CXCL8* is also important for tumor progression and the early up-regulation of the cytokine supports this thesis.

4. Materials and Methods

4.1. Cell Culture

The MCF-7 breast cancer cells were purchased from the American Type Culture Collection (MCF7, ATCC[®] HTB-22[™]). They were cultured in RPMI 1640 (Life Technologies, Paisley, UK), 10 % FCS (Sigma Aldrich, Steinheim, Germany) and 1% penicillin/streptomycin (Life Technologies, New York, NY, USA). The Lifeact-eGFP-IRES-mCherry-Tubulin MCF-7 expressing cells were cultured in the same medium, in addition to G418 (Geneticin) to allow the growth of the stably transfected cells. The cells were cultured in T-75 flasks and the cells were harvested and seeded into other flasks every 3-5 days to prevent confluence.

4.2. Construction of An Expression Cassette to Visualize F-actin and α -tubulin

We constructed a pcDNA3.1 LifeAct-eGFP-IRES-mCherry-Tubulin (pLAGICT) expression cassette for visualization of F-actin and α -tubulin. In order to construct this expression cassette, pUC57 plasmid was ordered from GenScript. The required cassette LifeAct-eGFP-IRES-mCherry-Tubulin was excised from the pUC57 plasmid with NotI/XbaI restriction enzymes. The excised part was further purified by gel extraction and ligated into pcDNA3.1 (+) (Invitrogen, Carlsberg, CA, USA). The constructed plasmid was transformed into ultra-competent *Escherichia coli* cells to produce more copies of the plasmid. QIAprep spin column (Qiagen, Hilden, Germany) was used to extract the plasmid from the bacteria. More details about the construction of the expression cassette are mentioned in [11,76].

4.3. Generation of MCF 7 Cells Expressing Lifeact-eGFP-IRES-mCherry-Tubulin

The MCF-7 cell line was stably transfected using a Sleeping Beauty (SB) transposon-based vector containing the LAGICT expression cassette for the visualization of F-actin and α -tubulin as described in [11,77,78]. In brief, LifeAct-eGFP-IRES-mCherry-Tubulin was excised from the pLAGICT plasmid with NotI/XbaI restriction enzymes, and sub-cloned into a Sleeping Beauty transposon-based vector pT2/CMV-linker-SV40-Neo [78,79] containing a linker enabling insertion of the NotI-LAGICT-XbaI fragment excised from the pLAGICT vector. The resulting plasmid, pT2/CMV-LAGICT-SV40-Neo, was

entitled pSB-LAGICT. In order to provide stable expression of the LifeAct-eGFP-IRES-mCherry-Tubulin expression cassette, MCF-7 cells were co-transfected with pSB-LAGICT and pCMV-SB100X [78], using X-tremeGENE 9 transfection (Roche, Basel, Switzerland) reagent according to the manufacturer's protocol [77]. Afterwards, the transfected cells were cultured in medium containing G418 (Geneticin) to allow growth of stably transfected cells only. A fluorescence microscope was used to validate the efficiency of the transfection.

4.4. Live Cell Imaging by the FLUMIAS Microscope

Approximately 7000 MCF-7 cells were seeded into one channel of an ibiTreat μ -slide VI 0.4 (Ibidi, Gräfelfingen, Germany). The slide was temperature controlled and loaded into the FLUMIAS microscope (developed by FEI Munich GmbH [11]) shortly before the launch (Figure 12). Five minutes prior to launch three z-stacks were obtained from pre-selected cells as a ground control. About 75s after launch the microgravity phase was reached, and the microscope started recording the pre-selected cells. Three z-stacks were taken every one minute with 125 ms exposure time. The thickness of the z-stack was 21 μ m with 0.5 μ m step size. The procedure was repeated four times with a total number of five active phases covering 6 min of microgravity.

After recovery of the image data, a single image was extracted from each z-stack taken during microgravity to allow analysis of all images in the focal plane. The extracted images were deconvolved by Huygens Essential Scientific Volume Imaging software 4.3 and compared to a control image taken on ground.

4.5. TEXUS 54 Sounding Rocket Mission

The late access unit (Figure 13) was transferred into the payload, along with the cells shortly before launch. The sounding rocket, used in the TEXUS 54 mission, was composed of the payload and a Brazilian two-stage solid propellant VSB 30 rocket. The rocket was launched on the 13th of May 2018 from ESRANGE space center in Kiruna, Sweden. After launch, the sounding rocket reached an altitude of ~ 260 km. And it entered microgravity 75 s later after launch. The microgravity phase of $< 10^{-4}$ g lasted for ~ 353 s. Following the microgravity phase, the rocket went back to Earth by a parachute-mediated deceleration. The payload was recovered after landing by a helicopter (Figure 13).

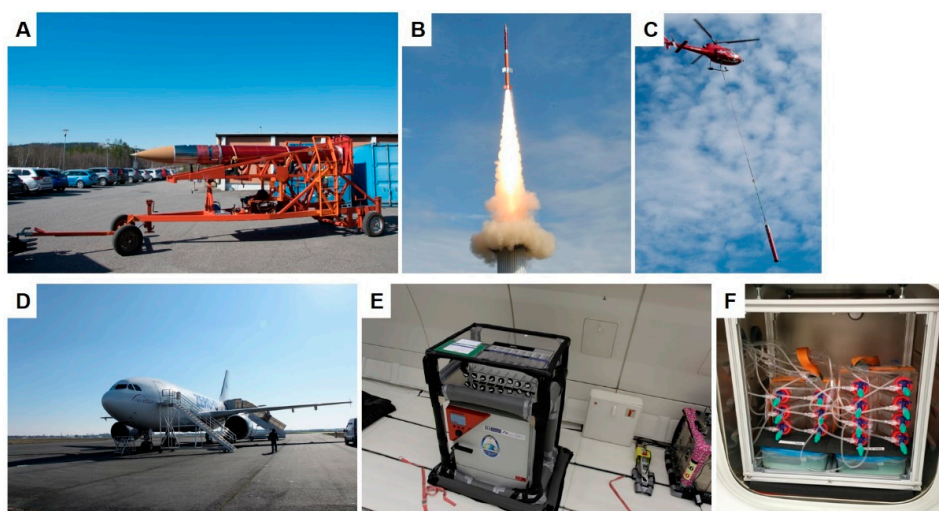


Figure 12. Shows the vehicles and experimental setups of the μ g-experiments. (A): TX 54 rocket transportation to the launch tower. (B): Launch of the TX 54 rocket (courtesy of Airbus, Defense & Space). (C): retrieval of the TX 54 rocket with a helicopter. (D): Airbus 310 aircraft used for the parabolic flight. (E): The incubator used for the experiment. (F): Inside of the incubator prior to take off of the flight.

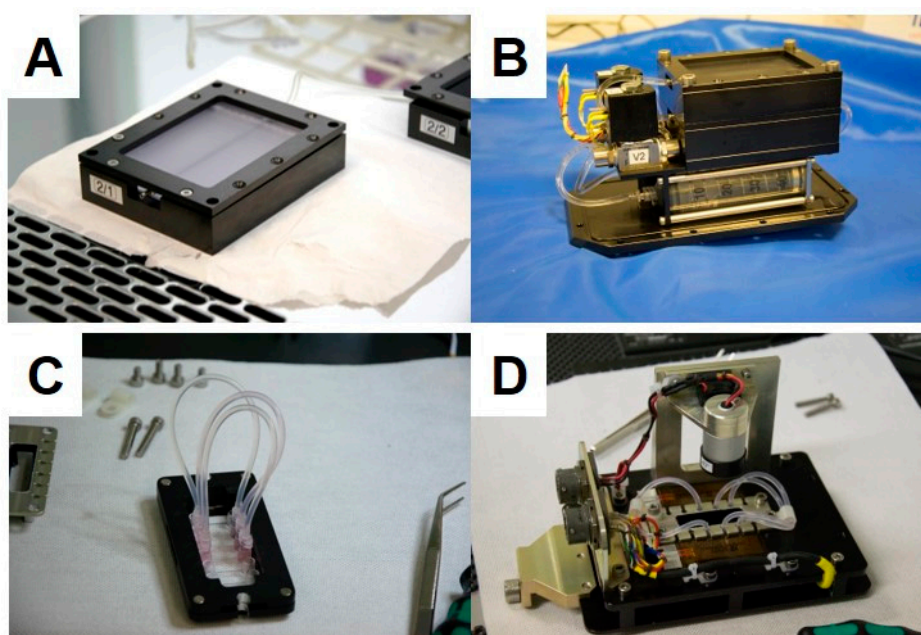


Figure 13. Late access units of the FLUFIX (A,B) and FLUMIAS (C,D).

4.6. FLUFIX and Immunocytochemistry of MCF-7 Fixed Cells during TEXUS 54

The MCF 7 cells were cultured in 18 well Ibidi slides. Approximately 2500 cells were seeded into each well. 4 slides were cultured on ground at 1g to be used as a control. Furthermore, there were four 18 well Ibidi slides on board of the rocket. The cells, on board of the rocket, were fixed with 4% paraformaldehyde (PFA) at two time points. Two Ibidi slides were fixed at the end of the hyper gravity phase and the other two slides were fixed at the end of the microgravity phase. The ground control slides were fixed with 4% PFA in parallel to the launch of the rocket. The slides were recovered and transferred back to the lab in 4% PFA.

To discard excess PFA, the cells were washed with DPBS three times. Afterwards, the slides were washed with 0.3% Triton X in DPBS for 10 min with agitation which was followed by washing with DPBS. To prevent non-specific binding, the slides were incubated in 3% BSA for one hour. Primary antibodies were added to the slides overnight at 4 °C (Table 1). The following day, the slides were washed with DPBS and the secondary antibody Alexa Fluor 488 anti-mouse/anti-rabbit was added for one hour (Table 1). The slides were washed again with DPBS and Alexa Fluor 568 phalloidin was added for one hour, followed by washing with DPBS and mounting with Fluoroshield with DAPI (Sigma). For the slides to be ready for examination, they were incubated overnight at 4 °C. Carl ZEISS LSM 800 Confocal laser scanning microscope was used to examine the cells. Three lasers were used to examine the slides: 488 nm, 561 nm and 405 nm for visualization of Alexa 488, Alexa 568 and DAPI, respectively.

The microscopic images were quantitatively analyzed by ImageJ 1.52b (U.S. National Institutes of Health, Bethesda, MD, USA) to detect the difference in protein expression between different conditions. The intensity of the fluorescence in every photo was measured by ImageJ after the areas of interest were defined by the wand (tracing) tool. Furthermore, all the values were normalized to background fluorescence.

4.7. 31st DLR Parabolic Flight Campaign

The parabolic flights were performed from the Bordeaux-Mérignac Airport between 6 and 9 March 2018. The cells were transferred on board of the Airbus 310 to a 37 °C pre-warmed incubator shortly before take-off and they were incubated at 37 °C for the whole time of the flight. The parabolic flight consisted of 31 parabolas. Each parabola had an initial phase of hyper gravity (1.8 g) for 22 s during pull up, followed by a microgravity phase for 22 s. At the end of the parabola, there is a second

phase of hyper gravity for 22 s during pull out. The flight maneuver is repeated 31 times per flight day [11] (Figure 12).

Table 1. Names, types, classes, companies, and dilutions of all the antibodies that were used for immunostaining.

Antibody Name	Class	Type	Company	Reference no.	Dilution
Matrix Metalloproteinase 9 (MMP9) (2C3)	mouse monoclonal AB	Primary Antibody	Santa Cruz	sc-21733	(1:100)
interleukin 6 (IL6) (E-4)	mouse monoclonal AB	Primary Antibody	Santa Cruz	sc-28343	(1:100)
interleukin 8 (IL8) (C-11)	mouse monoclonal AB	Primary Antibody	Santa Cruz	sc-376750	(1:100)
Vascular Endothelial Growth Factor (VEGF) (c-term)	Rabbit monoclonal	Primary Antibody	Epitomics, Inc	#1909-1	(1:250)
Alexa fluor plus 488 goat anti-mouse IgG (H + L)	Goat polyclonal	Secondary Antibody	Invitrogen by Thermo Fischer Scientific	A32723	(1:400)
Alexa fluor 488 F(ab') ₂ fragment of goat anti-rabbit IgG (H + L)	Goat polyclonal	Secondary Antibody	Invitrogen by Thermo Fischer Scientific	A11070	(1:500)
Alexa Fluor 568 phalloidin	bicyclic peptide toxin	Toxin	Invitrogen by Thermo Fischer Scientific	A12380	one unit in 200 μ L per slide
Fluoroshield with DAPI	fluorescent stain	fluorescent stain	Sigma Life science	F6057	no dilution

4.8. RNA Isolation and qPCR

During the parabolic flights, the MCF-7 cells were fixed with RNAlater (Invitrogen by Thermo Fischer Scientific) at the end of the first parabola (P1) and the end of the last parabola (P31). The cells were cultured in T-75 cell culture flasks (75 cm², SARSTEDT) with 10 mL medium in each flask. Each flask had a fixed three-way connector on the lid which was connected with 140 cm tubing to a 50 mL syringe filled with RNAlater. The RNAlater was injected manually into the flasks at the designated times. Additional MCF-7 cells were incubated on ground to serve as a ground control. The ground control cells were fixed with RNAlater in parallel to the samples on board of the flight. After landing, the medium and RNAlater mixture were thrown away and replaced with 3-5 mL of fresh RNAlater. Cells were harvested with 25 cm scraper (SARSTEDT) and incubated with RNAlater at 4 °C in 15 mL tubes until RNA isolation.

All the falcon tubes were centrifuged (2500 g for 10 min at 4 °C), followed by discarding the supernatant. The RNA was isolated afterwards by the RNeasy Mini Kit (Qiagen) according to the manufacturer's protocol. The quality of the RNA was evaluated with a spectrophotometer. The RNA was converted to cDNA with a High Capacity cDNA reverse Transcription Kit according to the manufacturer's protocol (Applied Biosystems, Darmstadt, Germany). The final volume of the reverse transcription reaction mix was 20 μ L with 1 μ g total RNA added to each reaction mix. The primers were designed using Primer Blast (primer designing tool from NCBI).

A total volume of 13 μ L SYBR green reaction mix (Applied Biosystems) was pipetted in each well in a 96 well plate. 1 μ L of cDNA was added to each reaction mix with a concentration of 100 μ M forward and reverse primers. 7500 Fast Real-Time PCR System (Applied Biosystems) was used to determine the transcription level of targeted genes (Table 2). The program consisted of initial 20 s holding stage of 95 °C followed by cycling stage. The cycling stage consisted of 40 cycles of 3 s at 95 °C and 30 s at 60 °C. A melt curve stage was implemented at the end which consisted of 15 s at 95 °C and 60 s at 60 °C. The data were collected and analyzed by the $\Delta\Delta$ CT method; 18s and TBP were used as reference genes [21].

Table 2. List of all the primer sequences used in the quantitative PCR. All the sequences are listed from 5'–3' direction.

Factor	Primer Name	Sequence 5'–3'
18S	18s-F	GGAGCCTGCCGCTTAATTT
	18s-R	CAACTAAGAACGGCCATGCA
ACTB	ACTB-F	TGCCGACAGGATGCAGAAG
	ACTB-R	GCCGATCCACACGGAGTACT
CAV1	CAV1-F	CCTCCTCACAGTTTTTCATCCA
	CAV1-R	TGTAGATGTTGCCCTGTTCC
CAV2	CAV2-F	GATCCCCACCGGCTCAAC
	CAV2-R	CACCGGCTCTGCGATCA
COL1A1	COL1A1-F	ACGAAGACATCCCACCAATCAC
	COL1A1-R	CGTTGTGCGAGACGCAGAT
EZR	EZR-F	GCAATCCAGCCAAATACAACCTG
	EZR-R	CCACATAGTGGAGGCCAAAGTAC
FN1	FN1-F	TGAGGAGCATGGTTTTAGGAGAA
	FN1-R	TCCTCATTTACATTCGGCGTATAC
ICAM1	ICAM1-F	CGGCTGACGTGTGCAGTAAT
	ICAM1-R	CTTCTGAGACCTCTGGCTTCGT
IL6	IL6-F	CGGGAACGAAAGAGAAGCTCTA
	IL6-R	GAGCAGCCCCAGGGAGAA
CXCL8	IL8-F	TGGCAGCCTTCCTGATTTCT
	IL8-R	GGGTGGAAAGGTTTGGAGTATG
KRT8	KRT8-F	GATCTCTGAGATGAACCGGAACA
	KRT8-R	GCTCGGCATCTGCAATGG
LAMA1	LAMA1-F	TGACTGACCTGGGTTTCAGGA
	LAMA1-R	TGCTAGCACTCCTTGCTTCC
LAMA3	LAMA3-F	AAAGCAAGAAGTCAGTCCAGC
	LAMA3-R	TCCCATGAAGACCATCTCGG
MMP9	MMP9-F	CCTGGAGACCTGAGAACCAATC
	MMP9-R	TTCGACTCTCCACGCATCTCT
MSN	MSN-F	GAAATTTGTCATCAAGCCCATTG
	MSN-R	CCATGCACAAGGCCAAGAT
TBP	TBP-F	GTGACCCAGCATCACTGTTTC
	TBP-R	GCAAACCAGAAACCCTTGCG
TIMP1	TIMP1-F	GCCATCGCCGAGATC
	TIMP1-R	GCTATCAGCCACAGCAACAACA
TLN1	TLN1-F	GATGGCTATTACTCAGTACAGACAACCTGA
	TLN1-R	CATAGTAGACTCCTCATCTCCTTCCA
TUBB	TUBB-F	CTGGACCGCATCTCTGTGTACTAC
	TUBB-R	GACCTGAGCGAACAGAGTCCAT
VEGFA	VEGFA-F	GCGCTGATAGACATCCATGAAC
	VEGFA-R	CTACCTCCACCATGCCAAGTG
VCL	VCL-F	GTCTCGGCTGCTCGTATCTT
	VCL-R	GTCCACCAGCCCTGTCATTT
PTK2	FAK1-F	TGTGGGTAAACCAGATCCTGC
	FAK1-R	CTGAAGCTTGACACCCTCGT
RDX	RDX-F	GAAAATGCCGAAACCAATCAA
	RDX-R	GTATTGGGCTGAATGGCAAATT
PAI1	PAI1-F	AGGCTGACTTCACGAGTCTTTCA
	PAI1-R	CACTCTCGTTACCTCGATCTTC
CDH1	CDH1-F	GCTGGACCGAGAGAGTTTCC
	CDH1-R	CAGCTGTTGCTGTTGTGCTT
ITGB1	ITGB1-F	GAAAACAGCGCATATCTGGAAATT
	ITGB1-R	CAGCCAATCAGTGATCCACAA

4.9. Western Blot Analysis

Western blot analysis, gel electrophoresis, trans-blotting, and densitometry were carried out following routine protocols as described previously [38–40]. Following lysis and centrifugation, aliquots of 30 µg were subjected to SDS-PAGE and Western blotting. The samples attained at the end of the P1 and P31 are compared to 1g control samples. Each condition is represented with 4 samples with a total number of 12 samples for all the conditions. The samples were loaded on Criterion XT 4–12% precast gels (Bio-Rad, Hercules, CA, USA) and run for 1h at 150 volts. Proteins were then transferred with a TurboBlot (Bio-Rad) (100 V, 30 min) to a PVDF membrane. Glyceraldehyde-3-phosphate-dehydrogenase (GAPDH) was used as a loading control. Membranes were then blocked for two hours in TBS-T containing 0.3% I Block (Applied Biosystems, Foster City, CA, USA). For detection of the selected antigens (see Table 3), the membranes were incubated overnight at room temperature in TBS-T and 0.3% I Block solutions of the antibodies. Following three washing steps of 5 min, membranes were incubated for additional two hours at room temperature with secondary antibody horseradish peroxidase (HRP)-linked antibody (Cell Signaling Technology Inc., Danvers, MA, USA) diluted 1:4000 in TBS-T and 0.3% I-Block. The respective protein bands were visualized using Bio-Rad Clarity Western ECL (Bio-Rad) and images were captured with Image Quant LAS 4000 mini (GE Healthcare Life Science, Freiburg, Germany). Images of stained membranes were captured on Syngene PXi 4EZ image analysis system (Synoptics, Cambridge, UK) and analyzed using the ImageJ software for densitometric quantification of the respective bands and total protein load [22].

Table 3. List of the names, sources, companies, molecular weight and dilutions of all the antibodies that were used for Western blots.

Antibody Name	Source	Company	Reference no.	MW kDa	Dilution
Anti-Cyclophilin B	Rabbit monoclonal	Abcam	#178397	24	1: 1000
Anti-Cytokeratin	Mouse monoclonal	Sigma	#C1801	68	1: 1000
Anti-E Cadherin	Mouse monoclonal	Abcam	ab1416	97	1:500
Anti-FAK	Rabbit monoclonal	Abcam	ab40794	125	1:1000
Anti-IL-8	Rabbit polyclonal	Abcam	ab7747	11	1:500
Anti-Integrin beta 1	Rabbit monoclonal	Abcam	#134179	88	1: 1000
Anti-Laminin	Rabbit polyclonal	Sigma	#L9393	220	1: 1000
Anti-PAI1	Rabbit polyclonal	Abcam	Ab66705	45	1:1000
Anti-Vinculin	Mouse monoclonal	Abcam	Ab18058	124	1:1000
Anti-β-Actin	Mouse monoclonal	Sigma	A5316	42	1:2000
Beta Tubulin Antibody	Rabbit Polyclonal	Santa Cruz Biotechnology	sc-9104	55	1: 1000
Ezrin	Rabbit polyclonal	Cell Signaling	#3145	81	1:500
Fibronectin	Mouse monoclonal	Invitrogen	#MA5-11981	250	1:1000
GAPDH (14C10)	Rabbit monoclonal	Cell signaling	#5014S	37	1:1000
MMP9	Mouse monoclonal	ThermoFisher	#MA5-14220	92	1: 500
Moesin (Q480)	Rabbit polyclonal	Cell signaling	#3150	78	1:500
Radixin	Rabbit monoclonal	Cell Signaling	#2636S	80	1: 1000
TIMP1	Mouse monoclonal	ThermoFisher	#MA5-13688	28	1: 500

4.10. Immunostaining of Fixed MCF-7 Cells Collected during the 31st Parabolic Flight Campaign

Approximately 20,000 MCF-7 cells were seeded into Ibidi slide flasks two days prior to the flight day. Four flasks were fixed at the end of the first parabola and additional four flasks were fixed at the end of the 31st parabola. Four slide flasks were cultured in parallel on ground to act as a control. Cells were fixed with 4% PFA and transferred to the lab to continue the staining procedure. MMP9, IL 6 and IL-8 were used as primary Antibodies. Alexa Fluor plus 488 goat anti-mouse IgG was used as a secondary antibody. DAPI and phalloidin were used additionally in all the slides (Table 1). The immunostaining procedure was performed as mentioned earlier [22].

4.11. Statistical Analysis

GraphPad prism 7.01 (GraphPad Software, Inc., California, USA) was used to analyze the data. The nonparametric Mann–Whitney U test was used as a statistical test of significance. The difference between groups was considered significant when the P-value was less than 0.05.

5. Conclusions

The FLUMIAS microscope has now been shown to be an elegant device suitable for live-cell imaging in real microgravity [11,30]. We could show for the first time, significant changes in the F-actin and microtubule cytoskeleton on living MCF-7 breast cancer cells in orbit. MCF-7 cells sense microgravity early and focal adhesion proteins are involved in this process. The actin cytoskeleton is contributing to adhesion and migration of the cancer cells. The early formation of lamellipodia and filopodia is the right step in this direction [66]. Early increases in *VEGFA* and *CXCL8* gene expression as well as the down-regulation of *VCL* mRNA and the reduced E-cadherin protein indicate a change to a more invasive function of the MCF-7 cells exposed to short-term microgravity which supports earlier data with thyroid cancer cells exposed to parabolic flight maneuvers [16]. Our future plan is to investigate these cells for a longer time in space to investigate the behavior of breast cancer cells on the ISS.

Author Contributions: Sounding rocket flight, A.S., B.S., and H.O.; Conceptualization, D.G., T.J.C. and S.K.; methodology, S.K., M.Z.N., D.M., T.J.B., T.J.C. and J.S.; Software, T.J.B. and S.K.; Validation, D.G., T.J.C., S.K., M.K. and D.M.; Formal analysis, S.K., J.S., and M.W.; Investigation, S.K.; Resources, M.I.; Writing—Original draft preparation, S.K., T.J.C, D.G., M.K., M.W.; Project administration, D.G.; funding acquisition, D.G. and M.I.

Funding: This research was funded by the German Space Agency (DLR; BMWi projects 50WB1524; 50WB1924).

Acknowledgments: We like to thank Otfried Joop, Michael Becker and Markus Braun (German Aerospace Center DLR, Bonn) for their support and for giving us the possibility to attend the TEXUS mission in Kiruna, Sweden and the 31st DLR Parabolic Flight Campaign in Bordeaux-Mérignac, France.

Conflicts of Interest: The authors declare no conflict of interest.

Abbreviations

2D	two-dimensional
3D	three-dimensional
<i>ACTB</i>	Beta-actin
<i>CAV1</i>	Caveolin-1
<i>CAV2</i>	Caveolin-2
<i>CDH1</i>	E-cadherin
<i>COL1A1</i>	Collagen type 1 alpha 1
<i>CXCL8</i>	Interleukin 8
DAPI	4',6-diamidino-2-phenylindole
DLR	German Aerospace Center
ECM	Extracellular matrix
ESRANGE	European Space and Sounding Rocket Range
<i>EZR</i>	Ezrin
FLUMIAS	spinning-disc Fluorescence Microscopy Analysis System
<i>FN1</i>	Fibronectin
FTC-133	Follicular thyroid cancer cell line 133
GFP	Green fluorescent protein
GLOBOCAN	Global Cancer Observatory
IL-6	Interleukin 6
IL-8	Interleukin 8
ISS	International Space Station
<i>ITGB1</i>	Integrin beta 1
<i>KRT8</i>	Cytokeratin 8

LAMA1	Laminin alpha 1
LAMA3	Laminin alpha 3
LIMA1	LIM domain and actin-binding protein 1
MCF-7	Michigan cancer foundation
MCS	Multicellular spheroids
MMP9	Matrix metalloproteinases 9
MSN	Moesin
MTSS1	Metastasis suppressor protein 1
P	Parabola
PAI1	Plasminogen activator inhibitor 1
PF	Parabolic flight
PFA	Paraformaldehyde
PFC	Parabolic flight campaign
pLAGICT	pcDNA3.1 LifeAct-eGFP-IRES-mCherry-Tubulin
pSB-LAGICT	Sleeping Beauty LifeAct-eGFP-IRES-mCherry-Tubulin
PTK2	Protein tyrosine kinase 2; Focal adhesion kinase 1
r- μ g	real microgravity
RDX	Radixin
RPM	Random positioning machine
s- μ g	simulated microgravity
SB	Sleeping beauty
TIMP1	Metalloproteinase inhibitor 1
TLN1	Talin-1
TUBB	Beta tubulin
TX (TEXUS)	'Technische Experimente unter Schwerelosigkeit'
VCL	Vinculin
VEGFA	Vascular endothelial growth factor A
WHO	World health organization

References

1. Bray, F.; Ferlay, J.; Soerjomataram, I.; Siegel, R.L.; Torre, L.A.; Jemal, A. Global cancer statistics 2018: Globocan estimates of incidence and mortality worldwide for 36 cancers in 185 countries. *CA Cancer J. Clin.* **2018**, *68*, 394–424. [[CrossRef](#)] [[PubMed](#)]
2. Cancer.net. Breast cancer: Statistics. Available online: <https://www.cancer.net/cancer-types/breast-cancer> (accessed on 14 May 2019).
3. Becker, J.L.; Souza, G.R. Using space-based investigations to inform cancer research on earth. *Nat. Rev. Cancer* **2013**, *13*, 315–327. [[CrossRef](#)] [[PubMed](#)]
4. Grimm, D.; Wehland, M.; Pietsch, J.; Aleshcheva, G.; Wise, P.; van Loon, J.; Ulbrich, C.; Magnusson, N.E.; Infanger, M.; Bauer, J. Growing tissues in real and simulated microgravity: New methods for tissue engineering. *Tissue Eng. Part B Rev.* **2014**, *20*, 555–566. [[CrossRef](#)] [[PubMed](#)]
5. Grimm, D.; Bauer, J.; Wise, P.; Kruger, M.; Simonsen, U.; Wehland, M.; Infanger, M.; Corydon, T.J. The role of sox family members in solid tumours and metastasis. *Semin. Cancer Biol.* **2019**. [[CrossRef](#)] [[PubMed](#)]
6. Vorselen, D.; Roos, W.H.; MacKintosh, F.C.; Wuite, G.J.; van Loon, J.J. The role of the cytoskeleton in sensing changes in gravity by nonspecialized cells. *FASEB J.* **2014**, *28*, 536–547. [[CrossRef](#)] [[PubMed](#)]
7. Corydon, T.J.; Mann, V.; Slumstrup, L.; Kopp, S.; Sahana, J.; Askou, A.L.; Magnusson, N.E.; Echevoyen, D.; Bek, T.; Sundaresan, A.; et al. Reduced expression of cytoskeletal and extracellular matrix genes in human adult retinal pigment epithelium cells exposed to simulated microgravity. *Cell Physiol Biochem* **2016**, *40*, 1–17. [[CrossRef](#)] [[PubMed](#)]
8. Hughes-Fulford, M. Function of the cytoskeleton in gravisensing during spaceflight. *Adv. Space Res.* **2003**, *32*, 1585–1593. [[CrossRef](#)]
9. Maier, J.A.; Cialdai, F.; Monici, M.; Morbidelli, L. The impact of microgravity and hypergravity on endothelial cells. *Biomed. Res. Int.* **2015**, *2015*, 434803. [[CrossRef](#)]

10. Carlsson, S.I.; Bertilaccio, M.T.; Ballabio, E.; Maier, J.A. Endothelial stress by gravitational unloading: Effects on cell growth and cytoskeletal organization. *Biochim. Biophys. Acta* **2003**, *1642*, 173–179. [[CrossRef](#)]
11. Corydon, T.J.; Kopp, S.; Wehland, M.; Braun, M.; Schutte, A.; Mayer, T.; Hulsing, T.; Oltmann, H.; Schmitz, B.; Hemmersbach, R.; et al. Alterations of the cytoskeleton in human cells in space proved by life-cell imaging. *Sci. Rep.* **2016**, *6*, 20043. [[CrossRef](#)]
12. Kopp, S.; Warnke, E.; Wehland, M.; Aleshcheva, G.; Magnusson, N.E.; Hemmersbach, R.; Corydon, T.J.; Bauer, J.; Infanger, M.; Grimm, D. Mechanisms of three-dimensional growth of thyroid cells during long-term simulated microgravity. *Sci. Rep.* **2015**, *5*, 16691. [[CrossRef](#)] [[PubMed](#)]
13. Kopp, S.; Kruger, M.; Feldmann, S.; Oltmann, H.; Schutte, A.; Schmitz, B.; Bauer, J.; Schulz, H.; Saar, K.; Huebner, N.; et al. Thyroid cancer cells in space during the texus-53 sounding rocket mission—the thyroid project. *Sci. Rep.* **2018**, *8*, 10355. [[CrossRef](#)] [[PubMed](#)]
14. Kopp, S.; Kruger, M.; Bauer, J.; Wehland, M.; Corydon, T.J.; Sahana, J.; Nassef, M.Z.; Melnik, D.; Bauer, T.J.; Schulz, H.; et al. Microgravity affects thyroid cancer cells during the texus-53 mission stronger than hypergravity. *Int. J. Mol. Sci.* **2018**, *19*. [[CrossRef](#)] [[PubMed](#)]
15. Grimm, D.; Egli, M.; Kruger, M.; Riwaldt, S.; Corydon, T.J.; Kopp, S.; Wehland, M.; Wise, P.; Infanger, M.; Mann, V.; et al. Tissue engineering under microgravity conditions-use of stem cells and specialized cells. *Stem Cells Dev.* **2018**, *27*, 787–804. [[CrossRef](#)] [[PubMed](#)]
16. Ma, X.; Pietsch, J.; Wehland, M.; Schulz, H.; Saar, K.; Hübner, N.; Bauer, J.; Braun, M.; Schwarzwälder, A.; Segerer, J.; et al. Differential gene expression profile and altered cytokine secretion of thyroid cancer cells in space. *FASEB J.* **2014**, *28*, 813–835. [[CrossRef](#)] [[PubMed](#)]
17. Vassy, J.; Portet, S.; Beil, M.; Millot, G.; Fauvel-Lafeve, F.; Gasset, G.; Schoevaert, D. Weightlessness acts on human breast cancer cell line mcf-7. *Adv Space Res* **2003**, *32*, 1595–1603. [[CrossRef](#)]
18. Vassy, J.; Portet, S.; Beil, M.; Millot, G.; Fauvel-Lafeve, F.; Karniguian, A.; Gasset, G.; Irinopoulou, T.; Calvo, F.; Rigaut, J.P.; et al. The effect of weightlessness on cytoskeleton architecture and proliferation of human breast cancer cell line mcf-7. *FASEB J.* **2001**, *15*, 1104–1106. [[CrossRef](#)] [[PubMed](#)]
19. Tewinkel, M.; Burfeindt, J.; Rank, P.; Volkmann, D. Automatic fixation facility for plant seedlings in the texus sounding rocket programme. *Microgravity Sci. Technol.* **1991**, *4*, 216–220. [[PubMed](#)]
20. Kopp, S.; Slumstrup, L.; Corydon, T.J.; Sahana, J.; Aleshcheva, G.; Islam, T.; Magnusson, N.E.; Wehland, M.; Bauer, J.; Infanger, M.; et al. Identifications of novel mechanisms in breast cancer cells involving duct-like multicellular spheroid formation after exposure to the random positioning machine. *Sci. Rep.* **2016**, *6*, 26887. [[CrossRef](#)]
21. Kopp, S.; Sahana, J.; Islam, T.; Petersen, A.G.; Bauer, J.; Corydon, T.J.; Schulz, H.; Saar, K.; Huebner, N.; Slumstrup, L.; et al. The role of nfkappab in spheroid formation of human breast cancer cells cultured on the random positioning machine. *Sci. Rep.* **2018**, *8*, 921. [[CrossRef](#)]
22. Aleshcheva, G.; Wehland, M.; Sahana, J.; Bauer, J.; Corydon, T.J.; Hemmersbach, R.; Frett, T.; Egli, M.; Infanger, M.; Grosse, J.; et al. Moderate alterations of the cytoskeleton in human chondrocytes after short-term microgravity produced by parabolic flight maneuvers could be prevented by up-regulation of bmp-2 and sox-9. *FASEB J.* **2015**, *29*, 2303–2314. [[CrossRef](#)] [[PubMed](#)]
23. Wehland, M.; Ma, X.; Braun, M.; Hauslage, J.; Hemmersbach, R.; Bauer, J.; Grosse, J.; Infanger, M.; Grimm, D. The impact of altered gravity and vibration on endothelial cells during a parabolic flight. *Cell Physiol. Biochem.* **2013**, *31*, 432–451. [[CrossRef](#)] [[PubMed](#)]
24. Pietsch, J.; Gass, S.; Nebuloni, S.; Echegoyen, D.; Riwaldt, S.; Baake, C.; Bauer, J.; Corydon, T.J.; Egli, M.; Infanger, M.; et al. Three-dimensional growth of human endothelial cells in an automated cell culture experiment container during the spacex crs-8 iss space mission - the spheroids project. *Biomaterials* **2017**, *124*, 126–156. [[CrossRef](#)] [[PubMed](#)]
25. Strauch, S.M.; Grimm, D.; Corydon, T.J.; Kruger, M.; Bauer, J.; Lebert, M.; Wise, P.; Infanger, M.; Richter, P. Current knowledge about the impact of microgravity on the proteome. *Expert. Rev. Proteomics* **2018**, 1–12. [[CrossRef](#)] [[PubMed](#)]
26. Hader, D.P.; Braun, M.; Grimm, D.; Hemmersbach, R. Gravireceptors in eukaryotes—a comparison of case studies on the cellular level. *NPJ Microgravity* **2017**, *3*, 13. [[CrossRef](#)] [[PubMed](#)]
27. Guignandon, A.; Faure, C.; Neutelings, T.; Rattner, A.; Mineur, P.; Linossier, M.T.; Laroche, N.; Lambert, C.; Deroanne, C.; Nusgens, B.; et al. Rac1 gtpase silencing counteracts microgravity-induced effects on osteoblastic cells. *FASEB J.* **2014**, *28*, 4077–4087. [[CrossRef](#)] [[PubMed](#)]

28. Mann, V.; Grimm, D.; Corydon, T.J.; Kruger, M.; Wehland, M.; Riwaltdt, S.; Sahana, J.; Kopp, S.; Bauer, J.; Reseland, J.E.; et al. Changes in human foetal osteoblasts exposed to the random positioning machine and bone construct tissue engineering. *Int. J. Mol. Sci.* **2019**, *20*. [[CrossRef](#)]
29. Tan, X.; Xu, A.; Zhao, T.; Zhao, Q.; Zhang, J.; Fan, C.; Deng, Y.; Freywald, A.; Genth, H.; Xiang, J. Simulated microgravity inhibits cell focal adhesions leading to reduced melanoma cell proliferation and metastasis via fak/rhoa-regulated mtorc1 and ampk pathways. *Sci. Rep.* **2018**, *8*, 3769. [[CrossRef](#)]
30. Thiel, C.S.; Tauber, S.; Seebacher, C.; Schropp, M.; Uhl, R.; Lauber, B.; Polzer, J.; Neelam, S.; Zhang, Y.; Ullrich, O. Real-time 3d high-resolution microscopy of human cells on the international space station. *Int. J. Mol. Sci.* **2019**, *20*. [[CrossRef](#)]
31. Moos, P.J.; Graft, K.; Edwards, M.D.; Stodieck, L.S.; Einhorn, R.; Luttgies, M.W. Gravity-induced changes in microtubule formation. *USGS Bull.* **1988**, *2*, 55.
32. Papaseit, C.; Pochon, N.; Tabony, J. Microtubule self-organization is gravity-dependent. *Proc. Natl. Acad. Sci. USA* **2000**, *97*, 8364–8368. [[CrossRef](#)] [[PubMed](#)]
33. Piepmeier, E.H.; Kalns, J.E.; McIntyre, K.M.; Lewis, M.L. Prolonged weightlessness affects promyelocytic multidrug resistance. *Exp. Cell Res.* **1997**, *237*, 410–418. [[CrossRef](#)] [[PubMed](#)]
34. Boonstra, J. Growth factor-induced signal transduction in adherent mammalian cells is sensitive to gravity. *FASEB J.* **1999**, *13*, S35–S42. [[CrossRef](#)]
35. Leung, D.W.; Cachianes, G.; Kuang, W.J.; Goeddel, D.V.; Ferrara, N. Vascular endothelial growth factor is a secreted angiogenic mitogen. *Science* **1989**, *246*, 1306–1309. [[CrossRef](#)] [[PubMed](#)]
36. Luo, M.; Hou, L.; Li, J.; Shao, S.; Huang, S.; Meng, D.; Liu, L.; Feng, L.; Xia, P.; Qin, T.; et al. Vegf/nrp-1axis promotes progression of breast cancer via enhancement of epithelial-mesenchymal transition and activation of nf-kappab and beta-catenin. *Cancer Lett.* **2016**, *373*, 1–11. [[CrossRef](#)] [[PubMed](#)]
37. Tuttle, R.M.; Fleisher, M.; Francis, G.L.; Robbins, R.J. Serum vascular endothelial growth factor levels are elevated in metastatic differentiated thyroid cancer but not increased by short-term tsh stimulation. *J. Clin. Endocrinol. Metab.* **2002**, *87*, 1737–1742. [[CrossRef](#)]
38. Grosse, J.; Wehland, M.; Pietsch, J.; Ma, X.; Ulbrich, C.; Schulz, H.; Saar, K.; Hubner, N.; Hauslage, J.; Hemmersbach, R.; et al. Short-term weightlessness produced by parabolic flight maneuvers altered gene expression patterns in human endothelial cells. *FASEB J.* **2012**, *26*, 639–655. [[CrossRef](#)]
39. Ulbrich, C.; Pietsch, J.; Grosse, J.; Wehland, M.; Schulz, H.; Saar, K.; Hubner, N.; Hauslage, J.; Hemmersbach, R.; Braun, M.; et al. Differential gene regulation under altered gravity conditions in follicular thyroid cancer cells: Relationship between the extracellular matrix and the cytoskeleton. *Cell Physiol. Biochem.* **2011**, *28*, 185–198. [[CrossRef](#)] [[PubMed](#)]
40. Lu, D.; Sun, S.; Zhang, F.; Luo, C.; Zheng, L.; Wu, Y.; Li, N.; Zhang, C.; Wang, C.; Chen, Q.; et al. Microgravity-induced hepatogenic differentiation of rbmscs on board the sj-10 satellite. *FASEB J.* **2019**, *33*, 4273–4286. [[CrossRef](#)]
41. dos Santos, P.B.; Zanetti, J.S.; Ribeiro-Silva, A.; Beltrao, E.I. Beta 1 integrin predicts survival in breast cancer: A clinicopathological and immunohistochemical study. *Diagn Pathol.* **2012**, *7*, 104. [[CrossRef](#)]
42. Theodosiou, M.; Widmaier, M.; Bottcher, R.T.; Rognoni, E.; Veelders, M.; Bharadwaj, M.; Lambacher, A.; Austen, K.; Muller, D.J.; Zent, R.; et al. Kindlin-2 cooperates with talin to activate integrins and induces cell spreading by directly binding paxillin. *Elife* **2016**, *5*, e10130. [[CrossRef](#)] [[PubMed](#)]
43. Shinde, A.; Libring, S.; Alpsy, A.; Abdullah, A.; Schaber, J.A.; Solorio, L.; Wendt, M.K. Autocrine fibronectin inhibits breast cancer metastasis. *Mol. Cancer Res.* **2018**, *16*, 1579–1589. [[CrossRef](#)] [[PubMed](#)]
44. Yamamoto, H.; Ehling, M.; Kato, K.; Kanai, K.; van Lessen, M.; Frye, M.; Zeuschner, D.; Nakayama, M.; Vestweber, D.; Adams, R.H. Integrin beta1 controls ve-cadherin localization and blood vessel stability. *Nat. Commun.* **2015**, *6*, 6429. [[CrossRef](#)] [[PubMed](#)]
45. Lee, T.H.; Seng, S.; Li, H.; Kennel, S.J.; Avraham, H.K.; Avraham, S. Integrin regulation by vascular endothelial growth factor in human brain microvascular endothelial cells: Role of alpha6beta1 integrin in angiogenesis. *J. Biol. Chem.* **2006**, *281*, 40450–40460. [[CrossRef](#)] [[PubMed](#)]
46. Das, M.; Ithychanda, S.; Qin, J.; Plow, E.F. Mechanisms of talin-dependent integrin signaling and crosstalk. *Biochim Biophys Acta* **2014**, *1838*, 579–588. [[CrossRef](#)] [[PubMed](#)]
47. Grosse, J.; Wehland, M.; Pietsch, J.; Schulz, H.; Saar, K.; Hubner, N.; Eilles, C.; Bauer, J.; Abou-El-Ardat, K.; Baatout, S.; et al. Gravity-sensitive signaling drives 3-dimensional formation of multicellular thyroid cancer spheroids. *FASEB J.* **2012**, *26*, 5124–5140. [[CrossRef](#)] [[PubMed](#)]

48. Ilic, D.; Kovacic, B.; Johkura, K.; Schlaepfer, D.D.; Tomasevic, N.; Han, Q.; Kim, J.B.; Howerton, K.; Baumbusch, C.; Ogiwara, N.; et al. Fak promotes organization of fibronectin matrix and fibrillar adhesions. *J. Cell Sci.* **2004**, *117*, 177–187. [[CrossRef](#)]
49. Guan, J.L. Integrin signaling through fak in the regulation of mammary stem cells and breast cancer. *IUBMB Life* **2010**, *62*, 268–276. [[CrossRef](#)]
50. Sullivan, N.J.; Sasser, A.K.; Axel, A.E.; Vesuna, F.; Raman, V.; Ramirez, N.; Oberyszyn, T.M.; Hall, B.M. Interleukin-6 induces an epithelial-mesenchymal transition phenotype in human breast cancer cells. *Oncogene* **2009**, *28*, 2940–2947. [[CrossRef](#)]
51. Kitadai, Y.; Haruma, K.; Mukaida, N.; Ohmoto, Y.; Matsutani, N.; Yasui, W.; Yamamoto, S.; Sumii, K.; Kajiyama, G.; Fidler, I.J.; et al. Regulation of disease-progression genes in human gastric carcinoma cells by interleukin 8. *Clin. Cancer Res.* **2000**, *6*, 2735–2740.
52. Cohen, T.; Nahari, D.; Cerem, L.W.; Neufeld, G.; Levi, B.Z. Interleukin 6 induces the expression of vascular endothelial growth factor. *J. Biol. Chem.* **1996**, *271*, 736–741. [[CrossRef](#)] [[PubMed](#)]
53. Martin, D.; Galisteo, R.; Gutkind, J.S. Cxcl8/il8 stimulates vascular endothelial growth factor (vegf) expression and the autocrine activation of vegfr2 in endothelial cells by activating nfkappab through the cbm (carma3/bcl10/malt1) complex. *J. Biol. Chem.* **2009**, *284*, 6038–6042. [[CrossRef](#)] [[PubMed](#)]
54. Lecuit, T.; Yap, A.S. E-cadherin junctions as active mechanical integrators in tissue dynamics. *Nat. Cell Biol.* **2015**, *17*, 533–539. [[CrossRef](#)] [[PubMed](#)]
55. Sahana, J.; Nassef, M.Z.; Wehland, M.; Kopp, S.; Kruger, M.; Corydon, T.J.; Infanger, M.; Bauer, J.; Grimm, D. Decreased e-cadherin in mcf7 human breast cancer cells forming multicellular spheroids exposed to simulated microgravity. *Proteomics* **2018**, *18*, e1800015. [[CrossRef](#)] [[PubMed](#)]
56. Hazan, R.B.; Kang, L.; Roe, S.; Borgen, P.I.; Rimm, D.L. Vinculin is associated with the e-cadherin adhesion complex. *J. Biol. Chem.* **1997**, *272*, 32448–32453. [[CrossRef](#)] [[PubMed](#)]
57. Yu, Z.; Sun, M.; Jin, F.; Xiao, Q.; He, M.; Wu, H.; Ren, J.; Zhao, L.; Zhao, H.; Yao, W.; et al. Combined expression of ezrin and e-cadherin is associated with lymph node metastasis and poor prognosis in breast cancer. *Oncol. Rep.* **2015**, *34*, 165–174. [[CrossRef](#)] [[PubMed](#)]
58. Thapa, N.; Tan, X.; Choi, S.; Wise, T.; Anderson, R.A. Pipkigamma and talin couple phosphoinositide and adhesion signaling to control the epithelial to mesenchymal transition. *Oncogene* **2017**, *36*, 899–911. [[CrossRef](#)] [[PubMed](#)]
59. Dudek, M.C.; Wong, K.E.; Bassa, L.M.; Mora, M.C.; Ser-Dolansky, J.; Henneberry, J.M.; Crisi, G.M.; Arenas, R.B.; Schneider, S.S. Antineoplastic effects of rhodiola crenulata treatment on b16-f10 melanoma. *Tumour Biol.* **2015**, *36*, 9795–9805. [[CrossRef](#)] [[PubMed](#)]
60. Cowden Dahl, K.D.; Symowicz, J.; Ning, Y.; Gutierrez, E.; Fishman, D.A.; Adley, B.P.; Stack, M.S.; Hudson, L.G. Matrix metalloproteinase 9 is a mediator of epidermal growth factor-dependent e-cadherin loss in ovarian carcinoma cells. *Cancer Res.* **2008**, *68*, 4606–4613. [[CrossRef](#)] [[PubMed](#)]
61. Grunewald, M.; Avraham, I.; Dor, Y.; Bachar-Lustig, E.; Itin, A.; Jung, S.; Chimenti, S.; Landsman, L.; Abramovitch, R.; Keshet, E. Vegf-induced adult neovascularization: Recruitment, retention, and role of accessory cells. *Cell* **2006**, *124*, 175–189. [[CrossRef](#)]
62. Zheng, P.S.; Wen, J.; Ang, L.C.; Sheng, W.; Vilorio-Petit, A.; Wang, Y.; Wu, Y.; Kerbel, R.S.; Yang, B.B. Versican/pg-m g3 domain promotes tumor growth and angiogenesis. *FASEB J.* **2004**, *18*, 754–756. [[CrossRef](#)] [[PubMed](#)]
63. Zheng, H.; Takahashi, H.; Murai, Y.; Cui, Z.; Nomoto, K.; Niwa, H.; Tsuneyama, K.; Takano, Y. Expressions of mmp-2, mmp-9 and vegf are closely linked to growth, invasion, metastasis and angiogenesis of gastric carcinoma. *Anticancer Res.* **2006**, *26*, 3579–3583. [[PubMed](#)]
64. Davis, G.E.; Bayless, K.J.; Mavila, A. Molecular basis of endothelial cell morphogenesis in three-dimensional extracellular matrices. *Anat. Rec.* **2002**, *268*, 252–275. [[CrossRef](#)] [[PubMed](#)]
65. Krüger, M.; Melnik, D.; Kopp, S.; Buken, C.; Sahana, J.; Bauer, J.; Wehland, M.; Hemmersbach, R.; Corydon, T.J.; Infanger, M.; et al. Fighting thyroid cancer with microgravity research. *Int. J. Mol. Sci.* **2019**, *20*. [[CrossRef](#)]
66. Mattila, P.K.; Lappalainen, P. Filopodia: Molecular architecture and cellular functions. *Nat. Rev. Mol. Cell Biol.* **2008**, *9*, 446–454. [[CrossRef](#)] [[PubMed](#)]
67. Jacquemet, G.; Hamidi, H.; Ivaska, J. Filopodia in cell adhesion, 3d migration and cancer cell invasion. *Curr. Opin. Cell Biol.* **2015**, *36*, 23–31. [[CrossRef](#)] [[PubMed](#)]

68. Jacquemet, G.; Green, D.M.; Bridgewater, R.E.; von Kriegsheim, A.; Humphries, M.J.; Norman, J.C.; Caswell, P.T. Rcp-driven alpha5beta1 recycling suppresses rac and promotes rhoa activity via the racgap1-iggap1 complex. *J. Cell Biol.* **2013**, *202*, 917–935. [[CrossRef](#)]
69. Paul, N.R.; Allen, J.L.; Chapman, A.; Morlan-Mairal, M.; Zindy, E.; Jacquemet, G.; Fernandez del Ama, L.; Ferizovic, N.; Green, D.M.; Howe, J.D.; et al. Alpha5beta1 integrin recycling promotes arp2/3-independent cancer cell invasion via the formin fhod3. *J. Cell Biol.* **2015**, *210*, 1013–1031. [[CrossRef](#)]
70. Shibue, T.; Brooks, M.W.; Inan, M.F.; Reinhardt, F.; Weinberg, R.A. The outgrowth of micrometastases is enabled by the formation of filopodium-like protrusions. *Cancer Discov* **2012**, *2*, 706–721. [[CrossRef](#)]
71. Shibue, T.; Brooks, M.W.; Weinberg, R.A. An integrin-linked machinery of cytoskeletal regulation that enables experimental tumor initiation and metastatic colonization. *Cancer Cell* **2013**, *24*, 481–498. [[CrossRef](#)]
72. Lindberg, U.; Karlsson, R.; Lassing, I.; Schutt, C.E.; Höglund, A.S. The microfilament system and malignancy. *Semin. Cancer Biol.* **2008**, *18*, 2–11. [[CrossRef](#)] [[PubMed](#)]
73. Ingber, D. How cells (might) sense microgravity. *FASEB J.* **1999**, *13*, S3–S15. [[CrossRef](#)] [[PubMed](#)]
74. Aleshcheva, G.; Sahana, J.; Ma, X.; Hauslage, J.; Hemmersbach, R.; Egli, M.; Infanger, M.; Bauer, J.; Grimm, D. Changes in morphology, gene expression and protein content in chondrocytes cultured on a random positioning machine. *PLoS One* **2013**, *8*, e79057. [[CrossRef](#)] [[PubMed](#)]
75. Grimm, D.; Bauer, J.; Kossmehl, P.; Shakibaei, M.; Schoberger, J.; Pickenhahn, H.; Schulze-Tanzil, G.; Vetter, R.; Eilles, C.; Paul, M.; et al. Simulated microgravity alters differentiation and increases apoptosis in human follicular thyroid carcinoma cells. *FASEB J.* **2002**, *16*, 604–606. [[CrossRef](#)] [[PubMed](#)]
76. Aronovich, E.L.; McIvor, R.S.; Hackett, P.B. The sleeping beauty transposon system: A non-viral vector for gene therapy. *Hum. Mol. Genet.* **2011**, *20*, R14–R20. [[CrossRef](#)] [[PubMed](#)]
77. Askou, A.L.; Aagaard, L.; Kostic, C.; Arsenijevic, Y.; Hollensen, A.K.; Bek, T.; Jensen, T.G.; Mikkelsen, J.G.; Corydon, T.J. Multigenic lentiviral vectors for combined and tissue-specific expression of mirna- and protein-based antiangiogenic factors. *Mol. Ther. Methods Clin. Dev.* **2015**, *2*, 14064. [[CrossRef](#)] [[PubMed](#)]
78. Pihlmann, M.; Askou, A.L.; Aagaard, L.; Bruun, G.H.; Svalgaard, J.D.; Holm-Nielsen, M.H.; Dagnaes-Hansen, F.; Bek, T.; Mikkelsen, J.G.; Jensen, T.G.; et al. Adeno-associated virus-delivered polycistronic microRNA-clusters for knockdown of vascular endothelial growth factor in vivo. *J. Gene Med.* **2012**, *14*, 328–338. [[CrossRef](#)]
79. Staunstrup, N.H.; Sharma, N.; Bak, R.O.; Svensson, L.; Petersen, T.K.; Aarenstrup, L.; Kristiansen, K.; Bolund, L.; Mikkelsen, J.G. A sleeping beauty DNA transposon-based genetic sensor for functional screening of vitamin d3 analogues. *BMC Biotechnol.* **2011**, *11*, 33. [[CrossRef](#)]



11.3. Publication #3

Nassef MZ, Kopp S, Melnik D, Corydon TJ, Sahana J, Krüger M, Wehland M, Bauer TJ, Liemersdorf C, Hemmersbach R, Infanger M, Grimm D. Short-Term Microgravity Influences Cell Adhesion in Human Breast Cancer Cells. *Int J Mol Sci* 20: 5730, 2019.



Article

Short-Term Microgravity Influences Cell Adhesion in Human Breast Cancer Cells

Mohamed Zakaria Nassef ¹, Sascha Kopp ^{1,*}, Daniela Melnik ¹, Thomas J. Corydon ^{2,3} , Jayashree Sahana ², Marcus Krüger ¹ , Markus Wehland ¹, Thomas J. Bauer ¹, Christian Liemersdorf ⁴ , Ruth Hemmersbach ⁴, Manfred Infanger ¹ and Daniela Grimm ^{1,2,5,*}

- ¹ Clinic for Plastic, Aesthetic and Hand Surgery, Otto von Guericke University Magdeburg, 39120 Magdeburg, Germany; mohamed.nassef@med.ovgu.de (M.Z.N.); daniela.melnik@med.ovgu.de (D.M.); marcus.krueger@med.ovgu.de (M.K.); markus.wehland@med.ovgu.de (M.W.); thomas.bauer@med.ovgu.de (T.J.B.); manfred.infanger@med.ovgu.de (M.I.)
- ² Department of Biomedicine, Aarhus University, 8000 Aarhus C, Denmark; corydon@biomed.au.dk (T.J.C.); jaysaha@biomed.au.dk (J.S.)
- ³ Department of Ophthalmology, Aarhus University Hospital, 8200 Aarhus N, Denmark
- ⁴ Institute of Aerospace Medicine, Department of Gravitational Biology, German Aerospace Center, 51147 Cologne, Germany; christian.liemersdorf@dlr.de (C.L.); ruth.hemmersbach@dlr.de (R.H.)
- ⁵ Gravitational Biology and Translational Regenerative Medicine, Faculty of Medicine and Mechanical Engineering, Otto von Guericke University, 39120 Magdeburg, Germany
- * Correspondence: sascha.kopp@med.ovgu.de (S.K.); dgg@biomed.au.dk (D.G.); Tel.: +49-391-6721267 (S.K.); +45-871-67693 (D.G.)

Received: 11 October 2019; Accepted: 12 November 2019; Published: 15 November 2019



Abstract: With the commercialization of spaceflight and the exploration of space, it is important to understand the changes occurring in human cells exposed to real microgravity (r- μ g) conditions. We examined the influence of r- μ g, simulated microgravity (s- μ g, incubator random positioning machine (iRPM)), hypergravity (hyper-g), and vibration (VIB) on triple-negative breast cancer (TNBC) cells (MDA-MB-231 cell line) with the aim to study early changes in the gene expression of factors associated with cell adhesion, apoptosis, nuclear factor “kappa-light-chain-enhancer” of activated B-cells (NF- κ B) and mitogen-activated protein kinase (MAPK) signaling. We had the opportunity to attend a parabolic flight (PF) mission and to study changes in RNA transcription in the MDA-MB cells exposed to PF maneuvers (29th Deutsches Zentrum für Luft- und Raumfahrt (DLR) PF campaign). PF maneuvers induced an early up-regulation of *ICAM1*, *CD44* and *ERK1* mRNAs after the first parabola (P1) and a delayed upregulation of *NFKB1*, *NFKBIA*, *NFKBIB*, and *FAK1* after the last parabola (P31). ICAM-1, VCAM-1 and CD44 protein levels were elevated, whereas the NF- κ B subunit p-65 and annexin-A2 protein levels were reduced after the 31st parabola (P31). The *PRKCA*, *RAF1*, *BAX* mRNA were not changed and cleaved caspase-3 was not detectable in MDA-MB-231 cells exposed to PF maneuvers. Hyper-g-exposure of the cells elevated the expression of *CD44* and *NFKBIA* mRNAs, iRPM-exposure downregulated *ANXA2* and *BAX*, whereas VIB did not affect the TNBC cells. The early changes in ICAM-1 and VCAM-1 and the rapid decrease in the NF- κ B subunit p-65 might be considered as fast-reacting, gravity-regulated and cell-protective mechanisms of TNBC cells exposed to altered gravity conditions. This data suggest a key role for the detected gravity-signaling elements in three-dimensional growth and metastasis.

Keywords: breast cancer cells; microgravity; hypergravity; cell adhesion; apoptosis; NF- κ B

1. Introduction

The GLOBOCAN statistics from 2018 showed that breast cancer is the most common cancer in women and the second leading cause of cancer deaths worldwide [1]. Breast cancer comprises multiple subtypes with characteristic histology, treatability and outcome [2]. Currently, seven molecular subtypes are known [3–6]: luminal A (estrogen receptor positive (ER+)/progesterone receptor positive (PR+)/androgen receptor positive (AR+)/human epidermal growth receptor 2 negative (HER2–)/antigen KI67 negative (KI67–)), luminal B (ER+/PR+/AR+/HER2–/KI67+), HER2 enriched (ER–/PR–/HER2+), molecular apocrine (ER–/PR–/AR+/HER2+/KI67+), basal-like/triple-negative (ER–/PR–/AR–/HER2–), normal breast-like (ER+/PR+/HER2–/KI67–) and claudin-low (ER–/PR–/HER2–). Survival of the patients is associated with prognostic factors like tumor size, hormone-receptor-profile and metastases at the time of diagnosis. An onset therapy is the surgical resection of the tumor tissue (lumpectomy or mastectomy). Tumor size and possible metastases to the sentinel lymph node are decisive for the choice of following therapy. Chemotherapy, radiation and anti-hormone therapy, targeted treatment against HER2 and anti-angiogenic therapy are often applied after surgery or in the case of advanced disease stages [7]. Despite the advanced therapy, it is estimated that about 626,679 deaths worldwide will occur from breast cancer per year [1]. Therefore, it is necessary to implement novel ideas to find drug targets and to test new treatment options. This study will focus on the well-described basal-like/triple-negative cancer (TNBC) and will study the TNBC cell line MDA-MB-231 exposed to short-term altered gravity conditions and vibration (VIB) [8]. Using altered gravity conditions in the field of cancer research is not typically the first method to search for target proteins [9], but more than 20 years ago it became clear that cells exposed to microgravity (μg) opened an alternative view on cancer cells as they revealed numerous changes like an altered gene expression, protein synthesis and secretion. With the help of simulated microgravity ($s\text{-}\mu\text{g}$) and mass spectrometry, we found novel protein targets involved in cancer [10–13]. A space journey and a longer stay on the International Space Station (ISS) provide altered gravity conditions, which are not found on Earth. On Earth, we can simulate μg to some extent by applying rotating devices like a 2D or 3D clinostat, the National Aeronautics and Space Administration (NASA)-developed rotating wall vessel or a random positioning machine (RPM) [14]. Exposure of different cancer cells types to real ($r\text{-}\mu\text{g}$) or simulated ($s\text{-}\mu\text{g}$)-conditions influences various biological processes, which are of importance in cancer research. Other researchers reported about changes in the morphological phenotype, growth behavior, gene expression, protein content and release, cytoskeletal reorganization, extracellular matrix composition, cell adhesion and others [14,15]. One important finding was that in $r\text{-}$ and $s\text{-}\mu\text{g}$ various cell types form three-dimensional (3D) aggregates also called multicellular spheroids (MCS), resembling the *in vivo* situation of tumors much closer than conventional cell cultures [14]. These MCS are of great interest in cancer research to test drugs and to find new treatment targets [16]. An activation of nuclear factor “kappa-light-chain-enhancer” of activated B-cells (NF- κB), a proinflammatory transcription factor, was often detected in breast cancer [17]. The “inhibitor of κB ” (I κB) proteins include I $\kappa\text{B}\alpha$, I $\kappa\text{B}\beta$, I $\kappa\text{B}\gamma$, I $\kappa\text{B}\epsilon$, and others [18]. Among them, I $\kappa\text{B}\alpha$, I $\kappa\text{B}\beta$ and I $\kappa\text{B}\epsilon$ are the most important regulators of NF- κB and are of high interest in cancer research and μg -based research. Interestingly, the NF- κB -signaling pathway was significantly altered in FTC-133 cancer cells [19] as well as in MCF-7 breast cancer cells [20] exposed to $s\text{-}\mu\text{g}$ when MCS were formed. Grosse et al. described an increase in NF- κB p65 protein, when cells were exposed to $s\text{-}\mu\text{g}$ on an RPM [19]. This discovery was in concert with findings by Kopp et al., who described an activation and increase in NF- κB and associated molecules in MCF-7 cells exposed to the RPM [20]. Through drug-initiated NF- κB inhibition, they were able to reduce the formation of MCS. As it is not clear when NF- κB signaling is triggered during MCS formation, we exposed MDA-MB-231 breast cancer cells to $r\text{-}\mu\text{g}$ during a parabolic flight campaign (PFC).

The principal aim of this study was, first, to investigate the early phases of $r\text{-}\mu\text{g}$ achieved by PF maneuvers on TNBC cells and to test whether there is a link between factors of apoptosis, changes in NF- κB signaling and cell adhesion. The second aim was to study VIB and hyper- g (1.8 g) effects on the MDA-MB-231 cells. In a third approach, we exposed the MDA-MD-231 cells to an incubator RPM (iRPM)

for 2 h to compare the effects of s- μ g with those from r- μ g. Afterwards, we performed quantitative polymerase chain reaction (qPCR) focusing on genes involved in NF- κ B signaling, cell adhesion and MAPK signaling as well as apoptosis. Furthermore, the molecular biological results were finally evaluated by STRING (Search Tool for the Retrieval of Interacting Genes/Proteins) analyses to visualize the mutual regulation and interactions of genes and proteins examined in this study.

2. Results

2.1. Viability Staining

To examine whether the MDA-MB-231 cells were viable after the VIB-, hyper-g-, and iRPM-exposure, a terminal deoxynucleotidyl transferase dUTP nick end labeling (TUNEL) assay for the detection of DNA fragmentation was performed to measure the amount of apoptotic cells (Figure 1). Comparing ground controls at Earth's normal gravity (1 g), VIB, 1.8 g hyper-g (comparable to the hyper-g exposure on the PFC), and iRPM cell samples, the cytoplasm was evenly stained green, while the nucleus showed no green staining. In contrast, the positive control, which was treated with DNase prior to the staining procedure, presents an intensive green staining of the nucleus. This finding shows, that altered gravity conditions or VIB did not induce apoptosis in MDA-MB-231 cells (Figure 1).

2.2. Nuclear Factor "Kappa-Light-Chain-Enhancer" of Activated B-Cells (NF- κ B) Signaling Factors in Triple-Negative Breast Cancer Cells during Altered Gravity Conditions

To verify the influence of PF maneuvers on factors involved in the NF- κ B-signaling pathway, the gene expression pattern of NF- κ B signaling factors was determined in MDA-MB-231 cells (Figure 2). As a PF comprises different conditions beside microgravity like hyper-g (1.8 g), and VIB, these factors had been additionally tested to isolate the effects derived from the exposure to μ g (Figure 3).

The major factors of the NF- κ B-signaling pathway are NF- κ B subunits p105/50, p100/52 and p65 (NFKB3, RELA) of which their corresponding genes are NFKB1, NFKB2 and NFKB3.

While the gene expression of NFKB1 (P31, up-regulation) (Figure 2A) and NFKB3, (RELA; P1, up-regulation, Figure 2C) are significantly changed after the PF conditions, VIB-, 1.8 g- and iRPM-exposure had no significant impact on these genes. The NFKB2 mRNA was not altered in any experimental condition (Figure 2B, Figure 3C,D). In contrast, the Western blot analyses of NF- κ B p65 protein presented a significant reduction after P1 and P31 (Figure 2D).

The NF- κ B-signaling pathway is modulated by its inhibitors NF- κ B-inhibitor-alpha, -beta and -epsilon (NFKBIA, NFKBIB, NFKBIE) and the NF- κ B essential modulator (IKBKG, NEMO). In the case of NFKBIA, NFKBIB and NFKBIE (Figure 2E,G,H) gene expression, a significant upregulation was only found for NFKBIA and NFKBIB after P31 compared to their corresponding controls. The NFKBIA mRNA was differentially expressed by hyper-g (Figure 3G). Protein analyses revealed no significant change in I κ B α and NEMO (Figure 2F,J). The NFKBIE and IKBKG gene expressions (Figure 2H,I) were not altered in any of the experimental conditions (Figure 3K–N).

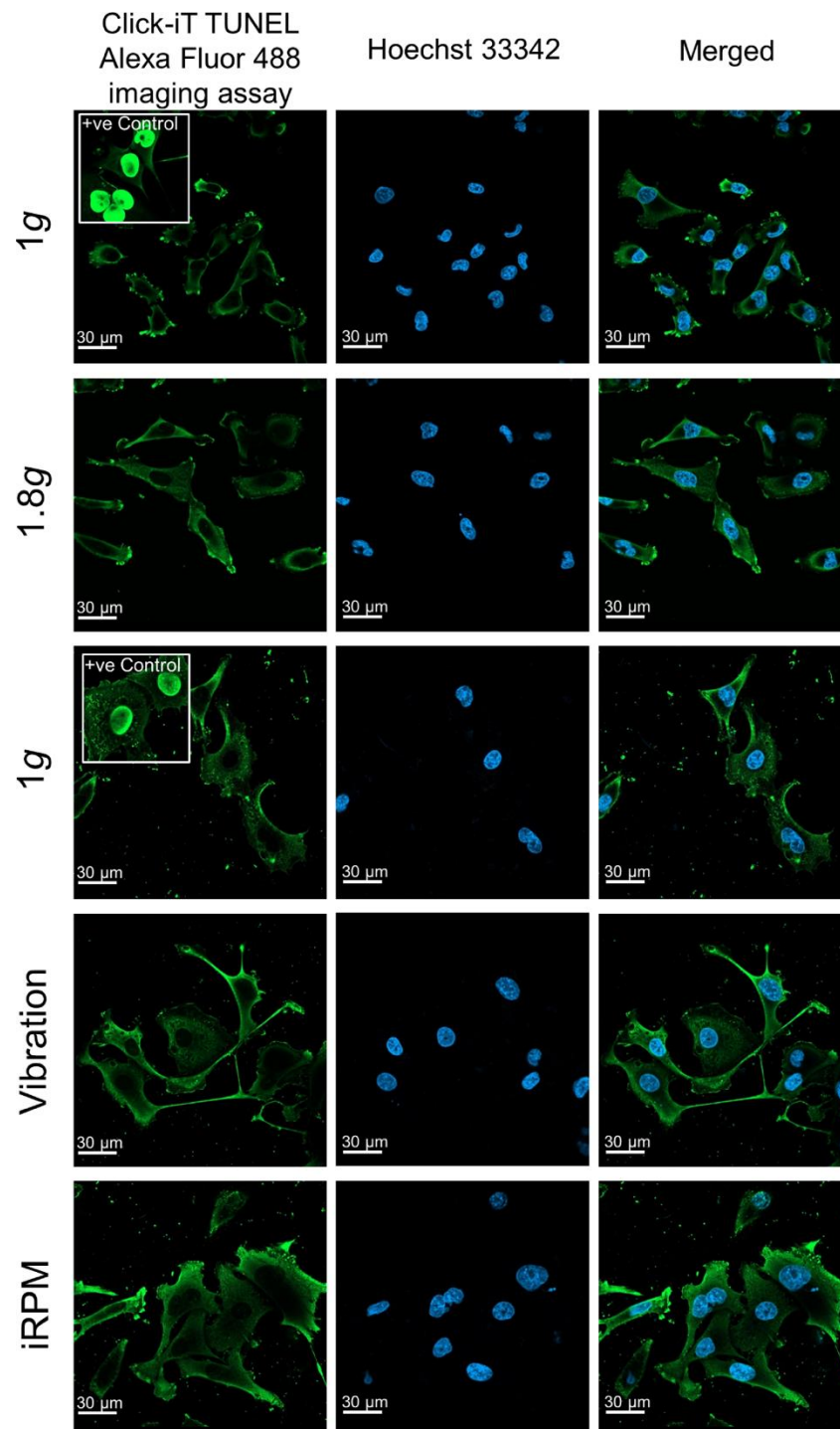


Figure 1. Click-IT terminal deoxynucleotidyl transferase dUTP nick end labeling (TUNEL) assay performed on MDA-MB-231 cells exposed to 1 g, 1.8 g hyper-g, vibration (VIB) and the incubator random positioning machine (iRPM). Green staining indicates free fluorophores in the cytoplasm in all images with the exception of the positive control. In the positive control, samples have been pretreated with DNase to induce DNA fragmentation, which is visualized by an enrichment of the fluorophores in the nucleus. Blue staining highlights the cells' nuclei. Green stained nuclei present apoptotic cells as shown in the inserted positive controls. None of the applied experimental approaches had induced apoptosis in the cells.

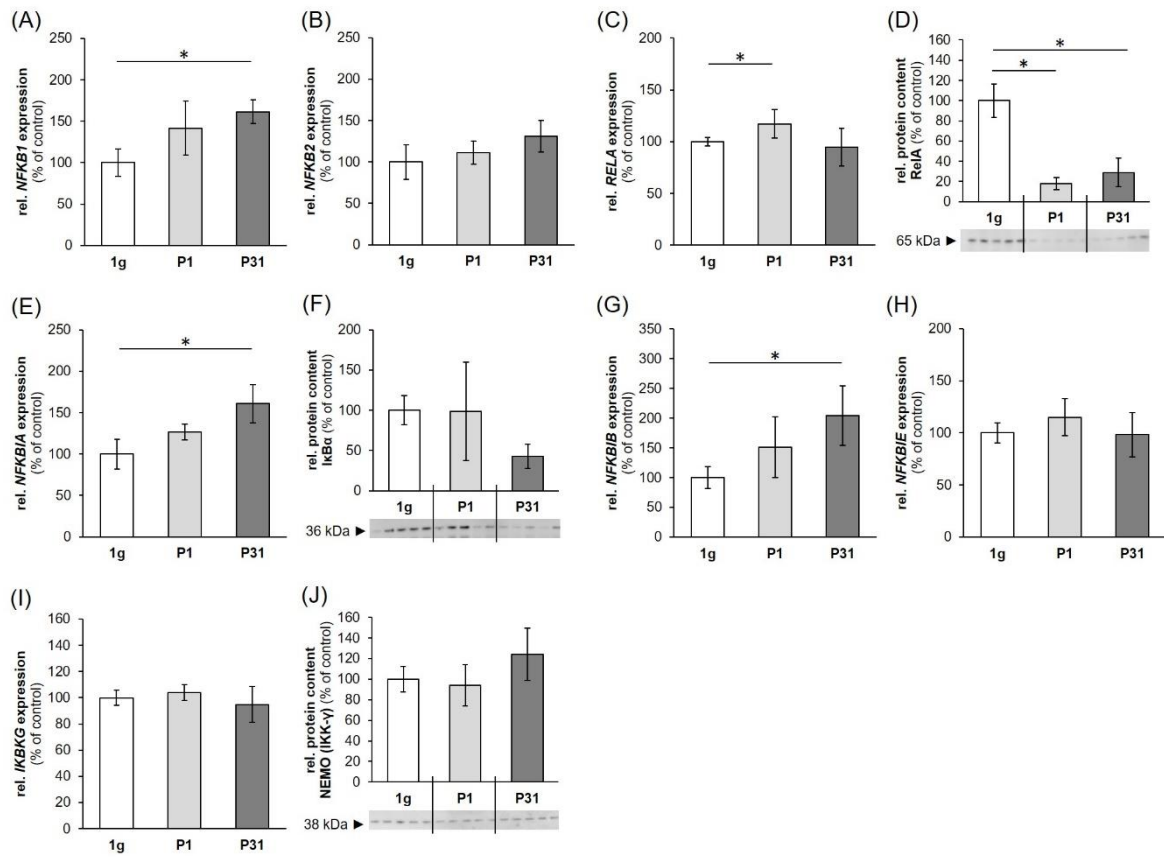


Figure 2. Influence of short-term microgravity on the gene expression: (A) *NFKB1*, (B) *NFKB2*, (C) *RELA*, (E) *NFKBIA*, (G) *NFKBIB*, (H) *NFKBIE*, (I) *IKBKG* and protein content: (D) RelA, (F) $I\kappa B\alpha$ (J) NEMO; of NF- κ B signaling factors. $n = 5$; The data are given as mean \pm standard deviation. * $p < 0.05$ vs. 1 g-control.

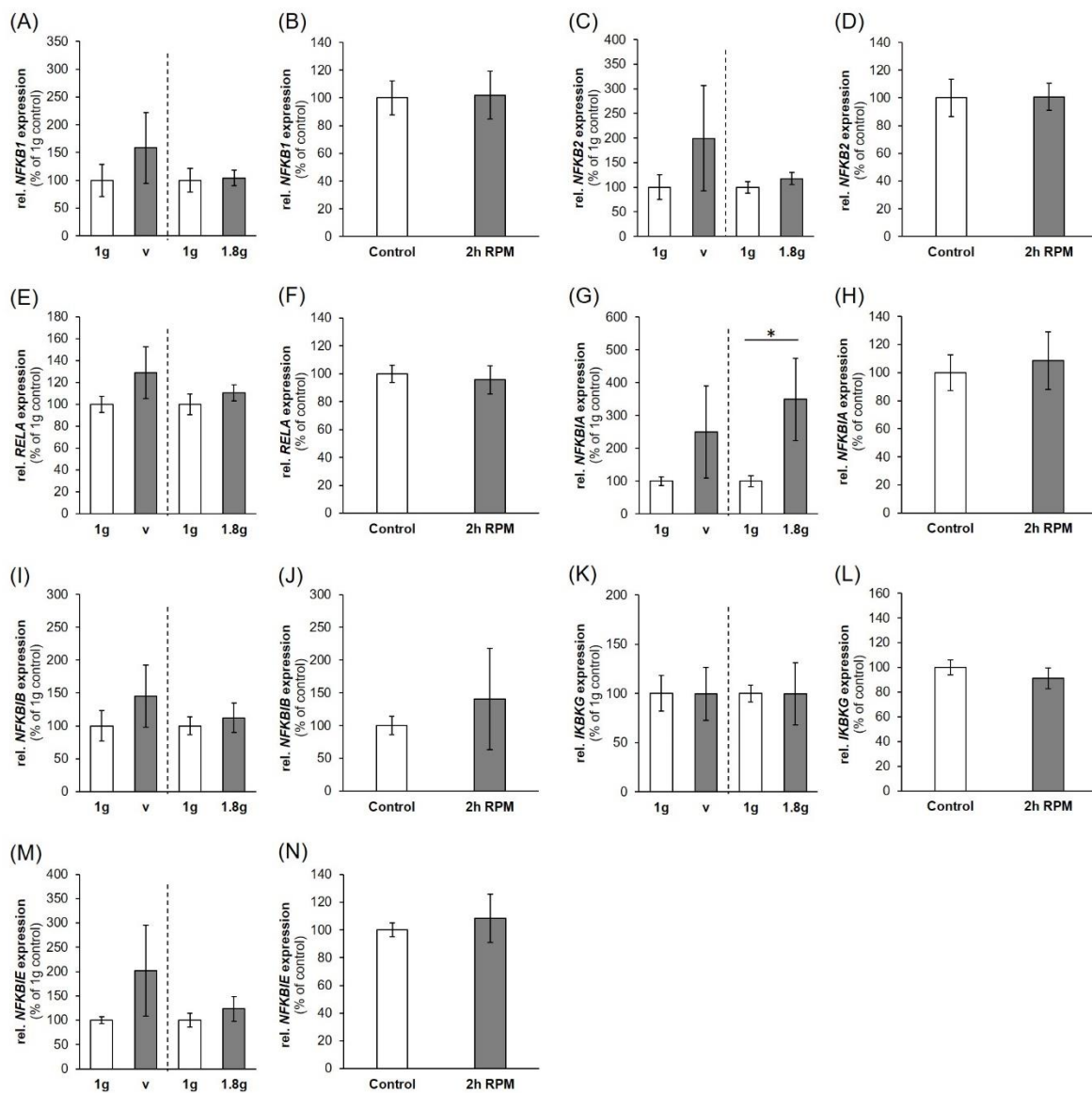


Figure 3. Influence of VIB (V), hyper-g and iRPM-exposure on the gene expression of NF- κ B signaling factors: (A,B) *NFKB1*, (C,D) *NFKB2*, (E,F) *RELA*, (G,H) *NFKBIA*, (I,J) *NFKBIB*, (K,L) *IKBKG*, (M,N) *NFKBIE*. $n = 5$. The data are given as mean \pm standard deviation. * $p < 0.05$ vs. corresponding 1 g-controls. The dashed vertical line separates two independent experiments.

2.3. Expression of Factors Belonging to the Biological Process of Apoptosis

Caspase 3 is a major factor in apoptosis [21]. Gene expression of *CASP3* was significantly upregulated after P1 and P31 (Figure 4A) while being not regulated after exposure to vibration and the RPM (Figure 5A,B). Measuring the cleaved caspase-3 protein by Western blot analysis and could not detect any active caspase-3, whereas the positive control colon cancer cells CX+ exerted a strong positivity [21] (Figure 4B).

The gene expression of *ANXA1* (Figure 4C, Figure 5C,D) was not significantly changed during any of the experimental procedures. *ANXA2* mRNA expression showed a similar behavior (Figure 4D, Figure 5E) except a downregulation after 2h of RPM exposure (Figure 5F). *ANXA2* (annexin A2) protein (Figure 4E) was first significantly increased after P1 and then re-adapted after P31, which is in agreement with the data obtained after a two-hour iRPM-exposure of the MDA-MB-231 cells (Figure 5F). In addition, the *BAX* mRNA was not differentially regulated (Figure 4F, Figure 5I,J), but *BCL2* mRNA

was reduced at both time points (Figure 4G). Finally, the *BAX* mRNA was not altered by VIB and hyper-g, but significantly reduced in MDA-MB-231 cells exposed to the iRPM (Figure 5G,H).

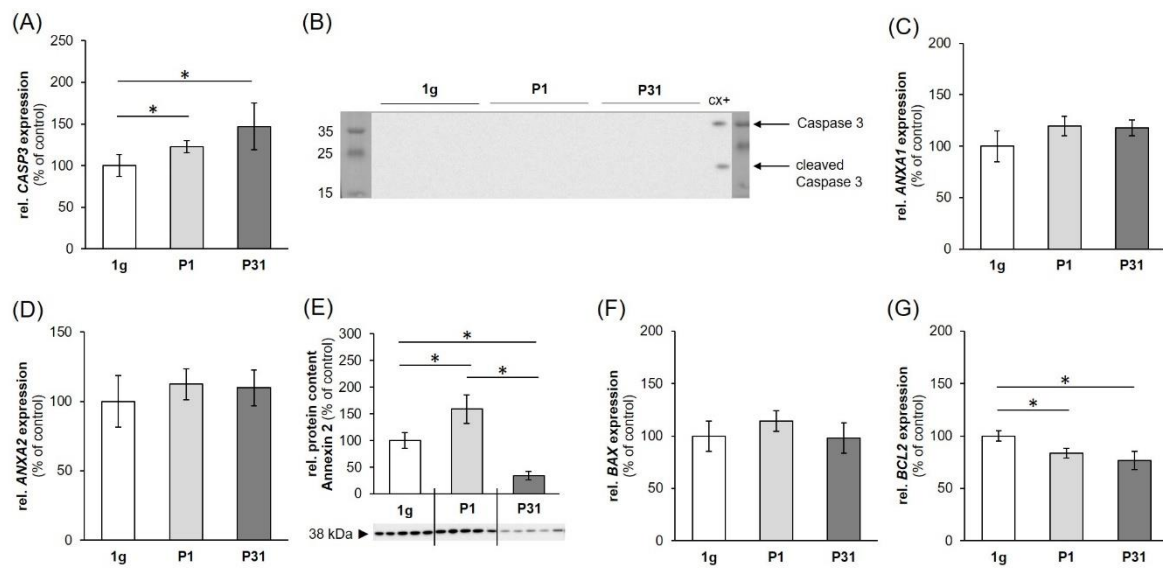


Figure 4. Influence of short-term microgravity on the gene expression: (A) *CASP3*, (C) *ANXA1*, (D) *ANXA2*, (F) *BAX*, (G) *BCL2*; and protein content (B) caspase 3, (E) annexin 2 regulators of apoptosis. The data are given as mean \pm standard deviation. * $p < 0.05$ vs. 1 g-control. CX+ colon cancer cells served as positive control for programmed cell death.

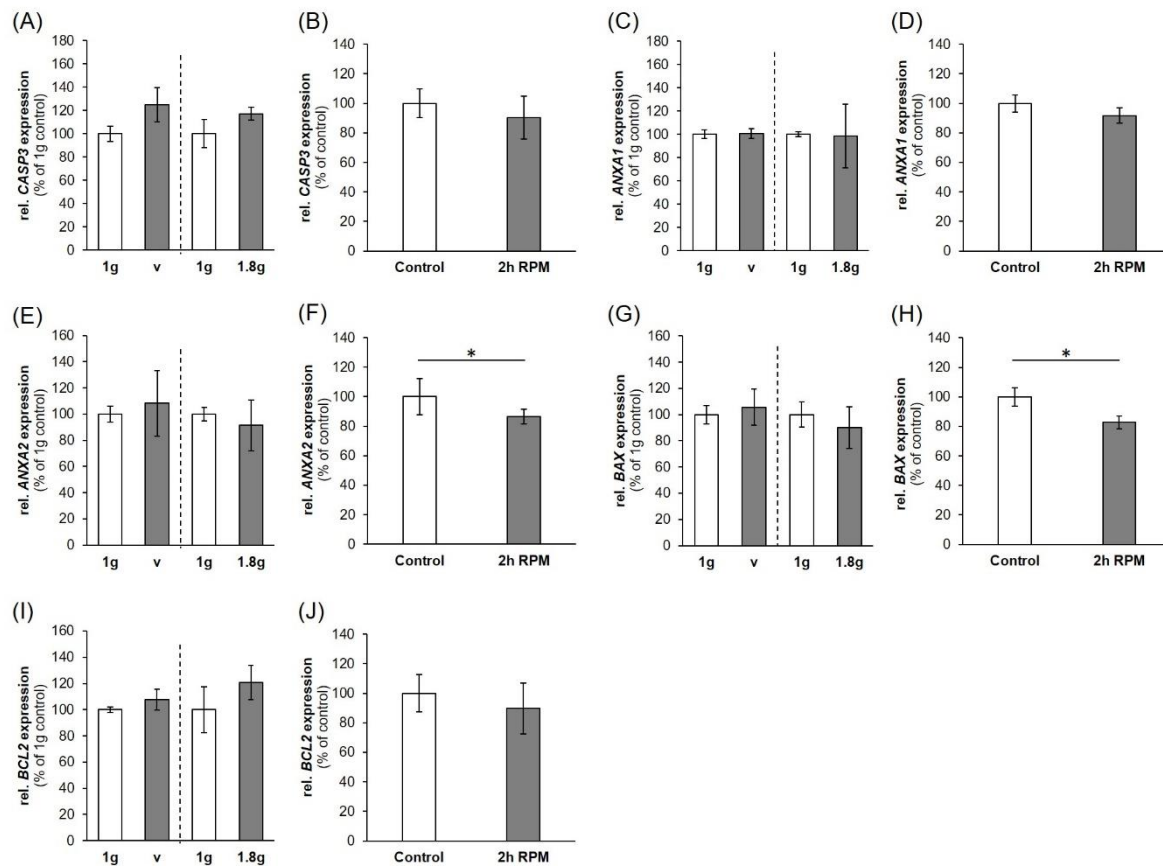


Figure 5. Influence of a VIB (V), hyper-g and iRPM-exposure on the gene expression of apoptosis signaling factors: (A,B) *CASP3*, (C,D) *ANXA1*, (E,F) *ANXA2*, (G,H) *BAX*, (I,J) *BCL2*. $n = 5$. The data are given as mean \pm standard deviation. * $p < 0.05$ vs. 1 g-control.

2.4. Regulation of Cell Adhesion Molecules in Triple-Negative Breast Cancer (TNBC) Cells

The *ICAM1* gene expression was significantly upregulated after one parabola. Although our data seem to hint towards an additional upregulation after 31 parabolas, the high variability of the measurements interfered with the statistical analysis (Figure 6A). *ICAM1* protein was significantly reduced after the first parabola and increased after 31 parabolas (Figure 6B). We did not observe changes in the *VCAM1* gene expression (Figure 6C), while *VCAM-1* protein levels were significantly elevated after one and 31 parabolas compared to static 1 g-controls (Figure 6D).

SPP1 gene expression was found to be significantly enhanced compared to the levels after one parabola, but not to 1 g-controls (Figure 6E). Osteopontin protein expression on the other hand was significantly downregulated compared to static controls after both one and 31 parabolas (Figure 6F).

Finally, the *CD44* gene expression showed a constant increase over the course of the experiment, with significant rises after one parabola vs. 1 g-controls and 31 parabolas vs. 1 g-controls and levels after one parabola (Figure 6G). *CD44* protein levels followed the same tendency with significant increases compared to static controls for both one and 31 parabola samples (Figure 6H).

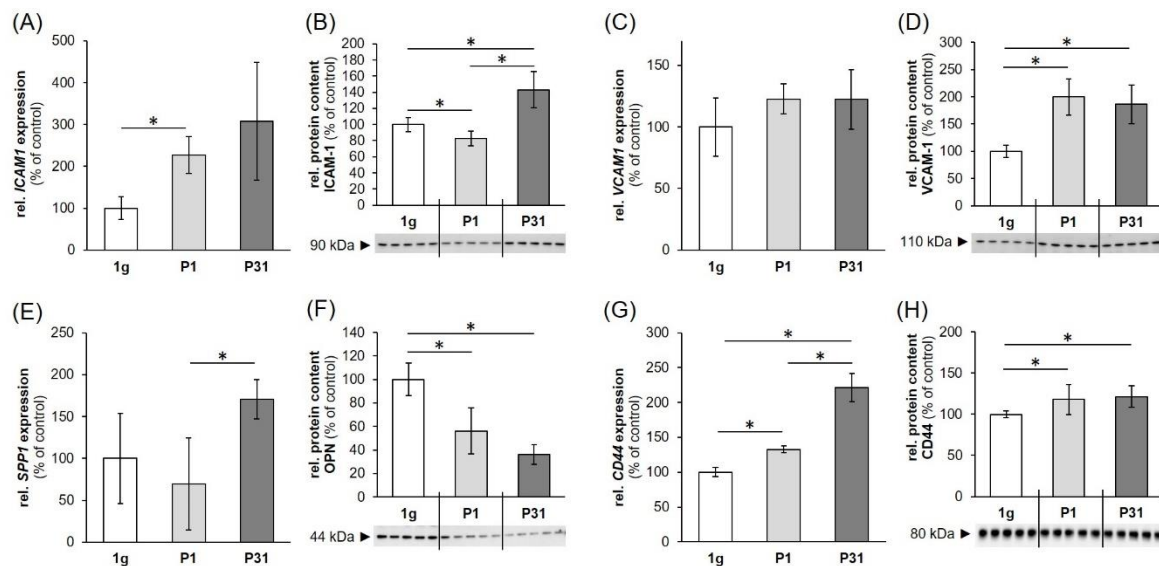


Figure 6. Expression of genes: (A) *ICAM1*, (C) *VCAM1*, (E) *SPP1*, (G) *CD44*; and proteins: (B) *ICAM-1*, (D) *VCAM-1*, (F) *OPN*, (H) *CD44* involved in cell adhesion. 1 g: ground control; P1: parabola 1; P31: parabola 31. The data are given as mean \pm standard deviation. * $p < 0.05$ vs. 1 g-control; ** $p < 0.01$ vs. 1 g-control.

ICAM1, *VCAM1*, and *SPP1* were not significantly regulated after VIB, hyper-g- or iRPM-exposure (Figure 7A–F). The *CD44* gene expression, on the other hand, was significantly enhanced under conditions of 1.8 g hyper-g, but remained unchanged by VIB- and iRPM-exposure (Figure 7G,H).

2.5. Factors of the Mitogen-Activated Protein Kinase (MAPK) Signaling Pathway Known to be Involved in Cancer Progression and Metastasis

First, we determined the gene expression of *PRKCA* (protein kinase C alpha, PKC α). The *PRKCA* mRNA was not significantly upregulated after the 31st parabola compared with corresponding 1 g-samples (Figure 8A).

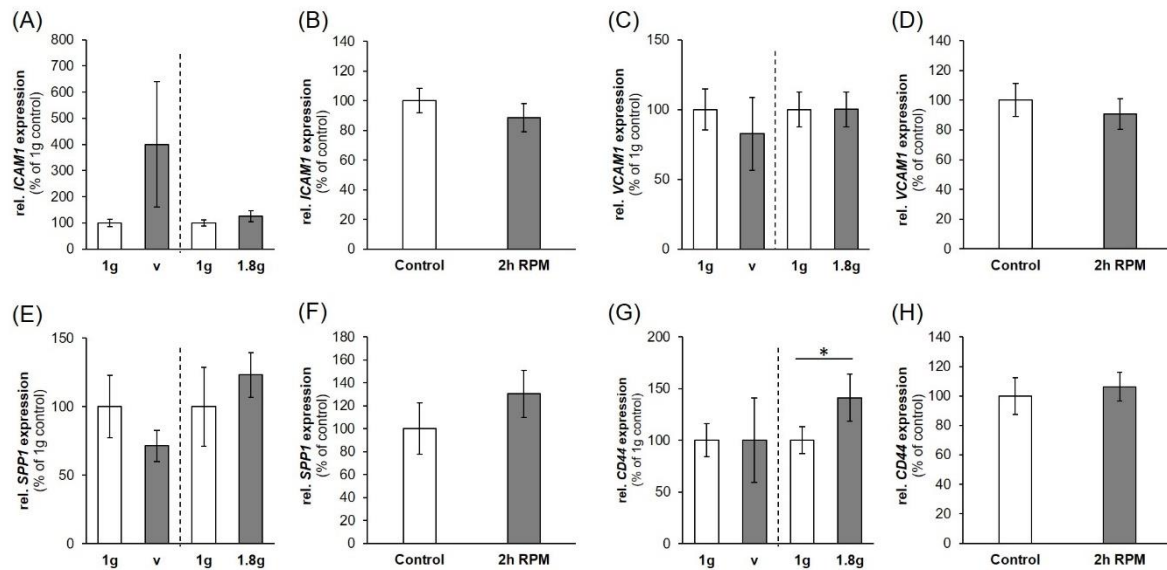


Figure 7. Influence of a VIB (V), hyper-g and iRPM-exposure on the gene expression of cell adhesion signaling factors: (A,B) *ICAM1*, (C,D) *VCAM1*, (E,F) *SPP1*, (G,H) *CD44*. 1 g: ground control; V: 2 h of vibration; 1.8 g: 2 h of hyper-g. The data are given as mean \pm standard deviation. * $p < 0.05$ vs. 1 g-control.

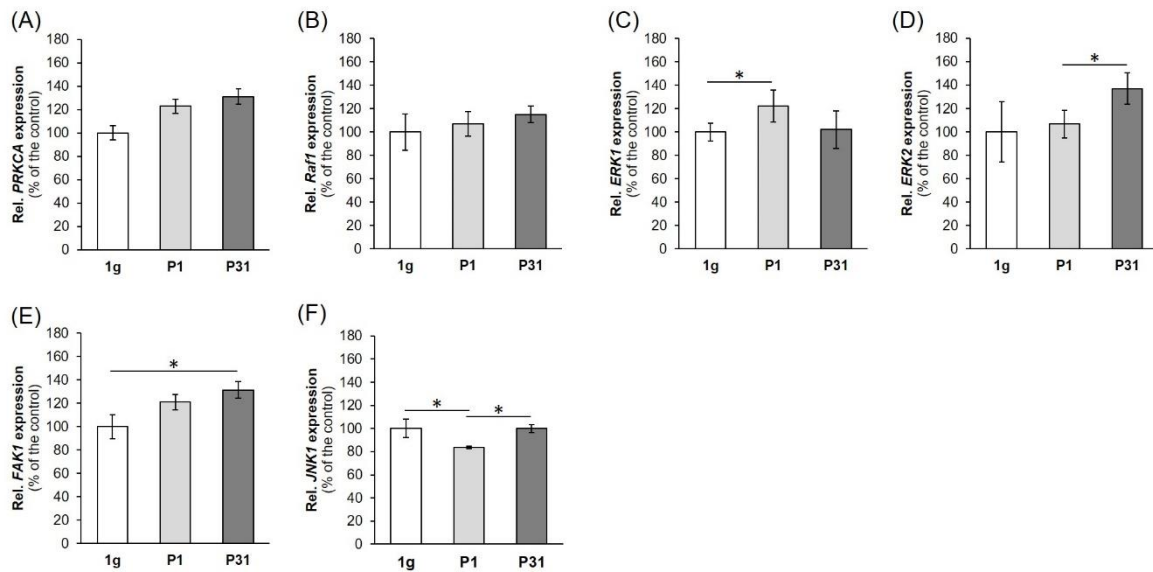


Figure 8. Expression of genes: (A) *PRKCA*, (B) *Raf1*, (C) *ERK1*, (D) *ERK2*, (E) *FAK1*, (F) *JNK1*, involved in cancer progression and metastasis. 1 g: ground control; P1: parabola 1; P31: parabola 31. The data are given as mean \pm standard deviation. * $p < 0.05$ vs. 1 g-control.

Then we focused on *RAF1* (RAF proto-oncogene serine/threonine-protein kinase). *RAF1* remained unchanged by PF maneuvers (Figure 8B). Afterwards, we measured the *ERK1* (extracellular signal-regulated kinase 1) (Figure 8C) and *ERK2* (extracellular signal-regulated kinase 2) (Figure 8D) gene expression. The *ERK1* gene expression was significantly up-regulated after the first parabola compared to 1 g-samples (Figure 8C). The *ERK2* mRNA was significantly elevated after the 31st parabola compared with P1 r- μ g-samples (Figure 8D). There is a direct interaction between *ERK1,2* and *FAK1* (focal adhesion kinase 1 also known as PTK2 (protein tyrosine kinase 2)). The *FAK1* mRNA was significantly up-regulated after P31 compared to 1 g-samples (Figure 8E).

In a next step we measured the *MAPK8* (mitogen-activated protein kinase 8) mRNA also called *JNK1* (c-Jun N-Terminal Protein Kinase 1) (Figure 8F). *JNK1* was down-regulated after P1 and was not significantly changed after P31, indicating a rapid short-term effect of microgravity.

2.6. Search Tool for the Retrieval of Interacting Genes/Proteins (STRING) Analysis

The various genes analyzed by qPCR were investigated in regard to their possible interaction and mutual expression dependence. A STRING/EMBL analysis of these items represented in molecule action mode is shown in Figure 9. It can be seen that the nuclear factors, whose expression was analyzed, are regulating each other very strongly, while the remaining items form a loose network. *RELA*, *NFKB1* and *NFKB2*, which represent three of the five members of the transcription factor NF- κ B family are strictly controlled at various levels [22]. Their activity is regulated by interaction with each other, with inhibitors such as *NFKBIA*, *NFKBIB*, *NFKBIE* and with kinases such as *IKBKB* (*NEMO*). The regulation occurs at various levels including the gene expression level. For example, *NFKB1* and *RELA* form protein heterodimers and are also associated in the regulation of their expression [23]. Moreover, *RELA* and *VCAM1* are upregulated after an injury of an artery, while *NFKBIA* is down-regulated [24] and if annexin A1 is upregulated, it forms a complex with *IKFKG* that activates *NFKB* [25]. On the other hand, the nuclear factors control the transcription of other genes. A target of *RELA* is *ICAM1* expression, which is also regulated by osteopontin [26,27]. Osteopontin is co-expressed with *CD44* [28], which co-localizes with annexin A2 [29]. Moreover, there are links between *NFKB1* and the expression of *CASP3* [30,31]. *CASP3* and *BAX* are upregulated during apoptosis, while *BCL2* is downregulated [32]. After the PF maneuvers, we measured increases in *CASP3* and a reduction of *BCL2* mRNAs, but no changes in their protein products and no signs of apoptosis. In addition, we detected an upregulation of *ERK1* after P1 compared to 1 g, *ERK2* after P31 compared to P1 samples, and *FAK1* after P31 compared to 1 g, whereas *PRKCA* and *RAF1* remained unchanged in short-term μ g. Moreover, the *JNK1* gene expression was down-regulated after the first parabola and unaltered after P31 compared to 1 g.

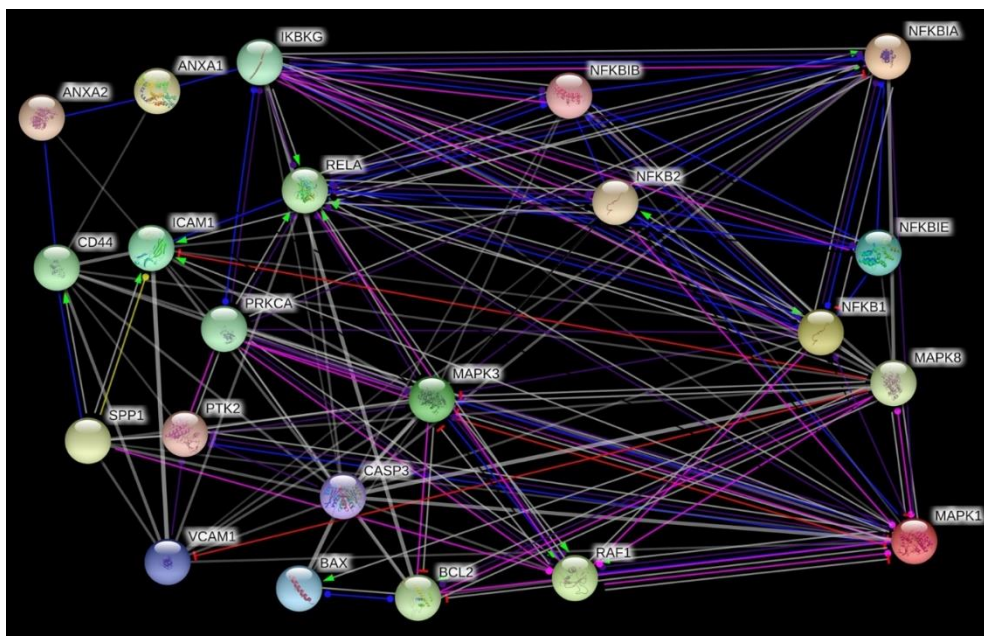


Figure 9. Network of the functional interaction of genes and their products analyzed in this study. The analysis was performed by STRING (Search Tool for the Retrieval of Interacting Genes/Proteins) v11.0 provided by the STRING Consortium (Available online: <https://string-db.org/>). The result is presented in the molecule action mode. Gene names are indicated.

3. Discussion

The basal-like or triple-negative form of breast cancer refers to tumors not expressing the *ER*, *PR*, *AR* and *HER2* genes [1]. This breast cancer type is very heterogeneous, which complicates treatment. The MDA-MB-231 cell line was isolated from a pleural effusion of a patient with invasive ductal carcinoma and is ER-, PR-, and E-cadherin negative and expresses mutated p53. Microarray profiling revealed that the MDA-MB-231 cell genome clusters with the basal subtype of breast cancer. In addition, MDA-MB-231 cells lack HER2 and thus this cell line is a good model of TNBC [8,33,34].

Gravity is permanently influencing the human body and all life on Earth. Gravitational unloading results in enormous changes in the organism, organs, tissues and cells [35,36].

Microgravity induces a large number of changes in thyroid and breast cancer cells, such as alterations of the cytoskeleton, extracellular matrix, focal adhesion, growth behavior, differentiation, proliferation, cell adhesion or an increased apoptosis [15,20,37–40].

We recently exposed MCF-7 breast cancer cells to the RPM and detected 3D MCS formation within 24 h [20]. The pathway analysis of 47 examined genes proposed that NF- κ B variants are involved in the formation of MCS [20]. This finding was in agreement with data obtained earlier from thyroid cancer studies [19]. Poorly differentiated FTC-133 follicular thyroid cancer cells cultured on an RPM for 24 h showed higher levels of NF- κ B-p65 protein and apoptosis than 1 g-controls [19]. Both studies indicated an involvement of NF- κ B in 3D growth. No information exists about the early phases when cells are exposed to μ g.

We had the opportunity to attend the 29th Deutsches Zentrum für Luft- und Raumfahrt (DLR) PF mission in Bordeaux Merignac, France, and to study cells in r- μ g (Available online: https://www.dlr.de/rd/desktopdefault.aspx/tabid-2285/3423_read-47055/; https://www.dlr.de/rd/desktopdefault.aspx/tabid-2285/3423_read-50372/). We investigated MDA-MB-231 cells in r- μ g during PF maneuvers. The cells were fixed with RNA*later* after the first and the 31st parabola, keeping in mind that this last time point represents a mixture of alternated acceleration phases. Postflight we focused on NF- κ B signaling, cell adhesion, and apoptosis. Furthermore, cells exposed to an iRPM, hyper-g cultures (1.8 g) and VIB samples were examined to evaluate the impact of these factors on the cells.

3.1. Influence of Altered Gravity Conditions and Vibration on Cell Survival

Apoptosis is involved in the pathogenesis of many diseases including among others ischemia, autoimmune and neurodegenerative diseases, as well as in tumor response to chemotherapy and/or radiotherapy [41].

It is known from earlier studies that cancer cells will become apoptotic when exposed to r- μ g and s- μ g and that apoptosis is involved in cell detachment and formation of spheroids [19]. Therefore, we investigated *CASP3*, *ANXA1*, *ANXA2*, *BAX* and *BCL2* mRNA expression patterns.

In our short-term experiments, after a 2-h exposure to s- μ g, hyper-g or vibration, TUNEL staining of TNBC cells revealed no signs of apoptosis and 100% viable cells. The gene expression of *CASP3* was elevated after the first and 31st parabola, but no uncleaved caspase-3 was detectable and no detectable cleavage of caspase-3 occurred. The *CASP3* gene expression was not changed in VIB-, hyper-g- and s- μ g-samples. This is in agreement with earlier findings obtained with endothelial cells exposed to PF maneuvers [42]. Furthermore, the gene expression of *CASP3* and *ANXA2* was reduced in endothelial cells exposed to a two-hour period of VIB or hyper-g conditions [43]. In MDA-MB-231 cells *ANXA1* mRNAs were not changed during the parabolic flight, hyper-g-, s- μ g- and VIB-exposure. However, *ANXA2* protein after PFC as well as *ANXA2* mRNA expression after s- μ g exposure was significantly altered. Thus, μ g has an impact on cell survival that is highly dependent on the cell type as well as on the duration of exposure.

3.2. Impact of Real Microgravity on NF- κ B Signalling in TNBC

NF- κ B is an interesting factor because it is associated with spaceflight-related health problems. Activation of NF- κ B is frequently observed in breast cancer as well. An *NFKB3* overexpression indicates increased aggressiveness of breast cancer and a poor prognosis [44]. In addition, NF- κ B is involved in endocrine therapy resistance [45]. Activation of NF- κ B promotes the survival of tumor cells. Several gene products that negatively regulate apoptosis in tumor cells are controlled by NF- κ B activation.

The NF- κ B proteins include the different variants NF- κ B-p50, -p52 and -p65, which are encoded by the gene loci *NFKB1*, 2 and 3 [45]. These proteins are bound and inhibited by I κ B proteins. The effectors and inhibitors are activated by external triggers and, thus, interesting in μ g-based research.

Human adherent cells exposed to s- μ g on a RPM showed elevated levels of NF- κ B p65 protein compared with 1 g-controls, a result found earlier in endothelial cells and in FTC-133 follicular thyroid cancer cells [19,46].

NF- κ B exerts several transcriptional regulatory functions important for programmed cell death [47] and is inactivated by binding to I κ B (inhibitor of NF κ B).

The *NFKB1* (Nuclear Factor Kappa B Subunit 1) mRNA was significantly elevated after the 31st parabola compared to 1 g, no changes were measured for the *NFKB2* (Nuclear Factor Kappa B Subunit 2) mRNA at each time point and an upregulated gene was found for *NFKB3* (*RELA* Proto-Oncogene (V-Rel Avian Reticuloendotheliosis Viral Oncogene Homolog A), Nuclear Factor NF-Kappa-B P65 Subunit) after the first parabola. *NFKB3* mRNA was unaltered after the last parabola (P31). Despite this result, the corresponding protein NF- κ B p65 was down-regulated after the first and 31st parabola. This counterregulatory effect was not due to VIB or hyper-g occurring during the PF (Figure 3E,F), as the *NFKB3* gene expression was unchanged in VIB and 1.8 g samples. The normalization of *NFKB3* after 31 parabolas and the down-regulation of NF- κ B p65 protein in short-term r- μ g (after one parabola, that means 22 s of r- μ g) is in agreement with earlier microarray data obtained from activated T cells cultured in space, which showed a suppressed expression of c-REL and NF- κ B gene targets after 1.5 h [48]. In addition, a four-hour exposure on the RPM of activated T cells revealed a suppressed expression of NF- κ B gene targets [49].

In many cell types, NF- κ B dimers are located in the cytoplasm in an inactive form through association with any of several I κ B inhibitor proteins (I κ B α , - β , - ϵ , - γ , p105 and p100) [50].

The NF- κ B signaling pathway is mainly regulated by inhibitor κ B (I κ B) proteins and the I κ B kinase complex through two major pathways: the canonical and non-canonical NF- κ B pathways [50]. We measured significantly elevated *NFKB1A* and *NFKB1B* mRNAs after the 31st parabola, whereas the *NFKB1E* and *IKBKG* gene expression were not altered by r- μ g (Figure 2). VIB did not affect the family of cellular I κ B proteins inhibiting the NF- κ B transcription factors, but hyper-g elevated the *NFKB1A* mRNA expression indicating that the measured elevation may be due to the hyper-g phase of the parabola, because an iRPM-exposure of the MDA-MB-231 cells demonstrated no changes in NF- κ B signaling. On the iRPM all investigated genes remained stably expressed. The RPM aims to simulate near weightlessness, but one should take note of increased fluid movements—and thus shear forces—occurring in the flasks, when the device is used for cell cultures experiments [51]. First, it is important to place the sample as close as possible to the center of rotation in order to minimize residual g-artifacts and second, the cell culture flasks have to be completely filled with medium without air bubbles to minimize shear stress. The RPM is used to prepare spaceflight missions and for tissue engineering purposes. It has proven to be a useful device for long-term cultures of cancer cells and benign cells [14]. Postflight data revealed that genes and proteins involved in the regulation of thyroid cancer cell proliferation and metastasis were similarly regulated under RPM and spaceflight conditions [52].

3.3. Parabolic Flight Maneuvers Changed Cell Adhesion Factors

It is known that s- μ g conditions induced changes in the cytoskeleton, ECM, and focal adhesion factors in various cell types [53,54]. Long-term RPM-exposure of human endothelial cells induced the

formation of 3D tubular structures and spheroids [55]. In parallel, secretion of the factors ICAM-1, and VCAM-1 were both increased, when the influence of gravity is minimized for 35 days [55]. In MDA-MB-231 cells exposed to short-term μg on a parabolic flight, an increased synthesis of ICAM-1 protein was found after the P31. A similar result was measured for VCAM-1 protein as given in Figure 6.

The adhesion molecules ICAM-1 and VCAM-1 are mediating the cell adhesion of cancer cells, lymphocytes and other cells to the vascular endothelium [56]. Moreover, ICAM-1 is involved in angiogenesis and is able to increase the survival of microvessels [57].

Primary human macrophages differentiated from monocytes exposed to 11 days r- μg in space on the ISS revealed a reduced surface expression of ICAM-1, defucosylation of surface proteins and an altered metabolite spectrum [58]. Another study examined the ICAM-1 protein synthesis and *ICAM1* gene expression in cells of the monocyte/macrophage system exposed to r- and s- μg obtained during 2D clinostat, parabolic flight, sounding rocket, and orbital experiments [59]. Murine BV-2 microglial cells showed a downregulated *ICAM1* expression, when exposed to a 2D clinostat and a rapid and reversible downregulation in the μg -phase of PF maneuvers [59].

Interestingly, an elevated *ICAM1* mRNA was measured in macrophage-like differentiated human U937 cells during the μg -phase of PFs. In non-differentiated U937 cells, no effect of μg was observed [59].

In addition, we studied the early effects of hyper-g, and VIB comparable to the conditions that occur during PFs on the gene expression of *ICAM1* and *VCAM1*. Both vibration and hypergravity had no effect on *VCAM1* expression. Hyper-g did not change the *ICAM1* mRNA expression, while VIB-exposure of the MDA-MB-231 cells revealed a non-significant result due to the high variation. Furthermore, the *SPP1* gene expression was not altered by VIB and hyper-g, whereas *CD44* was unchanged by VIB, but significantly elevated by hyper-g. Therefore, it can be assumed that the elevated *CD44* gene and protein expression after P31 (Figure 6G,H) is mainly due to hyper-g (Figure 7G). Comparable results were obtained when poorly differentiated ML-1 follicular thyroid cancer cells were investigated during a PFC. The *SPP1* mRNA was significantly elevated after P31 [60]. The *SPP1* gene expression was not changed by VIB and hyper-g in ML1 follicular thyroid cancer cells [60]. Corresponding data were obtained when human chondrocytes were studied during PF maneuvers [61]. No significant changes in the gene expression levels were observed during VIB and hyper-g experiments [61].

In a next step, we focused on the cell-surface glycoprotein CD44 antigen, which is involved in cell adhesion, migration and cell-cell interactions. The CD44 is a receptor for hyaluronic acid and interacts with osteopontin. The mRNA expression of *CD44* and the corresponding protein content were both significantly elevated after P1 and P31 compared to 1 g. Similar results were obtained earlier, when cells were exposed to a NASA rotary cell culture system (RCCS) grown as 3D spheroids and were CD44-positive [62]. The CD44-positivity of the cells grown in 3D MCS was determined by immunocytochemistry and was elevated in bladder cancer, prostate cancer, and glioma cell lines compared with 1 g-cultures [62].

Rat osteoblasts cultured for 4 or 5 days aboard the Space Shuttle and solubilized during spaceflight revealed strongly elevated *CD44* mRNA levels in the flight cultures [63]. In addition, FTC-133 follicular thyroid cancer cells exposed to an RPM for 24 h expressed a *CD44* mRNA which was significantly up-regulated in adherent cells but not significantly altered in MCS [19]. In addition, an increase in *SPP1* mRNA was measured in adherent FTC-133 cells cultured on the RPM. *CD44* can also interact with *SPP1*. The *SPP1* mRNA was elevated in MDA-MB-231 cells after P31 compared with P1 and 1 g-samples. The synthesis of the protein was reduced during the PF maneuvers (Figure 6F), whereas both hyper-g and VIB stress had no effect on *SPP1*. These results are in concert with data obtained from thyroid cancer cells exposed to the RPM. Simulated μg reduced the amount of osteopontin in adherent cells and MCS. Based on the role of osteopontin as a mediator of cell-matrix adhesion and communication, it is influencing tumorigenesis and invasion [64]. Osteopontin seems to be involved in motility regulation by interaction with CD44 in colon cancer cells, which suggests a role for osteopontin

in cancer progression [65]. Osteopontin is a potential cancer biomarker [66] and is involved in biological processes such as cell proliferation, survival, angiogenesis, progression and metastasis [66].

Another study demonstrated that in MDA-MB-231 cells, the inhibition of NF- κ B via the chemical compound Bay-11-7082 results in a CD44 suppression [67]. The NF- κ B inhibition and subsequent CD44 suppression reduced the cell proliferation and invasiveness of breast cancer cells. In contrast in μ g, the cells reacted with a down-regulation of NF- κ B p65 protein and an increase in CD44, a finding which has to be investigated in long-term μ g-studies in the future.

3.4. Interaction Network of Selected Genes Evaluated by STRING Analysis

The interaction between CD44 and osteopontin as a potential basis for cancer progression and metastasis formation is known for a long time [68]. In this study, the up-regulation of the *CD44* mRNA seems to be induced by the hyper-g phases of the PF maneuvers, whereas *SPP1* is mainly elevated by r- μ g. Interestingly, the synthesis of osteopontin is reduced, a finding only observed in r- μ g.

Furthermore, osteopontin regulates the *ICAM-1* and *VEGFA* expression mainly in triple-negative/basal-like breast cancer, supporting its role in tumor progression in TNBC [27]. Osteopontin protein was reduced in P31 samples, whereas the *ICAM-1* protein synthesis was elevated after 31 parabolas which may allow for both proteins to conclude a counterregulatory interaction mechanism in short-term μ g.

Another group demonstrated that purified native OPN induces NF- κ B activation and NF- κ B-dependent *ICAM-1* expression in breast cancer cells [69]. We measured a reduced amount of NF- κ B after P1 and P31 which may be due to the reduced osteopontin content (Figure 2D, Figure 6F).

Both cell adhesion molecules *ICAM-1* and *VCAM-1* are increased in patients with advanced breast cancer and the increase in *VCAM-1* is of prognostic significance [70]. In our study the *VCAM-1* protein synthesis was elevated after P1 and P31. *VCAM1* is one of five genes (*CXCL12*, *MMP2*, *MMP11*, *VCAM1*, and *MME*), which were associated with tumor progression, angiogenesis, and metastasis [71].

There is also an interaction between *CD44* and *ANXA2*. *ANXA1* together with *ANXA2* are both associated with the aggressive behavior of TNBC [72]. The prognostic impact of *ANXA1* relies on a high *ANXA2* expression and both are preferential for TNBC [72]. The MDA-MB-231 cells exhibited a high expression of *ANXA1* and *ANXA2*. *ANXA1* remained stable under all gravity conditions and VIB. Both, r- and s- μ g induced a reduction of *ANXA2* protein after 31 parabolas and *ANXA2* expression after 2h RPM exposure. This response seems to be due to altered gravity.

ANXA1 is known to constitutively activate NF- κ B in breast cancer cells by interacting with the IKK complex [25], an interaction that might not to be relevant in μ g.

ANXA2 is upregulated in many cancer types and is involved in cancer cell migration, adhesion, invasion, and metastasis [73]. Intracellular annexin A2 regulates NF- κ B signaling by binding to the p50 subunit in a calcium-independent manner [73]. The *ANXA2*-p50 complex translocated into the nucleus [73]. After the first parabola annexin A2 protein synthesis was elevated and then after the 31st parabola reduced. The *NFKB1* mRNA was upregulated after P31, but was not altered under all other experimental conditions (Figure 2A, Figure 3A,B).

MAPK3 (*ERK1*) was upregulated after the first parabola and is interacting with *RELA*, *CASP3* and *BCL2*. It is known that NF- κ B inhibits ERK activation to enhance cell survival during the development of tumor adaptive radioresistance in breast cancer cells [74]. In addition, ERK1/2 play a key role in controlling the *BCL2*-regulated, cell-intrinsic apoptotic pathway [75]. Other interactions are found for OPN, FAK and ERK1/2 as well as *RELA*. Integrin α v β 3 binding with OPN mediates the signaling pathways of FAK, ERK1/2, and NF- κ B to activate cellular migration [66], which is important for the dissemination of cancer cells to distant tissues.

3.5. MAPK Signaling Factors Involved in Cancer Progression and Metastasis

We investigated further factors known to enhance cancer growth and spreading. The protein kinase C alpha (PKC α) is implicated in cancer progression and associated with a poor prognosis in

breast cancer patients [76]. There is evidence that PKC α is a key regulator of migration and invasion in endocrine resistant ER+ breast cancer and basal A TNBC, but not in other subtypes such as endocrine sensitive ER+ [76]. In this study, we found a slight increase in *PRKCA* in TNBP exposed to short-term μ g after 31 parabolas. This result was not significant, and thus it may be speculated that *PRKCA* is upregulated later, when the cell detachment starts as well as the 3D aggregation of breast cancer cells [40]. In addition, *PRKCA* is also a key candidate gene in melanoma metastasis [77]. An important step for metastasis is that protein kinase C alpha activates RAF-1 by direct phosphorylation [78].

The biological process of the epithelial-mesenchymal transition (EMT) is known to increase migration and spreading of cancer cells, progression of the cell cycle, and resistance to apoptosis and chemotherapy. It supports tumor progression. One important signaling pathway involved in progression and metastasis is the MAPK pathway [79]. Therefore, we determined the *RAF1* mRNA expression. RAF1 works as a regulatory link between the membrane-associated Ras GTPases and the MAPK/ERK cascade and functions as a switch determining proliferation, differentiation, apoptosis, survival and oncogenic transformation of human cells [80]. RAF1 activation initiates a mitogen-activated protein kinase (MAPK) cascade [80]. The fact that it remained unaltered might explain that we did not find any apoptosis in TNBC exposed to short-term microgravity (Figure 8B).

Furthermore, we measured the expression of *ERK1* and *ERK2*. The ERK subfamily consists of typical (ERK 1/2/5), and atypical (ERK 3/4/7/8) members. ERKs are involved in the regulation of EMT and are thus promoting tumor progression. The *ERK1* gene expression was significantly up-regulated after the first parabola compared to 1 g-samples, and *ERK 2* after the 31st parabola compared with P1 r- μ g-samples (Figure 8D). ERK1 seems to give an initial signal to start 3D aggregation in μ g.

Moreover, we focused on the focal adhesion kinase 1 (FAK1), which is also called PTK2 protein tyrosine kinase 2 (PTK2) and known to increase cancer cell migration and promote metastatic dissemination to distant sites [81]. Blocking of FAK revealed that breast cancer cells became less metastatic due to decreased mobility [81]. The *FAK1* mRNA was significantly up-regulated after P31 compared to 1 g-samples. This is an interesting result indicating its importance for 3D aggregation, breast cancer progression and invasion. Chan et al. [82] had demonstrated that the depletion of FAK induced the formation of active invadopodia and impaired invasive cell migration.

Finally, we measured the *MAPK8/JNK1* mRNA in our experimental μ g-dependent approach. The *JNK1* gene was down-regulated after the first parabola in the μ g-exposed TNBP cells.

It has been shown that *JNK1* promotes cell survival in Her2/neu-positive breast cancer [83]. Human studies have shown the relevance of JNK activation to various human cancers [84]. These kinases are involved in the prevention of malignant transformation via the induction of apoptosis and in promoting cell survival in established tumors [85]. In addition, there is a potential to monitor JNK activity as an early biomarker of response to chemotherapy [85]. Therefore, the decrease in *JNK1* mRNA expression seems to promote a following 3D formation of the TNBC cells in real μ g-conditions.

Taken together, TNBC cells exposed to short-term μ g obtained by PF maneuvers kept all signs of a more aggressive phenotype as elevations of ICAM1 and VCAM1 proteins occurred soon.

MDA-MB-231 cells exposed to short-term r- μ g were relatively stable to this external stressor, vibration and hyper-g.

In summary, an early up-regulation of *NFKB1* (P1), *NFKB3 (RELA)* (P1), *ERK1* (P1), *ICAM1* (P1), *NFKBIA* (P31), *NFKBIB* (P31), *FAK1* (P31), *SPP1* (P31) and *CD44* (P1, P31) gene expression as well as a reduced protein content of NF- κ B p65 and osteopontin were found after the PF maneuvers. *CD44* and *NFKBIA* were upregulated in hyper-g, showing that the hyper-g-phase seems to influence both factors. For all other genes, our data indicate that the microgravity phase is the driving factor of most of these changes in gene expression. These results are very important because apoptosis is needed for cell detachment together with an activation of NF- κ B-p65 to form 3D growth (spheroids) of cancer cells when they were exposed to μ g. Changes in osteopontin protein suggest a role in survival, angiogenesis, invasion, and metastasis of TNBC cells.

4. Materials and Methods

4.1. Cell Culture

MDA-MB-231 cells were purchased from the American Type Culture Collection (ATCC[®] HTB26[™], Manassas, Virginia, USA). They were cultured in RPMI 1640 (Life Technologies, Paisley, UK), 10 % FCS (Sigma Aldrich, Steinheim, Germany) and 1% penicillin/streptomycin (Life Technologies, New York, USA). The cells were cultured in vented T75 cm² flasks (Sarstedt, Nümbrecht, Germany) and were split every 4–5 days to prevent confluence.

4.2. 29th. Parabolic Flight Campaign

The PFs were organized by the DLR in cooperation with Novespace, Bordeaux-Mérignac Airport, France. The cells were transferred on board of the Airbus A310 (Figure 10A) into a pre-warmed 37 °C incubator shortly before take-off and they were incubated at 37 °C for the whole time during the flight. The flight rack is shown in Figure 10B. Each parabola had an initial phase of hyper-g (1.8 g) for 22 s during pull-up and a final phase of hypergravity for 22 s during pull-out (Figure 10C). The two hyper-g-phases framed a 22-s long μ g-phase. The flight maneuver was repeated 31 times per flight day. During the PFs, the MDA-MB-231 cells were fixed with RNAlater (Invitrogen by Thermo Fischer Scientific, Vilnius, Lithuania) at the end of the first parabola (P1) and the end of the last parabola (P31). The cells were cultured in T75cm² cell culture flasks (Sarstedt, Nümbrecht, Germany) with 10 mL medium in each flask. Each flask had a fixed three-way connector on the lid which was connected with 140 cm tubing to a 50 mL syringe filled with RNAlater. The RNAlater was injected manually into the flasks at the designated times. Additional MDA-MB-231 cells were incubated on ground to serve as static 1 g-controls. The ground control cells were fixed with RNAlater in parallel to the samples on board of the flight. After landing, the medium and RNAlater mixture was removed and replaced with 5 mL of fresh RNAlater. The cells were harvested with a 25 cm scraper (Sarstedt, Nümbrecht, Germany) and stored suspended in RNAlater at 4 °C in 15 mL tubes until RNA isolation [54].

4.3. Vibration Experiments

As a PF implements different stressors, vibration was tested on the cells using the Vibraplex device (DLR, Cologne, Germany) [61,86]. MDA-MB-231 cells were seeded on μ -Slide VI ibiTreat channel slides (Ibidi, Gräfelfing, Germany) for immunostaining and in T25 cm² cell culture flasks for RNA isolation. The flasks and the slides were attached to the Vibraplex platform. The Vibraplex was transferred into a 37 °C incubator. Frequencies between 0.2 to 14 Hz were produced via the Vibraplex for a two-hour duration. These frequencies resemble the VIB produced during the PF. After the vibration procedure, the cells were fixed with either 4% PFA for immunostaining or RNAlater for RNA isolation. Ground control slides and flasks were cultured in parallel for comparison.

4.4. Hyper-g Experiments

MDA-MB-231 cells were counted and seeded into μ -Slide VI ibiTreat channel slides (Ibidi, Gräfelfing, Germany) comparable to [87] for immunostaining. For RNA isolation T 75 cm² flasks were used with a confluence of 90%. The flasks and the slides were fixed on swing-out gondolas inside the DLR multi-sample incubator centrifuge (MuSIC) located inside a 37 °C incubator. The centrifuge was rotating at a constant speed to produce 1.8 g for 2 h which is comparable to the hypergravity phases produced during the parabolic flight. The device designed by the DLR, Department of Gravitational Biology, is shown in Figure 10D. At the end of the run, the cells were fixed with either 4% PFA for immunostaining or RNAlater for RNA isolation. All slides and cell culture flasks were randomly assigned to centrifugation or 1 g-ground controls.

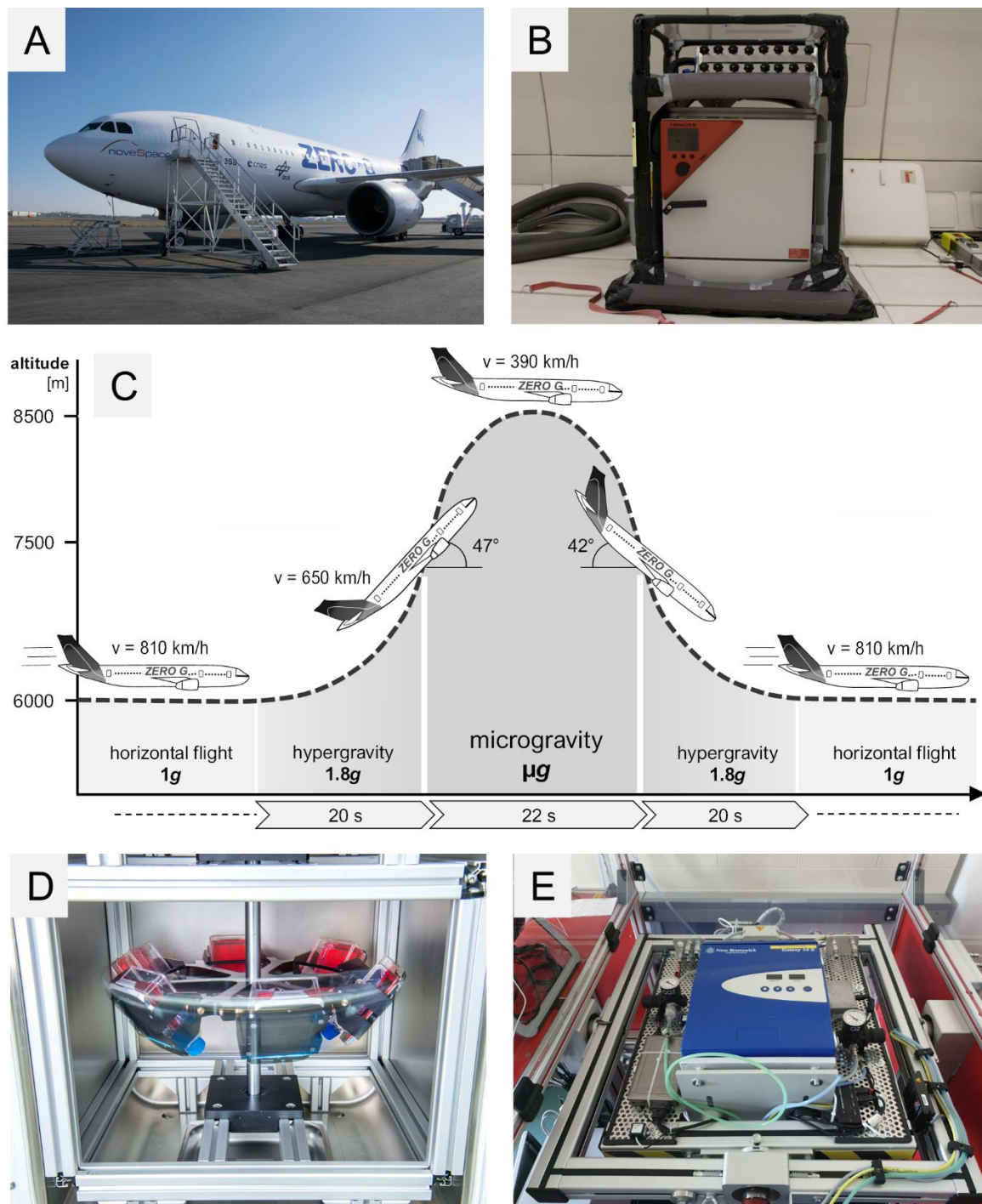


Figure 10. (A) Airbus A310 ZERO-G; (B) Deutsches Zentrum für Luft- und Raumfahrt (DLR) Flight rack; (C) Different phases of a parabolic flight; (D) DLR Multi-sample incubator centrifuge (MuSIC); (E) Incubator random positioning machine (iRPM).

4.5. Incubator Random Positioning Machine (iRPM)

The iRPM (Figure 10E) was designed and constructed by Prof. Jörg Sekler-Fachhochschule Nordwestschweiz. Details of the device were published in [88].

MDA-MB-231 cells were seeded in μ -Slide VI ibiTreat channel slides (Ibidi, Gräfelfing, Germany) for immunostaining and T25cm² flasks for RNA isolation. The slides and the flasks were placed inside a 37 °C pre-warmed iRPM. At the end of the 2 h, the cells were fixed with either 4% PFA for

immunostaining or RNAlater for RNA isolation. The RNA was isolated as mentioned earlier. All the slides and flasks were put in comparison to 1 g-ground control.

4.6. RNA Isolation and Quantitative Polymerase Chain Reaction (qPCR)

All falcon tubes were centrifuged (2500× g for 10 min at 4 °C), followed by discarding the supernatant. The RNA was isolated afterwards using the RNeasy Mini Kit (Qiagen, Hilden, Germany) according to the manufacturer's protocol. The quality of the RNA was evaluated with a spectrophotometer. Afterwards, RNA was converted to cDNA with the High Capacity cDNA reverse Transcription Kit according to the manufacturer's protocol (Applied Biosystems, Darmstadt, Germany). 1 µg total RNA in 20 µL reaction mix was prepared as stock for qPCR. The primers were designed using Primer Blast (primer designing tool from NCBI).

A total volume of 13 µL SYBR green reaction mix (Applied Biosystems, Darmstadt, Germany) was pipetted in each well in a 96 well plate. 1 µL of cDNA was added to each reaction mix with a concentration of 100 µM forward and reverse primers. The 7500 Fast Real-Time PCR System (Applied Biosystems, Darmstadt, Germany) was used to determine the transcription level of targeted genes (see Table 1). The program consisted of an initial 20 s long holding stage of 95 °C followed by the cycling stage. The cycling stage consisted of 40 cycles of 3 s at 95 °C and 30 s at 60 °C. A melting curve was implemented at the end of each run to verify the primer specificity. The data was collected and analyzed by the $\Delta\Delta C_T$ method. 18S rRNA and TBP were used as reference genes.

Table 1. List of primer used during the study. Primer sequences are given in 5' to 3' direction.

Factor	Primer Name	Sequence 5'–3'
18S rRNA	18s-F	GGAGCCTGCGGCTTAATTT
	18s-R	CAACTAAGAACGGCCATGCA
Annexin A1; ANXA1	ANXA1-F	GCCAAAGACATAACCTCAGACACAT
	ANXA1-R	GAATCAGCCAAGTCTTCATTACACA
Annexin A2; ANXA2	ANXA2-F	GGTACAAGAGTTACAGCCCTTATGACA
	ANXA2-R	CATGGAGTCATACAGCCGATCA
BCL2 Associated X, Apoptosis Regulator; BAX	Bax-F	GTCAGCTGCCACTCGGAAA
	Bax-R	AGTAACATGGAGCTGCAGAGGAT
B-cell lymphoma 2; BCL2	Bcl2-F	TCAGAGACAGCCAGGAGAAATCA
	Bcl2-R	CCTGTGGATGACTGAGTACCTGAA
Caspase 3; CASP3	Casp3-F	CTCCAACATCGACTGTGAGAAGTT
	Casp3-R	GCGCCAGCTCCAGCAA
CD44	CD44-F	ACCCTCCCCTCATTACCCAT
	CD44-R	GTTGTACTACTAGGAGTTGCCTGGATT
Extracellular signal-regulated kinases 1; ERK1	ERK1-F	ACCTGCGACCTTAAGATTTGTGA
	ERK1-R	AGCCACATACTCCGTCAGGAA
Extracellular signal-regulated kinases 2; ERK2	ERK2-F	TTCCAACCTGCTGCTCAACA
	ERK2-R	TCTGTCAGGAACCCTGTGTGAT
Focal adhesion kinase 1 (Protein-tyrosine kinase 2); pan-FAK1	FAK1-F	TGTGGGTAACACAGATCCTGC
	FAK1-R	CTGAAGCTTGACACCCCTCGT
Intercellular adhesion molecule 1; ICAM1	ICAM1-F	CGGCTGACGTGTGCAGTAAT
	ICAM1-R	CTTCTGAGACCTCTGGCTTCGT

Table 1. Cont.

Factor	Primer Name	Sequence 5'–3'
Mitogen-activated protein kinase 8 (MAPK8) (JNK1-a2); MAPK8/JNK1	JNK1-F	TCTCCTTTAGGTGCAGCAGTG
	JNK1-R	CAGAGGCCAAAGTCGGATCT
NF-kappa-B transcription complex P105/P50; NFKB1	NFKB1-F	CTTAGGAGGGAGAGCCCAC
	NFKB1-R	TGAAACATTTGTTTCAGGCCTTC
NF-kappa-B transcription complex P100/P52; NFKB2	NFKB2-F	GTACAAAGATACGGGACCC
	NFKB2-R	CCAGACCTGGGTTGTAGCA
NF-kappa-B transcription complex P65; NFKB P65	NFKB P65-F	CGCTTCTTCACACACTGGATTC
	NFKB P65-R	ACTGCCGGGATGGCTTCT
NF-kappa-B essential modulator (NEMO); IKBKG	Ikbkg-F	AACTGGGACTTTCTCGGAGC
	Ikbkg-R	GGCAAGGGCTGTCAGCAG
NF-kappa-B inhibitor alpha; NFKBIA	NFKBIA-F	AATGCTCAGGAGCCCTGTAAT
	NFKBIA-R	CTGTTGACATCAGCCCCACA
NF-kappa-B inhibitor beta; NFKBIB	NFKBIB-F	CCCGGAGGACCTGGGTT
	NFKBIB-R	GCAGTGCCGTGTCCCC
NF-kappa-B inhibitor epsilon; NFKBIE	NFKBIE-F	TGGGCATCTCATCCACTCTG
	NFKBIE-R	ACAAGGGATTCTCAGTCAGGT
Protein kinase C alpha type; PRKCA	PRKCA-F	TGGGTCAGTCTCTATGGACTTATC
	PRKCA-R	CGCCCCCTCTTCTCAGTGT
TATA-box binding protein; TBP	TBP-F	GTGACCCAGCATCACTGTTTC
	TBP-R	GCAAACCAGAAACCCTTGCG
Raf-1 Proto-Oncogene, Serine/Threonine Kinase; Raf1	Raf1-F	GGGAGCTTGGAAGACGATCAG
	Raf1-R	ACACGGATAGTGTGCTTGTC
Osteopontin (OPN); SPP1	SPP1-F	CGAGGTGATAGTGTGGTTTATGGA
	SPP1-R	CGTCTGTAGCATCAGGGTACTG
Vascular cell adhesion protein 1; VCAM1	VCAM1-F	CATGGAATTCGAACCCAAACA
	VCAM1-R	GGCTGACCAAGACGGTTGTATC

4.7. Western Blotting

Western blot analysis, gel electrophoresis, trans-blotting, and densitometry were carried out following routine protocols as described previously [21,54,61]. Following lysis and centrifugation, aliquots of 30 µg were subjected to sodium dodecyl sulphate-polyacrylamide gel electrophoresis (SDS-PAGE) and Western blotting. The samples were collected at the end of the P1 and P31 and were compared to 1 g control samples. Each condition is represented with 5 samples with a total number of 15 samples for all the conditions per cell line. The samples were loaded onto Criterion XT 4–12% precast gels (Bio-Rad, Hercules, CA, USA) and run for 1 h at 150 V. Proteins were then transferred with a TurboBlot (Bio-Rad) (100 V, 30 min) to a PVDF membrane. Cofilin-1 was used as a loading control. Membranes were then blocked for 2 h in TBS-T containing 0.3% I Block (Applied Biosystems, Foster City, CA, USA). For the detection of the selected antigens (see Table 2), the membranes were incubated overnight at room temperature in TBS-T and 0.3% I Block solutions of the antibodies. Following three washing steps of 5 min, the membranes were incubated for a further 2 h at room temperature with the secondary antibody Horseradish peroxidase (HRP)-linked antibody (Cell Signaling Technology Inc., Danvers, MA, USA) diluted 1:4000 in TBS-T and 0.3% I-Block. The respective protein bands were

visualized using Bio-Rad Clarity Western ECL (Bio-Rad) and images were captured with Image Quant LAS 4000 mini (GE Healthcare Life Science, Freiburg, Germany). Images of stained membranes were captured on Syngene PXi 4EZ image analysis system (SynGene, Cambridge, UK) and analyzed using the ImageJ software for densitometric quantification of the respective bands and total protein load.

Table 2. List of the names, sources, companies, molecular weight and dilutions of all the antibodies that were used for Western blots.

Antibody	kDa	Dilution	Company	Source
Annexin 2	38	1:1000	Abcam #ab41802	Rb
NFkBp65	65	1:1000	Thermo Fisher #PA1-186	Rb
IKBKG	38	1:500	Origene #TA812460	MS
IkB α /NFKBIA	36	1:1000	Invitrogen #MA5-15132	MS
Cofilin-1	20	1:2000	Abcam #ab 42824	Rb
CD44	80	1:500	CST#5640	MS
VCAM1	110	1:500	Sc80431	MS
Casp 3	35	1:800	CST#9662	Rb
ICAM1	90	1:500	CST#4915	Rb
Osteopontin	44	1:1000	SAB4200018	MS

4.8. Terminal Deoxynucleotidyl Transferase dUTP Nick End Labeling (TUNEL) Staining

The MDA-MB-231 cells were cultured in μ -Slide VI 0.4 ibiTreat Ibidi slides (IBIDI GmbH, Martinsried, Planegg, Germany), exposed to VIB, hyper-g and iRPM and subsequently collected for the detection of apoptosis. The method was published earlier in Lützenberg et al. [89].

TUNEL staining was performed according to the manufacturer's recommendation (Thermo Fisher Scientific, Waltham, Massachusetts, USA; Click-iT TUNEL Alexa Fluor 488 (cat# C10245)).

The stained cell samples (VIB, hyper-g, iRPM and corresponding static 1 g-controls) were examined utilizing a Leica DM 2000 microscope equipped with an objective with a calibrated magnification of 400 \times and connected to an external light source, Leica EL 6000 (Leica Microsystems GmbH, Wetzlar, Germany). To obtain positive controls the cells were treated with DNAase before the TUNEL staining.

4.9. STRING Analysis

Interactions between proteins were determined using the STRING 10 platform [90]. For each protein, the UniProtKB entry number was inserted in the input form "multiple proteins" and "Homo sapiens" was selected as organism. The resulting network view was downloaded in the molecular action view showing lines between interacting proteins and genes [91].

4.10. Statistical Analyses

GraphPad prism 7.01 (GraphPad Software, Inc., California, USA) was used to analyze the data. The nonparametric Mann-Whitney U test was used as a statistical test of significance. The difference between groups was considered significant when the *p*-value was less than 0.05 (* *p* < 0.05).

5. Conclusions

Short-term r- μ g produced by PF maneuvers induced the gene expression of cell adhesion molecules in triple-negative breast cancer cells. This finding is in agreement with long-term μ g (s- and r- μ g) data with other cell types grown on the NASA-developed high-aspect ratio vessel (HARV) or on the Space Shuttle in space for 4–5 days [62,63,92]. The CD44 upregulation in the r- μ g- and hyper-g-cultures may be involved in the compensative regulation to counteract cellular apoptosis occurring in μ g [93,94].

Cell adhesion molecules and factors of the MAPK pathway are involved in the adaptive response to perturbation of mechanical stress under short-term real microgravity. Overall, our study suggests that a fine balance between NF- κ B-p65 and osteopontin gene dosage is required to regulate metastasis, survival and angiogenesis of TNBC cells.

Author Contributions: Parabolic flight campaign: M.Z.N., D.M., T.J.C., S.K., and M.K.; VIB experiment: T.J.B. and M.Z.N.; iRPM experiment: M.Z.N., T.J.B., and hyper-g experiment: C.L., R.H., M.Z.N., S.K., M.K., T.J.B.; Conceptualization, D.G., T.J.C. and S.K.; methodology, S.K., M.Z.N., D.M., T.J.B., and J.S.; Software, T.J.B., M.W., and S.K.; Validation, D.G., T.J.C., S.K., M.K. and D.M.; Formal analysis, M.Z.N., S.K., J.S., and M.W.; Investigation, M.Z.N., and S.K.; Resources, M.I. and R.H.; Writing—Original draft preparation, M.Z.N., S.K., D.G., and M.W.; Project administration, D.G.; funding acquisition, D.G. and M.I.

Funding: This research was funded by the German Space Agency (DLR; BMWi projects 50WB1524; 50WB1924).

Acknowledgments: We would like to thank Katrin Stang, Michael Becker and Markus Braun (German Aerospace Center DLR, Bonn) for their support and for giving us the possibility to attend the 29th DLR Parabolic Flight Campaign in Bordeaux-Mérignac, France.

Conflicts of Interest: The authors declare no conflict of interest.

Abbreviations

2D	Two-dimensional
3D	Three-dimensional
ANXA1	Annexin A1
ANXA2	Annexin A2
AR	Androgen receptor
ATCC	American Type Culture Collection
BAX	BCL2 Associated X, Apoptosis Regulator
BCL2	B-cell lymphoma 2
CASP3	Caspase3
CD44	Cell surface glycoprotein CD44
Cx+	Connexin positive
CXCL12	C-X-C Motif Chemokine Ligand 12
CYC1	Cytochrome c1
DLR	Deutsches Zentrum für Luft- und Raumfahrt
ECM	Extracellular matrix
ER	Estrogen receptor
ERK1,2	Extracellular Signal-Regulated Kinase 1, 2
FAK1	Focal adhesion kinase 1
FCS	Fetal calf serum
FTC-133	Human follicular thyroid carcinoma cell line
GLOBOCAN	Global Cancer Observatory
HARV	High-aspect ratio vessel
HER2	Human epidermal growth receptor 2
hyper-g	Hypergravity
ICAM1	Intercellular adhesion molecule 1
IKBK	NF-kappa-B essential modulator (NEMO)
IKK	I κ B kinase
iRPM	Incubator random positioning machine
ISS	International Space Station
I κ B	Inhibitor of κ B
I κ B α	Inhibitor of κ B alpha
I κ B β	Inhibitor of κ B beta
I κ B γ	Inhibitor of κ B gamma
I κ B ϵ	Inhibitor of κ B epsilon
JNK1	Mitogen-activated protein kinase 8
KI67	Antigen KI67

µg	Microgravity
MAPK	Mitogen-Activated Protein Kinase
MCF-7	Michigan Cancer Foundation-7 cell line
MCS	Multicellular spheroids
MDA-MB-231	M.D. Anderson-Metastasis Breast cancer cell line
ML1	Human thyroid carcinoma cell line
MME	Membrane Metalloendopeptidase
MMP11	Matrix Metallopeptidase 11
MMP2	Matrix Metallopeptidase 2
MuSIC	Multi-sample incubator centrifuge
NFKB1	NF-kappa-B transcription complex P105/P50
NFKB2	NF-kappa-B transcription complex P100/P52
NFKB3/NFKB	NF-kappa-B transcription complex P65
P65	
NFKBIA	NF-κB-inhibitor-alpha
NFKBIB	NF-κB-inhibitor-beta
NFKBIE	NF-κB-inhibitor-epsilon
NFκB	Nuclear factor-kappaB
P	Parabola
PF	Parabolic flight
PFA	Paraformaldehyde
PR	Progesterone receptor
PRKCA	Protein kinase C alpha
PTK2	Protein tyrosine kinase 2 (known as FAK1)
qPCR	Quantitative polymerase chain reaction
RAF1	RAF proto-oncogene serine/threonine-protein kinase
r-µg	Real microgravity
RELA	V-Rel Avian Reticuloendotheliosis Viral Oncogene Homolog A
RPM	Random positioning machine
s-µg	Simulated microgravity
SPP1/OPN	Osteopontin
STRING	Search Tool for the Retrieval of Interacting Genes/Proteins
TBP	TATA-box binding protein
TNBC	Triple-negative breast cancer
TUNEL	Terminal deoxynucleotidyl transferase dUTP nick end labeling
VCAM1	Vascular cell adhesion protein 1
VIB	Vibration

References

1. Bray, F.; Ferlay, J.; Soerjomataram, I.; Siegel, R.L.; Torre, L.A.; Jemal, A. Global cancer statistics 2018: GLOBOCAN estimates of incidence and mortality worldwide for 36 cancers in 185 countries. *CA Cancer J. Clin.* **2018**, *68*, 394–424. [[CrossRef](#)]
2. Van't Veer, L.J.; Dai, H.; van de Vijver, M.J.; He, Y.D.; Hart, A.A.; Mao, M.; Peterse, H.L.; van der Kooy, K.; Marton, M.J.; Witteveen, A.T.; et al. Gene expression profiling predicts clinical outcome of breast cancer. *Nature* **2002**, *415*, 530–536. [[CrossRef](#)]
3. Soliman, N.A.; Yussif, S.M. Ki-67 as a prognostic marker according to breast cancer molecular subtype. *Cancer Biol. Med.* **2016**, *13*, 496–504. [[CrossRef](#)] [[PubMed](#)]
4. Dai, X.; Li, T.; Bai, Z.; Yang, Y.; Liu, X.; Zhan, J.; Shi, B. Breast cancer intrinsic subtype classification, clinical use and future trends. *Am. J. Cancer Res.* **2015**, *5*, 2929–2943. [[PubMed](#)]
5. Farmer, P.; Bonnefoi, H.; Becette, V.; Tubiana-Hulin, M.; Fumoleau, P.; Larsimont, D.; Macgrogan, G.; Bergh, J.; Cameron, D.; Goldstein, D.; et al. Identification of molecular apocrine breast tumours by microarray analysis. *Oncogene* **2005**, *24*, 4660–4671. [[CrossRef](#)] [[PubMed](#)]

6. Prat, A.; Parker, J.S.; Karginova, O.; Fan, C.; Livasy, C.; Herschkowitz, J.I.; He, X.; Perou, C.M. Phenotypic and molecular characterization of the claudin-low intrinsic subtype of breast cancer. *Breast Cancer Res.* **2010**, *12*, R68. [[CrossRef](#)] [[PubMed](#)]
7. Kristensen, T.B.; Knutsson, M.L.; Wehland, M.; Laursen, B.E.; Grimm, D.; Warnke, E.; Magnusson, N.E. Anti-vascular endothelial growth factor therapy in breast cancer. *Int. J. Mol. Sci.* **2014**, *15*, 23024–23041. [[CrossRef](#)]
8. Cailleau, R.; Young, R.; Olive, M.; Reeves, W.J., Jr. Breast tumor cell lines from pleural effusions. *J. Natl. Cancer Inst.* **1974**, *53*, 661–674. [[CrossRef](#)]
9. Becker, J.L.; Souza, G.R. Using space-based investigations to inform cancer research on Earth. *Nat. Rev. Cancer* **2013**, *13*, 315–327. [[CrossRef](#)]
10. Obermaier, C.; Jankowski, V.; Schmutzler, C.; Bauer, J.; Wildgruber, R.; Infanger, M.; Kohrle, J.; Krause, E.; Weber, G.; Grimm, D. Free-flow isoelectric focusing of proteins remaining in cell fragments following sonication of thyroid carcinoma cells. *Electrophoresis* **2005**, *26*, 2109–2116. [[CrossRef](#)]
11. Pietsch, J.; Kussian, R.; Sickmann, A.; Bauer, J.; Weber, G.; Nissum, M.; Westphal, K.; Egli, M.; Grosse, J.; Schonberger, J.; et al. Application of free-flow IEF to identify protein candidates changing under microgravity conditions. *Proteomics* **2010**, *10*, 904–913. [[CrossRef](#)] [[PubMed](#)]
12. Bauer, J.; Kopp, S.; Schlagberger, E.M.; Grosse, J.; Sahana, J.; Riwaldt, S.; Wehland, M.; Luetzenberg, R.; Infanger, M.; Grimm, D. Proteome Analysis of Human Follicular Thyroid Cancer Cells Exposed to the Random Positioning Machine. *Int. J. Mol. Sci.* **2017**, *18*, 546. [[CrossRef](#)] [[PubMed](#)]
13. Sahana, J.; Nassef, M.Z.; Wehland, M.; Kopp, S.; Kruger, M.; Corydon, T.J.; Infanger, M.; Bauer, J.; Grimm, D. Decreased E-Cadherin in MCF7 Human Breast Cancer Cells Forming Multicellular Spheroids Exposed to Simulated Microgravity. *Proteomics* **2018**, *18*, e1800015. [[CrossRef](#)] [[PubMed](#)]
14. Grimm, D.; Egli, M.; Kruger, M.; Riwaldt, S.; Corydon, T.J.; Kopp, S.; Wehland, M.; Wise, P.; Infanger, M.; Mann, V.; et al. Tissue Engineering Under Microgravity Conditions-Use of Stem Cells and Specialized Cells. *Stem Cells Dev.* **2018**, *27*, 787–804. [[CrossRef](#)]
15. Masiello, M.G.; Cucina, A.; Proietti, S.; Palombo, A.; Coluccia, P.; D'Anselmi, F.; Dinicola, S.; Pasqualato, A.; Morini, V.; Bizzarri, M. Phenotypic switch induced by simulated microgravity on MDA-MB-231 breast cancer cells. *BioMed Res. Int.* **2014**, *2014*, 652434. [[CrossRef](#)]
16. Kruger, M.; Melnik, D.; Kopp, S.; Buken, C.; Sahana, J.; Bauer, J.; Wehland, M.; Hemmersbach, R.; Corydon, T.J.; Infanger, M.; et al. Fighting Thyroid Cancer with Microgravity Research. *Int. J. Mol. Sci.* **2019**, *20*, 2553. [[CrossRef](#)]
17. Wang, W.; Nag, S.A.; Zhang, R. Targeting the NFkappaB signaling pathways for breast cancer prevention and therapy. *Curr. Med. Chem.* **2015**, *22*, 264–289. [[CrossRef](#)]
18. Zhang, Q.; Lenardo, M.J.; Baltimore, D. 30 Years of NF-kappaB: A Blossoming of Relevance to Human Pathobiology. *Cell* **2017**, *168*, 37–57. [[CrossRef](#)]
19. Grosse, J.; Wehland, M.; Pietsch, J.; Schulz, H.; Saar, K.; Hubner, N.; Eilles, C.; Bauer, J.; Abou-El-Ardat, K.; Baatout, S.; et al. Gravity-sensitive signaling drives 3-dimensional formation of multicellular thyroid cancer spheroids. *FASEB J.* **2012**, *26*, 5124–5140. [[CrossRef](#)]
20. Kopp, S.; Sahana, J.; Islam, T.; Petersen, A.G.; Bauer, J.; Corydon, T.J.; Schulz, H.; Saar, K.; Huebner, N.; Slumstrup, L.; et al. The role of NFkappaB in spheroid formation of human breast cancer cells cultured on the Random Positioning Machine. *Sci. Rep.* **2018**, *8*, 921. [[CrossRef](#)]
21. Murakami, N.; Kuhnel, A.; Schmid, T.E.; Ilicic, K.; Stangl, S.; Braun, I.S.; Gehrmann, M.; Molls, M.; Itami, J.; Multhoff, G. Role of membrane Hsp70 in radiation sensitivity of tumor cells. *Radiat. Oncol.* **2015**, *10*, 149. [[CrossRef](#)]
22. Oeckinghaus, A.; Hayden, M.S.; Ghosh, S. Crosstalk in NF-kappaB signaling pathways. *Nat. Immunol.* **2011**, *12*, 695–708. [[CrossRef](#)]
23. Huang, T.; Kang, W.; Zhang, B.; Wu, F.; Dong, Y.; Tong, J.H.; Yang, W.; Zhou, Y.; Zhang, L.; Cheng, A.S.; et al. miR-508-3p concordantly silences NFKB1 and RELA to inactivate canonical NF-kappaB signaling in gastric carcinogenesis. *Mol Cancer* **2016**, *15*, 9. [[CrossRef](#)]
24. Lindner, V. The NF-kappaB and IkappaB system in injured arteries. *Pathobiology* **1998**, *66*, 311–320. [[CrossRef](#)]
25. Bist, P.; Leow, S.C.; Phua, Q.H.; Shu, S.; Zhuang, Q.; Loh, W.T.; Nguyen, T.H.; Zhou, J.B.; Hooi, S.C.; Lim, L.H. Annexin-1 interacts with NEMO and RIP1 to constitutively activate IKK complex and NF-kappaB: Implication in breast cancer metastasis. *Oncogene* **2011**, *30*, 3174–3185. [[CrossRef](#)]

26. Anwar, K.N.; Fazal, F.; Malik, A.B.; Rahman, A. RhoA/Rho-associated kinase pathway selectively regulates thrombin-induced intercellular adhesion molecule-1 expression in endothelial cells via activation of I kappa B kinase beta and phosphorylation of RelA/p65. *J. Immunol.* **2004**, *173*, 6965–6972. [[CrossRef](#)]
27. Ortiz-Martinez, F.; Sanmartin, E.; Pomares-Navarro, E.; Perez-Balaguer, A.; Andres, L.; Sanchez-Paya, J.; Aranda, F.I.; Lerma, E.; Peiro, G. Osteopontin Regulates VEGFA and ICAM-1 mRNA Expression in Breast Carcinoma. *Am. J. Clin. Pathol.* **2015**, *143*, 812–822. [[CrossRef](#)]
28. Ue, T.; Yokozaki, H.; Kitadai, Y.; Yamamoto, S.; Yasui, W.; Ishikawa, T.; Tahara, E. Co-expression of osteopontin and CD44v9 in gastric cancer. *Int. J. Cancer* **1998**, *79*, 127–132. [[CrossRef](#)]
29. Chintagari, N.R.; Jin, N.; Wang, P.; Narasaraju, T.A.; Chen, J.; Liu, L. Effect of cholesterol depletion on exocytosis of alveolar type II cells. *Am. J. Respir. Cell Mol. Biol.* **2006**, *34*, 677–687. [[CrossRef](#)]
30. Tiys, E.S.; Ivanisenko, T.V.; Demenkov, P.S.; Ivanisenko, V.A. FunGeneNet: A web tool to estimate enrichment of functional interactions in experimental gene sets. *BMC Genom.* **2018**, *19*, 76. [[CrossRef](#)]
31. Zaczynska, E.; Kochanowska, I.; Kruzal, M.; Zimecki, M. Lactoferrin Prevents Susceptibility of WEHI 231 Cells to Anti-Ig-Induced Cell Death Promoting Cell Differentiation. *Folia Biol. (Praha)* **2018**, *64*, 16–22.
32. Reza, A.; Choi, Y.J.; Yasuda, H.; Kim, J.H. Human adipose mesenchymal stem cell-derived exosomal-miRNAs are critical factors for inducing anti-proliferation signalling to A2780 and SKOV-3 ovarian cancer cells. *Sci. Rep.* **2016**, *6*, 38498. [[CrossRef](#)]
33. Cailleau, R.; Olive, M.; Cruciger, Q.V. Long-term human breast carcinoma cell lines of metastatic origin: Preliminary characterization. *In Vitro* **1978**, *14*, 911–915. [[CrossRef](#)]
34. Brinkley, B.R.; Beall, P.T.; Wible, L.J.; Mace, M.L.; Turner, D.S.; Cailleau, R.M. Variations in cell form and cytoskeleton in human breast carcinoma cells in vitro. *Cancer Res.* **1980**, *40*, 3118–3129.
35. White, R.J.; Averner, M. Humans in space. *Nature* **2001**, *409*, 1115–1118. [[CrossRef](#)]
36. Hader, D.P.; Braun, M.; Grimm, D.; Hemmersbach, R. Gravireceptors in eukaryotes—a comparison of case studies on the cellular level. *NPJ Microgravity* **2017**, *3*, 13. [[CrossRef](#)]
37. Grimm, D.; Bauer, J.; Kossmehl, P.; Shakibaei, M.; Schoberger, J.; Pickenhahn, H.; Schulze-Tanzil, G.; Vetter, R.; Eilles, C.; Paul, M.; et al. Simulated microgravity alters differentiation and increases apoptosis in human follicular thyroid carcinoma cells. *FASEB J.* **2002**, *16*, 604–606. [[CrossRef](#)]
38. Qian, A.; Zhang, W.; Xie, L.; Weng, Y.; Yang, P.; Wang, Z.; Hu, L.; Xu, H.; Tian, Z.; Shang, P. Simulated weightlessness alters biological characteristics of human breast cancer cell line MCF-7. *Acta Astronaut.* **2008**, *63*, 947–958. [[CrossRef](#)]
39. Kopp, S.; Warnke, E.; Wehland, M.; Aleshcheva, G.; Magnusson, N.E.; Hemmersbach, R.; Corydon, T.J.; Bauer, J.; Infanger, M.; Grimm, D. Mechanisms of three-dimensional growth of thyroid cells during long-term simulated microgravity. *Sci. Rep.* **2015**, *5*, 16691. [[CrossRef](#)]
40. Kopp, S.; Slumstrup, L.; Corydon, T.J.; Sahana, J.; Aleshcheva, G.; Islam, T.; Magnusson, N.E.; Wehland, M.; Bauer, J.; Infanger, M.; et al. Identifications of novel mechanisms in breast cancer cells involving duct-like multicellular spheroid formation after exposure to the Random Positioning Machine. *Sci. Rep.* **2016**, *6*, 26887. [[CrossRef](#)]
41. Schoenberger, J.; Bauer, J.; Moosbauer, J.; Eilles, C.; Grimm, D. Innovative strategies in in vivo apoptosis imaging. *Curr. Med. Chem.* **2008**, *15*, 187–194. [[CrossRef](#)]
42. Grosse, J.; Wehland, M.; Pietsch, J.; Ma, X.; Ulbrich, C.; Schulz, H.; Saar, K.; Hubner, N.; Hauslage, J.; Hemmersbach, R.; et al. Short-term weightlessness produced by parabolic flight maneuvers altered gene expression patterns in human endothelial cells. *FASEB J.* **2012**, *26*, 639–655. [[CrossRef](#)]
43. Wehland, M.; Ma, X.; Braun, M.; Hauslage, J.; Hemmersbach, R.; Bauer, J.; Grosse, J.; Infanger, M.; Grimm, D. The impact of altered gravity and vibration on endothelial cells during a parabolic flight. *Cell Physiol. Biochem.* **2013**, *31*, 432–451. [[CrossRef](#)]
44. Sarkar, D.K.; Jana, D.; Patil, P.S.; Chaudhari, K.S.; Chattopadhyay, B.K.; Chikkala, B.R.; Mandal, S.; Chowdhary, P. Role of NF-kappaB as a Prognostic Marker in Breast Cancer: A Pilot Study in Indian Patients. *Indian J. Surg. Oncol.* **2013**, *4*, 242–247. [[CrossRef](#)]
45. Khongthong, P.; Roseweir, A.K.; Edwards, J. The NF-KB pathway and endocrine therapy resistance in breast cancer. *Endocr. Relat. Cancer* **2019**, *26*, 369–380. [[CrossRef](#)]
46. Ulbrich, C.; Westphal, K.; Baatout, S.; Wehland, M.; Bauer, J.; Flick, B.; Infanger, M.; Kreutz, R.; Vadrucchi, S.; Egli, M.; et al. Effects of basic fibroblast growth factor on endothelial cells under conditions of simulated microgravity. *J. Cell Biochem.* **2008**, *104*, 1324–1341. [[CrossRef](#)]

47. Ghobrial, I.M.; Witzig, T.E.; Adjei, A.A. Targeting apoptosis pathways in cancer therapy. *CA Cancer J. Clin.* **2005**, *55*, 178–194. [[CrossRef](#)]
48. Chang, T.T.; Walther, I.; Li, C.F.; Boonyaratanakornkit, J.; Galleri, G.; Meloni, M.A.; Pippia, P.; Cogoli, A.; Hughes-Fulford, M. The Rel/NF-kappaB pathway and transcription of immediate early genes in T cell activation are inhibited by microgravity. *J. Leukoc. Biol.* **2012**, *92*, 1133–1145. [[CrossRef](#)]
49. Boonyaratanakornkit, J.B.; Cogoli, A.; Li, C.F.; Schopper, T.; Pippia, P.; Galleri, G.; Meloni, M.A.; Hughes-Fulford, M. Key gravity-sensitive signaling pathways drive T cell activation. *FASEB J.* **2005**, *19*, 2020–2022. [[CrossRef](#)]
50. Gilmore, T.D. Introduction to NF-kappaB: Players, pathways, perspectives. *Oncogene* **2006**, *25*, 6680–6684. [[CrossRef](#)]
51. Wuest, S.L.; Stern, P.; Casartelli, E.; Egli, M. Fluid Dynamics Appearing during Simulated Microgravity Using Random Positioning Machines. *PLoS ONE* **2017**, *12*, e0170826. [[CrossRef](#)] [[PubMed](#)]
52. Ma, X.; Pietsch, J.; Wehland, M.; Schulz, H.; Saar, K.; Hubner, N.; Bauer, J.; Braun, M.; Schwarzwald, A.; Segerer, J.; et al. Differential gene expression profile and altered cytokine secretion of thyroid cancer cells in space. *FASEB J.* **2014**, *28*, 813–835. [[CrossRef](#)] [[PubMed](#)]
53. Buken, C.; Sahana, J.; Corydon, T.J.; Melnik, D.; Bauer, J.; Wehland, M.; Kruger, M.; Balk, S.; Abuagela, N.; Infanger, M.; et al. Morphological and Molecular Changes in Juvenile Normal Human Fibroblasts Exposed to Simulated Microgravity. *Sci. Rep.* **2019**, *9*, 11882. [[CrossRef](#)] [[PubMed](#)]
54. Nassef, M.Z.; Kopp, S.; Wehland, M.; Melnik, D.; Sahana, J.; Kruger, M.; Corydon, T.J.; Oltmann, H.; Schmitz, B.; Schutte, A.; et al. Real Microgravity Influences the Cytoskeleton and Focal Adhesions in Human Breast Cancer Cells. *Int. J. Mol. Sci.* **2019**, *20*, 3456. [[CrossRef](#)]
55. Dittrich, A.; Grimm, D.; Sahana, J.; Bauer, J.; Kruger, M.; Infanger, M.; Magnusson, N.E. Key Proteins Involved in Spheroid Formation and Angiogenesis in Endothelial Cells After Long-Term Exposure to Simulated Microgravity. *Cell Physiol. Biochem.* **2018**, *45*, 429–445. [[CrossRef](#)]
56. Eibl, R.H.; Benoit, M. Molecular resolution of cell adhesion forces. *IEE Proc. Nanobiotechnol.* **2004**, *151*, 128–132. [[CrossRef](#)]
57. Deng, C.; Zhang, D.; Shan, S.; Wu, J.; Yang, H.; Yu, Y. Angiogenic effect of intercellular adhesion molecule-1. *J. Huazhong Univ. Sci. Technol. Med. Sci.* **2007**, *27*, 9–12. [[CrossRef](#)]
58. Tauber, S.; Lauber, B.A.; Paulsen, K.; Layer, L.E.; Lehmann, M.; Hauschild, S.; Shepherd, N.R.; Polzer, J.; Segerer, J.; Thiel, C.S.; et al. Cytoskeletal stability and metabolic alterations in primary human macrophages in long-term microgravity. *PLoS ONE* **2017**, *12*, e0175599. [[CrossRef](#)]
59. Paulsen, K.; Tauber, S.; Dumrese, C.; Bradacs, G.; Simmet, D.M.; Golz, N.; Hauschild, S.; Raig, C.; Engeli, S.; Gutewort, A.; et al. Regulation of ICAM-1 in cells of the monocyte/macrophage system in microgravity. *BioMed Res. Int.* **2015**, *2015*, 538786. [[CrossRef](#)]
60. Ulbrich, C.; Pietsch, J.; Grosse, J.; Wehland, M.; Schulz, H.; Saar, K.; Hubner, N.; Hauslage, J.; Hemmersbach, R.; Braun, M.; et al. Differential gene regulation under altered gravity conditions in follicular thyroid cancer cells: Relationship between the extracellular matrix and the cytoskeleton. *Cell Physiol. Biochem.* **2011**, *28*, 185–198. [[CrossRef](#)]
61. Aleshcheva, G.; Wehland, M.; Sahana, J.; Bauer, J.; Corydon, T.J.; Hemmersbach, R.; Frett, T.; Egli, M.; Infanger, M.; Grosse, J.; et al. Moderate alterations of the cytoskeleton in human chondrocytes after short-term microgravity produced by parabolic flight maneuvers could be prevented by up-regulation of BMP-2 and SOX-9. *FASEB J.* **2015**, *29*, 2303–2314. [[CrossRef](#)]
62. Ingram, M.; Techy, G.B.; Saroufeem, R.; Yazan, O.; Narayan, K.S.; Goodwin, T.J.; Spaulding, G.F. Three-dimensional growth patterns of various human tumor cell lines in simulated microgravity of a NASA bioreactor. *In Vitro Cell Dev. Biol. Anim.* **1997**, *33*, 459–466. [[CrossRef](#)] [[PubMed](#)]
63. Kumei, Y.; Morita, S.; Katano, H.; Akiyama, H.; Hirano, M.; Oyha, K.; Shimokawa, H. Microgravity signal ensnarls cell adhesion, cytoskeleton, and matrix proteins of rat osteoblasts: Osteopontin, CD44, osteonectin, and alpha-tubulin. *Ann. N. Y. Acad. Sci.* **2006**, *1090*, 311–317. [[CrossRef](#)] [[PubMed](#)]
64. Weber, G.F. The cancer biomarker osteopontin: Combination with other markers. *Cancer Genom. Proteom.* **2011**, *8*, 263–288.
65. Irby, R.B.; McCarthy, S.M.; Yeatman, T.J. Osteopontin regulates multiple functions contributing to human colon cancer development and progression. *Clin. Exp. Metastasis* **2004**, *21*, 515–523. [[CrossRef](#)]

66. Wei, R.; Wong, J.P.C.; Kwok, H.F. Osteopontin—A promising biomarker for cancer therapy. *J. Cancer* **2017**, *8*, 2173–2183. [[CrossRef](#)]
67. Smith, S.M.; Lyu, Y.L.; Cai, L. NF-kappaB affects proliferation and invasiveness of breast cancer cells by regulating CD44 expression. *PLoS ONE* **2014**, *9*, e106966. [[CrossRef](#)]
68. Weber, G.F.; Ashkar, S.; Cantor, H. Interaction between CD44 and osteopontin as a potential basis for metastasis formation. *Proc. Assoc. Am. Physicians* **1997**, *109*, 1–9.
69. Ahmed, M.; Kundu, G.C. Osteopontin selectively regulates p70S6K/mTOR phosphorylation leading to NF-kappaB dependent AP-1-mediated ICAM-1 expression in breast cancer cells. *Mol. Cancer* **2010**, *9*, 101. [[CrossRef](#)]
70. O'Hanlon, D.M.; Fitzsimons, H.; Lynch, J.; Tormey, S.; Malone, C.; Given, H.F. Soluble adhesion molecules (E-selectin, ICAM-1 and VCAM-1) in breast carcinoma. *Eur. J. Cancer* **2002**, *38*, 2252–2257. [[CrossRef](#)]
71. Lee, J.Y.; Park, K.; Lee, E.; Ahn, T.; Jung, H.H.; Lim, S.H.; Hong, M.; Do, I.G.; Cho, E.Y.; Kim, D.H.; et al. Gene Expression Profiling of Breast Cancer Brain Metastasis. *Sci. Rep.* **2016**, *6*, 28623. [[CrossRef](#)] [[PubMed](#)]
72. Gibbs, L.D.; Vishwanatha, J.K. Prognostic impact of AnxA1 and AnxA2 gene expression in triple-negative breast cancer. *Oncotarget* **2018**, *9*, 2697–2704. [[CrossRef](#)] [[PubMed](#)]
73. Jung, H.; Kim, J.S.; Kim, W.K.; Oh, K.J.; Kim, J.M.; Lee, H.J.; Han, B.S.; Kim, D.S.; Seo, Y.S.; Lee, S.C.; et al. Intracellular annexin A2 regulates NF-kappaB signaling by binding to the p50 subunit: Implications for gemcitabine resistance in pancreatic cancer. *Cell Death Dis.* **2015**, *6*, e1606. [[CrossRef](#)] [[PubMed](#)]
74. Ahmed, K.M.; Dong, S.; Fan, M.; Li, J.J. Nuclear factor-kappaB p65 inhibits mitogen-activated protein kinase signaling pathway in radioresistant breast cancer cells. *Mol. Cancer Res.* **2006**, *4*, 945–955. [[CrossRef](#)]
75. Cook, S.J.; Stuart, K.; Gilley, R.; Sale, M.J. Control of cell death and mitochondrial fission by ERK1/2 MAP kinase signalling. *FEBS J.* **2017**, *284*, 4177–4195. [[CrossRef](#)]
76. Pham, T.N.D.; Perez White, B.E.; Zhao, H.; Mortazavi, F.; Tonetti, D.A. Protein kinase C alpha enhances migration of breast cancer cells through FOXC2-mediated repression of p120-catenin. *BMC Cancer* **2017**, *17*, 832. [[CrossRef](#)]
77. Chen, J.; Wu, F.; Shi, Y.; Yang, D.; Xu, M.; Lai, Y.; Liu, Y. Identification of key candidate genes involved in melanoma metastasis. *Mol. Med. Rep.* **2019**, *20*, 903–914. [[CrossRef](#)]
78. Kolch, W.; Heidecker, G.; Kochs, G.; Hummel, R.; Vahidi, H.; Mischak, H.; Finkenzeller, G.; Marme, D.; Rapp, U.R. Protein kinase C alpha activates RAF-1 by direct phosphorylation. *Nature* **1993**, *364*, 249–252. [[CrossRef](#)]
79. Olea-Flores, M.; Zuniga-Eulogio, M.D.; Mendoza-Catalan, M.A.; Rodriguez-Ruiz, H.A.; Castaneda-Saucedo, E.; Ortuno-Pineda, C.; Padilla-Benavides, T.; Navarro-Tito, N. Extracellular-Signal Regulated Kinase: A Central Molecule Driving Epithelial-Mesenchymal Transition in Cancer. *Int. J. Mol. Sci.* **2019**, *20*, 2885. [[CrossRef](#)]
80. Eblen, S.T. Extracellular-Regulated Kinases: Signaling From Ras to ERK Substrates to Control Biological Outcomes. *Adv. Cancer Res.* **2018**, *138*, 99–142. [[CrossRef](#)]
81. Crapoulet, N.; O'Brien, P.; Ouellette, R.J.; Robichaud, G.A. Coordinated expression of Pax-5 and FAK1 in metastasis. *Anticancer Agents Med. Chem.* **2011**, *11*, 643–649. [[CrossRef](#)] [[PubMed](#)]
82. Chan, K.T.; Cortesio, C.L.; Huttenlocher, A. FAK alters invadopodia and focal adhesion composition and dynamics to regulate breast cancer invasion. *J. Cell Biol.* **2009**, *185*, 357–370. [[CrossRef](#)] [[PubMed](#)]
83. Han, J.S.; Crowe, D.L. Jun amino-terminal kinase 1 activation promotes cell survival in ErbB2-positive breast cancer. *Anticancer Res.* **2010**, *30*, 3407–3412. [[PubMed](#)]
84. Zhang, J.Y.; Selim, M.A. The role of the c-Jun N-terminal Kinase signaling pathway in skin cancer. *Am. J. Cancer Res.* **2012**, *2*, 691–698.
85. Ashenden, M.; van Weverwijk, A.; Murugaesu, N.; Fearn, A.; Campbell, J.; Gao, Q.; Iravani, M.; Isacke, C.M. An In Vivo Functional Screen Identifies JNK Signaling As a Modulator of Chemotherapeutic Response in Breast Cancer. *Mol. Cancer Ther.* **2017**, *16*, 1967–1978. [[CrossRef](#)]
86. Lutzenberg, R.; Solano, K.; Buken, C.; Sahana, J.; Riwaldt, S.; Kopp, S.; Kruger, M.; Schulz, H.; Saar, K.; Huebner, N.; et al. Pathway Analysis Hints Towards Beneficial Effects of Long-Term Vibration on Human Chondrocytes. *Cell Physiol. Biochem.* **2018**, *47*, 1729–1741. [[CrossRef](#)]
87. Corydon, T.J.; Kopp, S.; Wehland, M.; Braun, M.; Schutte, A.; Mayer, T.; Hulsing, T.; Oltmann, H.; Schmitz, B.; Hemmersbach, R.; et al. Alterations of the cytoskeleton in human cells in space proved by life-cell imaging. *Sci. Rep.* **2016**, *6*, 20043. [[CrossRef](#)]

88. Benavides Damm, T.; Walther, I.; Wuest, S.L.; Sekler, J.; Egli, M. Cell cultivation under different gravitational loads using a novel random positioning incubator. *Biotechnol. Bioeng.* **2014**, *111*, 1180–1190. [[CrossRef](#)]
89. Lutzenberg, R.; Wehland, M.; Solano, K.; Nassef, M.Z.; Buken, C.; Melnik, D.; Bauer, J.; Kopp, S.; Kruger, M.; Riwaldt, S.; et al. Beneficial Effects of Low Frequency Vibration on Human Chondrocytes in Vitro. *Cell Physiol. Biochem.* **2019**, *53*, 623–637. [[CrossRef](#)]
90. Snel, B.; Lehmann, G.; Bork, P.; Huynen, M.A. STRING: A web-server to retrieve and display the repeatedly occurring neighbourhood of a gene. *Nucleic Acids Res.* **2000**, *28*, 3442–3444. [[CrossRef](#)]
91. Pietsch, J.; Riwaldt, S.; Bauer, J.; Sickmann, A.; Weber, G.; Grosse, J.; Infanger, M.; Eilles, C.; Grimm, D. Interaction of proteins identified in human thyroid cells. *Int. J. Mol. Sci.* **2013**, *14*, 1164–1178. [[CrossRef](#)] [[PubMed](#)]
92. Li, N.; Wang, C.; Sun, S.; Zhang, C.; Lu, D.; Chen, Q.; Long, M. Microgravity-Induced Alterations of Inflammation-Related Mechanotransduction in Endothelial Cells on Board SJ-10 Satellite. *Front. Physiol.* **2018**, *9*, 1025. [[CrossRef](#)] [[PubMed](#)]
93. Fedorchenko, O.; Stiefelhagen, M.; Peer-Zada, A.A.; Barthel, R.; Mayer, P.; Ecke, L.; Breuer, A.; Crispatsu, G.; Rosen, N.; Landwehr, T.; et al. CD44 regulates the apoptotic response and promotes disease development in chronic lymphocytic leukemia. *Blood* **2013**, *121*, 4126–4136. [[CrossRef](#)] [[PubMed](#)]
94. Lewis, M.L.; Reynolds, J.L.; Cubano, L.A.; Hatton, J.P.; Lawless, B.D.; Piepmeier, E.H. Spaceflight alters microtubules and increases apoptosis in human lymphocytes (Jurkat). *FASEB J.* **1998**, *12*, 1007–1018. [[CrossRef](#)]



© 2019 by the authors. Licensee MDPI, Basel, Switzerland. This article is an open access article distributed under the terms and conditions of the Creative Commons Attribution (CC BY) license (<http://creativecommons.org/licenses/by/4.0/>).

11.4. Publication #4

Lützenberg R, Wehland M, Solano K, **Nassef MZ**, Buken C, Melnik D, Bauer J, Kopp S, Krüger M, Riwaldt S, Hemmersbach R, Schulz H, Infanger M, Grimm D. Beneficial Effects of Low Frequency Vibration on Human Chondrocytes in Vitro. *Cell Physiol Biochem*. 2019;53:623–37.

Original Paper

Beneficial Effects of Low Frequency Vibration on Human Chondrocytes *in Vitro*

Ronald Lützenberg^a Markus Wehland^a Kendrick Solano^a Mohamed Z. Nassef^a
Christoph Buken^{a,b} Daniela Melnik^a Johann Bauer^c Sascha Kopp^a
Marcus Krüger^a Stefan Riwaldt^a Ruth Hemmersbach^d Herbert Schulz^e
Manfred Infanger^a Daniela Grimm^{a,b,f}

^aClinic for Plastic, Aesthetic and Hand Surgery, Otto-von-Guericke-University Magdeburg, Magdeburg, Germany, ^bDepartment of Biomedicine, Aarhus University, Aarhus, Denmark, ^cMax-Planck Institute of Biochemistry, Martinsried, Germany, ^dGerman Aerospace Center, Institute of Aerospace Medicine, Gravitational Biology, Cologne, Germany, ^eCologne Center for Genomics, University of Cologne, Cologne, Germany, ^fMicrogravity and Translational Regenerative Medicine, Faculty of Medicine and Mechanical Engineering, Otto-von-Guericke-University Magdeburg, Magdeburg, Germany

Key Words

Vibration • Chondrocytes • Extracellular matrix • Apoptosis • Focal adhesion • Annexin A2

Abstract

Background/Aims: In articular cartilage, chondrocytes are the predominant cell type. A long-term stay in space can lead to bone loss and cartilage breakdown. Due to the poor regenerative capacity of cartilage, this may impair the crewmembers' mobility and influence mission activities. Beside microgravity other factors such as cosmic radiation and vibration might be important for cartilage degeneration. Vibration at different frequencies showed various effects on cartilage *in vivo*, but knowledge about its impact on chondrocytes *in vitro* is sparse. **Methods:** Human chondrocytes were exposed to a vibration device, simulating the vibration profile occurring during parabolic flights, for 24 h (VIB) and compared to static controls. Phase-contrast microscopy, immunofluorescence, F-actin and TUNEL staining as well as quantitative real-time PCR were performed to examine effects on morphology, cell viability and shape as well as gene expression. The results were compared to earlier studies using semantic analyses. **Results:** No morphological changes or cytoskeletal alterations were observed in VIB and no apoptotic cells were found. A reorganization and increase in fibronectin were detected in VIB samples by immunofluorescence technique. *PXN*, *VCL*, *ANXA1*, *ANXA2*, *BAX*, and *BCL2* revealed differential regulations. **Conclusion:** Long-term VIB did not damage human chondrocytes *in vitro*. The reduction of *ANXA2*, and up-regulation of *ANXA1*, *PXN* and *VCL* mRNAs suggest that long-term vibration might even positively influence cultured chondrocytes.

© 2019 The Author(s). Published by Cell Physiol Biochem Press GmbH&Co. KG

R. Lützenberg and M. Wehland contributed equally to this study.

Dr. Ronald Lützenberg
and Prof. Daniela Grimm

Clinic for Plastic, Aesthetic and Hand Surgery, Otto-von-Guericke-University Magdeburg,
39120 Magdeburg (Germany);
Department of Biomedicine, Aarhus University, Høegh-Guldbergsgade 10, bygn. 1116 (SKOU),
8000 Aarhus C (Denmark)
Tel. +49-391-6721465, +45-871 67693, E-Mail ronald.luetzenberg@med.ovgu.de; dgg@biomed.au.dk

Introduction

Cartilage cells, also called chondrocytes, are the sole cellular component in cartilage tissue. They synthesize extracellular matrix (ECM) proteins, such as collagen II, proteoglycans, fibronectin and others.

Several publications demonstrated that mechanical stress influences human chondrocytes *in vitro* and alters various biological processes such as proliferation, cell adhesion, differentiation, and signal transduction [1, 2]. Human chondrocytes exposed to parabolic flight (PF) maneuvers showed an up-regulation of the cytoskeletal network genes and proteins suggesting that short-term microgravity (μg) influences the cells to respond by reorganizing the cytoskeleton [3]. Similar data were found when human chondrocytes were investigated for 24 h on the random positioning machine (RPM). The chondrocytes had changed their ECM synthesis while they reorganized their cytoskeleton prior to forming three-dimensional (3D) aggregates [4, 5].

In earlier studies an effect of vibration (VIB) was observed, when chondrocytes of human origin were investigated for 2 h and 24 h with vibraplex device developed by the German Aerospace Center (Deutsches Zentrum für Luft- und Raumfahrt, DLR) [3, 6]. Short-term VIB did not negatively influence the cartilage cells [3] and also long-term VIB did not alter the morphology of human chondrocytes *in vitro*. No signs of apoptosis were found. However, a reduction of osteopontin protein and a decrease in *PSMD4* and *TBX15* gene expression suggested that VIB might have positive effects on human chondrocytes [6].

Whole-body vibration (WBV) is currently under investigation to examine whether it is an option to treat the musculoskeletal disease osteoarthritis (OA). The effects are not clarified. A recent study showed that WBV induced cartilage degeneration in mice [7], while the application of lower frequencies of WBV showed a more differentiated picture. WBV of 10 Hz and 20 Hz resulted in a reduced cartilage resorption, an increased cartilage formation, and a delayed cartilage degradation, especially when applying 20 Hz, whereas higher frequencies of 30 Hz and 40 Hz induced worsening limb function, shrinking cartilage volume and cartilage resorption [8].

The principal aim of this study was first to address changes in the expression of selected genes of the ECM, focal adhesions and pathways of apoptosis in human chondrocytes exposed to VIB using a Vibraplex device, and secondly to compare these data with earlier μg results from studies reporting about the effects of simulated microgravity (*s- μg*) using a Random Positioning Machine (RPM) or of real microgravity (*r- μg*) achieved during PF or space missions. For this purpose, *in silico* analyses were performed. Moreover, the cells were examined by immunofluorescence staining and laser scanning microscopy to visualize the F-actin cytoskeleton, as well as vimentin, fibronectin and ICAM-1 proteins.

Materials and Methods

Cells and Culture Medium

Human chondrocytes from six different donors were bought from the company Provitro (Berlin, Germany). The cells were cultured in Chondrocyte Growth Medium (CGM; Provitro®, Berlin, Germany) supplemented with 10 % fetal calf serum (Provitro®, Berlin, Germany) and antibiotics – 100 IU penicillin/mL and 100 μg streptomycin/mL (Provitro®, Berlin, Germany). Chondrocytes of passage 3 grown in T25 cm² flasks (25 cm²; Sarstedt, Nümbrecht, Germany) were used for the experiments. The procedure was described in detail in [6].

For immunohistochemical studies, the cells were seeded in slide flasks (Thermo Fisher Scientific, Waltham, MA, USA) 24 h before the experiments (n=40 each group).

Vibration experiments

The vibration experiments were conducted as described in [3]. Briefly, the Vibraplex is a VIB platform designed and constructed by the Deutsches Zentrum für Luft- und Raumfahrt (DLR, German Center for

Aerospace Medicine) - Cologne, and can be used for studies to mimic the mechanical VIB encountered on an airplane during PFs.

The Vibraplex VIB platform (frequency range 0.2 Hz-14 kHz) was used to create VIB like to the ones occurring during PFs. The corresponding vibrations were recorded and analyzed by Schmidt [9]. The device is driven by an amplified wave signal equal to a $1/f^2$ noise (red noise), which was generated with the software WaveLab 4.0 from Steinberg.

The vibration treatment of the samples during the simulated free fall phase was alleviated by about -6 dB. This is half of the energy found during the simulated horizontal flight. During the simulated pull-up and pull-out phases, the vibrations were amplified by about +6 dB. The intensity of the noise applied was equivalent to 100 W/m^2 . The Vibraplex uses 2W with an experimental area of about 0.02 m^2 .

Table 1. Primary antibodies for immunofluorescence staining

Antibody	Dilution	Company
Vimentin Mouse	1:200	Sigma-Aldrich V5255
ICAM-1 Rabbit	1:25	Cell Signaling 4915
Fibronectin Rabbit	1:400	Sigma-Aldrich F3648

Immunofluorescence and F-actin staining

After the experimental procedures (VIB and static control experiments), the cell culture medium was immediately aspirated and the chondrocytes were fixed with 4% PFA for 30 minutes at room temperature (RT). Then the slides were washed two times in DPBS. Afterwards, the slides were washed with 0.1% Triton X in DPBS for 10 min with agitation, which was followed by three more washing steps with DPBS. To prevent non-specific binding, the slides were incubated in 3% BSA in a wet chamber for one hour. Primary antibodies diluted in 1% BSA were added to the slides overnight at 4°C (Table 1). The following day, the slides were washed 2 times in DPBS and the secondary antibody Alexa Fluor plus 488 goat anti-mouse IgG (H + L) (1:400) or Alexa Fluor 488 F(ab')₂ fragment of goat anti-rabbit IgG (H + L) (1:500) (both Invitrogen by Thermo Fischer Scientific) diluted in 1% BSA was added for one hour at RT. Afterwards, the slides were washed again with DPBS and Alexa Fluor 568 phalloidin (Invitrogen by Thermo Fischer Scientific) was added for one hour, followed by three times washing with DPBS and mounting with Fluoroshield with DAPI (Sigma Life Science). Then the slides were incubated overnight at 4°C . A Carl ZEISS LSM 800 Confocal laser scanning microscope was used to examine the cells. Three lasers were used to examine the slides: 488 nm, 561 nm and 405 nm for visualization of Alexa 488, Alexa 568 and DAPI, respectively.

Viability staining

TdT-mediated dUTP-biotin nick end labeling (TUNEL) staining was done according to the manual provided by the manufacturer (Thermo Fisher Scientific, Click-iT TUNEL Alexa Fluor 488 (cat# C10245)). The cells for 4',6-diamidino-2-phenylindole (DAPI) staining were fixed with 3.7% formaldehyde (room temperature, 10 min) and incubated in $1 \mu\text{g/mL}$ DAPI in PBS for 15 min (Invitrogen/Molecular Probes, Darmstadt, Germany). Stained cell samples (VIB and static CON) were investigated utilizing a Leica DM 2000 microscope equipped with an objective with a calibrated magnification of 400x and connected to an external light source, Leica EL 6000 (Leica Microsystems GmbH, Wetzlar, Germany). To obtain positive controls the cells were treated with DNAase before the TUNEL staining. The results were shown in the inserts of Fig. 1C, D.

Microscopy

The chondrocytes were examined with a Zeiss 510 META inverted confocal laser scanning microscope (Zeiss, Oberkochen, Germany), equipped with a Plan-Apochromat 363 1.4 objective [4]. Excitation and emission wavelengths were $\lambda_{exc} = 488 \text{ nm}$ and $\lambda_{em} = 505 \text{ nm}$ for FITC.

All samples were investigated with the image analysis program Scion Image (Version 1.63 Mac OS; Scion Corporation, Frederick, MD, USA). Phase contrast microscopy was performed using a LEICA DM2000 microscope equipped with a Leica DFC310 FX digital CCD color camera.

RNA isolation and quantitative real-time PCR (qPCR)

The RNA isolation and qPCR were performed as published earlier [6, 10]. Briefly, RNA was isolated with the RNeasy Mini Kit (Qiagen, Hilden, Germany), with an additional DNase digestion step (Qiagen) in order to eliminate residual DNA contaminations. Subsequently, the amount of RNA was quantified via a Photometer Ultraspec2010 (Amersham Biosciences, Freiburg, Germany). The first strand cDNA synthesis

kit (Thermo Fisher Scientific, Waltham, US) was used for reverse transcription. qPCR was performed using the 7500 Fast Real-Time PCR System (Applied Biosystems, Darmstadt, Germany) according to routine protocols [6, 11]. cDNA-selective-primers were synthesized by TIB Molbiol (Berlin, Germany) and were listed in Table 2. The primers were designed using Primer Express (Applied Biosystems, Darmstadt, Germany) to have a T_m of $\sim 60^\circ\text{C}$ and to span exon-exon boundaries. All samples were measured in triplicate. For normalization, 18S rRNA was used as a housekeeping gene. The comparative C_t ($\Delta\Delta C_t$) method was used for relative quantification of transcription levels and non-vibrated controls were defined as 100 % for reference.

Western blot analyses

Whole cell lysates were used for Western blotting following conventional protocols for gel electrophoresis and trans-blotting, as described earlier in [12]. Equal amounts of 10 μL lysate containing 2 $\mu\text{g}/\mu\text{L}$ protein were loaded on precast TGX stain-free gels (Bio-Rad, Munich, Germany). Transturbo blot PVDF membranes (Bio-Rad) were used for blotting. An overview of the used antibodies and their applied concentrations is given in Table 3. The analysis was performed using ImageQuant™ LAS 4000 (GE Healthcare UK Limited, Buckinghamshire, UK), and the densitometry was performed using ImageJ (NIH).

Pathway analyses

To study the mutual regulation of genes and to visualize localization and interactions between proteins, we entered relevant UniProtKB entry numbers in the Pathway Studio v.11 software (Elsevier Research Solutions, Amsterdam, The Netherlands). The graphs were generated for the gene expression and protein regulation and binding. The method was described in earlier studies [13, 14]. STRING analyses were done with STRING 11.0, available at <https://string-db.org/>.

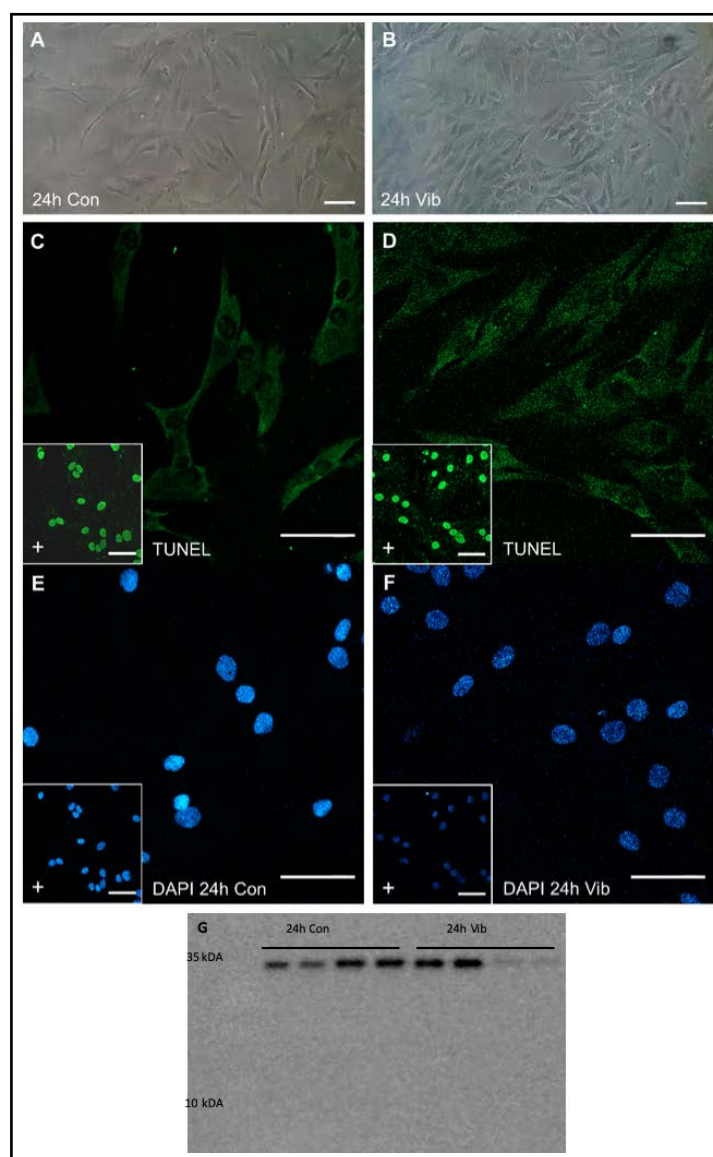


Fig. 1. Morphology of human primary chondrocytes in (A) static controls and (B) after 24h of VIB. TUNEL assay in comparison to DAPI counter staining (C, D) was used for apoptosis detection (green fluorescence). Positive controls (inserts) were initiated by DNase 1 prior to staining. DAPI staining (E, F) after fixation with PFA indicated no apoptotic bodies inside the nuclei or decomposition. (G) No cleaved caspase-3 (17 kDa) could be detected by Western blot. The uncleaved Cas-3 band visible at 32 kDa. Scale bars: 100 μm .

Statistical analysis

All statistical analyses were performed using SPSS 24 software (SPSS, Inc., Chicago, IL, USA). We used the Mann-Whitney-U-test to assess differences, which were considered significant at the level of $p < 0.05$. All data are presented as means \pm standard deviation.

Results

Morphology of the chondrocytes

After 24 h of VIB, no morphological differences between static control cells and vibrated chondrocytes were visible on commercially available human chondrocytes of passage 3 used for the experiments. The cells showed regular cell morphologies without any detectable alterations (Fig. 1A, B). Furthermore, all vibrated chondrocytes did not exhibit an increase in apoptosis (Fig. 1C-F). DAPI staining revealed normal nuclei in all samples (Fig. 1E, F). Positive controls given in the inserts showed apoptotic nuclei. In addition, Western blotting of cleaved caspase-3 demonstrated no activated caspase-3 (17 kDa) in all samples (Fig. 1G).

The F-actin cytoskeleton, vimentin, fibronectin and ICAM-1

Rhodamine-phalloidin staining was used to visualize the F-actin cytoskeleton after 24 h. Both static control as well as vibrated cells displayed a normal distribution and structure of actin fibers with no signs of damage, no disarrangements or deposits of F-actin at the cellular membranes (Fig. 2A, D, G, J, M, P).

The distribution and localization of the intermediate filament vimentin was similar in both groups (Fig. 2B, E).

Significant changes in the fibronectin content of chondrocytes exposed to mechanical vibration are shown in the Fig. 2H, K. A 24-hour-exposure to vibration showed that the cells started to secrete fibronectin into the extracellular space between adjacent cells, as can clearly be seen in Fig. 2K, L. An accumulation of this ECM protein was detectable as visualized by the green fluorescein isothiocyanate fluorescence.

ICAM-1 was strongly and constantly expressed by the chondrocytes in the control and VIB group. ICAM-1 was highly accumulated around the nucleus and spread out through the cell in both the control and vibration images. No difference was detected between both groups (Fig. 2N, Q).

Table 2. Primers used for quantitative real-time PCR. All sequences are given in 5'-3'-direction

Gene	Direction	Sequence
18S rRNA	forward	GGAGCCTGGCGCTTAATTT
	reverse	CAACTAAGAAGCCGCATGCA
ACAN	forward	AGTCCAACCTTCAAGGTGAAC
	reverse	ACTCAGCGAGTTGTCATGGT
ANXA1	forward	GCCAAAGACATAACCTCAGACACAT
	reverse	GAATCAGCCAAGTCTTCATTGACA
ANXA2	forward	GGTACAAGAGTTACAGCCCTTATGACA
	reverse	CATGGAGTCATACAGCCGATCA
BAX	forward	GTCAGCTGCCACTCGGAAA
	reverse	AGTAACATGGAGCTCGAGAGGAT
BCL2	forward	TCAGAGACAGCCAGGAAAATCA
	reverse	CCTGTGGATGACTGAGTACCTGAA
BIRC2	forward	GCTTTTGTGTGATGGTGGCT
	reverse	ACTCACACCTTGGAAACCACT
BIRC3	forward	TGCTGTGATGGTGACTCAG
	reverse	ACTCACACCTTGGAAACCACT
BIRC5	forward	GCCAGATGAGACCCCATAG
	reverse	CACCAAGGGTTAATCTTCAAACCTG
COL1A1	forward	ACGAAGACATCCCACCAATCAC
	reverse	CGTTGTGCGAGACGAGAT
COL2A1	forward	GGCAATAGCAGGTTACAGTACA
	reverse	CGATAACAGTCTTGCCCACTT
CYC1	forward	CACTGCGGGAAGGTCTCTAC
	reverse	GGGGTGCATCGTCAAACCTC
FADD	forward	CCTGGGGGAAGAAGCCTGTGTG
	reverse	TGATGCTGCGATCTTGGTG
FAS	forward	AGTCTGGTTTATCCCATTTGAC
	reverse	AGGGATTGGAATTGAGGAAGACT
FN1	forward	TGAGGAGCATGTTTTAGGAGAA
	reverse	TCCTCATTACATTCGGCGTATAC
NFKB1	forward	CTTAGGAGGAGAGCCAC
	reverse	TGAAACATTTGTTCCAGGCCTTC
PXN	forward	CATGGACGACCTCGACGC
	reverse	CAAGAACACAGCCGTTTGG
RELA	forward	CGCTTCTCACACACTGGATT
	reverse	ACTGCGGATGGCTTCT
TLN1	forward	GATGGCTATTACTCAGTACAGACAAGTGA
	reverse	CATAGTAGACTCTCATCTCTTCCA
VCL	forward	GTCTCGGCTGCTCGTATCTT
	reverse	GTCCACCAGCCCTGTCATTT

Table 3. Primary antibodies for Western blotting. Ms: mouse, Rb: rabbit

Antibodies	Company / No	Species	Detected MW (kDa)	Dilution
Anti-β-actin	Sigma / #A5316	Ms	42	1:5000
Anti-Caspase 3	Cell-Signaling / #9662S	Rb	17, 19, 35	1:800
Anti-NFκB p65	Cell-Signaling / #4764S	Rb	65	1:800

Expression of selected genes

In order to examine the influence of VIB on cultured chondrocytes, the gene expression of selected genes belonging to biological processes such as apoptosis, extracellular matrix, cell adhesion, or focal adhesions were studied. The chosen set of 19 genes comprised *ACAN*, *COL1A1*, *COL2A1*, *FN1* (Fig. 3), *VCL*, *TLN1*, *PXN* (Fig. 4), and *ANXA1*, *ANXA2*, *NFKB1*, *RELA*, *BIRC2*, *BIRC3*, *BIRC5*, *FADD*, *FAS*, *CYC*, *BAX*, *BCL2* (Fig. 5).

Significant changes were found for *VCL*, *PXN*, *ANXA1*, *ANXA2*, *BAX* and *BCL2* mRNAs. All others were not significantly altered (Fig. 3-5). Although the gene expression of *RELA* was not changed after a 24-hour vibration-exposure, the NF- κ B p65 protein was down-regulated in VIB samples, which hints to the cell-protective effects of low frequency VIB on human chondrocytes *in vitro* (Fig. 5).

Semantic analysis of observed gene and protein alterations in combination with earlier data

As determined by qPCR the majority of the 19 genes remained unchanged after 24 h of treatment (Fig. 3-5). Only 6 genes (*VCL*, *PXN*, *ANXA1*, *ANXA2*, *BAX* and *BCL2*) were significantly changed in the chondrocytes of the six donors after 24 h of incubation on a Vibraplex (Fig. 3-5). In order to estimate the relevance of this data, we compared them with earlier data shown in Tables 4-6 using the Pathway Studio program.

We did not find a significant up-regulation of *ACAN* and *COL2A1* (Fig. 3). According to the pathway analysis shown in Fig. 6, which is based on a number of

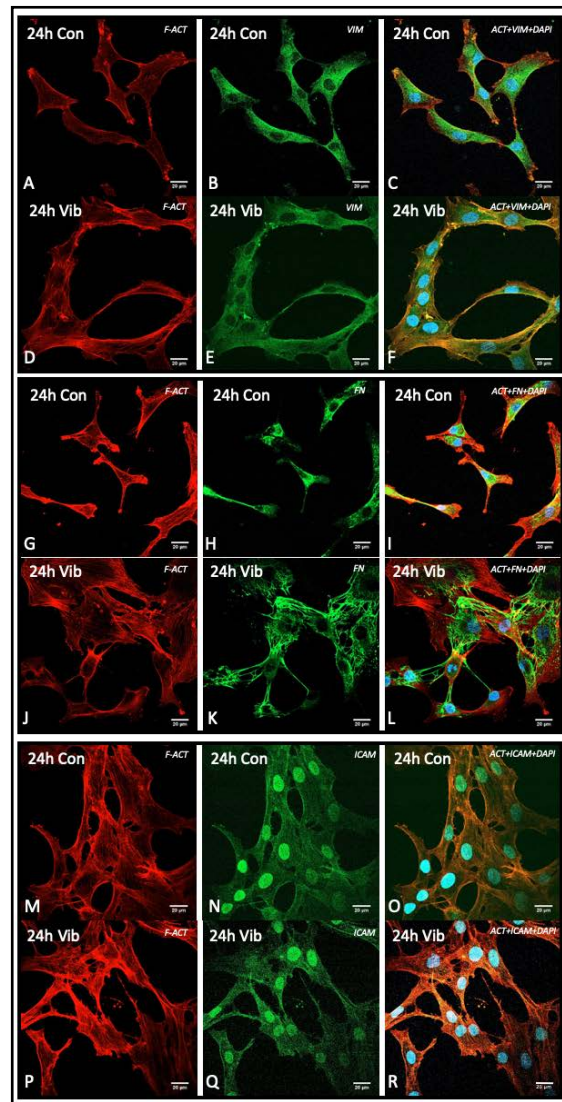


Fig. 2. Immunofluorescence staining of vimentin (B, E), fibronectin (H, K) and ICAM-1 (N, Q) (green), F-actin filaments (red; A, D, G, J, M, P) and the nucleus (blue - DAPI) in chondrocytes exposed to static control conditions (A-C, G-I, M-O) or to VIB (D-F, J-L, P-R) for 24 h. The scale bar is 20 μ m.

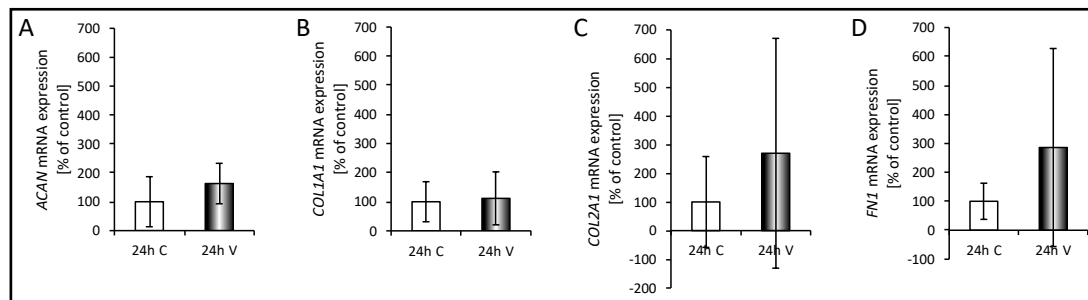


Fig. 3. Gene expression of ECM genes were determined by qPCR. Data is presented as means \pm standard deviation; n=6 (qPCR); C = control; V = VIB; * = p<0.05.

Fig. 4. Gene expression of focal adhesion genes were determined by qPCR. Data is presented as means \pm standard deviation; n=6 (qPCR); C = control; V = VIB; * = p<0.05.

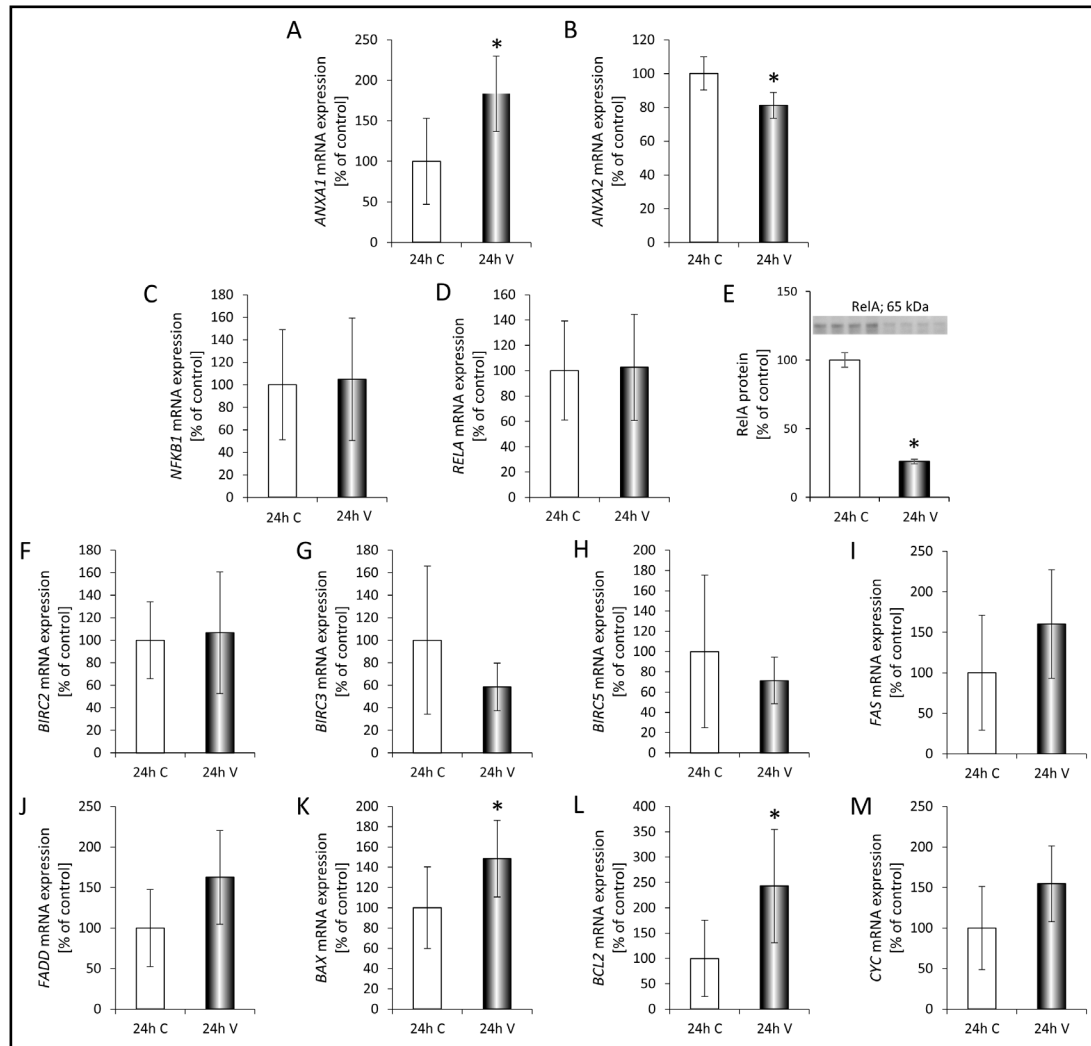
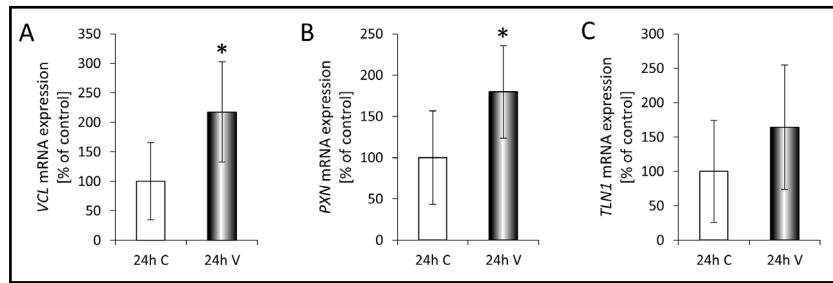


Fig. 5. Gene expression of the intrinsic and extrinsic pathway of apoptosis were determined by qPCR. In addition, the NF- κ B-p65 protein content was also analyzed by Western blot. Data is presented as means \pm standard deviation; n=6 (qPCR) and n=4 (Western blot); C = control; V = VIB; * = p<0.05.

studies described in the literature, an up-regulation of *COL2A1* may be supported by *ACAN*, as observed in [15] and by *RELA*. *COL2A1* may induce an up-regulation of *CXCL8* and *CASP3*, whereas *IL6* inhibits *COL2A1* expression.

According to [3], *ANXA2* was down-regulated while *SOX9* was up-regulated. *ANXA2* inhibits *CASP3* accumulation (Fig. 7). In addition, *COL2A1* inhibits *ACTB*. Enhanced *SOX5* and *SOX9* transcription factors are regulating the actin cytoskeleton (Fig. 7). In Fig. 3 we demonstrate that *COL2A1* was unchanged by VIB, but *COL1A1* was unchanged and expressed

at a low level. *ACTB* inhibits *SOX9* expression and activates *ACAN*, (Fig. 6) as it is described in [16].

In an earlier study, *SPP1* was also enhanced after 31P at gene and at protein levels [3]. At that time *ACTB*, *CAV1*, *ICAM1*, *SOX9*, *TUBB* and *VIM* were up-regulated together with *SPP1*, while *SOX5* was down-regulated. This may be explained by a mutual up-regulation of *SPP1*, *SOX9*, *VIM*, and *ICAM1* (Fig. 6, green arrows) [17-19]. *SPP1* had been shown to positively influence *IL6* and *CXCL8* genes (Fig. 6) [20]. Wehland *et al.* [21] had demonstrated that the *CXCL8* gene expression was up-regulated in vibrated chondrocytes and chondrocytes exposed to 31P during a PF mission (Table 5). They concluded that vibration was the major driving factor inducing the increase in *CXCL8* mRNA [21].

Above, we showed that the *ANXA2* mRNA was significantly down-regulated in the six donors (Fig. 5). Cleaved caspase-3 (17 kDa) was not detected in chondrocytes exposed to VIB for 24 h (Fig. 1G), as well as factors of the extrinsic pathway of apoptosis like FAS and FADD were not altered by vibration. Furthermore, *BAX* and *BCL2* genes were both elevated and thus inhibiting each other (Fig. 8).

Furthermore, *SPP1* could play an inhibitory role on *CASP3* gene expression (Fig. 6, red line with cross bar) [22]. NF- κ B p65 has an influence on aggrecan (Fig. 7). Interestingly, aggrecan and collagen type 2 were found enhanced in chondrocytes after 24 h on the RPM [15], but not significantly changed in VIB samples (Fig. 3), although there was a tendency to increase. In addition, after 16 days and 4 months of exposing chondrocytes to (s-) μ g, collagen type II was diminished, and collagen type 1 and type 10 were reduced already after 24 h [15, 23, 24]. In (s-) μ g, *SPP1* has shown an upregulating influence on the ECM components aggrecan and collagen type 2, but not on collagen type 1 and type 10 (Table 6) [25]. In patients suffering of OA, osteopontin may exert a protective effect against aggrecan degradation [26]. *SOX5* and *SOX9* play essential roles in producing aggrecan and collagen type 2 during cartilage formation [27-29].

Table 4. Comparison of gene and protein expression analyses with literature data from earlier experiments. ▼: significantly down-regulated; ○: no regulation; ▲: significantly up-regulated; n.d.: not determined; n.e.: not expressed; PFC: Parabolic flight campaign; RPM: Random Positioning Machine; VIB: Vibration; 31P: after 31 parabolas

Gene/Protein	Gene Expression				Protein Expression	
	VIB [6]		[3]		[3]	[15]
	VIB vs. 1g	PFC vs. 1g	VIB vs. 1g	1.8g vs. 1g	PFC 31P vs. 1g	24 h RPM vs. 1g
ACTB	○	▲	○	○	▲	n.d.
ANXA2	▼	n.d.	n.d.	n.d.	n.d.	n.d.
CASP3	○	n.d.	n.d.	n.d.	n.d.	▼
CAV1	○	▲	○	○	n.d.	n.d.
GAPDH	▲	n.d.	n.d.	n.d.	n.d.	n.d.
ICAM1	○	▲	○	○	▲	n.d.
ITGB1	○	n.d.	n.d.	n.d.	n.d.	n.d.
RELA	○	n.d.	n.d.	n.d.	n.d.	n.d.
SOX5	○	▼	○	○	n.d.	n.d.
SOX9	▲	▲	○	○	▲	n.d.
SPP1	○	▲	○	○	▲	n.d.
TUBB	○	▲	○	○	▲	n.d.
VIM	○	▲	○	○	▲	n.d.

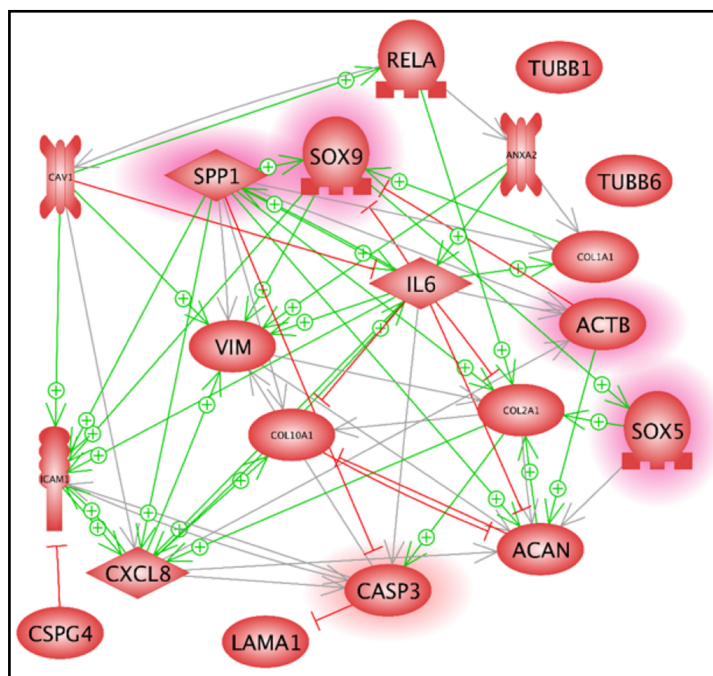
Table 5. The gravitational influence on the pro-inflammatory cytokines IL-6 and IL-8 [21]. ▼: significantly down-regulated; ○: no regulation; ▲: significantly up-regulated; n.d.: not determined; PFC: Parabolic flight campaign; VIB: Vibration

Gene/Protein	Gene Expression		Protein Expression	
	VIB 2h vs. 1g	PFC 2h vs. 1g	VIB 2h vs. 1g	1.8g 2h vs. 1g
IL6	▲	○	○	▲
CXCL8	▲	▲	n.d.	n.d.

Table 6. Regulation of extracellular matrix components under altered gravity. ▼: significantly down-regulated; ○: no regulation; ▲: significantly up-regulated; n.d.: not determined; PFC: Parabolic flight campaign; RPM: Random Positioning Machine; 31P: after 31 parabolas

Protein/ Gene	Protein Expression				Gene Expression
	[15]	[4]	[23]	[24]	[21]
	24h RPM vs. 1g	24h RPM vs. 1g	16d RPM/r- μ g vs. 1g	4mo r- μ g vs. 1g	PFC 31P vs. 1g
Aggrecan	▲	n.d.	▼	n.d.	n.d.
Chondroitin Sulfate	▲	n.d.	n.d.	n.d.	n.d.
Coll. Type I	▼	n.d.	▼	n.d.	n.d.
Coll. Type II	▲	▲	▼	▼	▼
Coll. Type X	▼	n.d.	n.d.	n.d.	n.d.
Laminin	○	n.d.	n.d.	n.d.	n.d.

Fig. 6. Mutual interaction of genes and their products on a genetic level. The genes were selected from the studies described in Tables 4-6. The graph was generated with Pathway Studio v.11 software (Elsevier Research Solutions, Amsterdam, The Netherlands).



Therefore, it may be suggested that microgravity induces an up-regulation of *SPP1* genes in chondrocytes and cartilage. The STRING analysis given in Fig. 8 demonstrated a central role for *FN1*, *VCL*, *NFKB1*, *RELA*, *FADD* and *CYC1*.

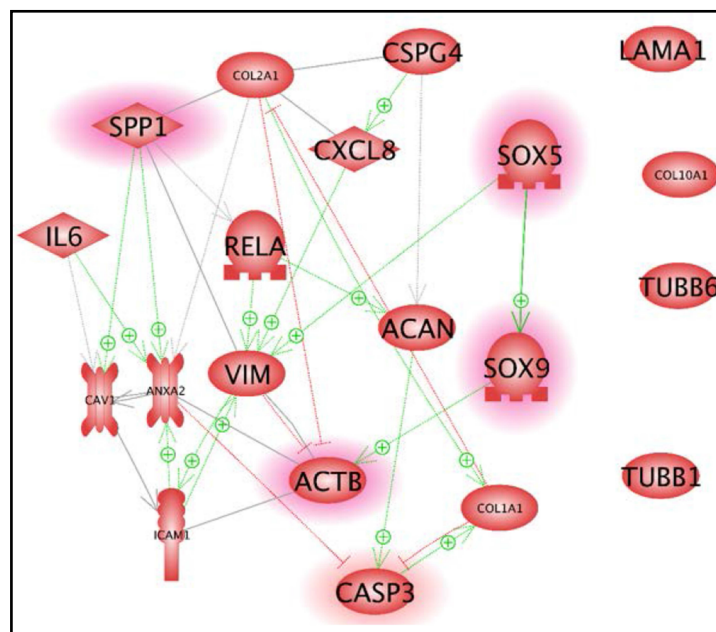
Discussion

In transportation systems like planes or spacecrafts one source of travelers' or crewmembers' discomfort are VIBs. They are experienced by the passengers due to the motion of the aircraft or the spacecraft in its operational mode. These VIBs can occur during normal passenger flights, but also during PF and space missions. Studies applying WBV have demonstrated an influence on bone and cartilage and propose WBV for the prevention of subchondral bone loss of knee OA [8]. Little is known about the direct effects of low frequency VIB on human chondrocytes, occurring during a long-term passenger flight. Therefore, we focused on the impact of low frequency VIB, measurable during a normal flight. It is known that short-term $r\text{-}\mu\text{g}$ occurring during PF maneuvers ($r\text{-}\mu\text{g}$) for about 2 hours induced only moderate changes in human chondrocytes and a two-hour-exposure to VIB exerted no damage of the cells [5].

Cartilage tissue has a low regeneration potential. The chondrocytes show a well-differentiated phenotype with unique physiological functions. Chondrocytes have shown to react to external stress and forces *in vitro* [3-6]. For example, culturing chondrocytes in simulated microgravity using μg -simulation devices like the NASA-developed rotating wall vessel (RWV) or the RPM induces three-dimensional growth of the chondrocytes and favor cartilage formation [30, 31].

However, long-term space missions revealed bone loss and cartilage breakdown in crewmembers, resulting in similar symptoms compared to OA [32, 33]. Therefore, it is of high interest to design and perform new studies focusing on chondrocytes *in vitro* or cartilage *in vivo*. Recently, a paper demonstrated the effects of low-magnitude WBV on cartilage degradation, bone/cartilage turnover, and OA joint function in a rabbit knee OA model [33, 34]. Lower frequency (20 Hz) WBV revealed beneficial effects for the bone micro-structure [34].

Fig. 7. Mutual interaction of proteins, which were selected from the studies described in the Tables 4-6. The graph was generated with Pathway Studio v.11 software (Elsevier Research Solutions, Amsterdam, The Netherlands).



We used human chondrocytes deriving from six different donors. The cells were exposed to the Vibraplex device *in vitro*. We did not detect any VIB-induced morphological changes and no cell death, which confirmed earlier data [6]. Recently, we had performed a whole genome microarray analysis on vibrated chondrocytes. Overall, we detected that VIB had only very little influence on the differential gene expression in chondrocytes [6].

In this study, we focused on selected genes belonging to the extracellular matrix which are characteristic for chondrocytes (*ACAN*, *COL2A1*), on focal adhesion markers and on factors of the intrinsic and extrinsic pathway of apoptosis. The objective was to further verify our hypothesis that VIB might have beneficial effects on chondrocytes and eventually on cartilage.

Long-term VIB of human chondrocytes *in vitro* promotes the interaction of cells leading to changes in extracellular matrix proteins or cell adhesion molecules such as fibronectin. Fibronectin was disorganized and accumulated in the extracellular space in vibrated chondrocytes compared to control cells (Fig. 2). Fibronectin is a key factor of the osteoarthritic process and it plays a central role in this study as demonstrated by the interaction network shown in Fig. 8. In particular, in the early stages of OA fibronectin has shown a rapid accumulation of the ECM, which might suggest an attempt of the tissue to repair itself [34]. A large elevation of *FN1* and *SPP1* mRNAs was measured in human OA-affected cartilage samples as compared with normal cartilage [35, 36]. Both cell adhesion molecules are involved in the inflammatory process of OA.

SPP1 was not significantly altered by vibration which hints to a more beneficial effect [6, 35], as an elevated osteopontin content could be involved in cartilage damage in astronauts, where osteopontin is linked to severity and progression of OA. Studies have shown that OA patients present higher concentrations of osteopontin as compared to healthy patients [3, 4, 8, 26, 37, 38].

We investigated whether focal adhesion genes are influenced by vibration in chondrocytes (Fig. 3-5). Focal adhesion proteins link the ECM and the actin cytoskeleton. They propagate signals arising from the activation of integrins following their engagement with ECM proteins like fibronectin. Fibronectin binding by cells influences vinculin (Fig. 8). Vibration significantly elevated the *VCL* mRNA expression. A fibronectin-vinculin transmembrane interaction is involved in differentiation processes [39].

Midpalatal suture cartilage cells exposed to expansive stimulation form actin stress fibers, and a reorganization of focal adhesion contacts (vinculin) occurred [40]. In parallel,

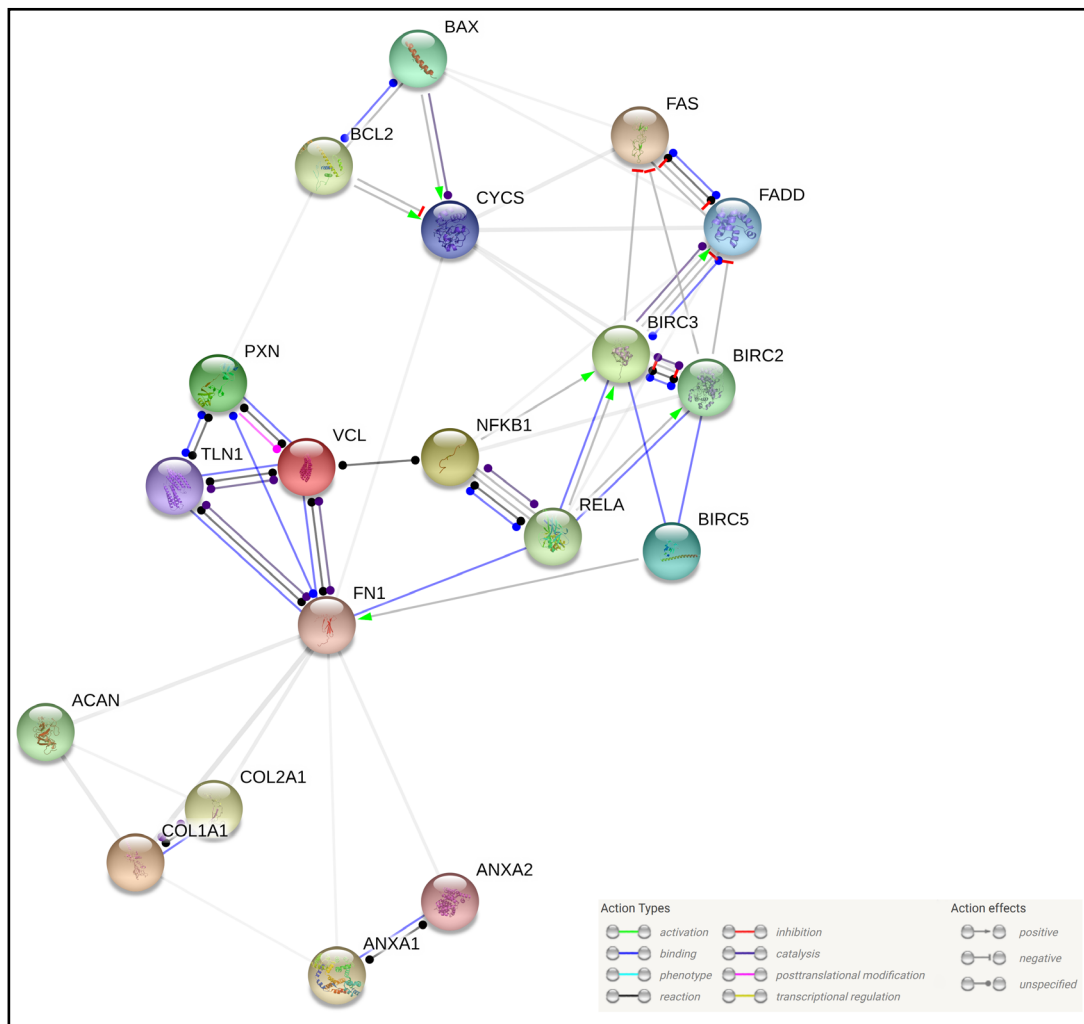


Fig. 8. STRING analysis with the major protein-protein interactions for chondrocytes experiments under mechanical vibration. The visualization was made using the online software STRING [https://string-db.org/].

fibronectin was elevated [39], which is comparable to our *in vitro* findings. Vibration also elevated the *PXN* mRNA in human chondrocytes (Fig. 4). The association of focal adhesion kinase with fibronectin and paxillin is required for precartilaginous condensation of chick mesenchymal cells [41]. Paxillin serves as a critical transducer of signals from fibronectin [42]. Vinculin has shown to regulate the survival of mouse embryonal cancer cells through regulating paxillin-FAK interactions to alter ERK1/2 activation [43]. In addition, paxillin is acting anti-apoptotic and is involved in the survival of mouse cells [44].

We have focused on apoptosis applying TUNEL staining. In all cultures of the six donors no morphological signs of programmed cell death were detectable. The *CASP3* and *RELA* gene expression was not significantly changed, but a significant reduction of the *ANXA2* gene expression was found in vibrated chondrocytes after 24 h. Cleaved caspase-3 protein (17 kDa) was not detectable. As the chondrocytes are the only cell type found in cartilage, inhibition of programmed cell death may be crucial for the maintenance of healthy cartilage [45]. The protein of *ANXA2* is annexin-A2, which is belonging to the annexin family. It plays a role in the development of OA. Annexin-A2 is involved in regulating cellular growth, cell motility and in signal transduction pathways (extracellular matrix). Human osteoarthritic chondrocytes undergo terminal differentiation, and are releasing, among other factors,

annexin A II-containing matrix vesicles which are able to initiate mineral formation, and ultimately die by apoptosis. Thus, these cells are involved in the destruction of articular cartilage in OA [46]. Moreover, we detected an up-regulation of *ANXA1* mRNA after vibration. *ANXA1* inhibits the activation of NF- κ B (nuclear factor κ -light-chain-enhancer of activated B cells) by binding to the p65 subunit [47], it is anti-proliferative, anti-apoptotic and associated with survival in gastric cancer [48].

In this study the gene expression of *RELA* was not changed after a 24-hour vibration-exposure, but the NF- κ B p65 protein was down-regulated in VIB samples, which hints to the cell-protective effects of low frequency VIB on human chondrocytes *in vitro*. In addition, we studied key factors of the intrinsic and extrinsic pathway of programmed cell death. *BAX* (Bcl-2 associated X-protein) and *BCL2* mRNAs were significantly up-regulated, whereas *CYC1* was not changed. In addition, *FAS* and *FADD* were not changed by vibration. In a next step, we investigated the *BIRC2*, *BIRC3*, *BIRC5*, which are members of the protein (IAP) family. IAPs are regulating the caspase activity, as well as proliferation and survival. None of these genes were changed in expression, neither *BIRC2*, which is the gene of the Baculoviral IAP repeat-containing protein 2, nor *BIRC3*, which inhibit apoptosis by binding to the tumor necrosis factor receptor-associated factors TRAF1 and TRAF2. *BIRC2* inhibits the activation of caspases-3, -7 and -9 [49]. *BIRC5* gene is coding for the surviving factor was also not changed by vibration. Hence, we did not find signs that vibration for 24h modulates chondrocyte apoptosis.

These experiments demonstrated that long-term VIB showed beneficial effects. The up-regulation of *VCL*, *PXN*, *ANXA1* and the down-regulation of *ANXA2* seem to protect the chondrocytes and inhibits dedifferentiation.

Conclusion

In conclusion, a 24-hour exposure to vibration as generated by the Vibraplex showed beneficial effects on human chondrocytes which did not reveal any noteworthy morphological alterations or damage. Pathway analyses hint towards a beneficial influence of this kind of vibration on human cartilage cells. The future of space exploration will involve long-duration spaceflights and stays on the International Space Station or flights to the Mars and beyond, and crewmembers will be subjected to a number of stressors like microgravity, vibration or cosmic radiation. Therefore, long-term vibration and microgravity studies on different cell types like endothelial cells [50] or lymphocytes [51] should be performed in the future.

Abbreviations

μ g (Microgravity); 3D (Three dimensional); ACAN (Aggrecan); ACTB (Beta-actin); *ANXA1* (Annexin a1); *ANXA2* (Annexin a2); *BAX* (Apoptosis regulator BAX); *BCL2* (Apoptosis regulator BCL2); *BIRC2* (Baculoviral IAP repeat-containing protein 2); *BIRC3* (Baculoviral IAP repeat-containing protein 3); *BIRC5* (Baculoviral IAP repeat-containing protein 5); BSA (Bovine serum albumin); *CASP3* (Caspase-3); *COL1A1* (Collagen alpha-1(I) chain); *COL2A1* (Collagen alpha-1(II) chain); CON (Control); *CXCL8* (Interleukin-8); *CYC1* (Cytochrome c1); DAPI (4',6-diamidino-2-phenylindole); DLR (Deutsches Zentrum für Luft- und Raumfahrt); DPBS (Dulbeccos phosphate buffered saline); ECM (Extracellular matrix); ERK1/2 (Mitogen-activated protein kinase 3/6); *FADD* (FAS-associated death domain protein); *FAS* (Tumor necrosis factor receptor superfamily member 6); FITC (Fluorescein isothiocyanate); FN1 (Fibronectin 1); IAP (Inhibitor of apoptosis protein); ICAM-1 (Intercellular adhesion molecule 1); IL6 (Interleukin-6); NF- κ B p65 (Nuclear factor NF-kappa-B p65 subunit); NFKB1 (Nuclear factor NF-kappa-B p105 subunit); OA (Osteoarthritis); PCR (Polymerase chain reaction); PF (Parabolic flight); PSMD4 (26S proteasome non-ATPase regulatory subunit 4); PVDF (Polyvinylidene fluoride); *PXN* (Paxillin); r- μ g (real microgravity); *RELA*

(Nuclear factor NF-kappa-B p65 subunit); RPM (Random positioning machine); RWV (Rotating wall vessel); s- μ g (simulated microgravity); SOX5 (Transcription factor SOX-5); SOX9 (Transcription factor SOX-9); SPP1 (Osteopontin); TBX15 (T-box transcription factor TBX15); TRAF 1/2 (TNF receptor-associated factor 1/2); TUBB (Beta-tubulin); TUNEL (TdT-mediated dUTP-biotin nick end labeling); VCL (Vinculin); VIB (Vibration); VIM (Vimentin); WBV (Whole body vibration).

Acknowledgements

The authors like to thank the European Space Agency (ESA; (DG, RH) ESA-CORA-GBF-Project 2014-03 "Vibrated Chondrocytes"), the German Space Agency (DLR; (DG) BMWi projects 50WB1524 and 50WB1924), and Aarhus University, Denmark, for funding of this study.

The views expressed herein can in no way be taken to reflect the official opinion of the German Space Agency and the European Space Agency.

Disclosure Statement

The authors declare no competing financial interests.

References

- 1 Chen CS, Ingber DE: Tensegrity and mechanoregulation: From skeleton to cytoskeleton. *Osteoarthritis Cartilage* 1999;7:81-94.
- 2 Davission T, Sah RL, Ratcliffe A: Perfusion increases cell content and matrix synthesis in chondrocyte three-dimensional cultures. *Tissue Eng* 2002;8:807-816.
- 3 Aleshcheva G, Wehland M, Sahana J, Bauer J, Corydon TJ, Hemmersbach R, Frett T, Egli M, Infanger M, Grosse J, Grimm D: Moderate alterations of the cytoskeleton in human chondrocytes after short-term microgravity produced by parabolic flight maneuvers could be prevented by up-regulation of bmp-2 and sox-9. *FASEB J* 2015;29:2303-2314.
- 4 Aleshcheva G, Sahana J, Ma X, Hauslage J, Hemmersbach R, Egli M, Infanger M, Bauer J, Grimm D: Changes in morphology, gene expression and protein content in chondrocytes cultured on a random positioning machine. *PLoS One* 2013;8:e79057.
- 5 Aleshcheva G, Bauer J, Hemmersbach R, Egli M, Wehland M, Grimm D: Tissue engineering of cartilage on ground-based facilities. *Microgravity Sci Technol* 2016;28:237-245.
- 6 Lützenberg R, Solano K, Buken C, Sahana J, Riwaldt S, Kopp S, Krüger M, Schulz H, Saar K, Huebner N, Hemmersbach R, Bauer J, Infanger M, Grimm D, Wehland M: Pathway analysis hints towards beneficial effects of long-term vibration on human chondrocytes. *Cell Physiol Biochem* 2018;47:1729-1741.
- 7 McCann MR, Yeung C, Pest MA, Ratneswaran A, Pollmann SI, Holdsworth DW, Beier F, Dixon SJ, Seguin CA: Whole-body vibration of mice induces articular cartilage degeneration with minimal changes in subchondral bone. *Osteoarthritis Cartilage* 2017;25:770-778.
- 8 Junbo W, Sijia L, Hongying C, Lei L, Pu W: Effect of low-magnitude different-frequency whole-body vibration on subchondral trabecular bone microarchitecture, cartilage degradation, bone/cartilage turnover, and joint pain in rabbits with knee osteoarthritis. *BMC Musculoskelet Disord* 2017;18:260.
- 9 Schmidt W: Quickly changing acceleration forces (QCAFs) vibration analysis on the A300 ZERO-G. *Microgravity Sci Technol* 2004;15:42-48.
- 10 Dittrich A, Grimm D, Sahana J, Bauer J, Krüger M, Infanger M, Magnusson NE: Key proteins involved in spheroid formation and angiogenesis in endothelial cells after long-term exposure to simulated microgravity. *Cell Physiol Biochem* 2018;45:429-445.

- 11 Pietsch J, Gass S, Nebuloni S, Echegoyen D, Riwaldt S, Baake C, Bauer J, Corydon TJ, Egli M, Infanger M, Grimm D: Three-dimensional growth of human endothelial cells in an automated cell culture experiment container during the spacex crs-8 iss space mission - the spheroids project. *Biomaterials* 2017;124:126-156.
- 12 Riwaldt S, Monici M, Graver Petersen A, Birk Jensen U, Evert K, Pantalone D, Utpatel K, Evert M, Wehland M, Krüger M, Kopp S, Frandsen S, Corydon T, Sahana J, Bauer J, Lützenberg R, Infanger M, Grimm D: Preparation of a spaceflight: Apoptosis search in sutured wound healing models. *Int J Mol Sci* 2017;18:pii:E2604.
- 13 Riwaldt S, Bauer J, Wehland M, Slumstrup L, Kopp S, Warnke E, Dittrich A, Magnusson NE, Pietsch J, Corydon TJ, Infanger M, Grimm D: Pathways regulating spheroid formation of human follicular thyroid cancer cells under simulated microgravity conditions: A genetic approach. *Int J Mol Sci* 2016;17:528.
- 14 Bauer J, Kopp S, Schlagberger EM, Grosse J, Sahana J, Riwaldt S, Wehland M, Luetzenberg R, Infanger M, Grimm D: Proteomic analysis of human follicular thyroid cancer cells exposed to the random positioning machine. *Int J Mol Sci* 2017;18:pii:E546.
- 15 Ulbrich C, Westphal K, Pietsch J, Winkler HD, Leder A, Bauer J, Kossmehl P, Grosse J, Schoenberger J, Infanger M, Egli M, Grimm D: Characterization of human chondrocytes exposed to simulated microgravity. *Cell Physiol Biochem* 2010;25:551-560.
- 16 Akiyama H, Chaboissier MC, Martin JF, Schedl A, de Crombrughe B: The transcription factor sox9 has essential roles in successive steps of the chondrocyte differentiation pathway and is required for expression of sox5 and sox6. *Genes Dev* 2002;16:2813-2828.
- 17 Kawai T, Yasuchika K, Ishii T, Miyauchi Y, Kojima H, Yamaoka R, Katayama H, Yoshitoshi EY, Ogiso S, Kita S, Yasuda K, Fukumitsu K, Komori J, Hatano E, Kawaguchi Y, Uemoto S: Sox9 is a novel cancer stem cell marker surrogated by osteopontin in human hepatocellular carcinoma. *Sci Rep* 2016;6:30489.
- 18 Ahmed M, Kundu GC: Osteopontin selectively regulates p70s6k/mtor phosphorylation leading to nf-kappab dependent ap-1-mediated icam-1 expression in breast cancer cells. *Mol Cancer* 2010;9:101.
- 19 Matsushima H, Kuroki T, Kitasato A, Adachi T, Tanaka T, Hirabaru M, Hirayama T, Kuroshima N, Hidaka M, Soyama A, Takatsuki M, Kinoshita N, Sano K, Nishida N, Eguchi S: Sox9 expression in carcinogenesis and its clinical significance in intrahepatic cholangiocarcinoma. *Dig Liver Dis* 2015;47:1067-1075.
- 20 Yang Y, Gao SG, Zhang FJ, Luo W, Xue JX, Lei GH: Effects of osteopontin on the expression of il-6 and il-8 inflammatory factors in human knee osteoarthritis chondrocytes. *Eur Rev Med Pharmacol Sci* 2014;18:3580-3586.
- 21 Wehland M, Aleshcheva G, Schulz H, Saar K, Hübner N, Hemmersbach R, Braun M, Ma X, Frett T, Warnke E, Riwaldt S, Pietsch J, Corydon TJ, Infanger M, Grimm D: Differential gene expression of human chondrocytes cultured under short-term altered gravity conditions during parabolic flight maneuvers. *Cell Commun Signal* 2015;13:18.
- 22 Zhao H, Chen Q, Alam A, Cui J, Suen KC, Soo AP, Eguchi S, Gu J, Ma D: The role of osteopontin in the progression of solid organ tumour. *Cell Death Dis* 2018;9:356.
- 23 Stamenkovic V, Keller G, Nestic D, Cogoli A, Grogan SP: Neocartilage formation in 1 g, simulated, and microgravity environments: Implications for tissue engineering. *Tissue Eng Part A* 2010;16:1729-1736.
- 24 Freed LE, Langer R, Martin I, Pellis NR, Vunjak-Novakovic G: Tissue engineering of cartilage in space. *Proc Natl Acad Sci U S A* 1997;94:13885-13890.
- 25 Grogan SP, Chen X, Sovani S, Taniguchi N, Colwell CW, Jr, Lotz MK, D'Lima DD: Influence of cartilage extracellular matrix molecules on cell phenotype and neocartilage formation. *Tissue Eng Part A* 2014;20:264-274.
- 26 Gao SG, Zeng C, Song Y, Tian J, Cheng C, Yang T, Li H, Zhang FJ, Lei GH: Effect of osteopontin on the mrna expression of adams4 and adams5 in chondrocytes from patients with knee osteoarthritis. *Exp Ther Med* 2015;9:1979-1983.
- 27 Lefebvre V, Dvir-Ginzberg M: Sox9 and the many facets of its regulation in the chondrocyte lineage. *Connect Tissue Res* 2017;58:2-14.
- 28 Lefebvre V, Behringer RR, de Crombrughe B: L-sox5, sox6 and sox9 control essential steps of the chondrocyte differentiation pathway. *Osteoarthritis Cartilage* 2001;9:S69-75.
- 29 Han Y, Lefebvre V: L-sox5 and sox6 drive expression of the aggrecan gene in cartilage by securing binding of sox9 to a far-upstream enhancer. *Mol Cell Biol* 2008;28:4999-5013.

- 30 Grimm D, Egli M, Krüger M, Riwaldt S, Corydon TJ, Kopp S, Wehland M, Wise P, Infanger M, Mann V, Sundaresan A: Tissue engineering under microgravity conditions-use of stem cells and specialized cells. *Stem Cells Dev* 2018;27:787-804.
- 31 Ulbrich C, Wehland M, Pietsch J, Aleshcheva G, Wise P, van Loon J, Magnusson N, Infanger M, Grosse J, Eilles C, Sundaresan A, Grimm D: The impact of simulated and real microgravity on bone cells and mesenchymal stem cells. *Biomed Res Int* 2014;2014:928507.
- 32 Grimm D, Grosse J, Wehland M, Mann V, Reseland JE, Sundaresan A, Corydon TJ: The impact of microgravity on bone in humans. *Bone* 2016;87:44-56.
- 33 Sanchez-Adams J, Leddy HA, McNulty AL, O'Connor CJ, Guilak F: The mechanobiology of articular cartilage: Bearing the burden of osteoarthritis. *Curr Rheumatol Rep* 2014;16:451.
- 34 Wang JB, Liu SJ, Chen HY, Wang P: [effects of low-magnitude whole body vibration (wbv) on knee osteoarthritis in rabbits]. *Sichuan Da Xue Xue Bao Yi Xue Ban* 2017;48:537-542.
- 35 Chevalier X: Fibronectin, cartilage, and osteoarthritis. *Semin Arthritis Rheum* 1993;22:307-318.
- 36 Attur MG, Dave MN, Stuchin S, Kowalski AJ, Steiner G, Abramson SB, Denhardt DT, Amin AR: Osteopontin: An intrinsic inhibitor of inflammation in cartilage. *Arthritis Rheum* 2001;44:578-584.
- 37 Gravallese EM: Osteopontin: A bridge between bone and the immune system. *J Clin Invest* 2003;112:147-149.
- 38 Li Y, Jiang W, Wang H, Deng Z, Zeng C, Tu M, Li L, Xiao W, Gao S, Luo W, Lei G: Osteopontin promotes expression of matrix metalloproteinase 13 through nf-kappab signaling in osteoarthritis. *Biomed Res Int* 2016;2016:6345656.
- 39 Lesot H, Kubler MD, Fausser JL, Ruch JV: A 165 kda membrane antigen mediating fibronectin-vinculin interaction is involved in murine odontoblast differentiation. *Differentiation* 1990;44:25-35.
- 40 Takahashi I, Onodera K, Sasano Y, Mizoguchi I, Bae JW, Mitani H, Kagayama M, Mitani H: Effect of stretching on gene expression of beta1 integrin and focal adhesion kinase and on chondrogenesis through cell-extracellular matrix interactions. *Eur J Cell Biol* 2003;82:182-192.
- 41 Bang OS, Kim EJ, Chung JG, Lee SR, Park TK, Kang SS: Association of focal adhesion kinase with fibronectin and paxillin is required for precartilage condensation of chick mesenchymal cells. *Biochem Biophys Res Commun* 2000;278:522-529.
- 42 Li D, Ding J, Wang X, Wang C, Wu T: Fibronectin promotes tyrosine phosphorylation of paxillin and cell invasiveness in the gastric cancer cell line ags. *Tumori* 2009;95:769-779.
- 43 Subauste MC, Pertz O, Adamson ED, Turner CE, Junger S, Hahn KM: Vinculin modulation of paxillin-fak interactions regulates erk to control survival and motility. *J Cell Biol* 2004;165:371-381.
- 44 Nah AS, Chay KO: Roles of paxillin phosphorylation in il-3 withdrawal-induced ba/f3 cell apoptosis. *Genes Genomics* 2019;41:241-248.
- 45 Matsuo M, Nishida K, Yoshida A, Murakami T, Inoue H: Expression of caspase-3 and -9 relevant to cartilage destruction and chondrocyte apoptosis in human osteoarthritic cartilage. *Acta Med Okayama* 2001;55:333-340.
- 46 Kirsch T, Swoboda B, Nah H: Activation of annexin ii and v expression, terminal differentiation, mineralization and apoptosis in human osteoarthritic cartilage. *Osteoarthritis Cartilage* 2000;8:294-302.
- 47 Zhang Z, Huang L, Zhao W, Rigas B: Annexin 1 induced by anti-inflammatory drugs binds to nf-kappab and inhibits its activation: Anticancer effects *in vitro* and *in vivo*. *Cancer Res* 2010;70:2379-2388.
- 48 Cheng TY, Wu MS, Lin JT, Lin MT, Shun CT, Huang HY, Hua KT, Kuo ML: Annexin a1 is associated with gastric cancer survival and promotes gastric cancer cell invasiveness through the formyl peptide receptor/ extracellular signal-regulated kinase/integrin beta-1-binding protein 1 pathway. *Cancer* 2012;118:5757-5767.
- 49 Saleem M, Qadir MI, Perveen N, Ahmad B, Saleem U, Irshad T, Ahmad B: Inhibitors of apoptotic proteins: New targets for anticancer therapy. *Chem Biol Drug Des* 2013;82:243-251.
- 50 Krüger M, Pietsch J, Bauer J, Kopp S, Carvalho DTO, Baatout S, Moreels M, Melnik D, Wehland M, Egli M, Jayashree S, Kobbero SD, Corydon TJ, Nebuloni S, Gass S, Evert M, Infanger M, Grimm D: Growth of endothelial cells in space and in simulated microgravity - a comparison on the secretory level. *Cell Physiol Biochem* 2019;52:1039-1060.
- 51 Battista N, Meloni MA, Bari M, Mastrangelo N, Galleri G, Rapino C, Dainese E, Agro AF, Pippia P, Maccarrone M: 5-lipoxygenase-dependent apoptosis of human lymphocytes in the international space station: Data from the roald experiment. *FASEB J* 2012;26:1791-1798.